A Study of Processing Methods for Producing Biaxial Orientation in Thermotropic Liquid Crystalline Polymers

by

Kent Gordon Blizard

Dissertation submitted to the Graduate Faculty of the Virginia Polytechnic Institute and State University in partial fulfillment of the requirements for the degree of

DOCTOR OF PHILOSOPHY
in
Chemical Engineering

APPROVED:

Donald G. Baird, Chairman

Garth L. Wilkes

Thomas C. Ward

William L. Conger

Daniel Frederick

February, 1988
Blacksburg, Virginia

PROCESSING METHODS FOR PRODUCING BIAXIAL ORIENTATION IN THERMOTROPIC LIQUID CRYSTALLINE POLYMERS

by

Kent G. Blizard

Abstract

Four methods of biaxial deformation were considered in an attempt to obtain biaxial orientation and properties in two thermotropic copolyesters: hydroxybenzoic acid-co-polyethylene terephthalate (HBA/PET) and hydroxybenzoic acid/2,6 hydroxynaphthoic acid (HBA/HNA). They consisted of solid phase forming, extrusion blow molding, biaxial stretching, and film blowing. Some measure of biaxial properties and orientation was obtainable in all four processes, from the layered structure apparent in the blow molded bottles to the uniplanar orientation in the stretched film. Tensile and flexural properties were exceptional in the blown film in comparison to the other processes considered: tensile strengths of 300 to 400 MPa and moduli of 13 GPa were observed in the axial direction, for example. This result is believed due to the absence of a skin-core texture in which the core often remains relatively unoriented.

A second objective of this work was to determine the feasibility of using Doi's theory for anisotropic solutions of rigid rods to predict the structure developed during the deformation processes for these thermotropic systems. Doi's theory of nematics, although limited to monodomains and containing numerous mathematical approximations in order to obtain a closed form for the kinetic equation, was used to predict the orientation development in the blown film process. Although qualitative agreement with experiment was found, quantitative agreement could not be expected.

Since Doi's theory was developed by examining an isolated rigid rod in solution and modifying the resultant equations to account for interactions of neighbors, transient predictions on a lyotropic solution were also made and compared to experimental results. In particular, stress growth on the inception of a steady simple shear flow was examined for the system of poly(p-phenylene terephthalamide)/ 100% sulfuric acid. Comparisons to Doi's theory were made for both isotropic and anisotropic solutions. Quantitatively the theory was found to be unacceptable, particularly at higher shear rates in which the equilibrium stress was at least an order of magnitude lower than experimental results showed. It did, however, predict an overshoot in the shear stress, which increases with deformation rate.

ACKNOWLEDGMENTS

The author wishes to express his sincere appreciation to his advisor, ., for his criticism, advice, and support in the course of this study. He would also like to thank his advisory committee, , , and for their interest and suggestions. The use of laboratory for part of the experimental work is greatly appreciated.

experimental work on PPT/H_2SO_4 solution rheology contributed significantly to finishing this degree. Thanks also go to , ., and for their help in the laboratory and their frequent advice, solicited or otherwise. help on the electron microscope has been invaluable. Not to be remiss, , ., and other students currently struggling through their graduate careers under the aegis of deserve commendation and this author's appreciation for their forbearance.

Finally, the author would like to thank his brother, ., for the excellent drawings he did as well as the long hours spent in the darkroom salvaging amateur photographic work.

TABLE OF CONTENTS

LIST OF ILLUSTRATIONS

LIST OF TABLES

1. INTRODUCTION

Over the past two decades a new class of polymers has been developed which has received a great deal of attention in the literature. Frequently termed liquid crystalline polymers (LCPs), these macromolecules have a structure intermediate between a liquid and a solid. The liquid crystalline mesophase may exist in polymers either in solution, in which case they are referred to as lyotropic, or in the melt state, in which instance they are designated as thermotropic. Although LCP fluids possess anisotropic optical properties like some solids, their molecules are relatively free to move about like a liquid; hence the term mesophase, meaning intermediate structure, has been applied to them.

Experimental observations have shown that the moities responsible for liquid crystalline behavior typically form elongated rigid rod molecules which exhibit a high degree of orientation within a domain. Flory has justified these observations from thermodynamics; the phase change from a liquid crystal to an isotropic solution could be attributed solely to the shape of the molecule [1]. Early work primarily was concerned with the lyotropic systems, of which poly(p-phenylene terephthalamide) (PPT), spun from

sulfuric acid solution to form Kevlar, is the most well known [2]. Because of the processing difficulties and limitations inherent in solution-spun fibers, melt-processable thermotropic LCPs have of late received great industrial interest. By combining the ease of processing found in most industrially important thermoplastics with potentially outstanding properties associated with highly oriented materials, thermotropic LCPs should play an ever more important role in the high performance plastics industry.

Much research and development remains, however, if the potential of the thermotropes is to be exploited. These systems should find a niche in applications where properties such as high strength and modulus, superior chemical resistance, high use temperatures, or specific electrical capabilities are required. Property-processing relationships are still rather vague and ill-defined in most instances. The importance of thermal and deformation history cannot be exaggerated when the process engineer tries to optimize the properties of the material. Traditional processing steps, particularly in the fabrication of multi dimensional articles, do not in general by themselves yield the optimal properties that one would desire.

The thermal and rheological properties exhibited by some thermotropic LCPs, though, permit processing options that may substantially enhance their physical and mechani-

cal properties. These processes in one way or another utilize the "orientability" of the domains and the molecules themselves in order to give the outstanding properties required in the competitive high performance materials market. For example, the long relaxation times associated with orientation in the thermotropic mesophase coupled with the phenomenon of supercooling permit processing below the usual flow temperature of the material.

This research looks at two aromatic systems, p-hydroxybenzoic acid, and 2,6 hydroxynaphthoic acid (HBA/HNA) system marketed by Celanese and hydroxybenzoic acid/ poly(ethylene terephthalate) (HBA/PET) thermotropic copolyester produced by Tennessee Eastman. This work attempts to answer the criticisms associated with these and other thermotropic LCPs. In particular, although properties in one direction may be outstanding, the anisotropy usually present is such that transverse properties are grossly inferior. Hence, if one were capable of predicting and producing biaxial or multiaxial orientation without excessive deterioration of properties in the machine direction, the polymers would have a wider range of applications.

Several processes for producing biaxial orientation in the melt or solid phase are discussed. Specifically, blow molding, a biaxial stretching process, squeezing flow, and free film blowing will be examined, the last both experimentally and theoretically (using Doi's

theory). The correlations of processing variables with orientation and properties in each instance will be undertaken.

In order to place this research in an appropriate framework, the recent technical literature concerned with the orientation and properties of thermotropic LCPs and the systems of interest in particular, will be reviewed in Chapter 2. An exhaustive review of the liquid crystalline literature is not contemplated; several such reviews are available [3-8]. The governing equations for free film blowing will also be summarized in preparation for the proposed theoretical work.

2. LITERATURE REVIEW

For one to comprehend the subtleties of the development of anisotropic properties in polymeric liquid crystals (LCPs), some phenomonological background is requisite. Section 2.1 thus gives an introduction, albeit brief, to the subject of liquid crystalline order in polymers. Second, the orientation and properties of thermotropic systems in general are considered, with emphasis on processing routes to achieving desired orientations. In section 2.3 the optical properties and domain orientation in thermotropic LCPs are then considered. The gross structure of liquid crystalline polymers from a mechanics viewpoint, including composite theory, is then considered in the next section. After that, in section 2.5 the thermal and flow properties of the systems of interest are considered. Points of contradiction of various research will be brought out, to emphasize the less than perfect state of fundamental knowledge in this rapidly developing field.

In view of the objective of this research to develop biaxial orientation in the copolyesters of interest, the next two sections will review the process of free film blowing. Following a theoretical development of the

governing equations in section 2.6, the following section concerns the practical considerations of the experimental techniques and methods used by other researchers. It should be emphasized that, although the equations presented were specific to film blowing, other processes to achieve biaxial orientation, such as blow molding, thermoforming, or a biaxial stretching process, could also be analyzed from such a perspective if the kinematics are known. This work will consider only film blowing from a modelling approach, although other processes will be studied in the laboratory.

It is one objective of this work to determine whether Doi's theory can be extended to thermotropic systems and used to predict orientation in the film blowing process. To this end his theory of polymer nematics will be summarized in the last section.

2.1 Liquid Crystalline Order in Polymers

Besides the distinctions made between lyotropic and thermotropic systems, liquid crystalline polymers may be further differentiated based on the type of molecular ordering exhibited in the liquid crystalline phase, which is a function of the molecular structure. Rigid rod molecules, helical molecules, and block or comb-like molecules each tend to form a specific mesophase type, of which there are three chief ones: nematic, cholesteric, and smectic.

A schematic representation of these three mesophase types is shown in Fig. 2.1. The nematic mesophase is that of lowest order and consists of aggregates of rod-like molecules. Within each aggregate, or domain, the molecules have a distribution about a common axis. No order exists, however, concerning the center of gravity of the individual molecules in a domain; they are free to slide over each other, maintaining their relative orientations. The cholesteric mesophase is closely related to the nematic, and thus has been termed a twisted or chiral nematic. Molecules are arranged in layers, each one resembling a nematic mesophase. The orientation in successive layers differs by a certain amount, the twist. The chiral nature of the substituent molecules gives rise to this helical packing, and results in the Bragg scattering

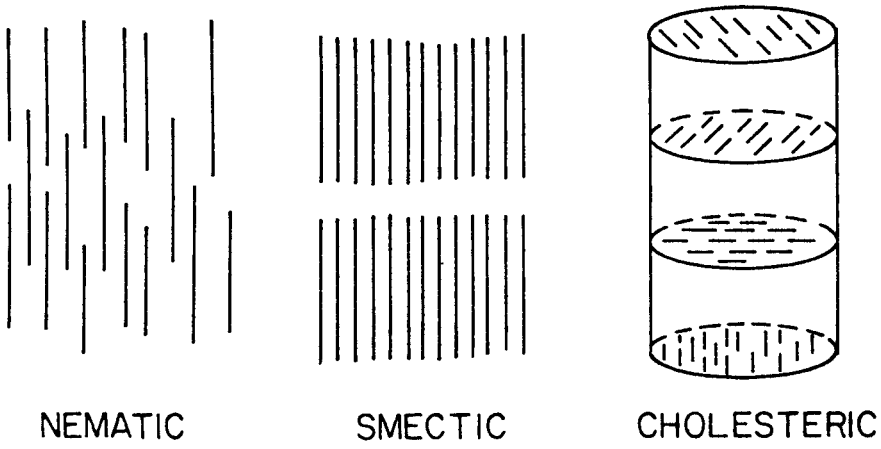

Figure 2.1 Schematic representation of the three mesophase types

frequently observed from these materials [60]. In the two dimensional smectic mesophase, the molecules reside in stratified layers separated by well-defined distances which can be detected by x-ray scattering. Unlike the nematic mesophase, there is an ordering of the centers of gravity of the molecules and they are not free to slide over one another. Both interactions between main chain and side chain groups may determine the ordering of the mesophase. Several reviews consider the chemistry of thermotropic LCPs [4,9], which is beyond the scope of the present work, concerned as it is primarily with orientation and properties.

2.2 Orientation and Properties of Thermotropic LCPs

The orientation and concomitant properties of numerous thermotropic systems, as well as various processing steps to generate these properties, have been reported in the literature [10-24]. Before examining these results, however, it is instructive to briefly review the concept of an order parameter, a good explanation of which was recently given by Ericksen [58].

A schematic representation of a single rod oriented at some angle in a Cartesian coordinate system is reproduced in Fig. 2.2. For rigid rod molecules having indistinguishable ends, odd moments of the orientation distribution disappear. In liquid crystal research the second moment is routinely used:

$$M_{ij} = \langle m_i m_j \rangle \qquad (2.2\text{-}1)$$

with **m** a unit vector and the brackets indicating the integral of the distribution function over a solid angle. The eigenvalues of **M**, M_n, n=1,2,3 must satisfy: $0<M_n<1$; $M_1+M_2+M_3=trM=1$. More common is to use the deviator of **M**, **S** = **M** - 1/3trMδ with the eigenvalues S_n satisfying: $-1/3<S_n<2/3$, $S_1+S_2+S_3=0$. In terms of the eigenvalues of **S**, three possibilities may exist. If all are equal, **S**=0, and an isotropic phase is defined. If two are equal, axial symmetry exists and S can be represented by

$$S_{ij} = S(n_i n_j - 1/3\delta_{ij}) \qquad (2.2\text{-}2)$$

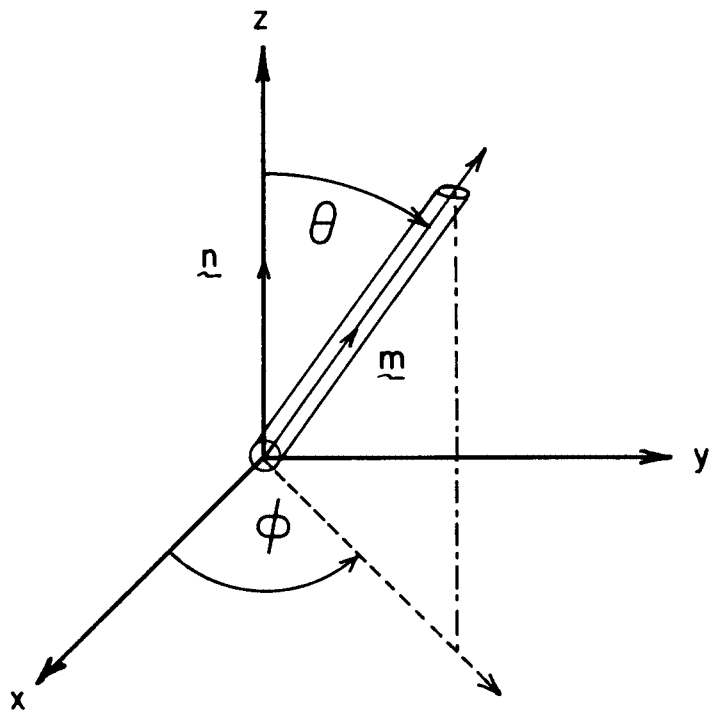

Figure 2.2 Schematic representation of a rigid rod oriented in a Cartesian coordinate system.

with **n** being a unit vector corresponding to the distinct eigenvalue (the director). In this case a nematic phase is defined. S, the order parameter, provides a scalar measure of how well the molecules are aligned and is defined such that $-\frac{1}{2} \leq S \leq 1$ with S=0 corresponding to random orientation. For perfect orientation along the director S=1. For $S=-\frac{1}{2}$, the molecules are confined to a plane perpendicular to **n**. Common measurements on nematic polymers place S in the range of .3 to .7; thus, alignment is usually far from perfect. Many theories have considered S to be characteristic of a given material. External fields, such as flow and magnetic fields, were used to control the director, **n**. The assumption of a constant S may not be valid for polymeric thermotropes because of chain flexibility, molecular weight distribution, and a polydomain structure, however, and an obvious compromise is to regard S as spatially variable and predict how its variations relate to an imposed field.

This remainder of this section will summarize some recent research findings concerning the orientation and properties of several thermotropic systems. With the above background on the definition of the order parameter, experimental results can be understood more readily and comparisons drawn between the often disparate findings.

Several authors have examined melt spun thermotropic systems in terms of the effect of processing variables

on orientation and mechanical properties of the fiber [10-16]. In most respects their findings are in agreement, but some differences should be pointed out. Acierno, et al. [10] studied fiber extrusion into air at room temperature of two compositions of the HBA/PET copolyester: 30/70 and 60/40. Only the latter exhibited the nematic phase. Among other results, they found mechanical properties, specifically tensile modulus, to decrease with increasing extrusion temperature for the 60/40 system. In particular, the highest value (30 GPa) was obtained at a temperature of only 225°C. At the highest temperature, 285°C, the initial modulus was only 1/10th of its maximum value. Material was extruded through a 2 mm orifice at 0.1 m/min with take-up velocities in the range of 10 to 300 m/min. Modulus increased with the take-up ratio, v_f/v_0, to an asymptotic value for each processing temperature. Their results are summarized in Fig. 2.3. The values of tensile strength, σ_B, also increased with take-up rate, but exhibited a discontinuity which was not fully accounted for. At high draw ratios ($v_{f/v0=2500}$), the tensile strength reached a maximum of about 300 MPa.

Ide and Ophir [12] described the melt extrusion of a naphthalene-containing terpolymer. The polyester was extruded through a 0.76 mm orifice at 340°C. Drawdown ratios of 1.1 to 50 were used. Tensile strengths increased from 0.1 to 0.7 GPa with drawdown ratios up to

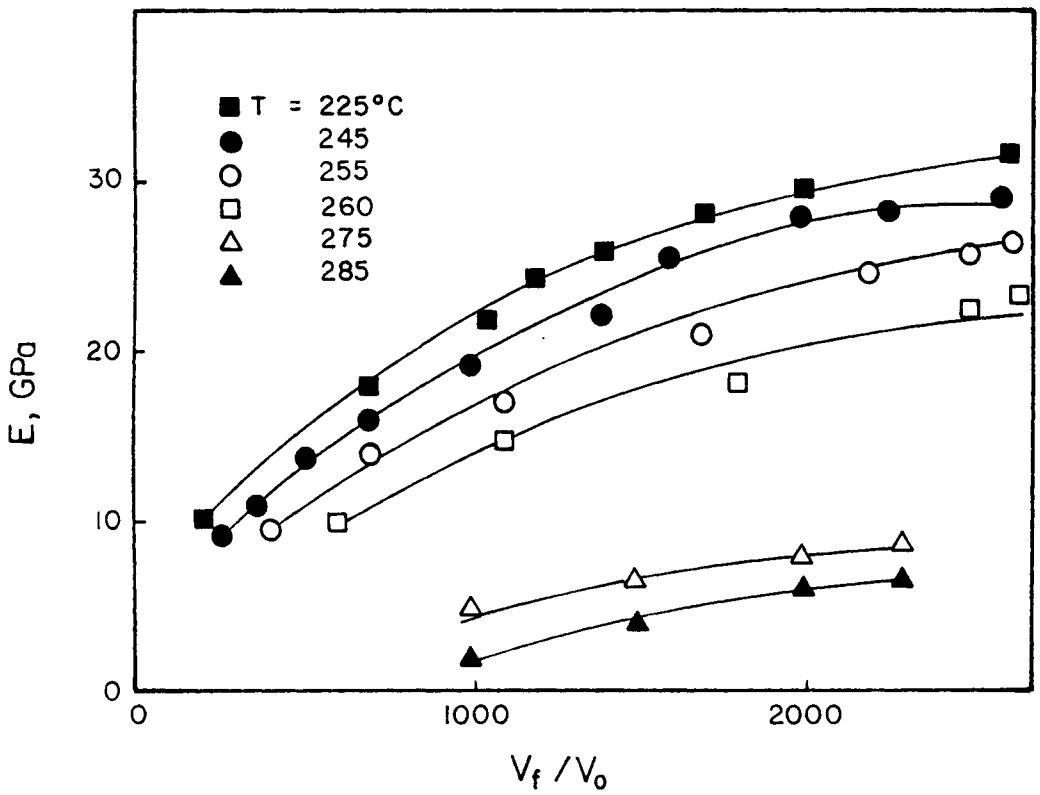

Figure 2.3 Elastic modulus for as spun $T_{2/60}$ vs. the V_f/V_0 ratio. Extrusion temperatures are indicated [10].

11, then decreased to about 0.5 GPa above draw ratios of 50. Tensile strengths were unaffected by increasing extrusion or shear rates. Tensile moduli decreased with shear rate from 5 GPa to 3.5 GPa at low draw ratios, but increased from 5 to 50 GPa at high draw ratios. These results are depicted in Fig. 2.4. The authors concluded that elongational, and not shear flow, contributed to the high degree of orientation observed in melt-spun fibers, and only small elongational strains were required for exceptional properties.

Sugiyama and coworkers [13] also reported on the melt spinning of the 60% HBA/PET copolyester. Although tensile properties were not reported, the effect of extrusion temperature and take-up ratio on fiber orientation were discussed. Fibers were melt spun between 230°C and 300°C through a 0.74 mm diameter capillary at 0.085 to 0.85 m/min with take-ups in the range of 500 to 1124 m/min. The authors did not report on how the fibers were cooled. Orientation, measured by x-ray scattering and determined by Hermans' orientation function,

$$f_H = [3\langle\cos 2\Theta\rangle - 1]/2 \qquad (2.2\text{-}3)$$

increased from 0.2 to 0.65 with no take-up as the temperature was increased from 230°C to 280°C. (Random orientation gives an f_H of zero, and perfectly aligned molecules an f_H of unity). A similar trend was noted at higher extrusion rates. This temperature dependence of orienta-

tion is summarized in Fig. 2.5. The limiting nature of Hermans' orientation function was interpreted as the result of "plug" flow in the capillary. The authors did not specify what exactly they meant by plug flow, how they determined its existence or how this would relate to the development of orientation in the extrudate. However, the flow curves indicated that no plug flow occurred. Little change of f_H with draw ratio was observed in contrast to the results of Ide and Ophir. Thus, Sugiyama and coworkers concluded that almost all of the orientation developed in the capillary itself.

Chung [11] has also conducted studies of the fiber extrusion of a nematic mesophase. The extrudate was run through a sizing ring and quenched. Various draw-down ratios were used, but the author does not specify these nor relate them to the orientation. Examining f_H for the HBA/HNA system, he correlated the modulus with the orientation function. He found that only a slight improvement in domain alignment led to a great enhancement in modulus. In Fig. 2.6, these results are seen. The initial tensile modulus increased from less than 2 MPsi to more than 10 MPsi if f_H was increased from approximately 0.8 to 0.95.

Muramatsu and Krigbaum [14] have recently reported their results on fiber spinning of 60% HBA/PET from the melt. The material was spun into a silicone oil below the die exit. Wide angle x-ray (WAXS) patterns showed better

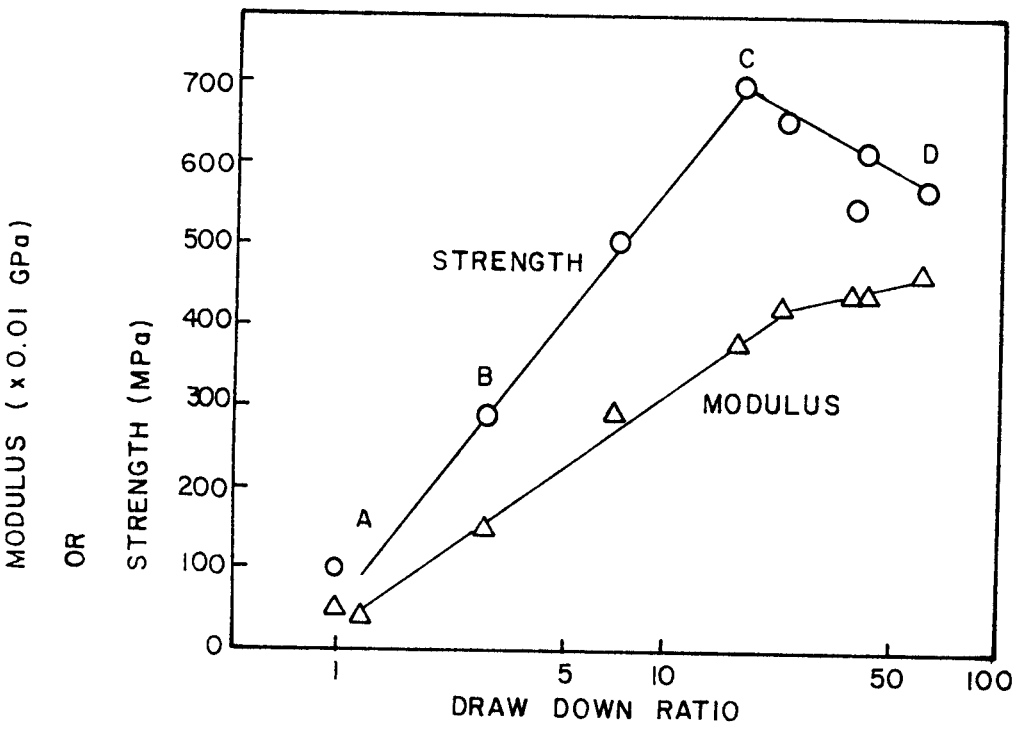

Figure 2.4 Mechanical properties of filaments drawn down at varying ratios [12].

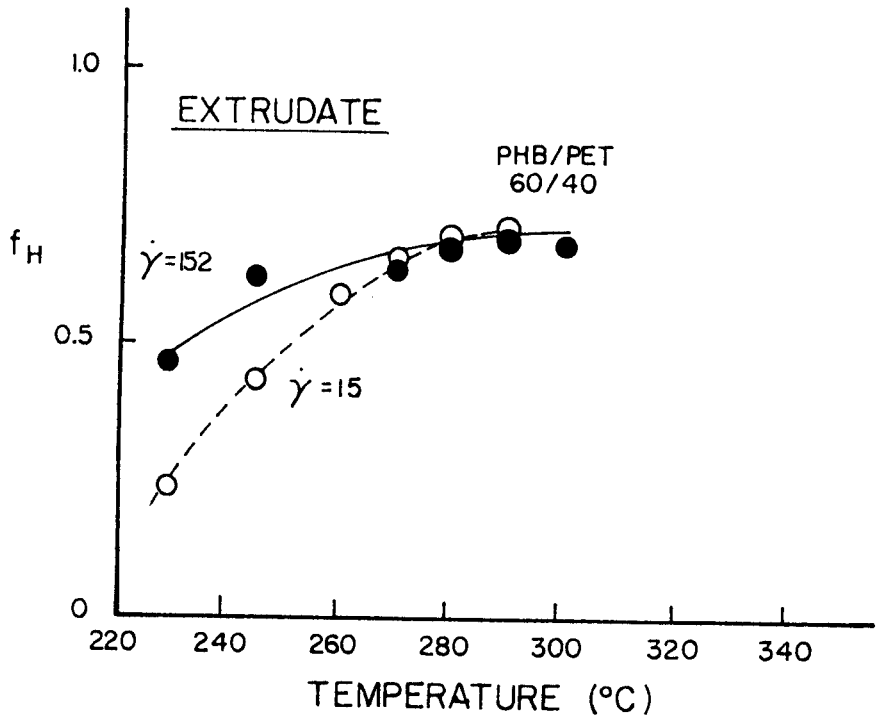

Figure 2.5 Temperature dependence of Hermans orientation factor, f_H, for 60/40 HBA/PET extrudates [13].

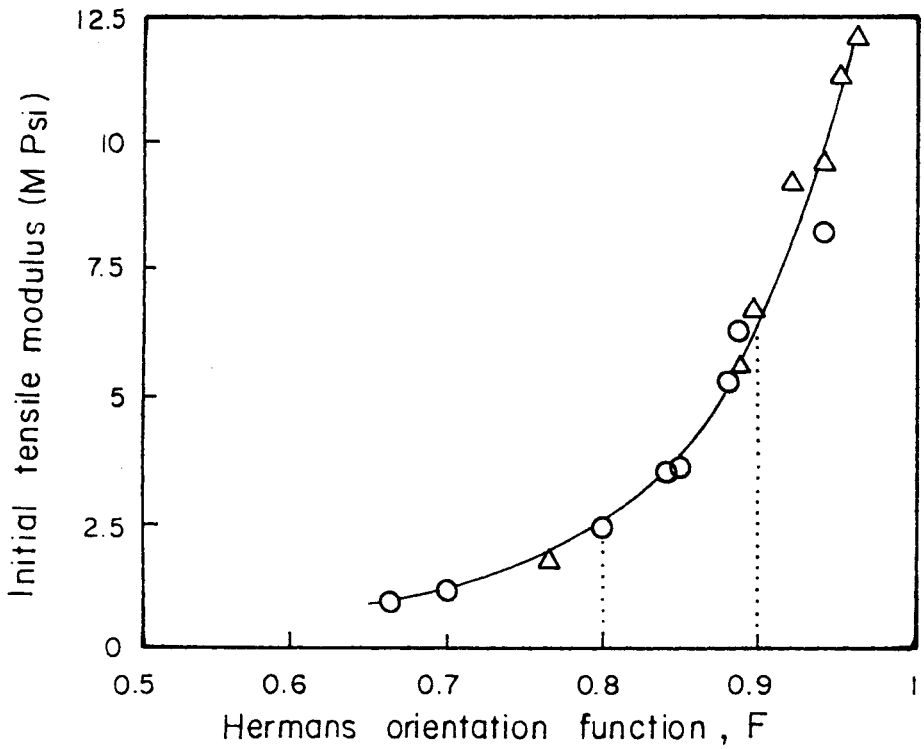

Figure 2.6 Initial modulus as a function of Hermans orientation function: (O) Polymer 1; (△) Polymer 2 [11].

orientation in the crystalline phase when the fibers were spun from the melt at 260°C or above where no HBA crystallites would remain. In contrast to Sugiyama's findings, some spin draw was required to improve the modulus. Fig. 2.7 gives the initial modulus as a function of take up ratio. Modulus increases with capillary length to diameter (L/D) ratio, but only between the short and intermediate capillary is the trend pronounced. The initial modulus as a function of $v_{f/v0}$ for various temperatures is reproduced in Fig. 2.8. The authors (incorrectly) concluded that the modulus increases with draw at a more rapid rate above 250°C than at 240° or 250°; actually, the reverse, based on these data, is more nearly correct. The authors conclude, that orientation is primarily developed through shear in the capillary, although some spin draw was required to avoid losing this orientation. Judging by their results in Figure 2.8, this conclusion should also be questioned. Draw appears to increase the modulus of the extrudate significantly in the limited region of $v_{f/v0}$ which they considered. How they attribute the orientation of the undrawn extrudate to shear in the capillary barrel and not to the converging extensional flow at its entrance is unclear.

Tealdi, Ciferri, and Conio [15] have recently published their melt spinning findings on the 60% HBA/PET system. The authors did not specify whether the extrudate

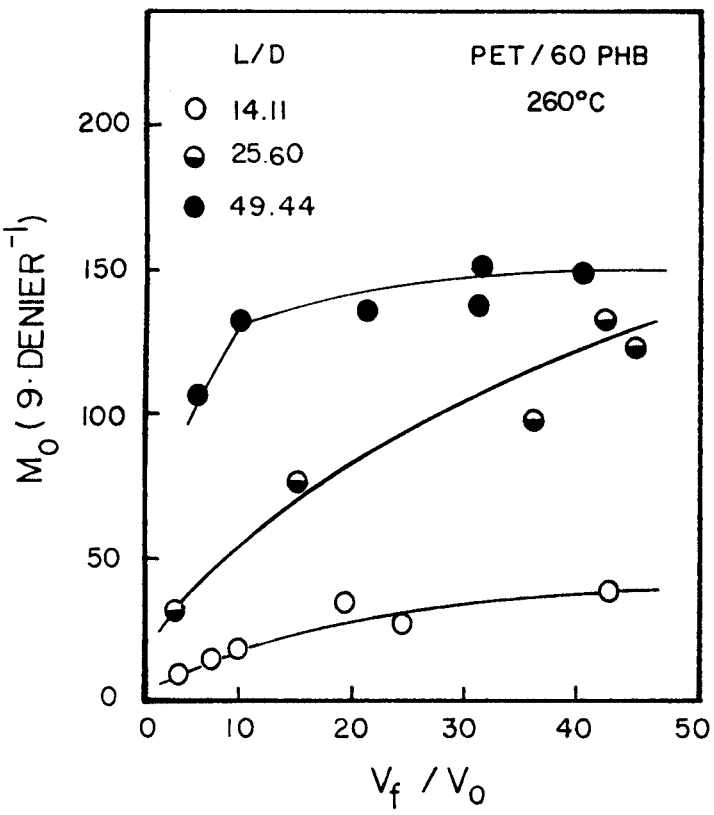

Figure 2.7 Initial modulus measured for three L/D ratios shown as a function of the spin draw ratio $V_{f/V0}$ [14].

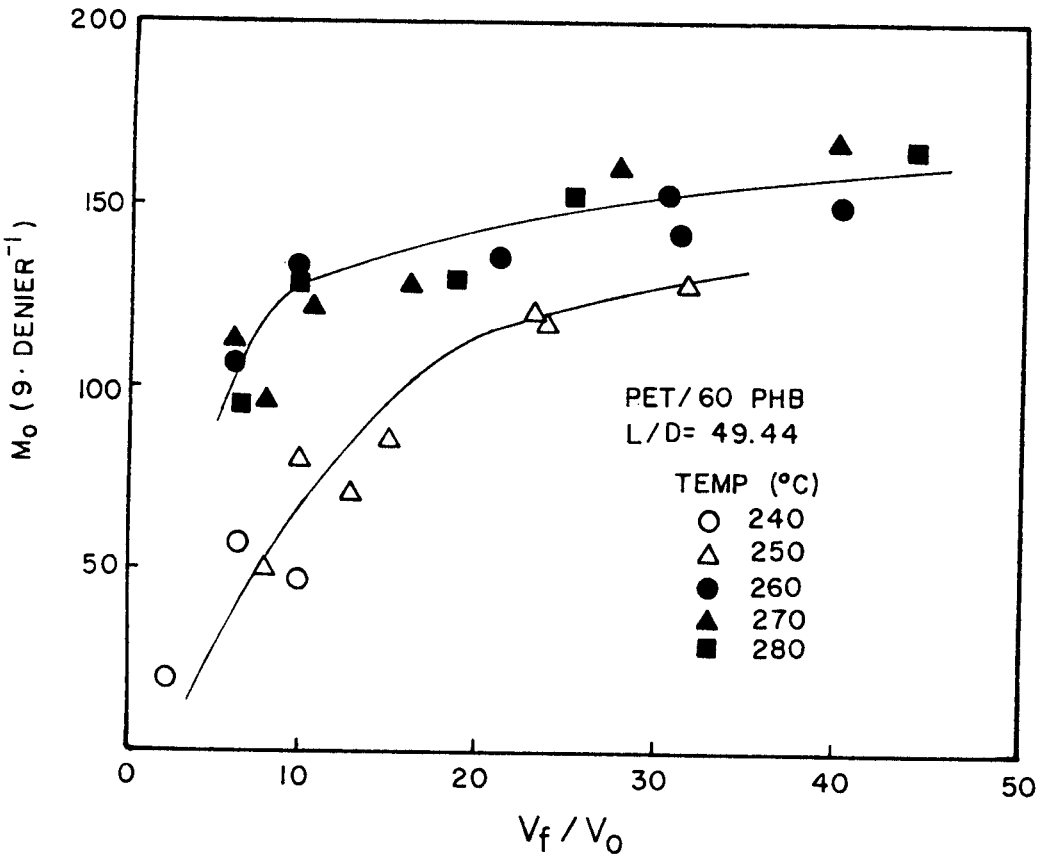

Figure 2.8 Initial modulus as a function of the spin draw ratio for five different spinning temperatures [14].

was quenched before take-up onto the bobbin. They found that, contrary to Acierno, modulus did not increase with extrusion temperature. It did, however, increase to a limiting value with draw-down ratio, as shown in Fig. 2.9. Also, unlike Acierno's findings, fiber could not be spun below 245°C: the other researcher had managed to process the copolyester as low as 225°C. A final difference between the two studies was that the modulus determined by Tealdi, et al. was not found to decrease with increasing temperature. With a relatively small draw, the modulus became quite large, and did not increase further with $v_{f/v0}$. One possible explanation for differences reported in the literature for this system is batch-to-batch variations, which appear as differences in intrinsic viscosity (IV). This explanation alone, attributing the contradictions to molecular weight variations seems inadequate.

Finally, Lewis and Fellers [16] have recently reported their studies on HBA/PET. They employed an isothermal gap below their spinneret analogous to a dry jet in solution spinning, and examined f_H and tensile properties as a function of this parameter in addition to the variables of processing temperature and $v_{f/v0}$. They found that Hermans' orientation function decreased with increasing extrusion rate (at a constant draw ratio), particularly at temperatures greater than 250°C. They interpreted this finding as indicating that a maximum in orientation occurs

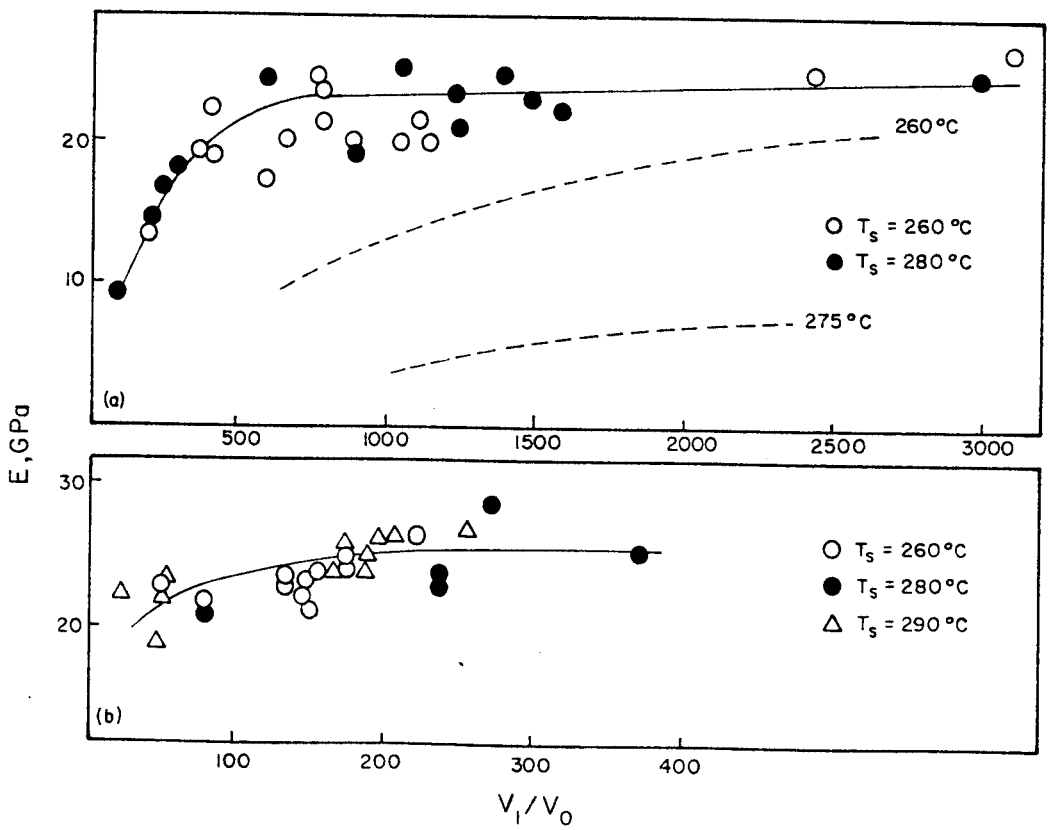

Figure 2.9 Elastic modulus for as-spun $T_{2/60}$ vs. V_1/V_0 ratio at varying extrusion temperatures. a) 2mm at the level die, V_0=10cm/min; b) 0.75mm die, V0=65cm/min [15]. Broken lines represent data of Acierno et al [10].

at low shear rates. With the presence of the isothermal gap, of orientation decreased relative to "nonisothermal" extrusion. Although the authors were surprised that their dry jet analogy failed, in view of possible relaxation of orientation at the melt temperature, this result might have been expected. Drawdown ratio did not have a significant effect on f_H, especially above a vf/v0 of about 200. Indeed, the conclusion they reached is that the extrusion temperature was the most effective processing variable for altering the extrudate orientation. The melting transition at 255°C appears to allow the level of orientation to increase since short segments of crystalline HBA are able to become involved in the orientation process. They further concluded that orientation is primarily developed by the flow in the die, and only marginally enhanced by the elongational flow outside the die.

The disparate results discussed above seem to indicate that there exists a maximum degree of orientation possible in the fiber drawing process and that this is not usually achieved in the die alone, but rather some post draw is required. The degree of orientation obtained in the die itself varied among the researchers, but seemed to depend on the thermal history (temperature, whether the fibers were quenched or supercooled, etc.) to a large extent. Thus it appears that control of the thermal history, along with the flow history enables one to orient thermotropes

to a high degree in the fiber process.

Injection molding of thermotropic liquid crystalline polymers has also been reported in the literature [17-20]. These results are among the earliest and best known concerning the orientation and mechanical properties of thermotropes and have in part spurred on recent work in the area. One of the first thermotropic systems studied was HBA/PET, reported by researchers at Tennessee Eastman [17] in 1976. Jackson and Kuhfuss examined mechanical properties of the copolyesters as a function of composition, mold thickness, and temperature profile in the molding machine. For the 60% HBA polymer, which exhibited some of the most encouraging properties as well as liquid crystalline behavior, further investigation was conducted on injection molded plaques. In particular, the high degree of anisotropy and the dependence of mechanical properties on mold thickness was noted. In Fig. 2.10 these results are shown. As can be seen, the flexural modulus along the flow direction increased ten-fold if the mold thickness was reduced from 1/2" to 1/16". The transverse direction modulus, in contrast, remained essentially constant, irrespective of mold thickness.

Mold filling studies of HBA/PET were conducted by Baird and coworkers [19]. Microtomed sections from end-gated plaques were examined under the electron microscope

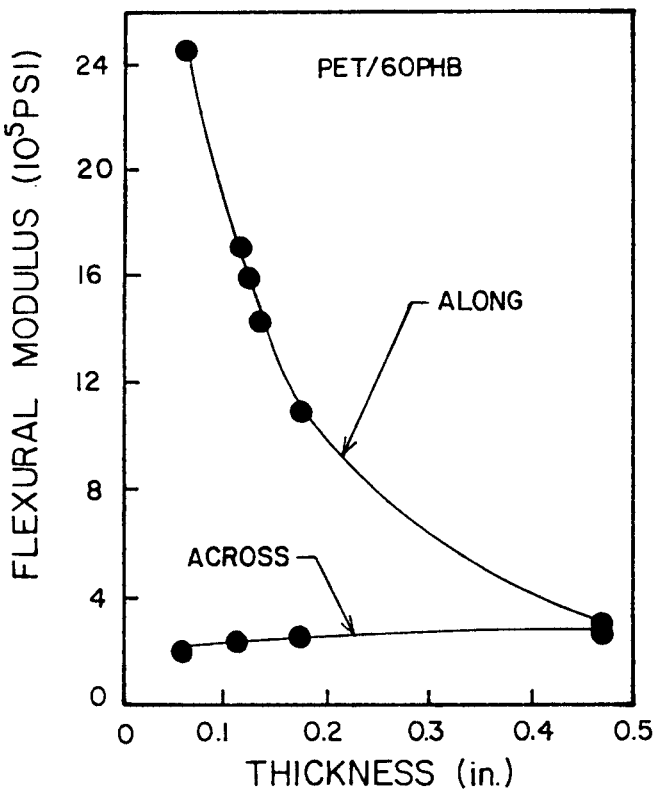

Figure 2.10 Effect of thickness on along and across flow modulus of 60 HBA/PET [17].

(SEM). A skin/core morphology was observed and confirmed by x-ray scattering (WAXS), which showed a relatively unoriented center and an edge consisting of highly oriented fibers. The radial flow in the center-gated specimens resulted in a more uniform degree of orientation in both the r and Θ directions.

Ophir and Ide [20] investigated the injection molding of naphthalene thermotropic polyesters (NTPs). They noticed a skin/core structure similar to that reported by Baird and coworkers and attributed it to fountain flow into the end-gated mold; the extensional flow near the surface, coupled with the more rapid cooling there, produced a far greater degree of orientation than was present at the center of the mold, in which shear flow and slower polymer cooling prevailed. The polymer exhibited superior mechanical properties, but transverse properties were not commented upon. Tensile strengths were up to 300 MPa and flexural moduli around 15 GPa were reported.

The shortcomings observed in traditional injection molding have provided the impetus to find other processing options to improve the properties of the thermotropic LCP systems. In particular, the elimination of an unoriented core is expected to improve mechanical properties. In order to better understand the effects of thermal and deformation history, some fundamental work on the development of molecular orientation and texture in HBA/PET has

also been published [21,22]. The effect of flow history, in particular simple shear, extensional flow, and biaxial squeezing flows, were examined by Baird and coworkers [21] using SEM and WAXS. Shear flow between the plates of a Rheometrics Mechanical Spectrometer (RMS) imparted little, if any, orientation and a spongy morphological texture was observed when the sample was etched with n-propylamine. If the specimens were simultaneously cooled while being sheared, however, a greater degree of orientation was observed.

By far the most effective method of inducing uniaxial orientation, though, was to draw ribbons of the material. With this extensional flow field the resulting WAXS patterns showed an exceptionally high degree of azimuthal intensity associated with uniaxial alignment of the molecules. The morphological texture of the etched specimens was fibrillar, reflecting the high degree of alignment shown by WAXS.

Finally, if compression molded samples were squeezed between lubricated plates, biaxial orientation could be seen, as suggested by the presence of four high intensity lobes on the diffraction patterns. However, this result could not be reproduced. Squeezing flow did, however, tend to produce a uniplanar orientation in which the molecules has a high degree of preferential orientation normal to the squeezing direction [23].

The differences in molecular orientation produced in shear versus extensional flow were explained in terms of the flow kinematics. The rotational (non-zero vorticity tensor) nature of shear flow may cause the domains to tumble rather than align themselves along one specific direction. If the material is cooled while it is being sheared at high rates, these domains may actually break up and molecular orientation occur. In extensional flow the material is stretched along one axis, resulting in the elongation of the domains and hence a high degree of orientation and fibrillar texture.

One final study relating to orientation of thermotropes was conducted by Farell and Fellers [24] and consisted of examining the orientation in cellulosic derivatives induced by rotating an annular die during a tube extrusion process. Some tubes were then inflated with nitrogen. Several techniques, including WAXS, SEM, and mechanical property measurement, were used to determine the level of biaxiality present. The authors concluded that the rotating annular die process is more effective in controlling orientation in thermotropic LCPs than in polyolefins due to the longer relaxation times. By controlling the angular velocities of the rotating surfaces, the average polymer chain axis, as determined from White-Spruiell biaxial orientation factors, could be placed anywhere between the machine and transverse directions (MD

and TD). These factors, calculated in both the MD and TD, may be conveniently represented by a triangular orientation diagram (see Fig. 2.11). For hydroxyproply cellulose extrudates these values ranged from 0.8 to 0.17 for f_{1B} (MD) and from 0.021 to 0.71 for f_{2B} (TD). The directionality of the mechanical properties could likewise be controlled; however, the properties in the transverse direction increased only at the expense of those in the MD as was expected.

Although fiber orientation and properties in thermotropes have been fairly extensively reported on, little work has been done concerning the optimization of properties in these systems in the form of film and other two and three dimensional articles. The effect of thermal and deformation history on properties and orientation is still not completely clear.

In the next section the optical properties and orientation of these materials will be examined. Research in this area has primarily been concerned with correlating optical textures with molecular orientation and mechanical properties.

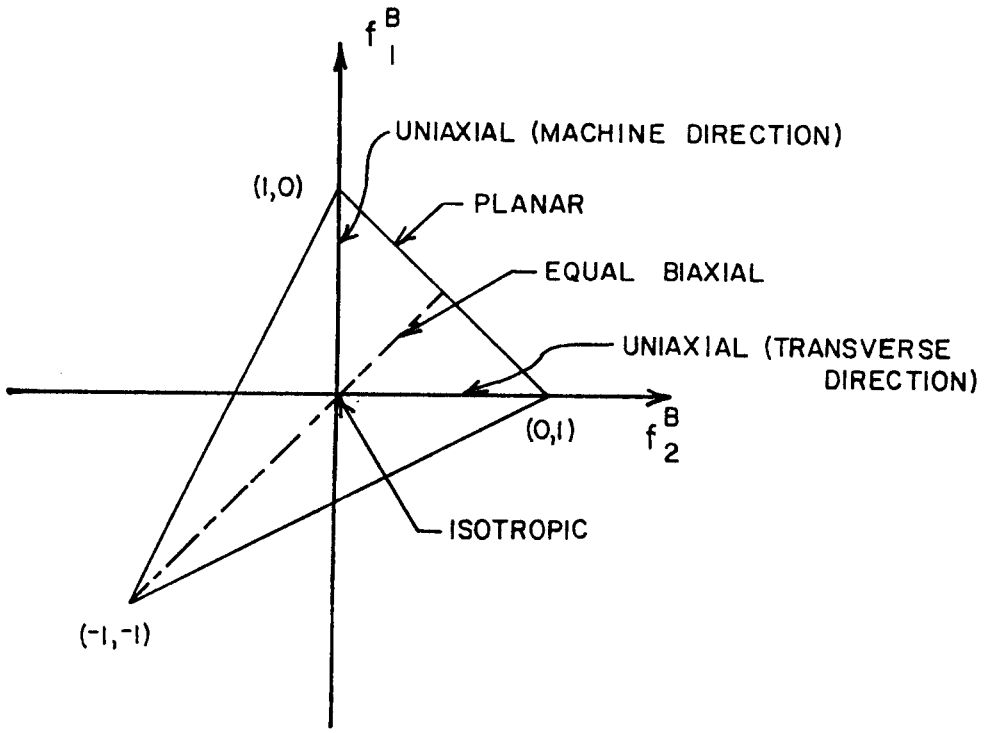

Figure 2.11 Graphical representation of orientation, the orientation triangle diagram [61].

2.3 Optical Properties and Orientation

The determination of mesophasic transitions, mesophasic structure, and optical orientation in thermotropic liquid crystalline polymers has been thoroughly investigated by Viney, Donald, Mitchell, and Windle, who collaborated on a series of publications in the past few years [25-31]. Mackley and coworkers [32], and Zacchariades and Logan [33] have also contributed to the literature. This section will focus on optical orientation in thermotropic LCPs, both in the quiescent and deformed states, and to what extent this orientation and the observed optical textures correlate with molecular orientation. This section does not intend to review the use of the microscope, or details of domains, walls, and structures that have been observed as Viney has recently published a very thorough account of the technique [34].

Mackley, Pinaud, and Siegmann [32] published the first work on the observations and optical anisotropy of a mesomorphic copolyester, 60 mole% HBA/PET. They noticed complex anisotropic effects in the quiescent melt which subsequently became frozen into the material at room temperature. By ordering the material in a magnetic field, disclinations typical of a liquid crystalline mesophase were observed. The actual molecular trajectory associated with these disclinations could not be identi-

fied, however.

In 1983, Donald et al. [25] reported on the appearance of banded structures in several thermotropic LCPs that had been drawn as fibers or shear-oriented as thin films. The 60% HBA/PET system, as well as HBA/HNA systems, exhibited bands or striations perpendicular to the shear or fiber axis direction. The authors noted that this structure closely resembled that observed in lyotropes, suggesting that, although the details were not understood, the bands were characteristic of oriented LCPs in general.

The presence of banded structures in sheared specimens was attributed by Zachariades [33] to the ordering of the macroscopic domains. These structures arose if the material was heated to 265-295°C and then sheared while cooled to 200°C. Bands were only present in thin sections of the specimens, which also gave better mechanical properties. The banded texture has recently been attributed to the twisting of molecules about the chain axis with the period of the bands [26]. This interpretation alludes to the presence of an out-of-plane component of molecular orientation. Specifically, twisting of the plane of the phenyl rings may occur.

These findings further support the view that the molecular axis cannot be taken as synonymous with the local optical director. The anomaly that led to this proposition was reported by Viney et al. [27]. They

noticed that although WAXS diffraction patterns showed a pronounced uniaxial orientation, optical patterns of two thermotropes showed no preferred orientation when observed between crossed polars. This contradictory observation led them to the conclusion that either the optical indicatrix was not uniaxial or that its unique axis was not aligned with the local chain axis, or both. Either way, the implication was that a rotational correlation about the long axes of adjacent molecules exists.

Even if the structure of thermotropic LCPs is explained satisfactorily from optical microscopy, permitting one to grasp fundamentally what is occurring, its limitations from an applications perspective become apparent when one tries to correlate mechanical properties on this basis. The materials approach in analyzing the structure of LCPs through property correlation schemes such as composite theory, may, on the other hand, be more helpful in correlating and explaining observed properties. The next section will take this approach in contrast to the molecular interpretation of optical textures of this section.

2.4 The Structure of Thermotropic Copolyesters

The materials approach in analyzing the structure of LCPs through property correlation schemes such as composite theory will be examined in this section in terms of some recent literature on the subject. In this regard, Ide and Chung considered thermotropic polymer sheets as macromolecular composites [35]. Tsai and Hill have developed a failure theory for anisotropic materials [36]. According to them, the tensile strength of a unidirectional sheet with reinforcing fiber obeys the relationship:

$$1/\sigma^2(\Theta) = X^{-2}\cos^4\Theta + Y^{-2}\sin^4\Theta + (S^{-2}-X^{-2})\sin^2\Theta\cos^2\Theta \qquad (2.4\text{-}1)$$

where $\sigma(\Theta)$ is the tensile strength at an angle Θ from the flow direction; X is $\sigma(0)$, Y is $\sigma(\pi/2)$, and S is the shear strength. Lees simplified a similar equation for the angular dependence of the tensile modulus [37]:

$$E(\Theta) = E_1E_2/[E_1-(E_1-E_2)\cos4\Theta] \qquad (2.4\text{-}2)$$

where E_1 and E_2 are the Young's moduli in the flow and transverse directions, respectively. Ide and Chung reported excellent agreement of both σ and E with the equations, as shown in Fig. 2.12 and Fig. 2.13. These results suggest that highly oriented liquid crystal domains may be thought of as reinforcing fibers in the extruded articles, and their mechanical properties are

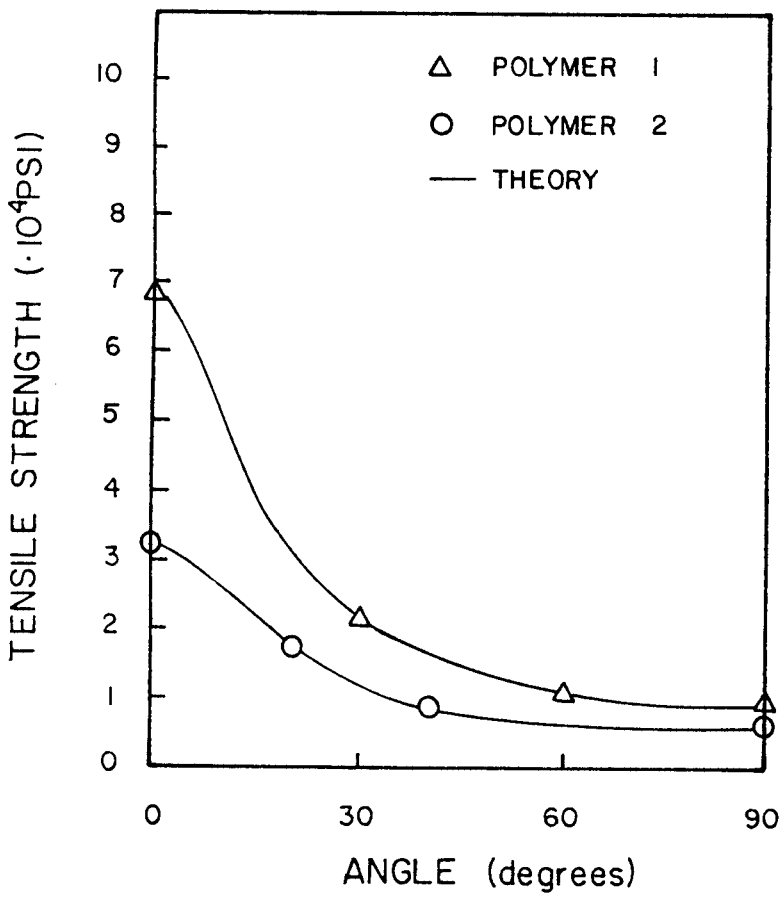

Figure 2.12 Angular dependence of tensile strength for extruded sheets [35].

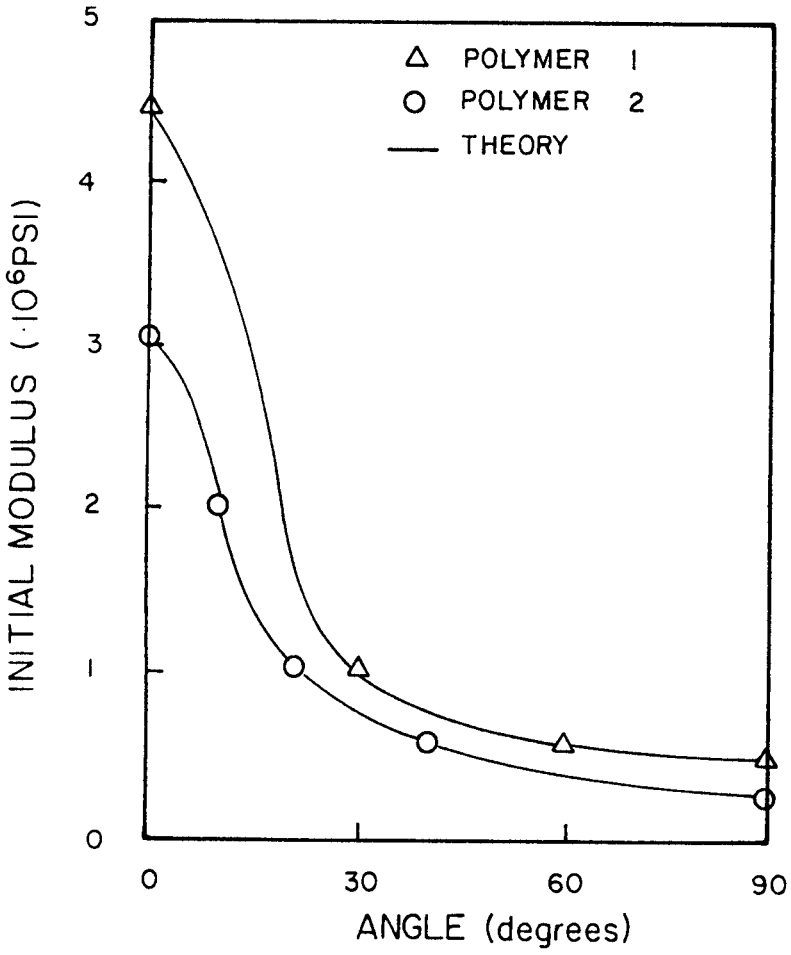

Figure 2.13 Angular dependence of Young's modulus for extruded sheets [35].

then predictable from existing composite theories. Although this theory sounds reasonable, more thermotropic systems need to be studied in this regard.

The structure of thermotropic copolyesters containing naphthalene rings was recently reported on by Sawyer and Jaffe [38]. Extensive characterization (SEM, TEM, optical microscopy, among others) of these materials resulted in the deliniation of a fibrillar, hierarchical structural model to account for the morphology seen in a broad range of fibers, extrudates, and molded articles. Three distinct fibrillar species, shown in Fig. 2.14 as an artists perception were identified: microfibrils of about 50 nm diameter, fibrils of about 500 nm diameter, and macrofibrils of about 50 μm diameter. Orientational variations, layering, and skin/core structures were viewed as the effect of local flow fields on the basic structural units during the deformation process. They did, however, fail to recognize the importance of thermal history on the resultant structure.

The authors have observed the same basic hierarchy for both lyotropic and thermotropic systems. The microfibrillar structure of all highly oriented polymers, including polyethylene, appeared similar to them. They speculated that once the orientational distribution in the layers of processed articles is elucidated, mechanical properties may be better understood in terms of composite

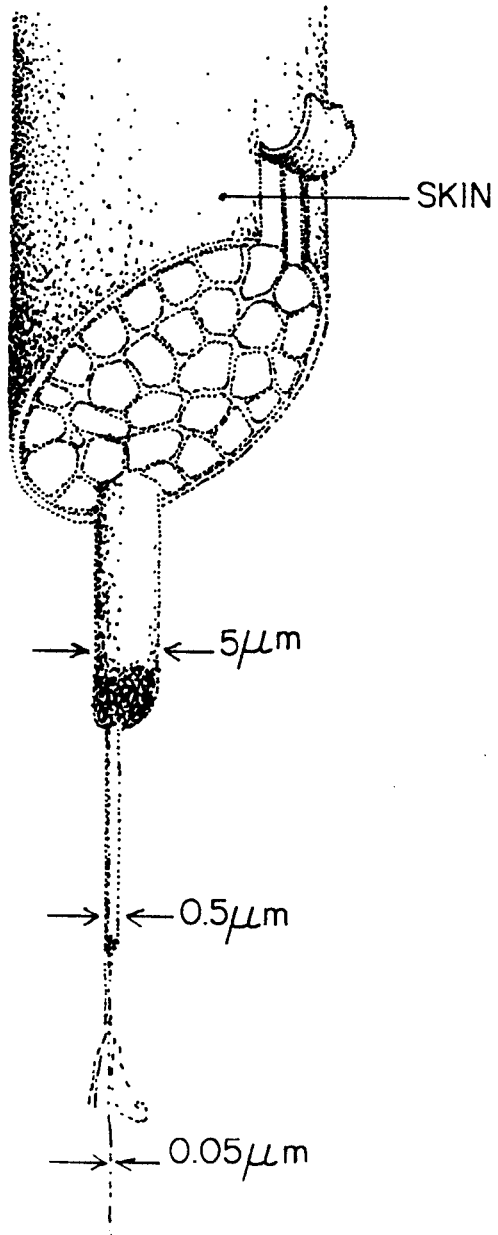

Figure 2.14 The LCP structural model shows the hierarchical fibrillar texture of the materials in an artist's perception [35].

theory. They neglected do discuss, though, how one gets to these properties.

Having discussed the orientation and properties in thermotropes in general, the focus will now center on the copolyesters being studied in the present work. The thermal and flow properties of both materials studied will be examined in some detail in the next section to provide a framework for processing these materials.

2.5 Thermal and Flow Properties of HBA/PET and HBA/HNA

Thermal transitions, frequently measured by differential scanning calorimetry (DSC), vary so widely in the literature for these materials due to their small magnitude, different scan rates, processing histories, and possibly molecular weight variations, that they will not be considered in this review. Annealing of both systems results in sharper first order transitions in comparison with the virgin sample [39]. Annealing of some thermotropic polymers may drastically improve the physical properties [40], particularly stress at break. For the HBA/PET system, however, no such improvement has been seen, even after 5 days of heat treatment [10]. For HBA/HNA, WAXS showed an amorphous material if quenched and some crystallinity upon subsequent annealing. DSC thermograms, however, did not change appreciably. Blundell concluded that microcrystals may develop on annealing that are too small to be seen by x-rays [41].

A review of the rheology of thermotropic systems is beyond the scope of the present survey. Several such articles have been published over the past decade [23, 42-44,76]. Some intriguing flow properties of both copolyesters being studied do, however, give direction to the processing possibilities which exist, and thus will be discussed in this section.

Done and Baird [45] have studied the effect of thermal history on the rheological properties of 60% and 80% HBA/PET and an NTP ("LCP 2000"). In particular, the possibility of deforming them below their normal melting points was examined. In Fig. 2.15 the complex viscosity is shown for two different thermal histories for the 60% HBA/PET copolyester. The viscosity was significantly reduced at 240°C if the material was cooled from 275°C prior to shearing. These data were taken in the range of 0.1 to 100 Hz. Time sweeps at 275°C showed no decrease in viscosity over twenty minutes, suggesting that the decrease in rheological properties was not due to degradation, but perhaps a supercooling of the nematic state. Crystallinity changes on heating to 275°C were not discussed, but may be of some importance.

In order to determine whether the solidification point could be observed, the samples were cooled while the small strain dynamic properties were measured. The data obtained are shown in Fig. 2.16. The G' values for 60% HBA/PET and 80% HBA/PET remained unchanged down to 200°C and 270°C, respectively. These nearly constant values of G' were obtained over a time span of 4 to 5 minutes and occurred 20-40° below the materials' normal flow temperatures.

By monitoring the value of G' as a function of time for these LCPs below their melting points, the authors

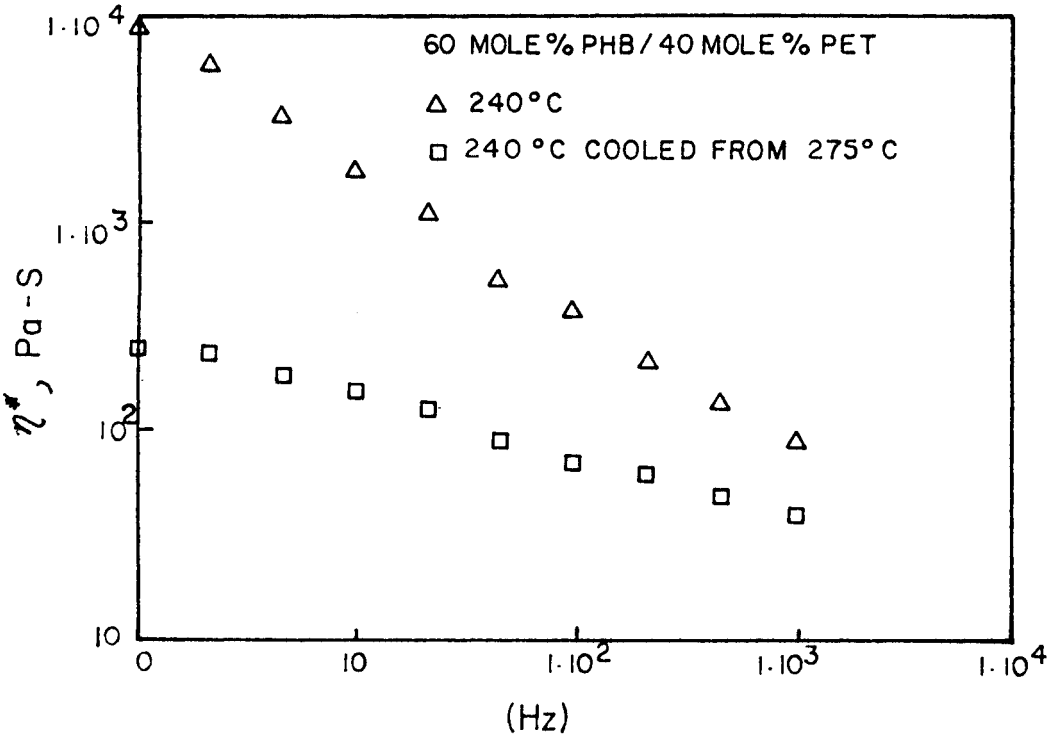

Figure 2.15 Dynamic viscosity vs. frequency for 60 HBA/PET with different thermal histories [45].

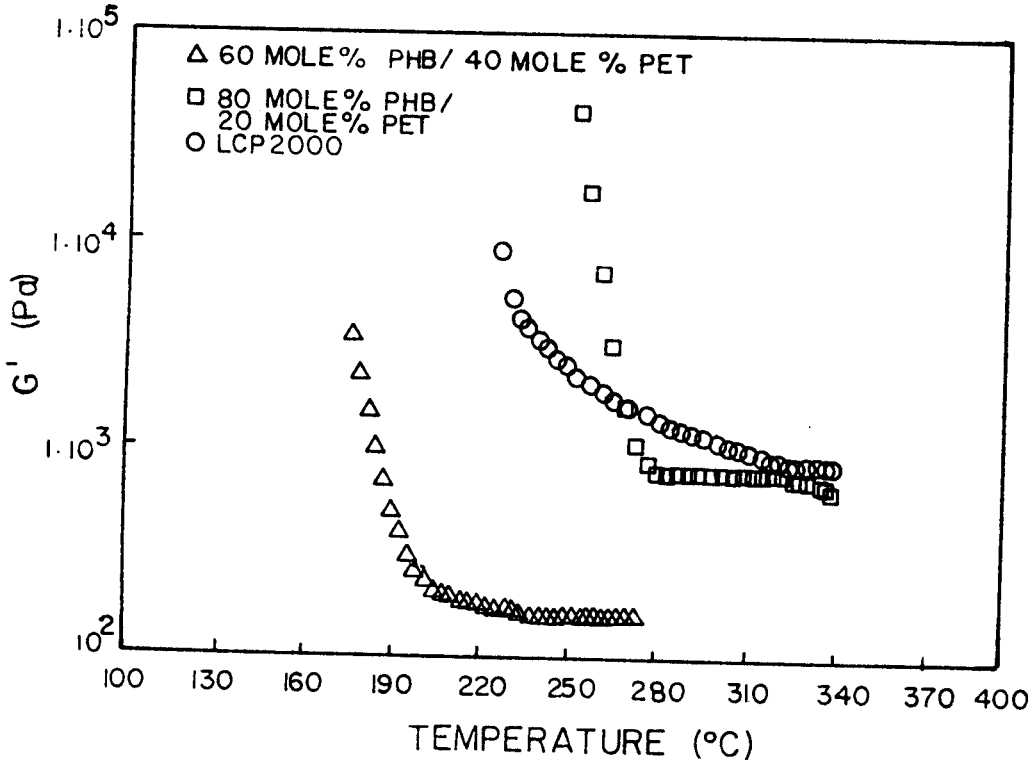

Figure 2.16 G' vs. temperature during cooling from the melt state at a strain of 5% [45].

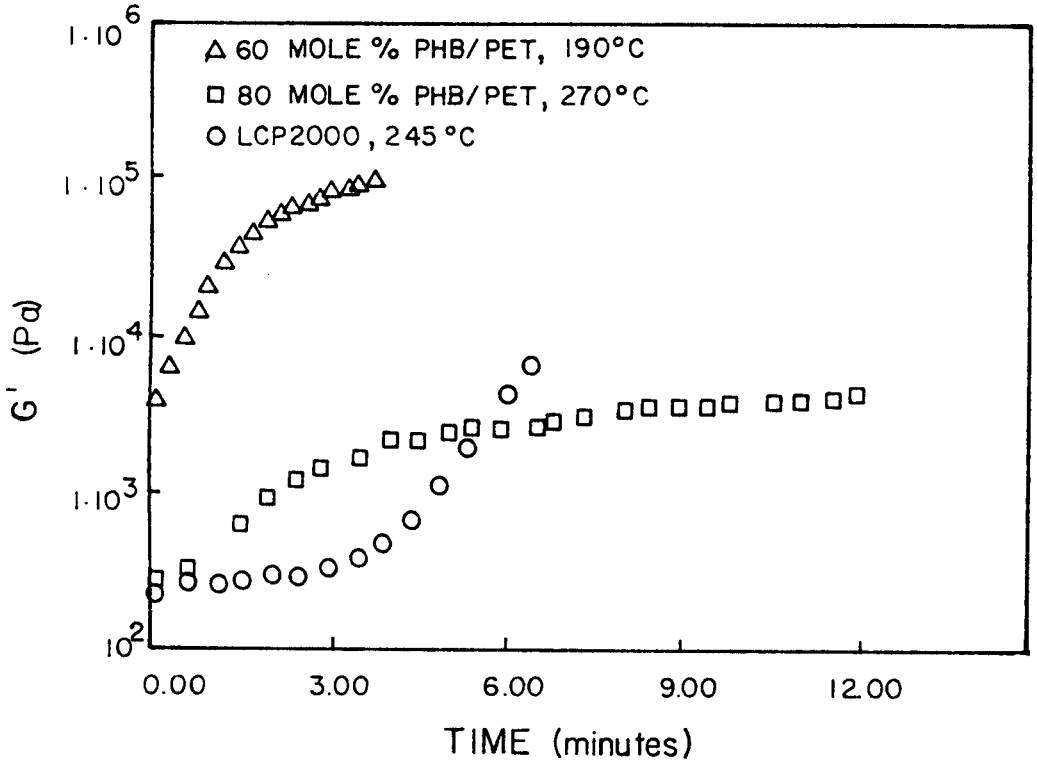

Figure 2.17 G' as a function of time at temperatures below their flow temperature at 0.1 sec-1; samples were preheated above the melt temperatures [45].

obtained the results in Fig. 2.17 showing that a true equilibrium state was not present. However, the kinetics of the rate of solidifaication are slow, requiring several minutes before the modulus reaches values beyond which deformation is difficult. The fact that the recovery of the solid phase occurred so slowly indicates that there may be another mechanism besides transesterification responsible for the super-cooling [46]. The higher elasticity of the super-cooled state as indicated by the increase in G' also promised some processing advantages such as increased melt strength relative to the "normal" melt state.

Recent work in processing thermotropic liquid crystalline polymers has been reviewed. One process that permits some control of the deformation is film blowing. By varying the blow up and draw, the kinematics will vary, and the resultant properties and structure of the polymer will thus change. Because this process permits a range of deformation histories and holds possibilities relative to the processing of thermotropic LCPs, it will now be reviewed. First, the theoretical development is presented, followed by experimental and numerical considerations.

2.6 Film Blowing: Theoretical Development

Various researchers over the past two decades have tackled the problem of free film blowing from a theoretical perspective [47-53]. The governing equations of continuity, energy, and momentum have been developed in the literature to the point that the greatest difficulty lies in the implementation of an appropriate numerical scheme with corresponding boundary conditions to solve the analytically intractable equations. This section will develop logically the governing equations, noting any assumptions made, for the general case and for the specific simplifications of isothermal Newtonian flow and a non-isothermal power law approximation. The choice of a constitutive equation may often severely complicate the resulting system since the material parameters for many materials of current interest are not known.

Pearson and Petrie [47] have developed a mathematical model for Newtonian isothermal flow between the annular die exit and the freeze line. Three other major assumptions, common to all development in the area, are axisymmetry, homogeneity, and a thin film. In addition, they also limited that early work by ignoring gravity, surface tension, air drag, and inertia. (Of these forces, gravity in particular should not be ignored). Pearson and Gutteridge [48] have extended that work to include non-

isothermal effects and have employed Funt's elastic model, applicable to their solid phase blowing of polypropylene. Petrie has also compared a non-isothermal Newtonian and isothermal Maxwell model to experiments, including gravity and inertia terms. Han and Park [51,52] have attempted to determine elongational viscosity with a blown film apparatus. They derived the elongational viscosities from theory primarily following Pearson and Petrie. They also extended Petrie's work to non-isothermal power law fluids. Both gravity and temperature dependence of the physical properties were accounted for (although the former incorrectly). Lastly, Pearson has reviewed film blowing in his recent text, perhaps the most concise treatment to date [54]. It is from this last reference that the following developments are in large part abstracted.

Film blowing is a method for economically producing thin sheets of thermoplastics with biaxial properties and cylindrical geometry by simultaneously stretching and inflating a moving tube of polymer melt extruded through an annular die. The blowing bubble of molten polymer is cooled while this process is occurring and crystallizes or vitrifies at a frost line beyond which no further deformation takes place (see Fig. 2.18).

The prime goal in blowing film is usually to maintain a uniform sheet thickness, and therefore axisymmetry and a

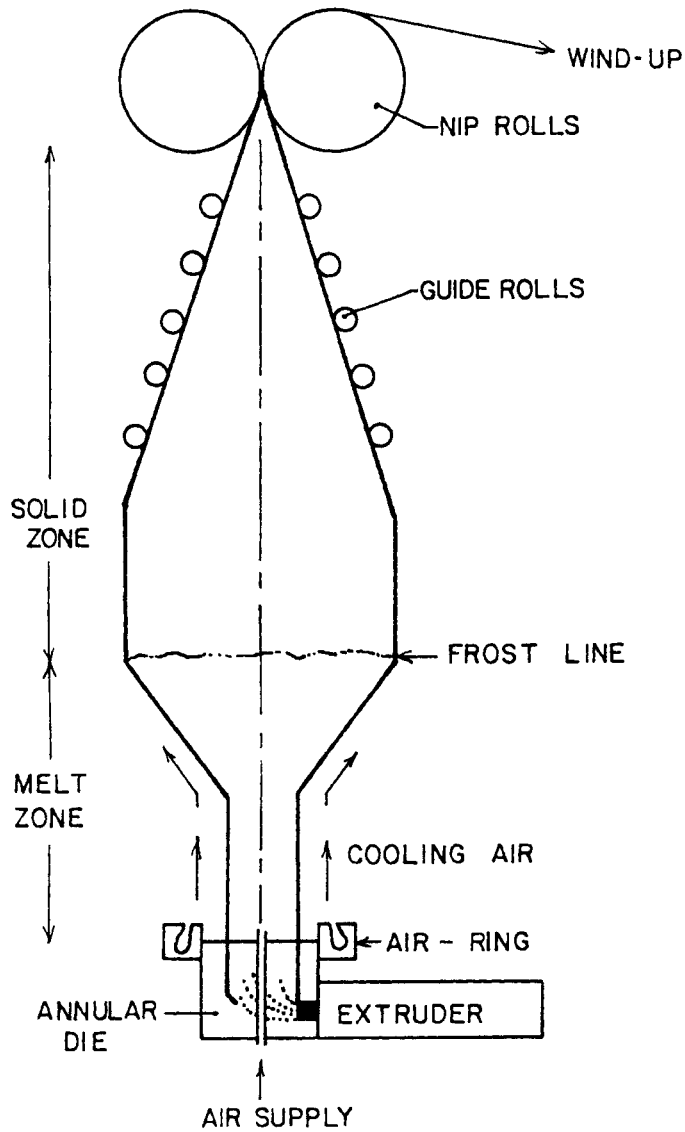

Figure 2.18 General view of melt film-blowing process [54].

steady flow in the molten portion of the bubble are assumed. The final film thickness is given by

$$h_f = h0/(Bu*Dr) \qquad (2.6\text{-}0)$$

for the assumption of constant density where h_0 is the die gap, usually 1-2 mm, Bu is the blow ratio, usually from 1.5 to 3, and Dr is the draw ratio, typically in the range of 5 to 15. The film thickness will thus be on the order of 50 μm, and hence is everywhere small compared to the bubble dimensions, justifying the flat sheet approximation. The film is usually assumed to be of uniform temperature throughout its thickness since for a flight time of 10 seconds in a molten section which cools 75 K, the Fourier number will be on the order unity for most conventional polymers [54].

General formulation of the governing equations must be founded on a careful consideration of the geometry of the moving surface. Far easier, avoiding complex co- and contra-variant tensors in two and three dimensions, is to use special coordinate systems that exploit any symmetries inherent in the problem. The simplest representation of this problem is the circular cylindrical coordinate system (r, φ, z) shown in Fig. 2.19. The z axis is the machine direction, frequently vertically upward. The position of the inner surface of the bubble is given by

$$r = a(\varphi,z,t).$$

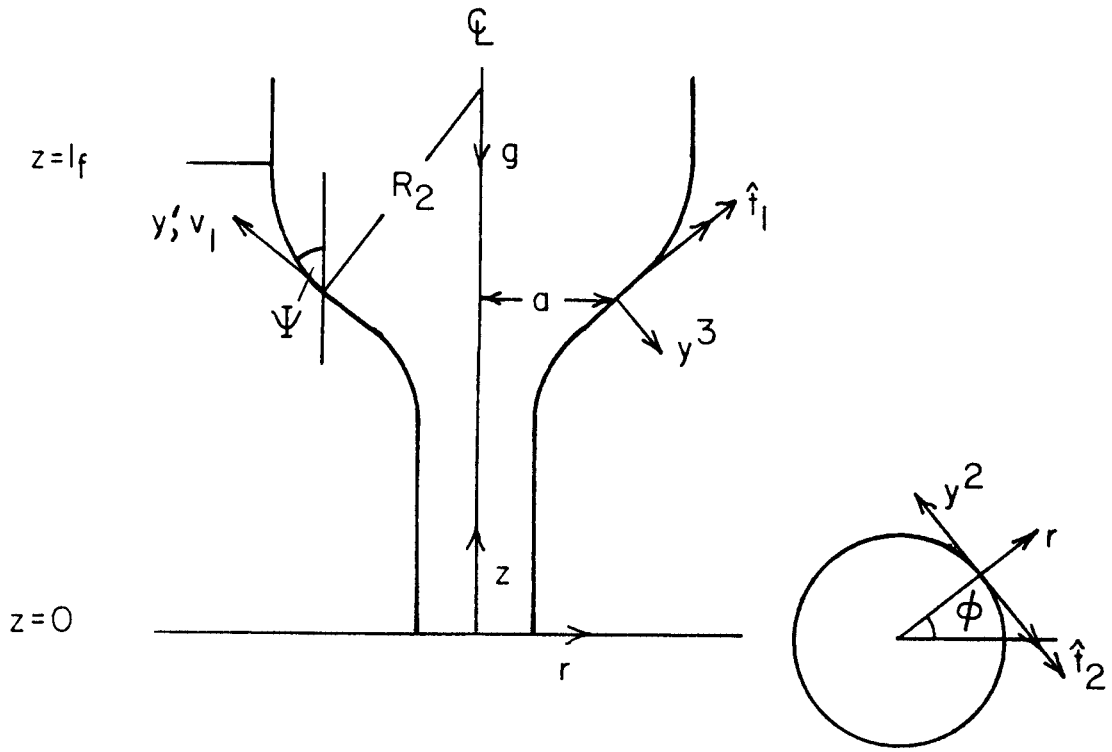

Figure 2.19 Coordinate systems: (r,φ,z) based on centerline axis of process; (y1,y2,y3) based on local tangent plane to blowing sheet [54].

For steady, axisymmetric flow, r becomes a function of z only. A local Cartesian coordinate system ($y1$, $y2$) may be described by the local values of (z,φ), orthogonality existing when a is not a function of φ. In this case, the physical component representation

$$\mathbf{v}(z,t) = (v_1, v_2, v_3)$$

for the velocity in the (y1,y2,y3)-directions, with y3 normal to the surface, can be used; $v_2 = 0$ unless the die is rotating, and $v_3 = 0$ for steady flow. The metric tensor is given for the (y1,y2) system by

$$\begin{bmatrix} g_{11} & 0 \\ 0 & g_{22} \end{bmatrix} = \begin{bmatrix} 1+(da/dz)^2 & 0 \\ 0 & a^2 \end{bmatrix}$$

where $ds^2 = g_{11}(dy1)^2 + g_{22}(dy2)^2$ is the square of a differential line element along the surface (dy1,dy2). Inertial forces are generally negligible, Re being on the order of 10-2 or less. Surface tension forces, which are the order of the inverse of the capillary number times as large as viscous forces, can likewise be shown to be negligible [54]. Gravity may be significant depending on the choices of length, viscosity, and velocity and have been included in the analysis. This treatment has the effect of including body force terms in the mechanical force balance equations:

$$\nabla_{surf} \cdot T + Ft = 0 \qquad (2.6\text{-}1)$$

$$\hat{t}_{1/R1} = \hat{t}_{2/R2} = \Delta p + Fn \qquad (2.6\text{-}2)$$

where F_t is the tangential force vector, Fn is the normal component, and Δp is the air pressure difference across the film. R_1 and R_2 are the principal radii of curvature:

$$R_1 = -1/(\cos\psi d\psi/dz) \text{ and } R_2 = a/\cos\psi$$

where ψ is the angle between the y1 and z axes and

$$\tan\psi = da/dz \qquad (2.6\text{-}3)$$

The mass conservation equation is simply:

$$2\pi\rho v_1 \, ah = M \qquad (2.6\text{-}4)$$

where M is the constant mass flow rate. For MD vertically upward, an axial force balance yields:

$$2\pi a\hat{t}_1\cos\psi - \pi a^2\Delta p = F(lf) \qquad (2.6\text{-}5)$$

where $df/dz = 2\pi\rho gah/\cos\psi$. $F(l_f)$ is the net axial force on the nip rolls. Equation 2.6-5 thus replaces 2.6-1 and 2.6-2 becomes:

$$\Delta p + \rho gh \sin\psi = \hat{t}_2 \cos\psi/a - \hat{t}_1 \cos\psi d\psi/dz \qquad (2.6\text{-}6)$$

Completion of the model requires knowledge of the temperature of the film as a function of z so that the rheological and physical properties can be correctly incorporated into the computations. The knowledge of the position of the freeze line is crucial, for the boundary conditions involve assumptions about the freeze line as well as the die exit region. The energy equation may be written [55]:

$$\dot{M}\, d(\gamma T)/dz = -\{h(T-T_c) + \epsilon\sigma(T4-T_a4)\} * 2\pi r/\cos\psi \quad (2.6\text{-}7)$$

where T(z) is the film temperature, γ is the specific heat, T_c is the temperature of the cooling air, h is the heat transfer coefficient, ϵ is the emissivity of the molten polymer, σ is the Stephan-Boltzmann constant, and T_a is the ambient temperature. In writing this equation, the heat transfer to the interior of the bubble is ignored; the dominant mechanism for cooling the film is the external forced convection, so h must be known or estimated. Radiative cooling may account for up to 20% of the heat transfer, and ϵ is typically taken to be in the range of 0.4 to 0.6. Freeze line height will be that value of z at which the film temperature reaches the point where solidification takes place. This might occur significantly below the actual melting point of the material, so care must be used in its estimation.

The unknown principal stresses

$$t_{11} = \hat{t}_1 / h \text{ and } t_{22} = \hat{t}_2 / h$$

will be given by the constitutive equation in terms of the histories of the principal strains

$$e_1 = v_1/v_1(0);\ e_2 = a/a_0;\ e_3 = h/h_0 \qquad (2.6\text{-}8)$$

(or by the rates of strain) where the e_i are the elements of the Finger tensor. As expected from equation 2.6-3, it follows that for constnat density

$$e_1e_2e_3 = \text{constant} \qquad (2.6\text{-}9)$$

The boundary conditions on the flow field also need to be considered. The inlet to the bubble flow is taken to be at, or very near, the exit of the die, z=0, where

$$a = \tfrac{1}{2}d_0,\ h = h_0,\ T = T_0, \text{ and } v_1 = v_{10}. \qquad (2.6\text{-}10)$$

Shear deformation will cease at the frost line, as yet unspecified, which is the exit from the bubble flow. The in-line velocity is usually specified at this point, neglecting shrinkage farther on:

$$v_1(l_f) = v_{1f} = Dr*v_{10} \qquad (2.6\text{-}11)$$

while

$$da/dz = \tan\psi(l_f) = 0 \qquad (2.6\text{-}12)$$

For commercial processes, $a(l_f) = a_0Bu$ will be specified. Thus, inlet and outlet requirements on the bubble flow specify eight boundary conditions if the freeze line temperature is estimated. These conditions are applied to the five equations, 2.6-3 to 2.6-7; the system is made determinate by suitably choosing $\dot{M}$, l_f, F_f, and Δp. If Δp is specified, Bu will be determined from the solution; if F_f is specified, Dr will be determined from the solution; $\dot{M}$ is effectively given by the product of h_0, a_0, and v_{10}.

Several constitutive equations have been substituted into the governing equations in the literature in order to compute the solutions. The following paragraphs will consider two cases: isothermal Newtonian and non-isothermal power law approximations.

For an isothermal Newtonian fluid [47] with constant density, the rheological equations become:

$$\hat{t}_1 = 2\eta_o(\dot{e}1-\dot{e}3)h; \quad \hat{t}2 = 2\eta_o(\dot{e}2-\dot{e}3)h \qquad (2.5\text{-}13a)$$

or,

$$\hat{t}_1 = 2\eta_o v_1 \cos\psi(2\ dh/dz + h/a\ da/dz)$$
$$\hat{t}_2 = 2\eta_o v_1 \cos\psi(h/a\ da/dz - dh/dz) \qquad (2.6\text{-}13b)$$

using equations 2.6-4 and 2.6-8. Using dimensionless parameters to define the effects of internal air pressure and gravity, v_1 can be eliminated and the problem becomes a two point boundary value problem. One weakness of the

viscous approach is that elastic effects become prominent near the frost line as evidenced by the rheology of the HBA/PET system, for example [45]. Elasticity cannot realistically be ignored under such conditions.

Another approach in the literature is a power law empiricism of the Generalized Newtonian Fluid model incorporating non-isothermal effects. Since the materials can usually be determined for this case, the theoretical predictions, however simplified, can be compared to the experimental results. Han [52] proposed the following semi-empirical expression for the material function:

$$\eta = \eta_0 \exp[E/R(1/T - 1/T_0)] \prod_2^{(n-1)/2} \qquad (2.6\text{-}14)$$

where $\prod_2$ is the second invariant of the rate of deformation tensor, E is the activation energy for elongational flow, R is the gas constant, η_0 is the viscosity at reference temperature T_0, and n is the material constant. Two weaknesses of Han's development were that his selection of l_f appeared unjustified and he did not calculate T(z).

Next, some experimental considerations of the blown film process will be reviewed since the modeling of the process requires relatively complicated analysis of the laboratory results.

2.7 Film Blowing: Experimental Considerations

In this section some practical aspects of film blowing and the experimental results and correlations other researchers have found will be discussed. Farber and Dealy have developed techniques to measure strain and thermal history of the fluid elements between the die and freeze line [56]. A radiation pyrometer was used to measure the temperature of the film. Videos were analyzed to determine rates of extension in the machine and transverse directions. The maximum extensional strain rates in the MD and TD were 0.15 to 0.6 sec-1 for the blowing of polyethylene. Bubble shape, strain history, and thermal history were each determined for a series of mass fluxes and blow ratios, the latter ranging from 1.8 to 3. The authors concluded that, at least for their system with fast relaxation times, the melt rheology did not play an important role in the generation of orientation in the films; more important by far was the change in the morphology near the freeze line.

Petrie [50] compared his theoretical predictions (non-isothermal Newtonian and isothermal elastic) with published experimental results. Bubble shape could be reproduced quite well, falling intermediate between elastic and viscous predictions. Velocity and strain rate predictions were more sensitive to the details of tempera-

ture profile and melt rheology. Although gravity and inertia were included, comparisons of his velocity and strain rate predictions with experiment were only fair. The main lines of improvement Petrie suggested were the modeling of the heat transfer along with a viscoelastic constitutive equation.

As mentioned earlier, Han and Park [51] used film blowing with an isothermal chamber to calculate elongational viscosities of three different thermoplastics: PP, LDPE, and HDPE. One major difficulty they encountered was the fact that elongation rate is not constant over the length of the melt. Also, only unequal biaxial and uniaxial (no Bu) extension was possible. From the practical standpoint, Han and Park found it virtually impossible to control the elongation rate; the draw ratio, v_1/v_0, was much easier to specify.

In order to analyze the experimental results of the blown film process, some constitutive equation is required. The next section will outline one such theory, that of Doi for monodomains of rigid rods.

2.8 Development of Doi's Theory

In this work the temporal evolution of $S_{\alpha\beta}$ will be studied by adapting Doi's theory of nematic solutions. The theory as has been presented in the literature will now be outlined. As it is not the intent of this review to present a detailed derivation of Masao Doi's theory, only a cursory development with the major assumptions and results will be presented. For a more detailed development, one should consult Doi [59,60].

Doi's theory for the dynamics of rod-like polymers in concentrated (anisotropic) solutions is an extension of Doi and Edwards' theory [61,62] which predicts the dynamics of an isotropic phase of rigid rods of length L and diameter d. Nonlinear viscoelasticity of both the isotropic and nematic phases, as well as the phenomonological coefficients from molecular parameters are determined by the theory. An important limitation of the theory, however, is that it fails to consider spatially variant systems; that is, the director is independent of location in an homogeneous flow field.

Choosing one rod in the solution, let u be a unit vector parallel to it, and f(u,t) be its distribution function. In very dilute solutions ($c<<L^{-3}$) the rotational motion of the rods is independent and can be described by the theory of Kirkwood and Auer [63]:

$$\partial f/\partial t = D_{r0}\,\nabla u\cdot\nabla u f + \nabla u\cdot \dot{u} f \qquad (2.8\text{-}1)$$

where $D_{r0} = kT\ln(L/d)(3\pi\mu_s L^3)^{-1}$, μ_s is the solvent viscosity, ∇u is the gradient operator on the surface of an arbitrary sphere $|u|=1$ through which rods diffuse, and $\dot{u}$ is the rate of change of u due to macroscopic flow:

$$\dot{u} = \kappa\cdot u - (u\cdot\kappa\cdot u)u \qquad (2.8\text{-}2)$$

where κ is the velocity gradient tensor.

For $c>>L^{-3}$ the rotational motion of the rods becomes restricted by other rods; consequently, D_r becomes quite small. If one views the rod as being confined in a tube of radius a, it may change its direction a small amount, $\Delta\Theta$, if it escaped the tube by a translational motion. For Θ small, $\sin\Theta \approx \Theta$, and $\Delta\Theta \approx a/L$. Since a rod will repeat this process D_{r0} times in unit time, the rotational diffusion coefficient may be expressed as:

$$D_r = D_{r0}(\Delta\Theta)^2 \qquad (2.8\text{-}3)$$

Estimating the tube radius from the distance to its nearest neighbor, Doi and Edwards [62] obtained the value of D_r from D_{r0}, c, L, u, f(u,t), and an undetermined constant, ν :

$$D_r = D_{r0}\nu(cL^3)^{-2}(4/\pi\int d^2u' f(u',t)\sin(u,u'))^{-2} \qquad (2.8\text{-}4)$$

With this modified diffusivity expression, one may use D_r in the kinetic equation:

$$\partial f/\partial t = \nabla u\cdot D_r\nabla u f + \nabla u\cdot \dot{u} f \qquad (2.8\text{-}5)$$

This equation is limited only to the semi-dilute concentration region since the only equilibrium solution is the

isotropic one.

Doi then proceeds to generalize the equation for regions of higher concentration. He employs Onsager's expression for the free energy of a solution based on the packing of rods [64], retaining only the first two terms in an infinite power series; with the constraint that the free energy should be a minimum at equilibrium, he obtains:

$$f(u) - \text{const}\cdot\exp(-V(u)/kT) \qquad (2.8\text{-}6)$$

where $V(u)$ is the mean field potential which acts on the test rod by the surrounding rods:

$$V(u) = 2cdL^2kT \int d^2u' f(u')\sin(u',u) \qquad (2.8\text{-}7)$$

Since the rod will feel the same potential in the presence of Brownian motion, the kinetic equation was generalized by Doi:

$$\partial f/\partial t = \nabla u\cdot D_r(\nabla uf + f/(kT)\nabla uV) + \nabla u\cdot \dot{u}f \qquad (2.8\text{-}8)$$

To simplify this equation, which is only semi-quantitative due to the numerous physical and mathematical approximations made, sin (u,u') may be written in terms of irreducible tensors by employing the properties of spherical harmonics:

$$\sin(u,u') = \pi/4[1-15/16(u_{\alpha u\beta}-\delta\alpha\beta/3)(u\alpha' u\beta'-\delta\alpha\beta/3) + \ldots \qquad (2.8\text{-}9)$$

By neglecting tensors of fourth rank and higher, Doi obtained

$$V(u) = -3/2CkT(u_{\alpha u\beta}-\delta\alpha\beta/3)S\alpha\beta(t) \qquad (2.8\text{-}10)$$

where $C = \text{const} \cdot cdL^2$ and

$$S_{\alpha\beta}(t) = \int d^2u f(u,t)(u_\alpha u_\beta - \delta_{\alpha\beta}/3) \qquad (2.8\text{-}11)$$

is the orientational order parameter tensor. This potential is that used by Maier and Saupe in their theory of the phase transition of thermotropic liquid crystals [65].

Doi obtained the stress tensor by considering a hypothetical small deformation. After some mathematics, he obtained the stress tensor using the Maier-Saupe potential:

$$\sigma_{\alpha\beta} = 3ckT\{S_{\alpha\beta} - C[S_{\alpha\mu}(S_{\beta\mu}+\delta_{\beta\mu}/3) - \langle u_\alpha u_\beta u_\mu u_\nu \rangle S_{\mu\nu}]\} \qquad (2.8\text{-}12)$$

In this equation, $\boldsymbol{\sigma}$ represents only the deviatoric portion of the stress tensor; its symmetry arises from the fact that the system was assumed uniform and no external field was present (Doi derived $\boldsymbol{\sigma}$ for the presence of a magnetic field in reference [66]). In order to proceed and obtain a closed form for $S_{\alpha\beta}$, the author first manipulated the kinetic equation to obtain $\partial S_{\alpha\beta}/\partial t$ explicitly and then decoupled the term $\langle u_\alpha u_\beta u_\mu u_\nu \rangle$ arbitrarily to obtain:

$$\partial S_{\alpha\beta}/\partial t = F_{\alpha\beta}(\mathbf{S}) + G_{\alpha\beta}(\mathbf{S}) \qquad (2.8\text{-}13)$$

where $\mathbf{S}$ is a traceless symmetric tensor. Here,

$$F_{\alpha\beta}(S) = -6D_r[(1-C/3)S_{\alpha\beta} - C(S_{\alpha\mu}S_{\beta\mu} - S_{\mu\nu}^2\delta_{\alpha\beta}/3) + CS_{\alpha\beta}S_{\mu\nu}^2] \qquad (2.8\text{-}14)$$

and

$$G_{\alpha\beta}(S) = 1/3(\kappa_{\alpha\beta}+\kappa_{\beta\alpha}) + (\kappa_{\alpha\mu}S_{\mu\beta}+\kappa_{\beta\mu}S_{\mu\alpha} - 2/3\delta_{\alpha\beta}\kappa_{\mu\nu}S_{\mu\nu}) - 2\kappa_{\mu\nu}S_{\mu\nu}S_{\alpha\beta} \qquad (2.8\text{-}15)$$

Hence, the equation for the stress tensor becomes

$$\sigma_{\alpha\beta} = 3ckT[S\alpha\beta(1-C/3)-C(S\alpha\mu S\mu\beta-(\delta\alpha\beta/3)S^2\mu\nu)+ CS\alpha\beta S^2\mu\nu] \quad (2.8\text{-}16)$$

Equations 2.8-13 and 2.8-16 are the rheological constitutive equations for the Doi model. One method of solution is to input the velocity field and deformation rate, as well as the parameters C and D_r. One then calculates the components of the orientation order parameter tensor from 2.15, and finally the stress tensor components from 2.16. Such a strategy was followed in the present work, which is the subject of the next chapter. In it the transient predictions of Doi's theory are studied in some detail by following the path of a particle during the deformation.

In Chapter 2 the published work in the literature concerning the orientational behavior of thermotropic liquid crystalline polymers, specifically HBA/PET and HBA/HNA, has been reviewed. Their characterization by DSC, WAXS, SEM, and optical microscopy was discussed. In sections 2.6 and 2.7 the free film blowing problem was reviewed from both a theoretical and experimental perspective. Finally, Doi's theory for nematics was examined in section 2.8.

In Chapter 3 the predictions of Doi's theory in the transient state will be analyzed, and the theory adapted

to thermotropic systems undergoing extensional deformations in order to predict the development of orientation during the process and make comparisons with experimental results. Transient shear flow predictions will also be made, to compare to PPT solution rheology with the RMS. Since the major thrust of this work is to compare the orientational order predictions of Doi with experimental results in extensional deformations, the predictions of S(t) in the next chapter are particularly relevant.

3. PREDICTIONS OF DOI'S THEORY

Masao Doi's theory was summarized at the end of the previous chapter. Although he developed it to account for the rheological behavior of solutions of rigid rods in the nematic state, with some further assumptions and generalizations, it may also be useful to predict the flow behavior of thermotropic systems. It should be noted that some of Doi's recent work has attempted to extend his theory to low molecular weight thermotropes [66].

This chapter is divided into three sections. In the first section the assumptions and simplifications made in applying Doi's theory to polymeric thermotropes are examined. Section 3.2 then gives the predictions of the simplified theory in extensional flows. The final section, 3.3, gives the predictions of Doi's theory for shearing flows.

3.1 Justification

In this chapter predictions of equations 2.8-13 and 2.8-16 for the order parameter tensor components and the components of the deviatoric stress tensor were calculated by employing the IMSL differential equation solver DGEAR. For these polymeric thermotropes, $F_{\alpha\beta}$ was found to be negligible in comparison to the flow term, $G_{\alpha\beta}$ (see Appendix B). The following paragraphs outline these calculations.

The term $F_{\alpha\beta}$ contains, in addition to $S_{\alpha\beta}$, the rotational diffusivity constant, D_r, and the parameter C:

$$C = \nu cdL^2 \qquad (3.1\text{-}1)$$

where c is the concentration of rods, d and L characterize the molecular dimensions of the rods, and ν represents a conglomeration of constants on the order of unity [59]. For these systems, there is no good way to determine the value of ν experimentally, hence the equations' predictions are only semi-quantitative, even given the validity of all the assumptions made. If one knows the Trouton ratio at low deformation rates, though, an equilibrium value of S can be obtained from the theory, and hence a dimensionless concentration can be found. As extensional viscosity data on these systems are virtually nonexistent, another method of estimating C must be found. To solve equation 2.8-16 one can either pick a value of $C > C_{crit}$ to

assess the importance of $F_{\alpha\beta}$ and determine the stress in that manner, or one can choose a value of C to fit experimental results such as shear stress growth. This latter method is shown for the HBA/PET system in Appendix B.

It should be noted that the calculations for c on the 60% HBA/PET system gave a value almost identical to those for lyotropes - 4.0 at 523K (see Appendix B). Despite the general agreement, the approximate nature of the calculations indicated that several values of C should be chosen to gauge the effect of this parameter on the equations.

Since the $F_{\alpha\beta}$ term is a collection of terms all multiplied by D_r, this value needs to be first determined. Although one experimental method to obtain D_r is through a Trouton ratio or zero shear rate viscosity, the paucity of data generally precludes such an option. Particularly for thermotropes, the zero shear rate viscosity may not be possible to determine anyway. Hence a method to calculate D_r will be presented.

The rotational diffusivity constant for dilute solutions was given by Doi as [60]:

$$D_{r0} = 3kT/(\pi L^3 \mu_s)[\ln(L/d)-\delta] \qquad (3.1\text{-}2)$$

where L/d is the length to diameter ratio, $\delta \approx 0.8$, k is Boltzmann's constant, and μ_s is the solvent viscosity. Since one can estimate L and d given the number average molecular weight and molecular information (bond angles, lengths, atomic radii) and the temperature T is known, the

important experimental parameter that must be determined is the shear viscosity of the solvent.

This diffusivity is extended by Doi to account for concentrated solution dynamics and a nematic environment. For example, in Appendix B calculations for the HBA/PET copolyester extruded at a temperature of 250°C show that D_r (for a concentrated isotropic solution) is on the order of 10-3. These estimates ignore the effects of supercooling which occur under realistic processing conditions in which the material is extruded with a die temperature significantly below the DSC endotherm. At these temperatures the time constant for relaxation is orders of magnitude longer than the processing time (see Chapter 2).

The calculations for shear flows in section 3.3 include the F_β term with different values of D_r in order to determine how large the diffusivity needs to be to affect the predictions of the equations. It will be seen that the $F_{\alpha\beta}$ term is not important in shear flow for thermotropic systems. The 1,1 component of $F_{\alpha\beta}$ and $G_{\alpha\beta}$ was calculated (see Appendix B) for uniaxial extension with an extension rate of 1.0 sec^{-1}, which is typical of many processing operations. For all input values of S_{11} except for perfect orientation, in which case the G term vanishes, the flow term G_{11} was at least 250 times larger than F_{11} at a temperature of 250°C and C=4 for the HBA/PET system. In these calculations, D_r was determined from

Doi's equations as outlined in the preceding paragraphs. These results show that for the thermotropes considered here under the given flow fields, only the flow term $G_{\alpha\beta}$ need be considered in predicting the orientation and stress development. However, for the calculations on transient behavior of solutions, the full equations will need to be utilized.

3.2 Extensional Flow Predictions

In this section predictions of the development of both $S_{\alpha\beta}$ and $\sigma_{\alpha\beta}$ on the inception of shearfree flows will be made. The effect of an inhomogeneous flow field will also be evaluated.

By considering only the flow term, $G_{\alpha\beta}$, and following the path of the particle, one obtains the derivative of $S_{\alpha\beta}$ with respect to time equal to a function of the kinematics of the flow field and $S_{\alpha\beta}$ only. This system of first order ordinary differential equations may be solved by choosing various initial values of $S_{\alpha\beta}$ and incrementing over time, thus determining the temporal evolution of the components of the orientation order parameter tensor. For extensional flow, only the terms S_{11}, S_{22}, and S_{33} are present. For a nematic two of these are equal to $-\frac{1}{2}$ of the third as mentioned in section 2.8.

Appendix A contains the source listing of the program for shear and shearfree flows. The kinematics of the deformation and the extension rates are the only inputs to the equations, from which the components of the orientational order parameter tensor S are obtained. If the $F_{\alpha\beta}$ term is retained, in contrast, a dimensionless concentration and diffusivity must also be input. The initial value of the orientational order components must be specified also; the effect of changing this parameter will be

examined closely.

The solution of the differential equation system required the selection of various parameters which were held constant. These parameters are contained in the source listing, but may be summarized as follows:

METH: Gear's method of backward differentiation

MITER: The chord iteration method was used with the Jacobian calculated internally by finite differences.

TOL: The relative error bound was set at 0.0001.

H: The step size of incrementation was 0.00001

The several figures included here summarize the results. In all cases of uniaxial extension, 1 was the stretch direction; for other shearfree flows, the 3-direction was compression. First the uniaxial case will be considered. With no initial orientation (Fig. 3.1) one can see that S_{11}, the component of the orientation parameter tensor in the deformation direction, saturates at its predicted value at approximately 1½ strain units (S.U.) regardless of extension rate, and is shown over four orders of magnitude, from 0.01 to 10.0 sec-1. These saturation values by definition indicate perfect uniaxial alignment in the direction of the deformation axis.

In Fig. 3.2 similar results for S_{22}, the direction perpendicular to the deformation, are shown. This com-

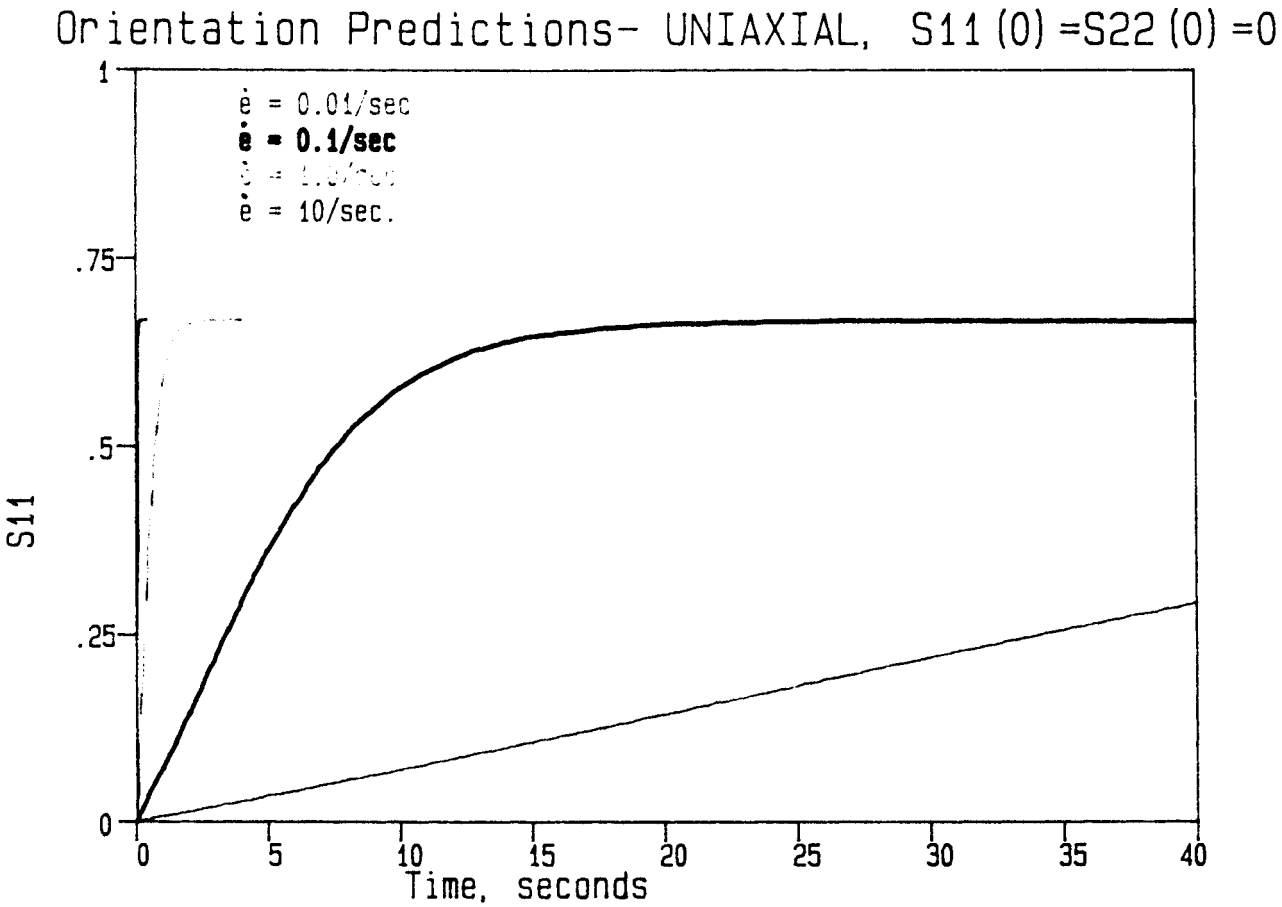

Figure 3.1 Orientation development (S_{11}) for uniaxial extension with $S_{\alpha\beta(0)}=0$ as a function of extension rate.

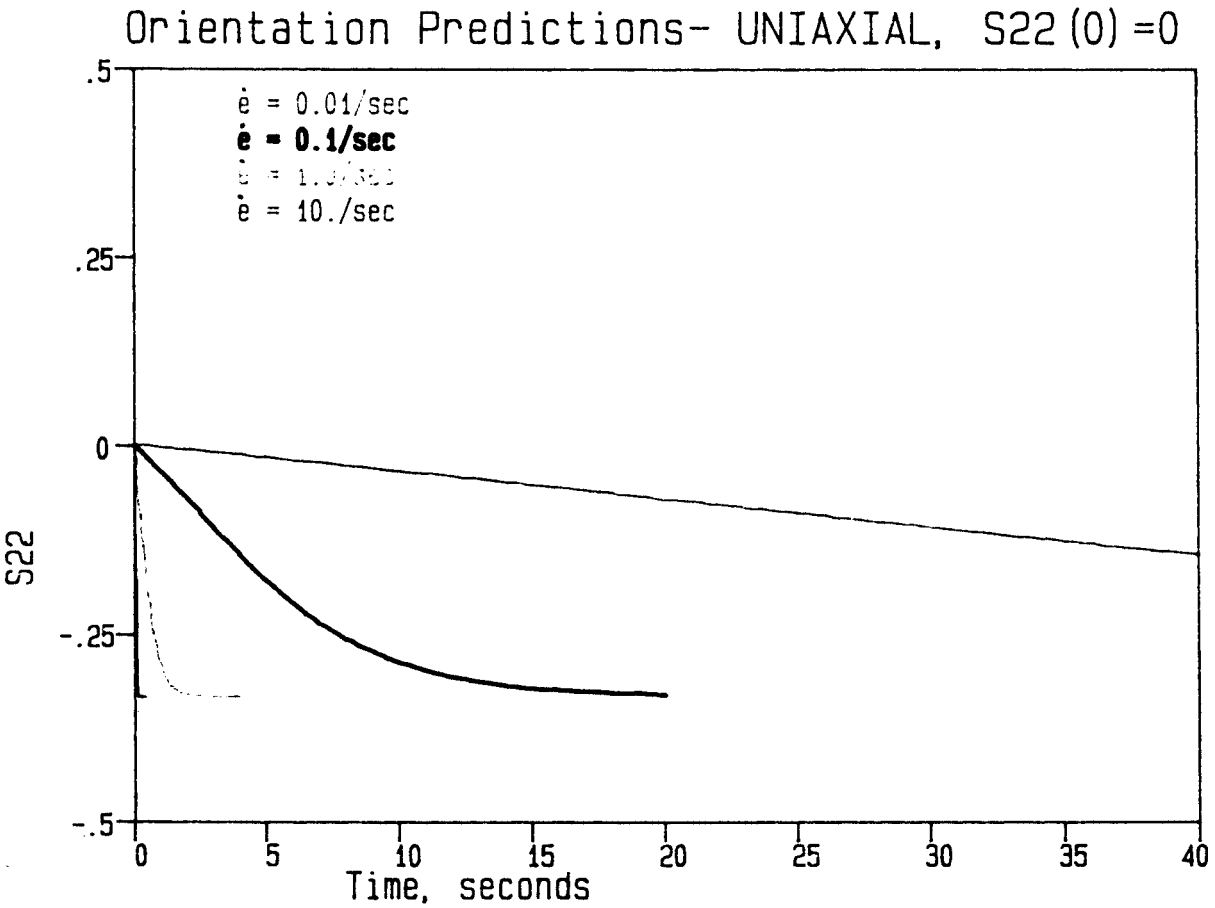

Figure 3.2 Orientation development (S_{22} for uniaxial extension with $S_{\alpha\beta(0)}=0$ as a function of extension rate.

ponent of the orientation parameter tensor saturates at -1/3, representing perpendicular orientation to the 2-direction. Further analyses of Doi's predictions for the uniaxial case were made at a constant extension rate of 1.0 sec-1 for varying initial orientations with the constraint that the order parameter tensor be traceless. In Fig. 3.3 the results for $S_{11(0)}=\{0,1/3,-1/3\}$ are shown. For the extreme of $S_{11(0)}=2/3$, Doi predicts the solution to remain stable at that value as expected. For the perpendicular extreme, $S_{11(0)}=-1/3$, saturation takes about 4 S.U. With an isotropic initial condition, 1½ S.U. are required, and only 1 strain unit is required if $S_{11(0)}=1/3$.

A comment on the assumption of an initial state with no preferential orientation needs to be made. Doi's theory fails to account for the multidomain structure present. It is physically meaningless, however, to start with an isotropic condition unless the material is not in the nematic state. These systems are in fact nematic, although globally they may be isotropic. Therefore, the assumption of no initial orientation is a formalism used to show the behavior of orientation and stresses. (An infinitesimal perturbation in orientation from the isotropic state would result in near identical predictions, although in that case a nematic phase would be defined). Thus, although not physically meaningful, $S_{\alpha\beta(0)}=0$ does

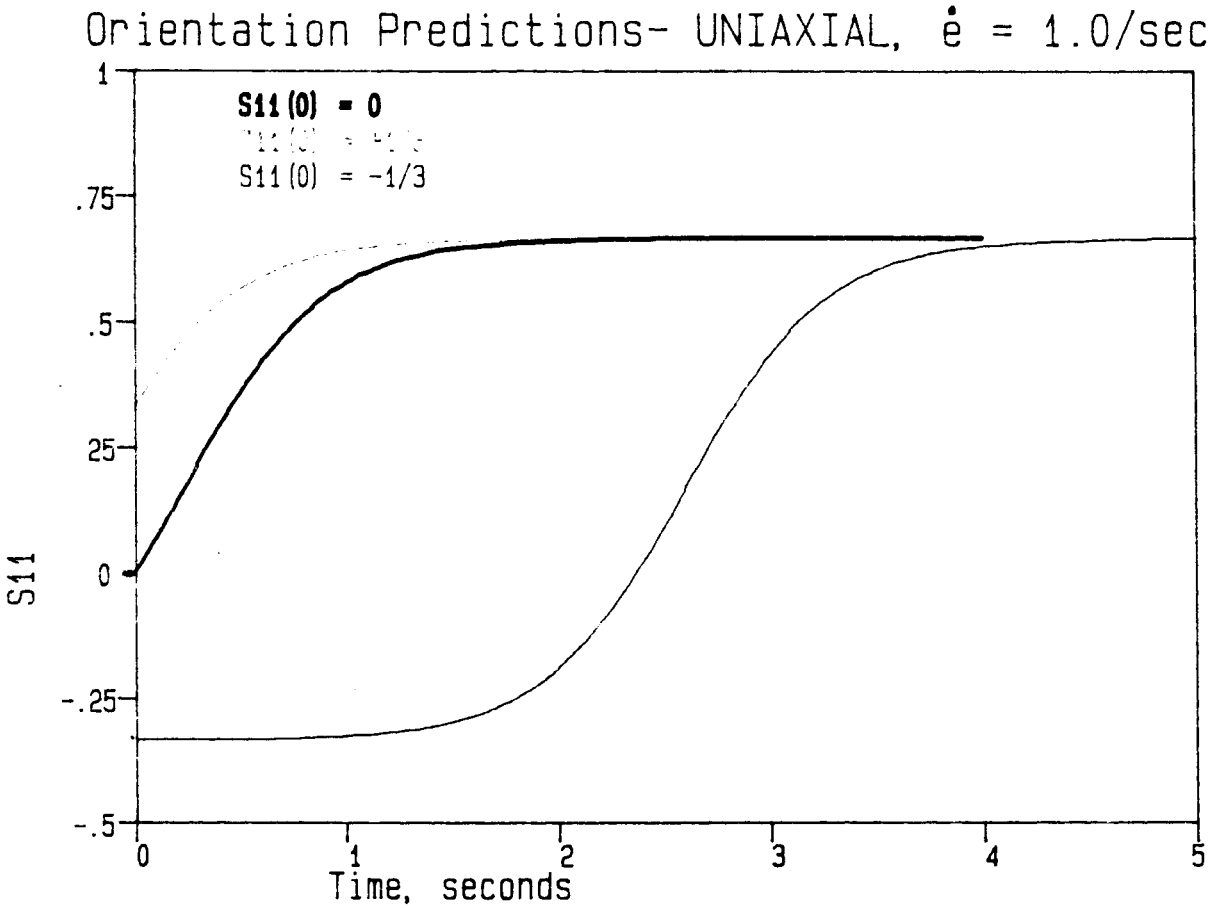

Figure 3.3 Orientation development (S_{11}) for uniaxial extension at 1.0 sec-1 for different $S_{\alpha\beta(0)}=0$

provide a "composite" or average of all orientation, and thus is a convenient way to view the predictions of the equations.

The results for the equal biaxial extension case (extension occurs in the 1- and 2-directions) with no initial preferential orientation and stretch rates of 0.01 to 1.0 sec-1 are summarized in Fig. 3.4. S_{11} saturates in about 7 S.U. at a value of 1/6. The orientation development of S_{11} for equal biaxial flow for different $S_{\alpha\beta}(0)$ is shown in Fig. 3.5. If $S_{11(0)}$ is either 2/3 or -1/3 (the extrema) it is predicted to remain constant; otherwise it will tend to reach a plateau at some value $0<S_{11(\infty)}<2/3$ for $S_{11(0)}>0$. Likewise, for $S11(0)<0$, S11 will saturate at some value approaching -1/3 as $S_{11(0)}$ approaches that value. As can be seen in Fig. 3.6, $S_{22(t)}$ shows corresponding behavior, increasing in all but the extreme case of $S_{22(0)}=-1/3$, more dramatically and to a higher equilibrium value as $S_{22(0)}$ is increased.

Equal biaxial deformation results in unique predictions of orientational behavior, as seen in Fig. 3.7 in which eight different ratios of 1- to 2-direction extension rates, ranging from uniaxial to planar extensional to equal biaxial, are shown. With no initial orientation all other shearfree flows give an ultimate value for S_{11} of 2/3, and the closer they approach uniaxial flow, the quicker they saturate. For equal biaxial deformation,

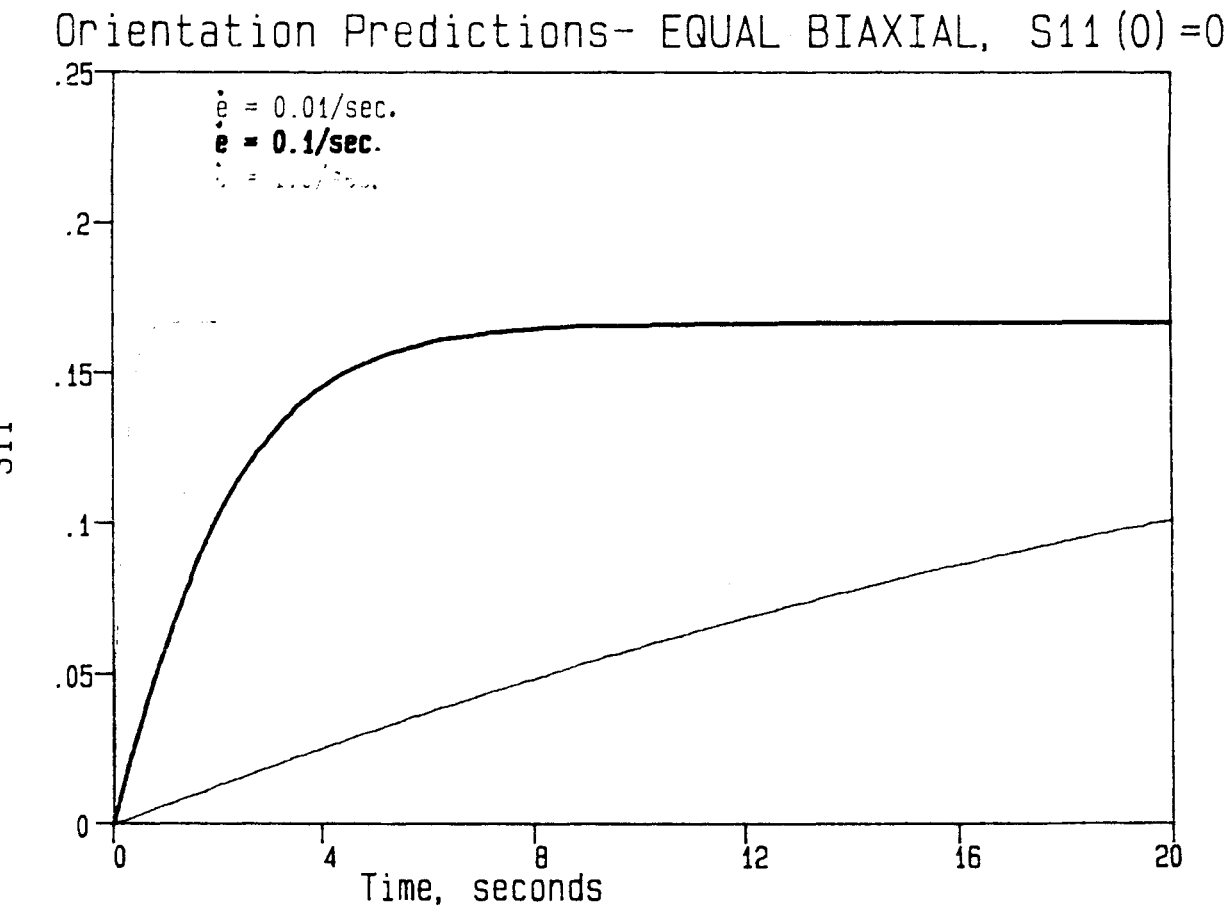

Figure 3.4 Orientation development for equal biaxial extension with $S_{\alpha\beta}(0)=0$ as a function of extension rate (S_{11})

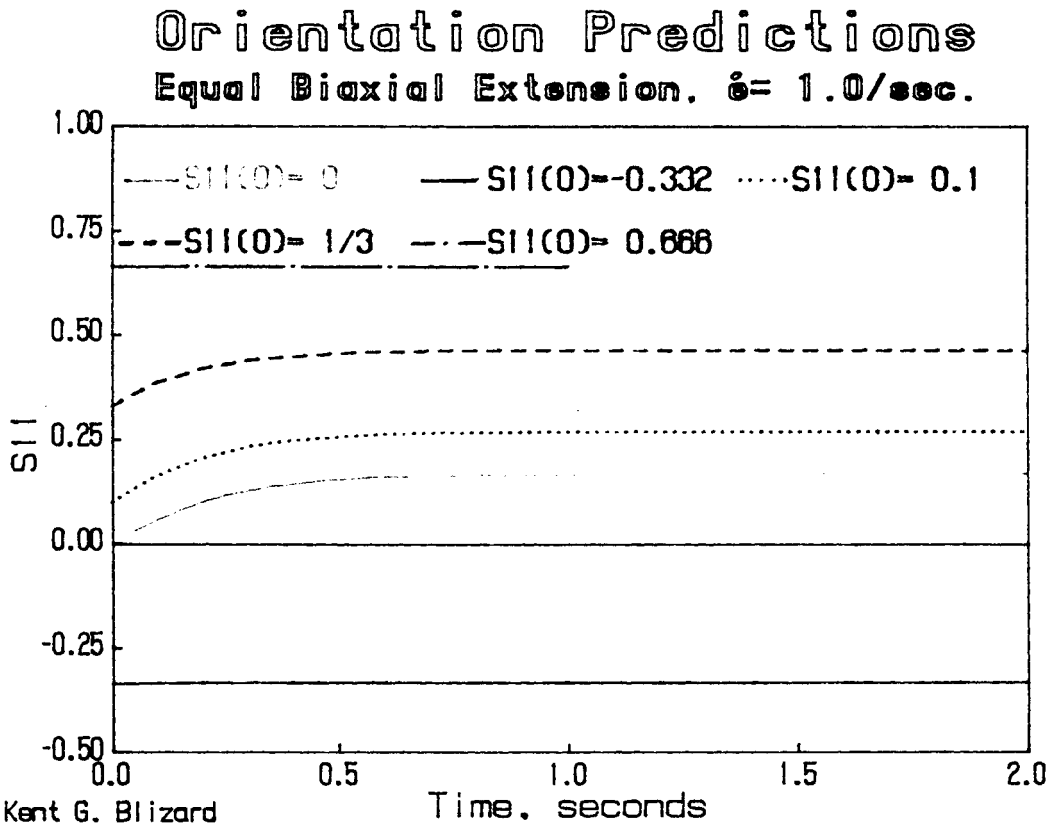

Figure 3.5 Orientation development (S_{11}) for equal biaxial extension at 1.0 sec-1 with different $S_{\alpha\beta}(0)$

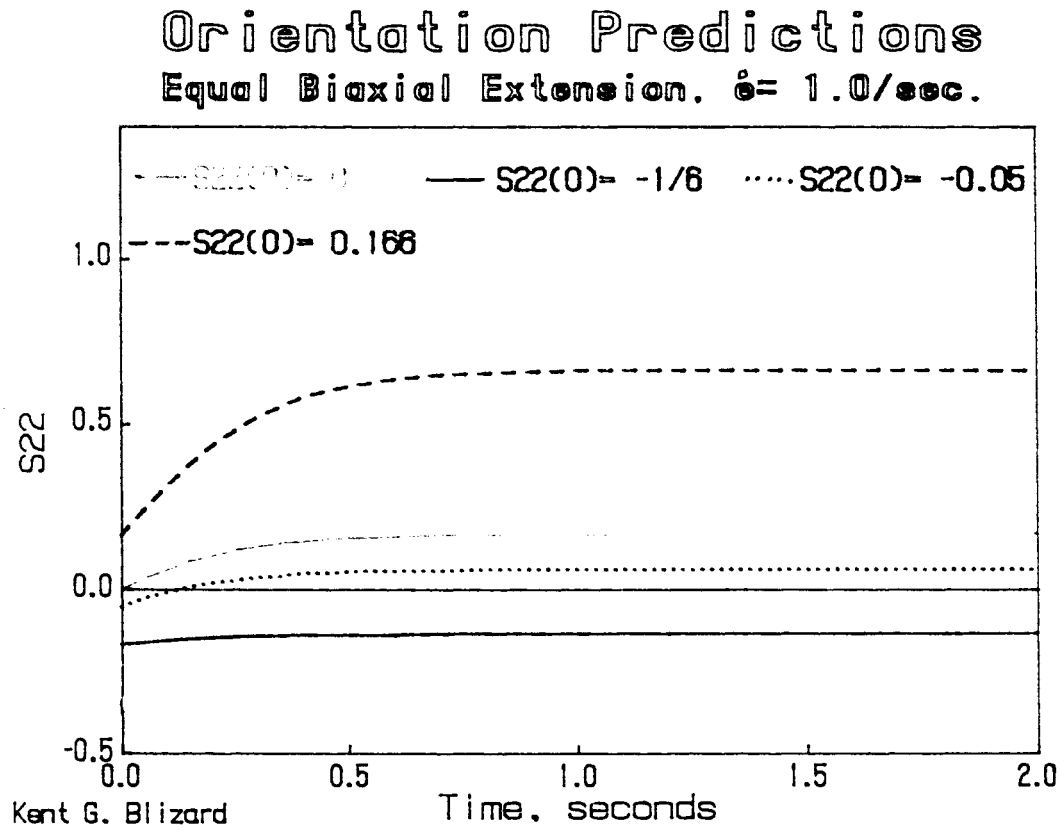

Figure 3.6 Orientation development (S_{22}) for equal biaxial extension at 1.0 sec-1 with different $S_{\alpha\beta(0)}$

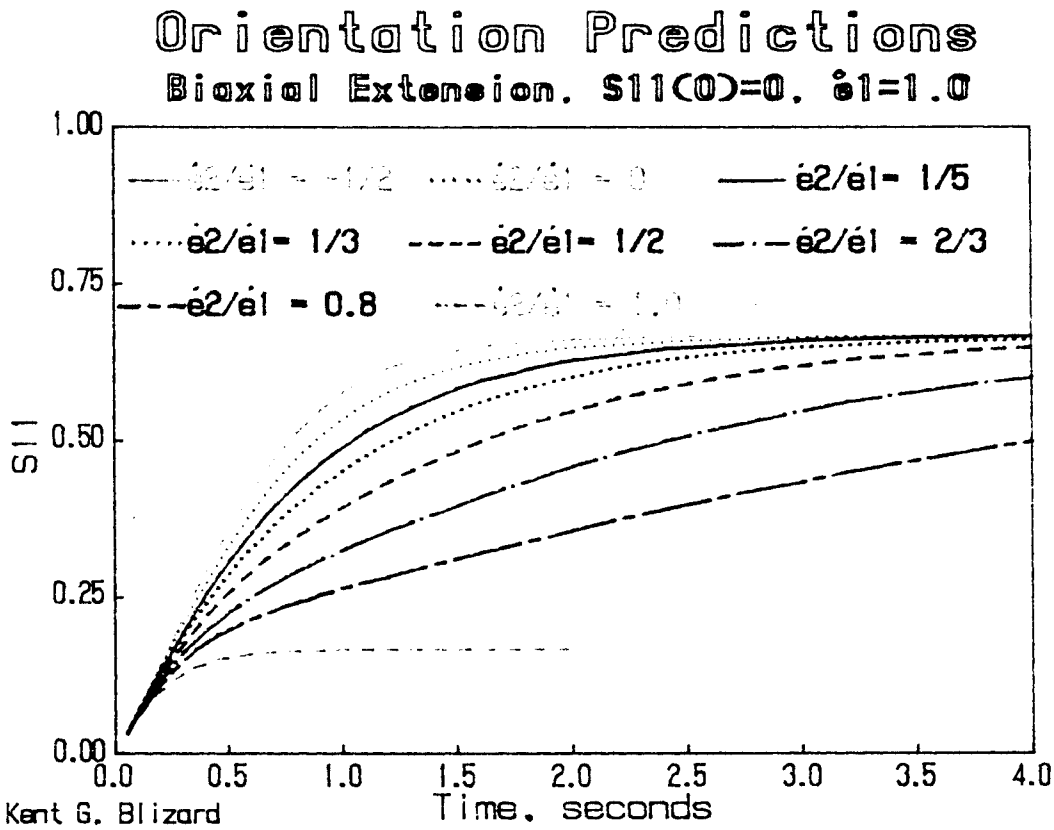

Figure 3.7 Orientation development (S_{11}) for shear-free flows in the 1,2 plane with $S_{\alpha\beta}(0)=0$

however, S_{11} reaches a plateau at 1/6, the same as S_{22}.

In Fig. 3.8 the corresponding behavior of S_{22} is shown. S_{22} approaches -1/3 except for equal biaxial extension, in which case it saturates at 1/6 along with S_{11}. An interesting phenomenon is that if the ratio of extension rates is greater than zero, $S_{22(t)}$ will increase from 0 before decreasing to its equilibrium value; this increase becomes more pronounced the nearer the flow is to equal biaxial extension.

The development of orientation in extensional flows where the extension rate is not constant (inhomogeneous flows) was also determined. The development of S_{11} is shown in Fig. 3.9 when the extension rate may arbitrarily given by the increasing function 2t/(1+t) as well as by a constant value of unity. The overall effect of such an extension is seen to be minor in the case of equal biaxial extension and somewhat more pronounced for uniaxial extension. In both instances the time for saturation of S_{11} increases slightly because the initial extension rate is quite low, but of course the saturation value remains constant as expected.

In Fig. 3.10 the interesting case of an extensional flow in which the transverse rate increases, while the machine direction rate simultaneously decreases to a value less than that of the TD rate, is shown. In this instance the orientation in the machine direction (S_{11}) goes

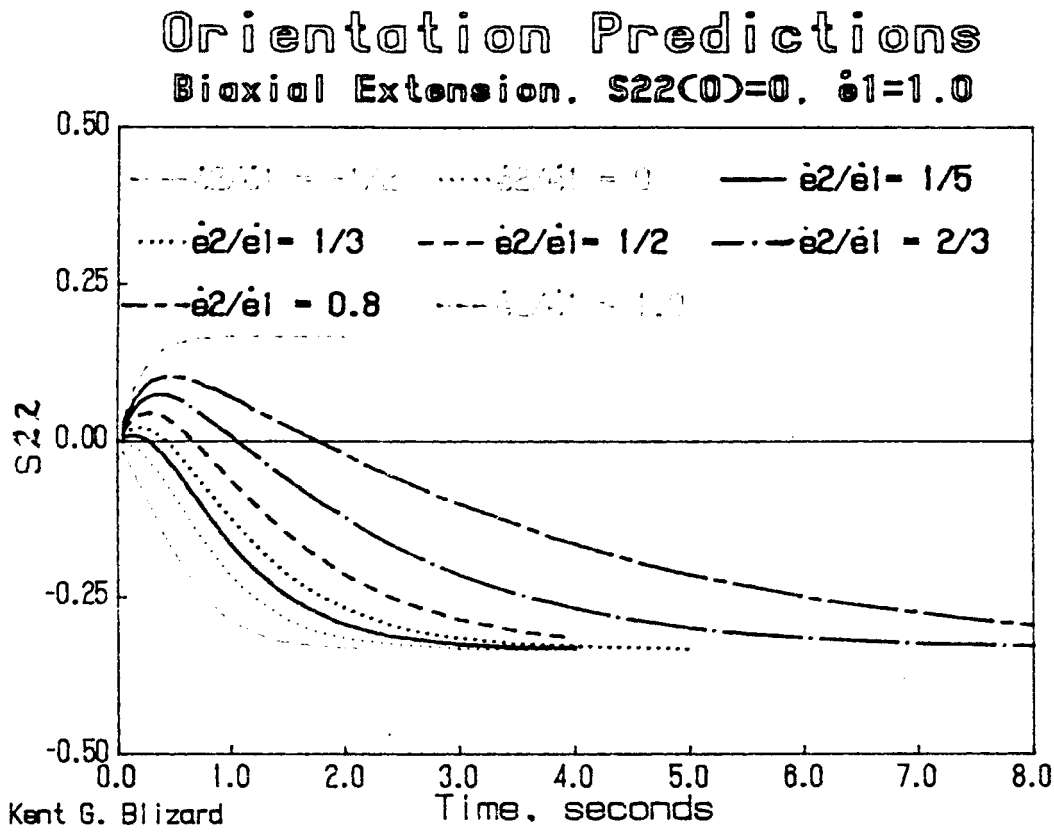

Figure 3.8 Orientation development (S_{22}) for shear-free flows in the 1,2 plane for different $S_{\alpha\beta}(0)$

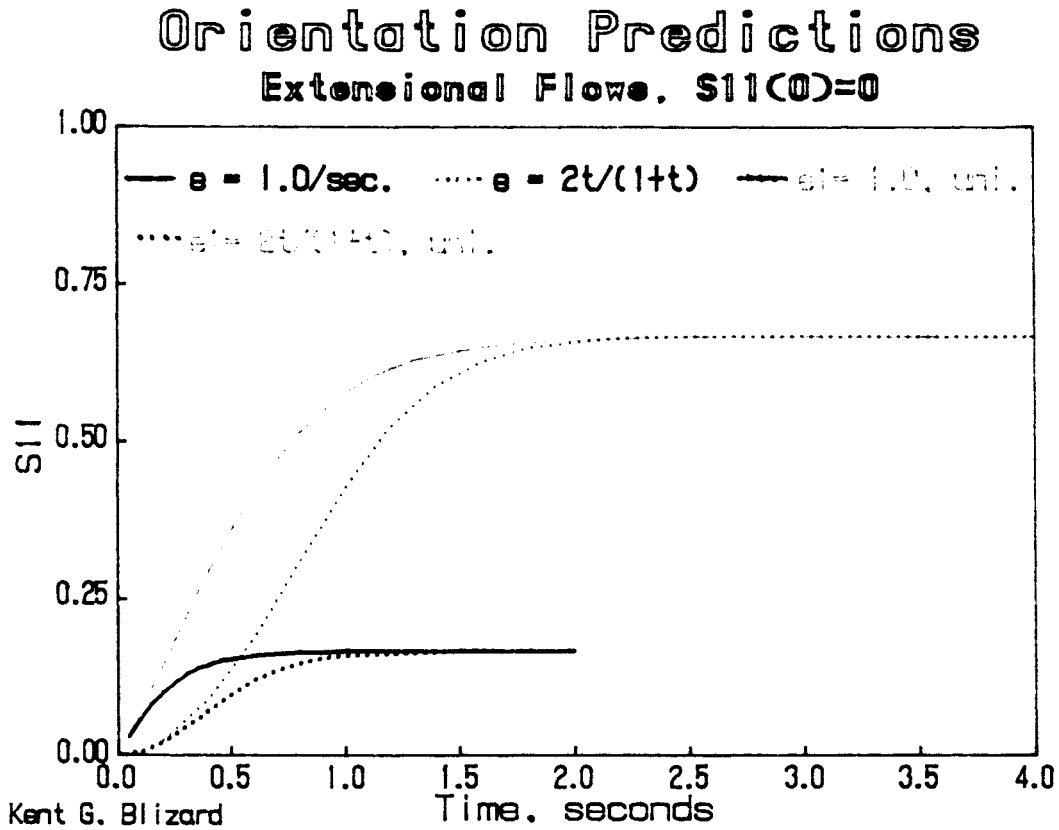

Figure 3.9 Orientation development for equal biaxial extension and uniaxial extension - the effect of an inhomogeneous flow field

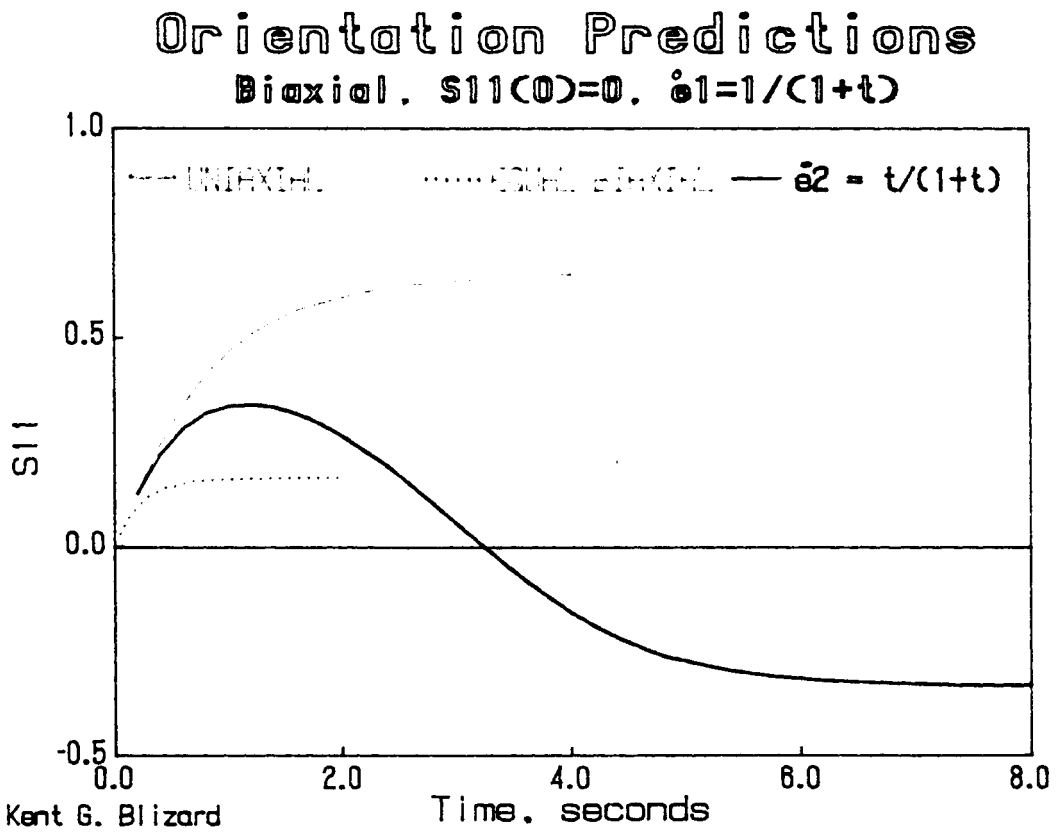

Figure 3.10 Orientation development (S_{11}) for shearfree flows - effect of different inhomogeneous fields

through a maximum before decreasing to its ultimate value of -1/3. The corresponding trends for S_{22} may be seen in Fig. 3.11, in which the orientation goes through a minimum before increasing monotonically to its steady state value of 2/3.

The transient stress predictions ($\sigma_{11}-\sigma_{33}$) for various extensional flows are summarized in Figs. 3.12 to 3.16. In these graphs the stress has been made dimensionless by dividing by ckT. In Fig. 3.12 the initial state of orientation was assumed to be random. The growth of $\sigma_{11}-\sigma_{33}$ follows that of the orientation with the difference that, apart from equal biaxial extension, σ passes through a minimum within $\frac{1}{2}$ second from the inception of flow before increasing to its steady state value.

Long time stress behavior for different $S_{11(0)}$ for equal biaxial extension is shown in Fig. 3.13. Except for the extreme case of $S_{11(0)}\approx 2/3$, in which case the stress remains essentially constant at its extreme positive value, the stress growth follows this pattern: the greater the initial orientation, the less the stress difference tends to increase or decrease during the deformation. The value of $\sigma_{11}-\sigma_{33}$ reaches a plateau at some value between zero and unity for all except the one extreme value of initial orientation.

For determining stress growth using the Doi equations,

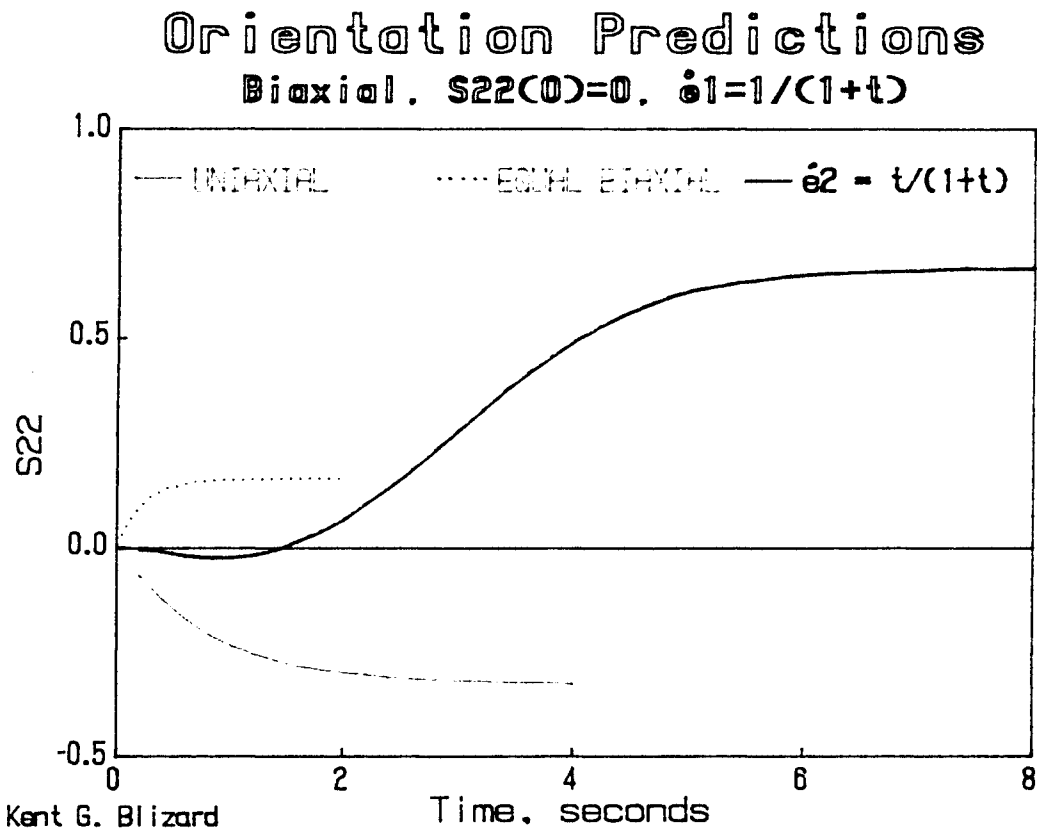

Figure 3.11 Orientation development (S_{22}) for shearfree flows - the effect of different inhomogeneous flow fields

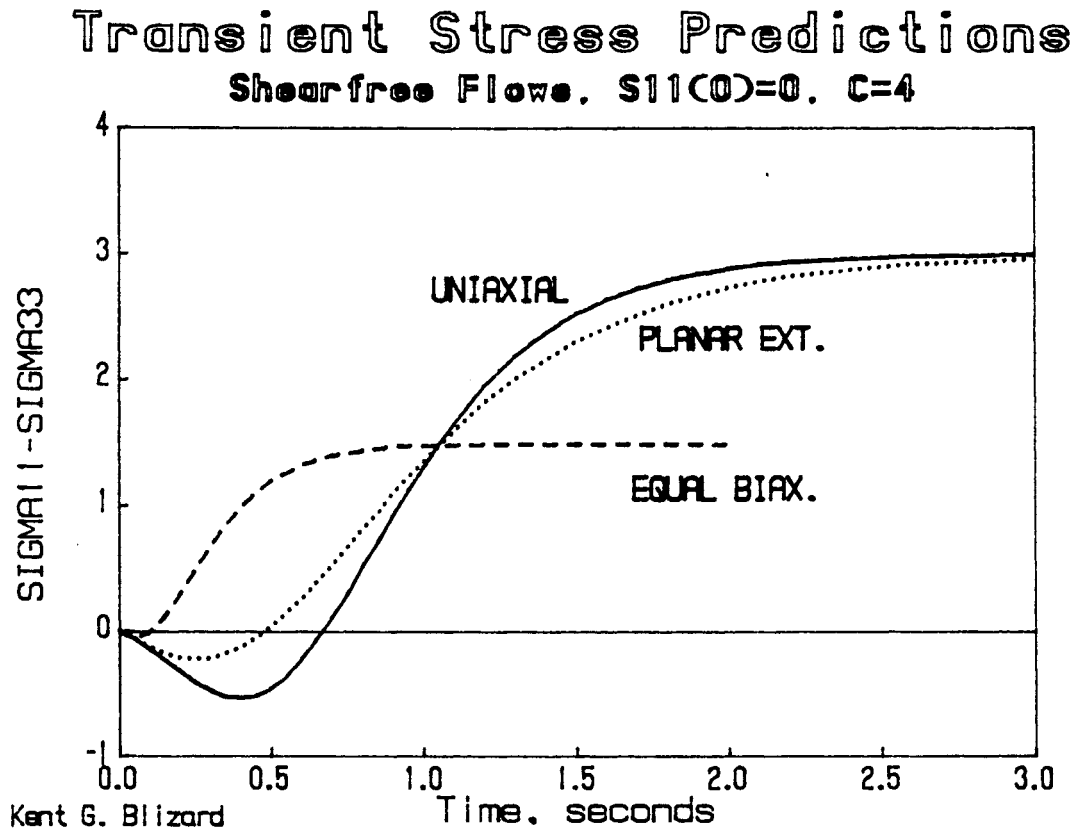

Figure 3.12 Stress development ($\sigma_{11}-\sigma_{33}$) in shearfree flows with $S_{\alpha\beta}(0)=0$ and C=4

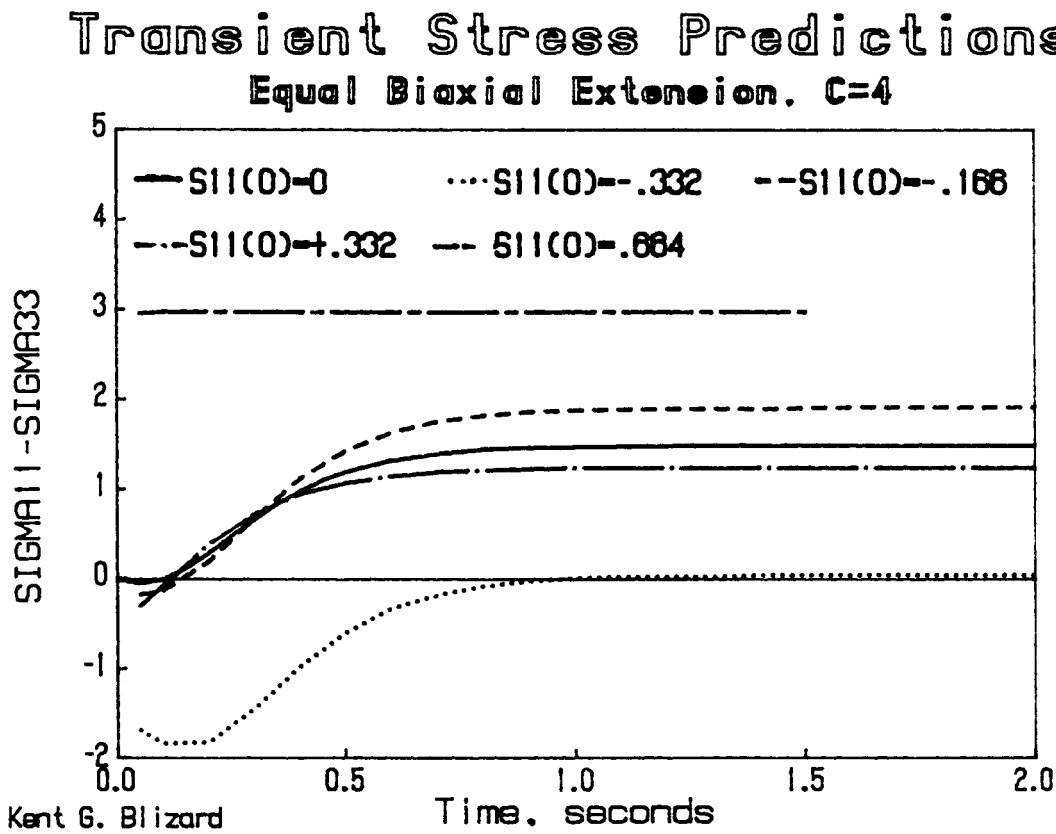

Figure 3.13 Stress development ($\sigma_{11}-\sigma_{33}$) for equal biaxial extension with different $S_{\alpha\beta}(0)$ and C=4

one must input a value for the parameter C, a dimensionless concentration. For equal biaxial extension, the effect of increasing C from the critical value of 3 to 4, a more typical value for anisotropic solutions, to 6, or even to 100, is shown in Fig. 3.14. (For C<3 there exists more than one solution to the equations). Subsequent calculations in this chapter arbitrarily chose C=4. As can be seen from reasonably small values of C, the affect on stress growth of varying C is similar to its affect on orientation: the larger the value of C, the longer the time required to achieve steady state at a given deformation rate. The case of C=100 is included since preliminary calculations indicated that C may be on that order for thermotropic systems (see Appendix A). More reasonable estimates can be obtained by considering a thermotropes response in simple shear, the subject of the next section.

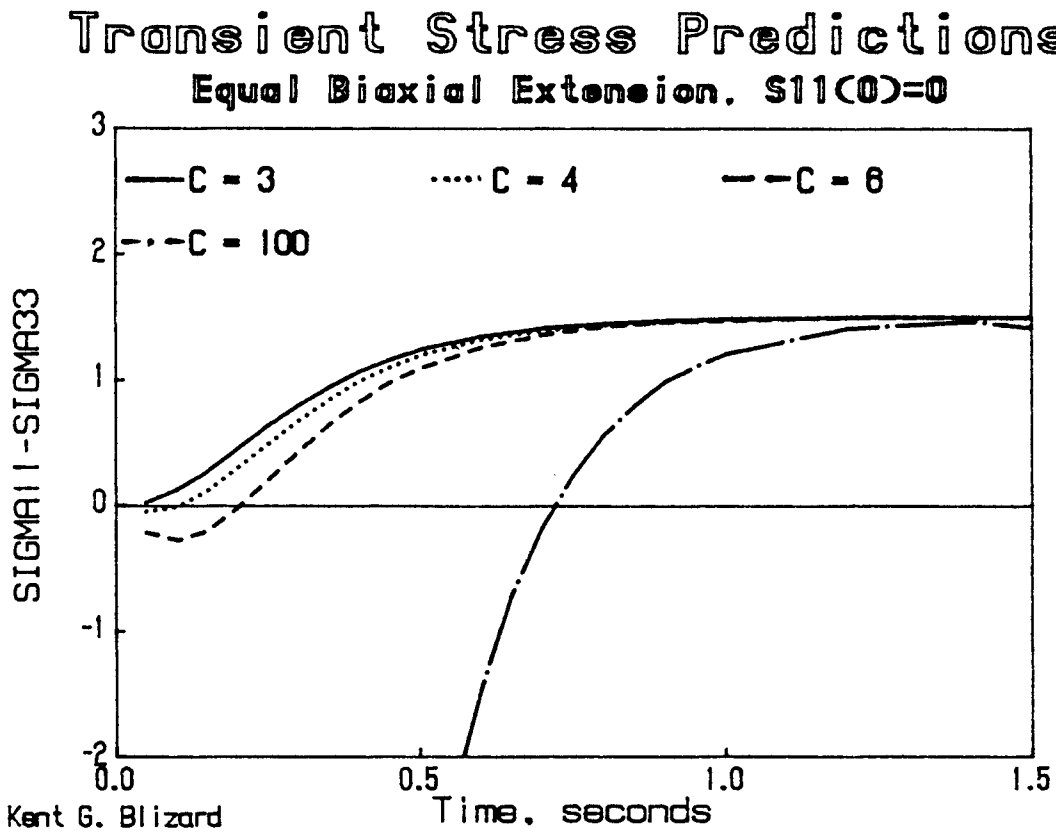

Figure 3.14 Stress development ($\sigma_{11}-\sigma_{33}$) for equal biaxial extension with $S_{\alpha\beta}(0)=0$ and different C values

3.3 Simple shear Flow Predictions

The remainder of this chapter concerns orientation and stress development on the inception of simple shear flow:

$$\dot{\gamma} = \dot{\gamma} \begin{pmatrix} 0 & 1 & 0 \\ 1 & 0 & 0 \\ 0 & 0 & 0 \end{pmatrix}$$

Four components of the orientation order parameter are present for simple shear flow: the three from extensional flow and S_{12}. As with extensional flow, S22 and S33 are equal for a nematic. The orientation development from an initial isotropic state in simple shearing flow with no diffusivity ($F_{\alpha\beta=0}$) is shown in Fig. 3.15. S11 reaches a plateau of 2/3 in about 6 S.U., at which time S_{22} and S33 (not shown) reach their minima of -1/3. The component S_{12} increases to a maximum at about 1½ strain units, and then is predicted to gradually decrease to zero as time approaches infinity. Physically, S_{12} may be viewed as the orientation in the 1,2 plane, which from the product of the direction sines and cosines, is a maximum when the director lies midway between the 1- and 2-directions.

The effect of increasing values of D_r on the order parameter tensor (and hence stresses) may be seen for the S_{11} component in Fig. 3.16. Here, Dr for a concentrated isotropic solution is varied from 0 to 10 sec-1. The effect of D_r on the development of the orientation in simple shear is only noticeable if D_r = O(0.1) or more.

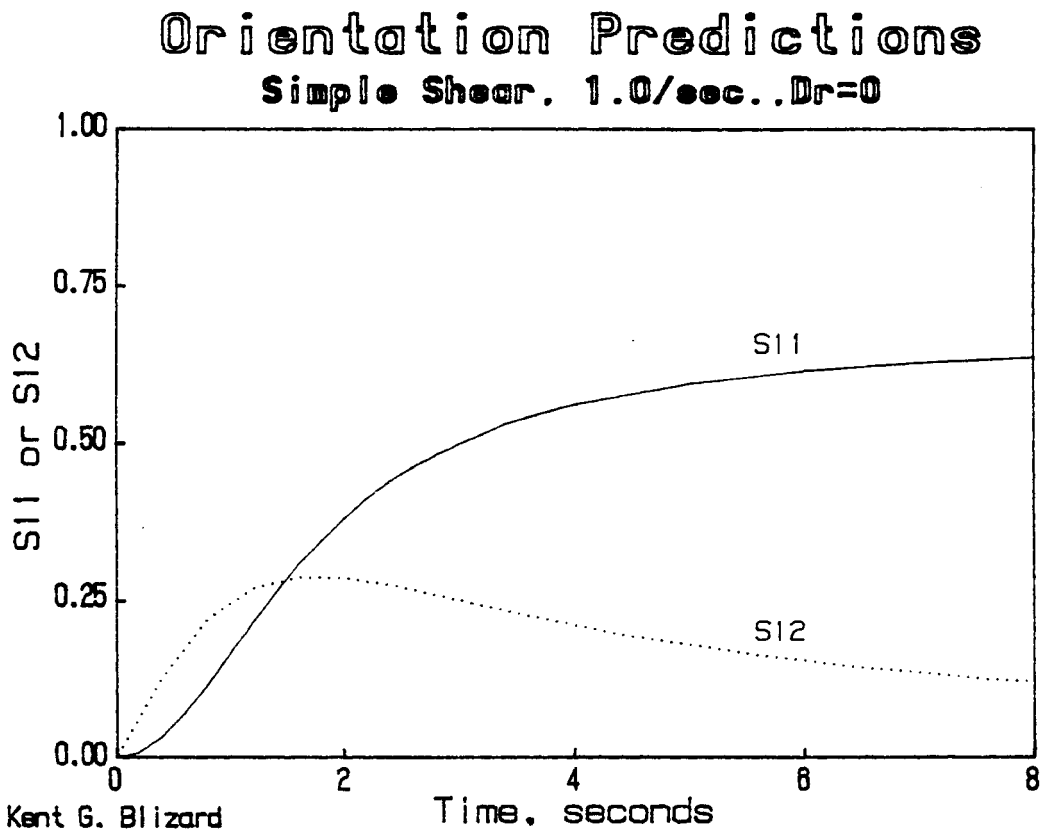

Figure 3.15 Orientation development in simple shear for $S_{\alpha\beta}(0)=0$ and Dr at 1.0 sec-1

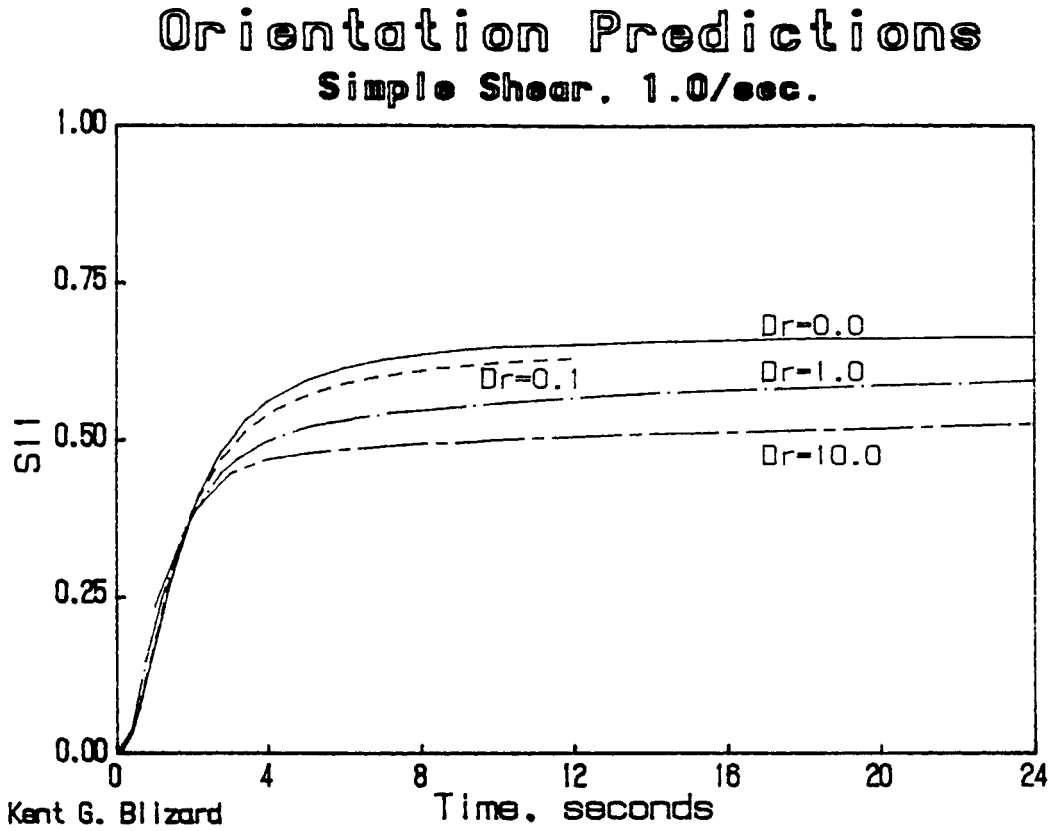

Figure 3.16 Orientation development in simple shear for different D_r for $S\alpha\beta(0)=0$ at 1.0 sec^{-1}

Typical values encountered for rod-like solutions are of the order unity. Thermotropes, on the other hand, seem to have diffusivities several orders of magnitude less, as would be expected. With diffusivities on the order of unity or more, the effective plateau of S_{11} is lowered from 2/3 to as little as ½ (for $D_{r=10}$), although the initial slope versus time remains unchanged since the flow term still dominates in this region.

The effect on the order parameter development of starting with a non-isotropic orientation is identical to the case of extensional flows, and is shown in Fig. 3.17. The closer the initial orientation is to the steady state value, the more gradual is the increase, although saturation does still tend to occur slightly earlier. Saturation does still occur in the 6-8 S.U. range, which is much greater than the 1-1½ for extensional flows of the same magnitude.

Transient stress predictions of Doi's theory in simple shear give trends similar to the orientation predictions, as seen in Figs. 3.18 and 3.19. Normal and shear stresses tend to take longer (10-16 or more S.U.) to stabilize than do the corresponding orientation components. As with the orientation, diffusivity tends to depress the value of shear stress noticeably if $D_{r>0.1}$. Indeed, the initial overshoot observed in σ_{12} disappears entirely if the diffusivity is on the order of unity. Although the

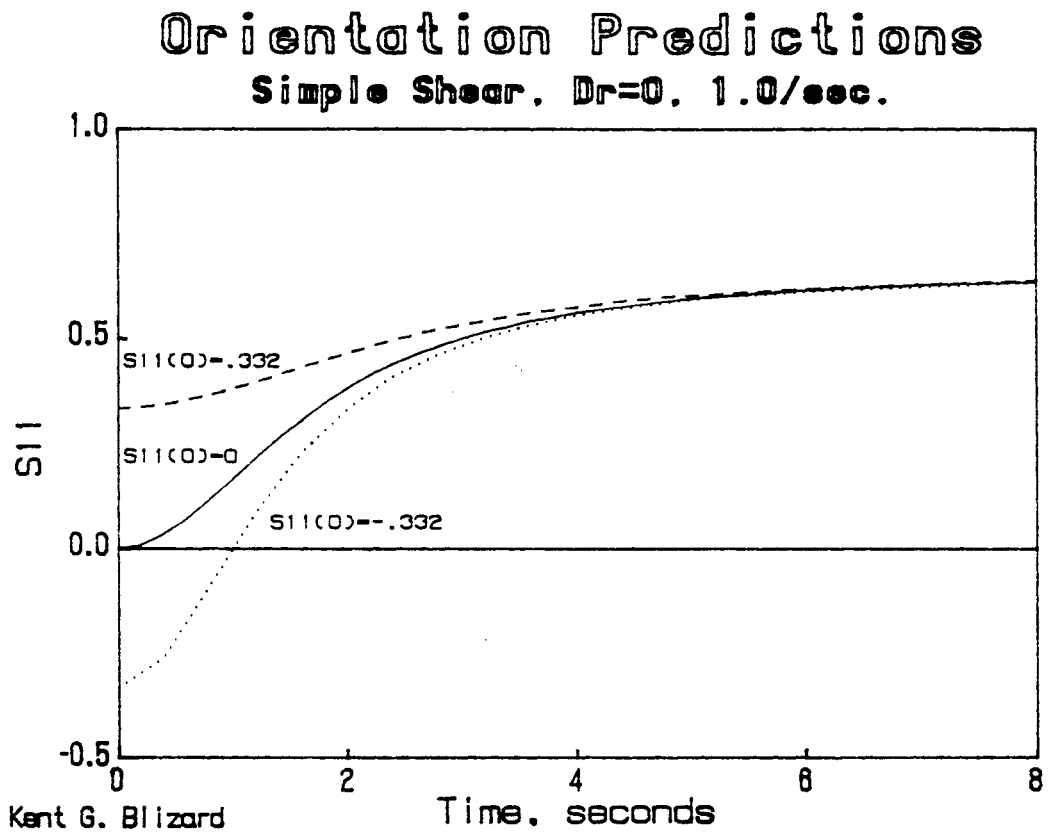

Figure 3.17 Orientation development in simple shear for different $S_{\alpha\beta(0)}$ at 1.0 sec-1

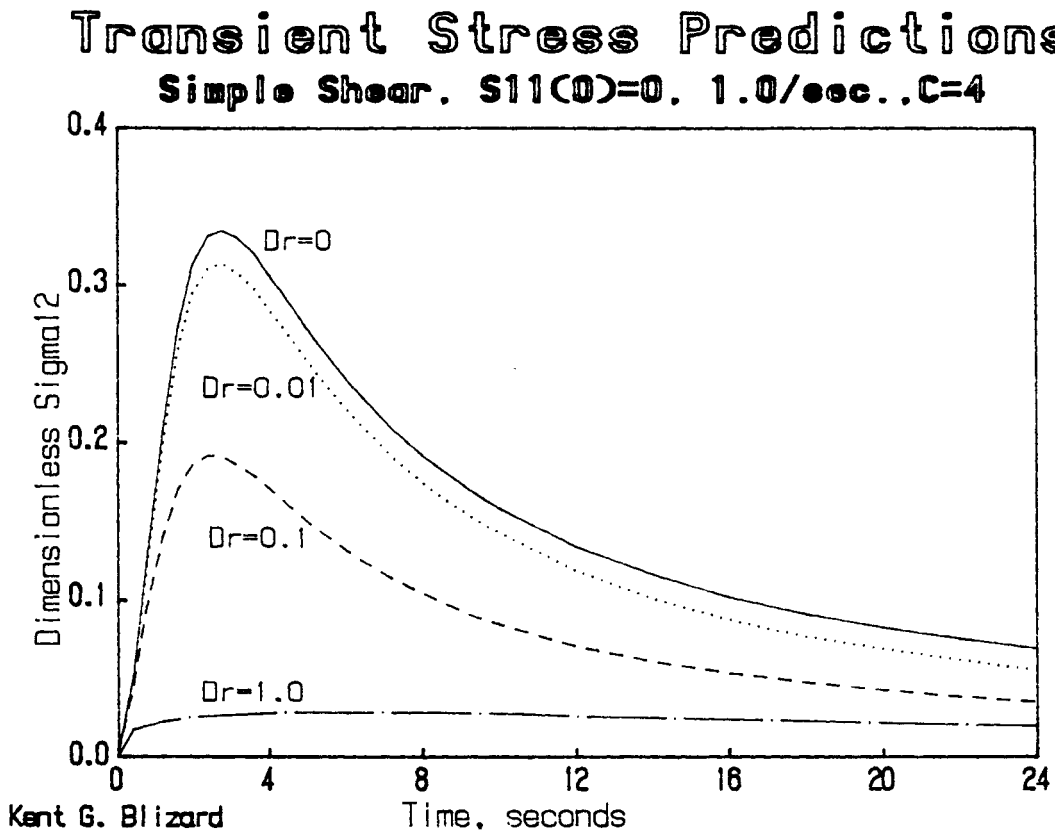

Figure 3.18 Shear stress development, σ_{12}, in simple shear at 1.0 sec-1, C=4, and different D_r

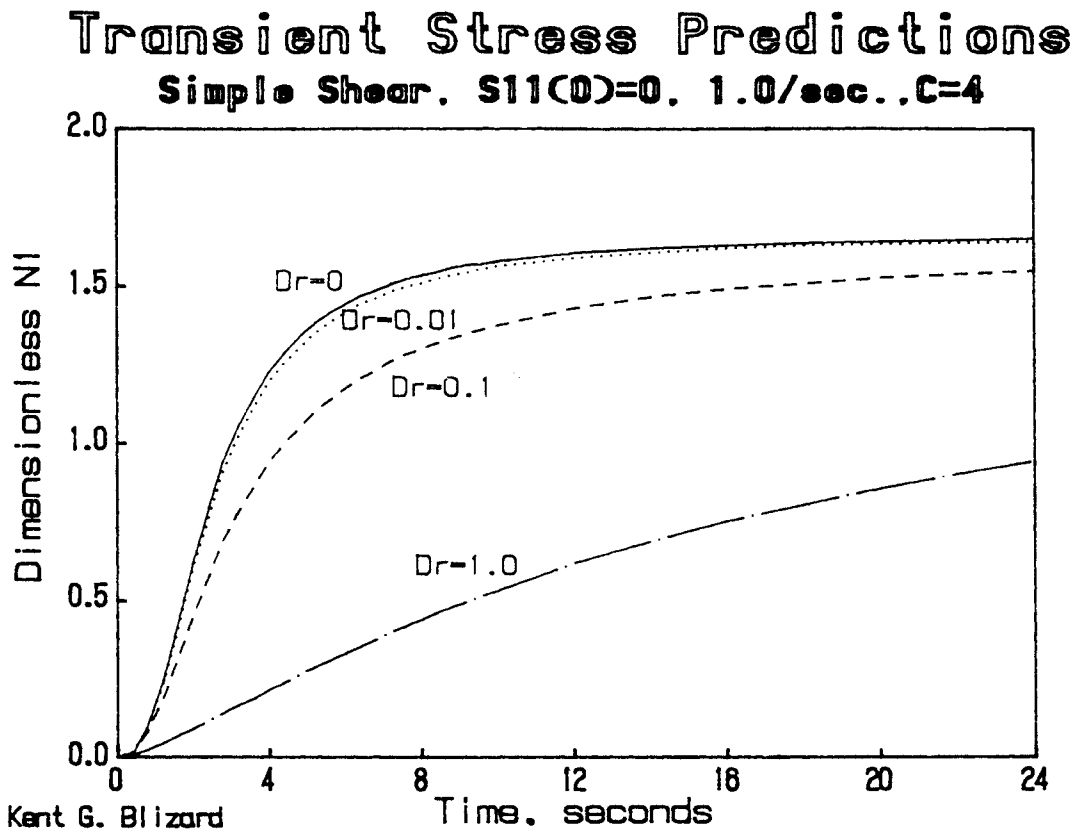

Figure 3.19 Normal stress development (σ_{11}-σ_{22}) in simple shear at 1.0 sec-1, C=4, $S_{\alpha\beta}(0)$=0, and different Dr

equilibrium value of N1, the first normal stress difference ($\sigma_{11}-\sigma_{22}$), appears to remain unchanged, the time to approach this value becomes extremely long for high values of D_r.

As with the extensional stress predictions, a value of C=4 was chosen for convenience to make predictions for the nematic state. The stresses saturate at approximately the same amount of strain, independent of the initial orientation, as can be observed in Fig. 3.20. For $S_{11}(0)<0$, a small amount of undershoot occurs in the first normal stress difference, N1.

Finally, in Fig. 3.21, one may see the effect of varying the parameter C on the stress growth in simple shear with isotropic initial orientation. The plateau value is seen to be highly dependent on the parameter C, increasing from less than unity (made dimensionless by dividing by ckT) for C=3 to around 3 for C=6.

In this chapter the predictions of Doi's theory for the development of orientation and stress after the inception of extensional and shear flows were made, considering the effect of the diffusivity on the equations. Although only the flow term was necessary for the thermotropic systems of interest, the full set of equations was required when studying the responses of concentrated solutions.

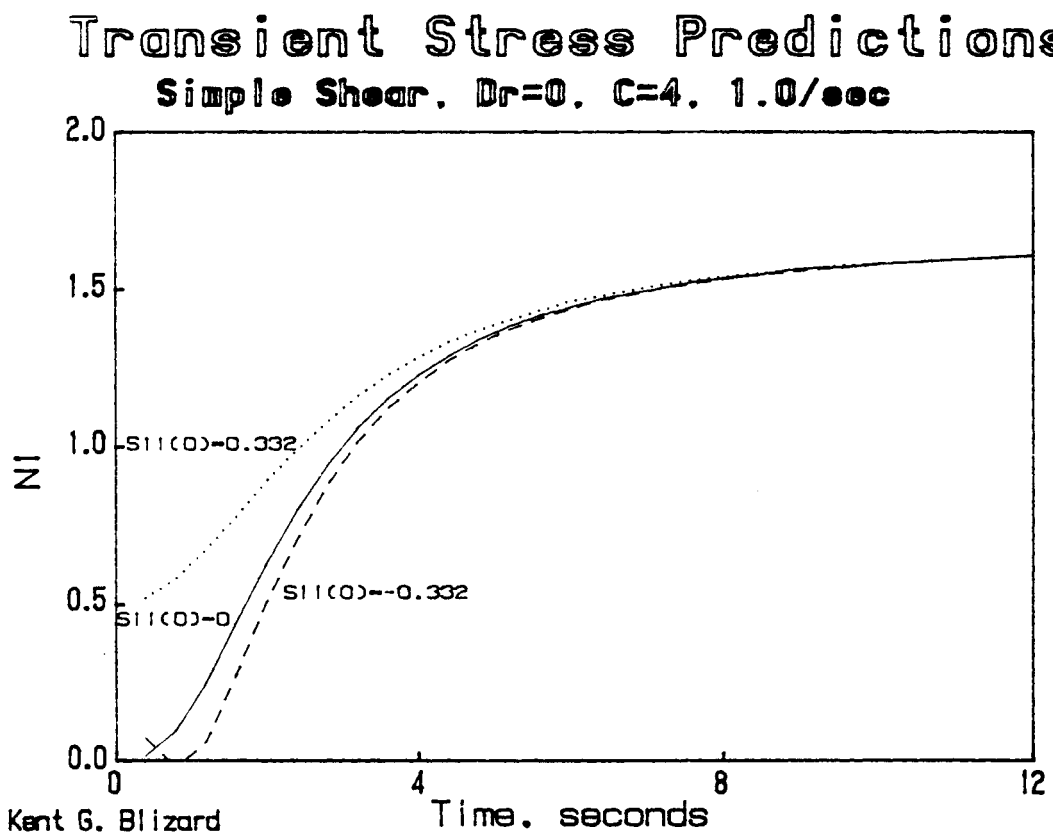

Figure 3.20 Normal stress development ($\sigma_{11}-\sigma_{22}$) in simple shear at 1.0 sec-1, C=4, $D_{r=0}$, and different S11(0)

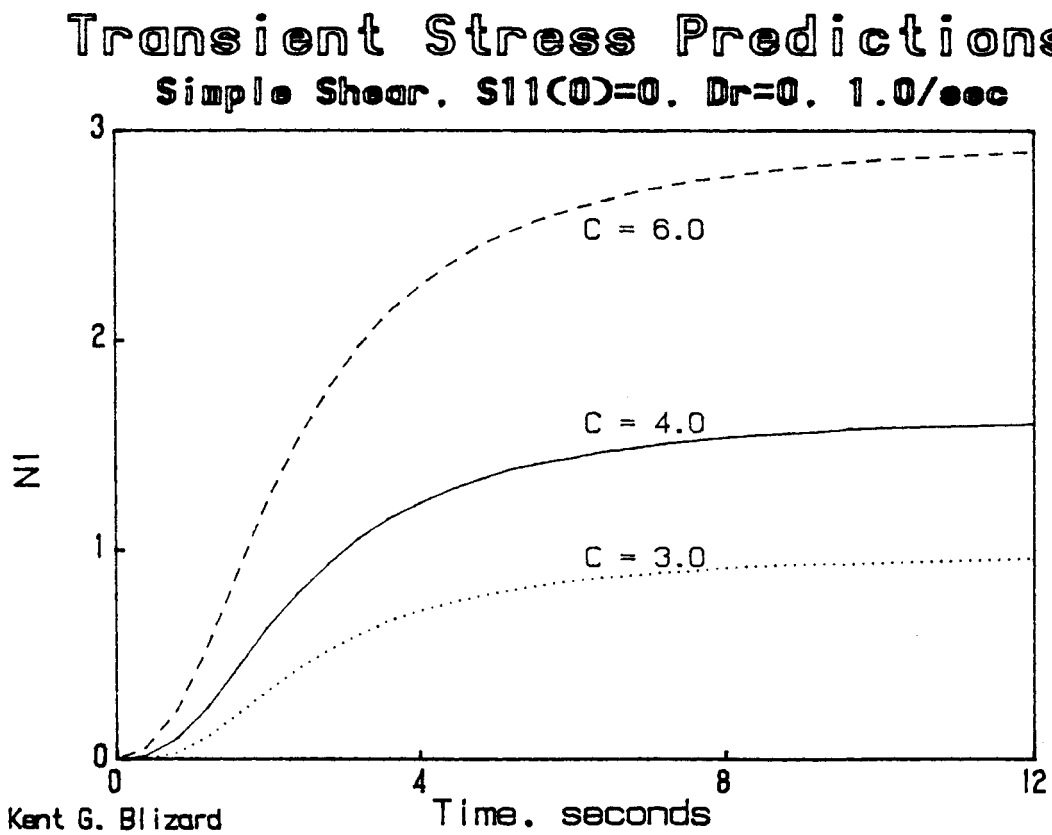

Figure 3.21 Normal stress development in simple shear at 1.0 sec-1, $D_{r=0}$, S11(0)=0, and different C

Next, the theoretical predictions for thermotropes will be compared to experimental results from a blown film line and the shear flow equations will be compared to the transient rheology of PPT/H_2SO_4 solutions. In Chapter 4 the experimental apparatus and techniques for this as well as other biaxial deformations studied will be examined. Results and discussion will then follow in the fifth chapter.

4. EXPERIMENTAL INVESTIGATION

The experimental plan of investigation used to study the liquid crystalline polymers is discussed in this chapter, which is divided into six sections. The materials used and preparation techniques are described in section 4.1. Then in the following four sections the processing methods are described. First the "solid phase forming" apparatus is discussed. Next, film stretching is described, followed by extrusion blow molding and finally in section 4.5 the film blowing apparatus is detailed. Lastly, characterization techniques, such as rheological and mechanical testing, scanning electron microscopy, and wide angle x-ray are discussed in section 4.6. The difficulties encountered and methods to overcome them are elaborated upon in the appropriate sections. The results of the experimental investigation and the pursuant calculations will then be discussed in Chapter 5.

4.1 Materials and Preparation

The polymers used in this work were an experimental aromatic copolyester of 60 mole% p-hydroxybenzoic acid (HBA) and 40 mole% polyethylene terephthalate (PET) made by Tennessee Eastman Company in pellet or chip form. In the latter case the material was pelletized to facilitate further processing. Molecular weight (number average) was about 20,000. Celanese' Vectra A900, which consisted of 73 mole% HBA and 27 mole% 6-hydroxy-2-naphthoic acid (HNA), was supplied as pellets. The preparation and physical properties of these copolymers have been described in detail elsewhere [9,17].

Both anisotropic and isotropic solutions of poly-(p-phenylene terephthalate) (PPT) in 100% sulfuric acid were used in this study. The acid was prepared by mixing the correct amounts on a molar basis of an aqueous solution consisting of 96.5% H_2SO_4 with Oleum (30% free SO_3). The PPT polymer was supplied in the form of Kevlar fiber by Monsanto Corporation, and had a weight average molecular weight of 40,100 and an M_w/M_n of about 2.

The preparation of the solutions of 4, 8, and 12 weight percent PPT consisted of a series of steps. First, the fiber was chopped into inch-long pieces which were then placed in a Soxhlet apparatus. The extraction in acetone took six hours, following which the fibers were

dried in vacuo overnight at 60°C. The mixing of the fibers with the acid was then accomplished under pre-purified nitrogen in a jacketed Helicone mixing bowl, also maintained at 60°C. Up to six hours were required to homogenize the solution, which was subsequently maintained in a vacuum oven at ambient temperature until needed for rheological measurements. The oven was then opened under nitrogen to reduce exposure to the humid air.

4.2 Solid Phase Forming

Injection molded plaques of both LCPs (1/8"x2.5"x2.5" end-gated plaques molded in an Arburg Allrounder Model 221-55-250) were pressed with an hydraulic press (Pasadena Hydraulics, Inc.) at 25,000 pounds force. As the materials studied were hydroscopic, they were dried for 24 hours under 30" of vacuum at 110°C prior to any processing.

Samples pressed isothermally were done so at 190°C and 205°C for the HBA/PET and at 210° and 240°C for the HBA/HNA. Plaques were also pressed non-isothermally. These samples were removed from the hot press after equilibrating at one of the above temperatures and placed in a cold press (water cooled to 10°C) and then pressed with 25,000 lbs. force. Steel shims were made to provide 10% and 26% reductions in the nominal thickness of the plaques. In all cases the sample was pressed between sheets of Teflon. The lubrication oil, when used, was a Dow Corning 1000 cs. oil.

4.3 Film Stretching

Films of 60% HBA/PET were extruded through a 6" film die with die temperatures ranging from 210°C to 230°C and taken up on chill rolls at 125°C (at Tennessee Eastman). These films were then stretched on a 4x4 T.M. Long stretcher in the transverse direction. No additional stretch could be imparted in the machine direction because of slippage from the grips. The stretch ratio varied from 1.5 to 3. Preheat time was one minute to stretch temperatures of 90° or 100°C. Grip pressure was approximately 350 psig., and was chosen to reduce the material's propensity to either tear or be pulled out during the stretch process.

The copolyester was also compression molded in the hydraulic press (260°C, 600 psi.) and the resulting unoriented film stretched biaxially to 1.5 X 1.5. Despite varying the stretch rate from 2 to 14 inches/sec., some tearing invariably resulted. Even soak times of three minutes at 130°C were insufficient to resolve this difficulty. Thus, the results will not be included. Results of independent research at the University of Tennessee (Fellers) confirmed this difficulty for the HBA/PET copolyester. Similarly, compression molded samples of HBA/HNA could not be stretched, even at 200°C, the limit of the heaters on the T.M. Long.

4.4 Extrusion Blow Molding

The copolyesters to be blowmolded were extruded through a 3/4" single screw extruder and then vertically downward through a 1/16" annular die. Barrel temperatures (single zone) were either 220, 260, or 275°C and the die temperatures either 180, 190, or 200°C for the HBA/PET material; 300 and 320°C barrel temperatures were used for the HBA/HNA, with die temperatures of 290 and 300°C, respectively. The die temperatures were limited primarily by freeze off at the lower end and a decreased melt strength at the upper extreme. Blowing pressure was 30 psig. for most runs, but could be varied to control the time required to blow the bottle. The time to form a parison was clocked with a stopwatch and a temperature probe was used to check the temperature of the lower end of the parison. The mold was air cooled to 25°C.

4.5 Film Blowing

Both the HBA/HNA and HBA/PET copolyesters were processed in a blown film line. Figure 4.1 is a photograph of the experimental setup, showing the laboratory extruder (1" Killion) with the blown film die (h_0 = 0.63 mm, a_0 = 2.45 cm) attached, adjustable height film tower with takeoff rolls, and the torque winder onto which the sheet was wound.

For each copolyester two different barrel temperatures were used. Melt temperatures for the HBA/PET system were 267°C and 247°C with a die profile of 215°C-195°C (initial and final zones) in both instances. For the naphthoic system final barrel zone temperatures of 338°C and 319°C were employed. A die profile of 275°-250°C was used for both barrel temperatures. As with the extrusion blow molding, the die temperature could not be varied to any large extent.

Screw speed was held constant at 46 RPM for both copolyesters, generating pressures of about 250 psi in the barrel. Nip roll speed was not varied, but held constant for a given polymer. Thus, the major adjustable parameter was the pressure of the nitrogen blown into the bubble, which could be increased up to 30 psig. Blow up ratios of 1 to about 3.1 were obtained. No air ring was required to cool these materials because of the supercooling that

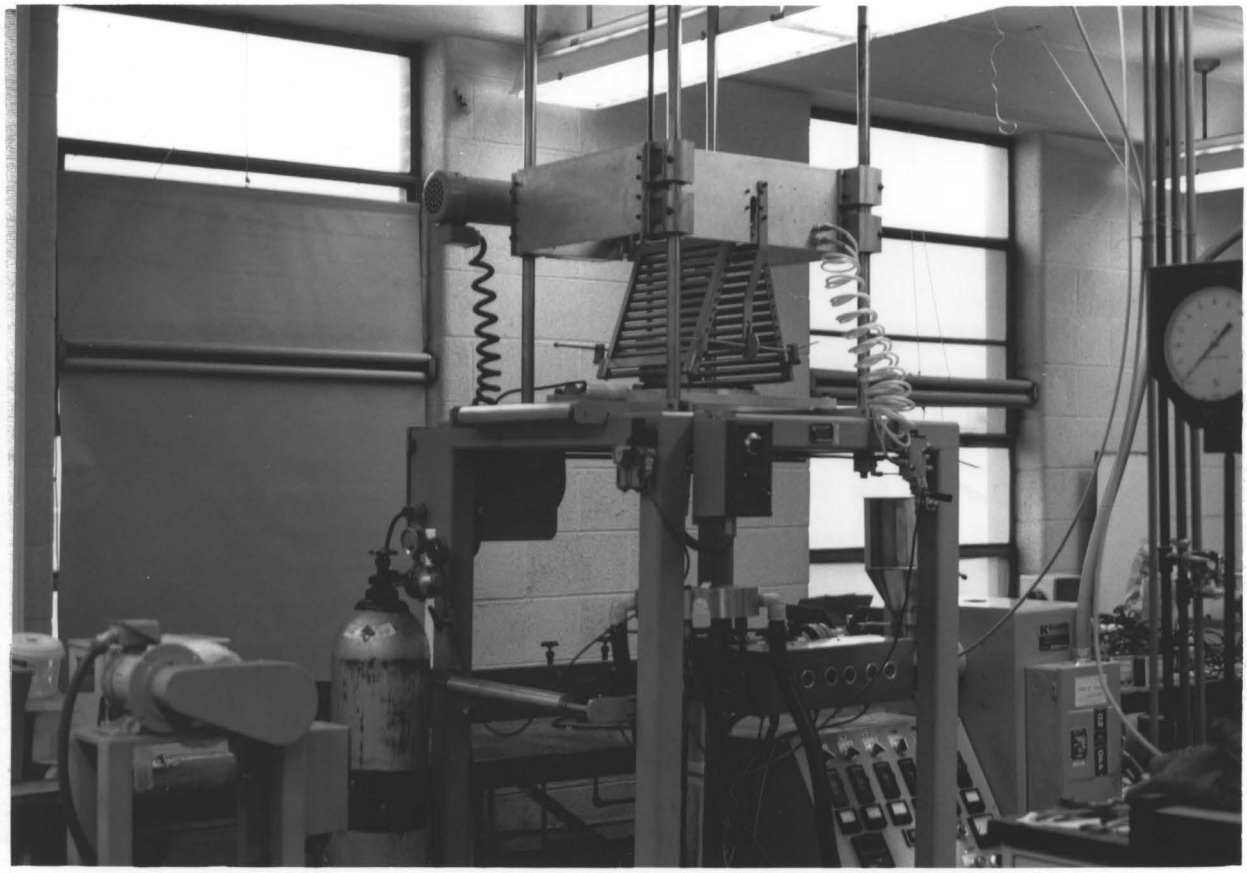

Figure 4.1 Photograph of experimental setup for the blown film process.

occurred in the die itself.

A video camera coupled to a VHS recorder was used to record the shape of the bubble under different conditions. In addition, a black permanent marker was used to provide a point of reference on the bubble from which to calculate the velocity of a particle in the axial direction on playback of the video.

4.6 Characterization

Once processed, several characterization techniques were utilized in order to measure the properties of the resulting material. The following subsections explain the methods used to measure the rheological and mechanical properties, texture, and molecular orientation.

4.6.1 Rheological Measurements

Transient, steady shear, and dynamic rheological measurements on the PPT solutions were conducted with a cone-and-plate geometry (0.04 radian angle, 25 mm diameter) on the Rheometrics Mechanical Spectrometer (RMS 605). In steady shear the viscosity and first normal stress difference were obtained from standard equations, as were the dynamic viscosity, storage, and loss moduli in the dynamic oscillatory mode [71]. A description of the measurement technique for the transient response experiments, however, is provided.

Transient rheological measurements include a number of tests in which the non-steady response of the shear and normal stresses are investigated. Typically these experiments consist of stress growth and relaxation tests, although such a jump strain and interrupted stress growth are possible. In a stress growth experiment the fluid is

assumed to be at rest for all times prior to t=0. At that point steady shear flow is initiated at a constant known value of $\dot{\gamma}$. In a stress relaxation experiment the material is assumed to have achieved steady state in shear flow for t<0. At time t=0 the shearing is stopped and the stresses are monitored as they relax to a constant value.

For all transient tests the data can be represented in terms of four time-dependent viscosity and normal stress functions:

$$\mu+(t) = \tau_{12(t)}/\dot{\gamma}$$

$$N1+(t) = \tau_{11(t)}-\tau 22(t)$$

$$\mu-(t) = \tau_{12(t)}/\dot{\gamma}$$

$$N1-(t) = \tau_{11(t)}-\tau 22(t)$$

where by convention the + sign signifies the stress growth behavior and the - sign the stress relaxation behavior of the material.

Specific data gathering techniques were employed on the transient experiments to ensure that an accurate measure of the response of the material was obtained. The RMS was equipped with a digital storage oscilloscope (Gould model OS4100) to which torque and normal force measurements were directly sent. After storage the signals were dumped onto a strip chart recorder. This arrangement avoided the effect of a slow pen response time which would exist if the measurements were directly

recorded on the plotter. Pre-purified nitrogen was used instead of air for all tests to eliminate the effects of moisture of the PPT solutions.

4.6.2 Mechanical Testing

Samples to be mechanically tested were obtained in both the machine and transverse directions (where possible). Tensile tests of 1 cm dumbbells and three point flex tests of rectangular strips were carried out on an Instron Mechanical Tester (model 1122) at equilibrium with the laboratory surroundings. In some instances it was not possible to obtain dumbbell samples for tensile testing: highly oriented thin film tended to splinter when the dumbbell cutter was used. Rectangular strips were cut for testing in these cases. Crosshead speeds were 0.5 mm/min for tensile and 5.0 mm/min for flex tests. The arithmetic average and standard deviation of the strength, modulus, and elongation to break were calculated for several specimens taken from the same film, bottle, or plaque.

4.6.3 Scanning Electron Microscopy

Scanning Electron Microscopy (SEM) was done with either a Jeol microscope (JSM-35C) with an accelerating voltage of 15kV or a Cambridge instrument (Stereoscan 200)

with an accelerating voltage of 25kV. Samples of the HBA/PET copolyester were either selectively etched of their PET-rich regions with n-propylamine and rinsed with water or were fractured under liquid nitrogen prior to mounting. The Vectra samples had to be etched with sulfuric acid (96.5%, aqueous solution) to enhance their texture for viewing. The samples were mounted with silver conducting paint and coated with 100-150 angstroms of gold prior to analysis. Photomicrographs on the JEOL instrument were taken with Polaroid type 55 film, primarily at 480x magnification. On the Cambridge instrument type 52 film was employed in preference to the type 55 because of the higher resolution, particularly at the higher magnifications used (sometimes greater than 20,000x).

4.6.4 Wide Angle X-Ray Scattering

Wide angle x-ray (WAXS) diffraction patterns were obtained from a Philips x-ray generator (model PW 1720) at 40kV and 20 milli amperes. A Wahrus camera was used to photographically record the scattering patterns. Samples were exposed from 4 to 24 hours, depending on their thickness. The impingement direction was perpendicular to the surface of the bottle, film, or plaque, except where noted.

In Chapter 4 the experimental portion of the investigation was detailed, with emphasis on the processing methods employed. The results obtained from the theoretical and experimental studies are discussed in the next chapter.

5. DISCUSSION

This study was conducted to determine whether thermotropic liquid crystalline copolyesters could be processed in a manner that would result in biaxial orientation and properties in the final product. Also of importance to this work was determining whether the molecular orientation could be successfully predicted by adapting Doi's theory of anisotropic solutions to the processing of thermotropes. Doi's theory predicts the stresses and orientation present in such solutions, but with appropriate modifications may be applicable to the melt state, as shown in Chapter 3. This chapter is broadly divided into two parts: the first part considers the experimental results on the thermotropic copolyesters. The second portion of the discussion focuses on the transient predictions of the Doi theory. The shear flow predictions of the theory are examined through the rheology of PPT/H_{2SO4} solutions and shearfree predictions are analyzed in terms of the film blowing results.

The chapter has been divided as follows. The processing methods are first discussed: solid phase forming in section 5.1, extrusion blow molding in section 5.2, film stretching in section 5.3, and film blowing in section

5.4. The processing and characterization results are included for each processing method with a discussion of the results at the end of each section. The transient orientation predictions of the theory for biaxial flows are then discussed in section 5.5 and compared to the results obtained from film blowing the two copolyesters of interest. In section 5.6 the transient rheological behavior of the PPT/H_2SO_4 solutions is discussed, followed by the predictions of Doi's theory for the anisotropic solution subjected to transient shear flows.

5.1 Solid Phase Forming

Mechanical properties of injection molded end-gated plaques do not approach those reported for fibers and films. It has been well documented that for relatively thick plaques, such as the 1/8" thick ones examined here, the core is mostly unoriented and amorphous in texture although the skin region may be highly oriented in the flow direction [72]. Thus, not only are the properties poor in the transverse direction, but they are less than ideal even in the machine direction. This deficiency provides the impetus for further processing of plaques of HBA/PET and HBA/HNA to improve the mechanical properties, either in one direction or by imparting biaxial properties and orientation.

Initial modulus and strength values have been determined for a variety of pressing conditions for the HBA/PET copolyester. Tables 5.1 and 5.2 summarize these results for the tensile and flexure modes, respectively. No significant change in the transverse direction properties can be seen under the range of processing conditions studied: tensile and flexural moduli remained below 2 GPa and stress at break was approximately 20-30 MPa. These values indicate an orientation perpendicular to the transverse direction. For the isothermal pressing of the HBA/PET copolyester even when the modulus increased sig-

TABLE 5.1: Tensile Calculations - HBA/PET Plaques

Conditions	Direction	E_T (MPa)	σBreak (MPa)
As molded	MD	3285 (148)	84.0 (2.76)
190, no press	MD	3106 (277)	71.9 (12.3)
205, no press	MD	3285 (249)	79.1 (6.66)
190,NL,10%	MD	3712 (328)	56.6 (19.6)
190,L,10%	MD	4054 (393)	55.4 (6.09)
190,NL,26%	MD	4436 (445)	58.3 (12.0)
205,NL,10%	MD	3793 (127)	51.0 (13.9)
205,L,10%	MD	4130 (212)	44.5 (6.81)
205CP,NL,10%	MD	3679 (348)	81.2 (5.98)
205CP,L,10%	MD	4018 (80)	79.9 (4.69)
205CP,NL,26%	MD	4326 (211)	77.9 (8.89)
205CP,L,26%	MD	4188 (481)	74.9 (9.92)
As molded	TD	1681 -	34.8 -
190, no press	TD	1226 (146)	24.2 (1.57)
205, no press	TD	1364 (111)	23.8 (1.86)
190,NL,10%	TD	1395 (301)	22.0 (9.64)
190,NL,26%	TD	1594 (115)	21.3 (3.44)
205,NL,10%	TD	1359 (40)	21.4 (1.84)
205,L,10%	TD	1489 (165)	19.7 (2.39)
205CP,NL,10%	TD	1447 (103)	24.6 (1.51)
205CP,L,10%	TD	1522 (107)	26.1 (2.80)
205CP,NL,26%	TD	1633 (42)	25.8 (4.57)
205CP,L,26%	TD	1668 (224)	24.1 (2.36)

Here, CP indicates cooled-while-pressing, L and NL indiate lubricated and not lubricated, respectively. The percentage nominal reduction is also given. Standard deviations are given in parentheses.

TABLE 5.2: Flexure Calculations - HBA/PET Plaques

Conditions	Direction	E_B (MPa)	σ_{Break} (MPa)
As molded	MD	10580 (1470)	98.8 (6.96)
190, no press	MD	12680 (513)	103.8 (1.97)
205, no press	MD	9690 (325)	101.5 (1.22)
190,NL,10%	MD	8357 (995)	50.0 (22.3)
190,L,10%	MD	9443 (676)	56.3 (15.3)
190,NL,26%	MD	7303 (336)	50.7 (18.1)
205,NL,10%	MD	9142 (898)	76.2 (10.0)
205,L,10%	MD	9913 (1756)	75.8 (5.71)
205CP,NL,10%	MD	12800 (365)	106.9 (0.68)
205CP,L,10%	MD	11330 (580)	94.2 (3.14)
205CP,NL,26%	MD	11570 (167)	93.3 (6.55)
205CP,L,26%	MD	13490 (897)	93.6 (15.8)
As molded	TD	1728 (264)	31.3 (3.57)
190, no press	TD	1534 (59)	27.2 (1.89)
205, no press	TD	1400 (87)	25.8 (1.19)
190,NL,10%	TD	1541 (236)	24.6 (3.19)
190,L,10%	TD	1572 (152)	3.1 (4.61)
190,NL,26%	TD	1732 (250)	25.2 (4.00)
205,NL,10%	TD	1524 (503)	21.4 (7.50)
205,L,10%	TD	1132 -	16.1 -
205CP,L,10%	TD	1689 (97)	27.1 (1.27)
205CP,NL,26%	TD	1353 (165)	22.2 (2.92)
205CP,L,26%	TD	1982 (106)	30.2 (0.85)

Here, CP indicates cooled-while-pressing, L and NL indiate lubricated and not lubricated, respectively. The percentage nominal reduction is also given. Standard deviations are given in parentheses.

nificantly in the MD, the strength was adversely affected, being reduced up to 50% compared to the as molded specimens. For the samples that were cooled while they were pressed, however, enhancement in the tensile modulus was observed with no corresponding reduction in the stress at break of the material. The flexure results follow the same trend: here again, loss of strength was detected only if the plaques were pressed isothermally.

Pressed plaques of HBA/PET were examined by means of electron microscopy (SEM). Fracture specimens taken parallel to the flow direction were examined edgewise. Thus, the horizontal direction in Figs. 5.1-5.3 is the thickness direction and the vertical is the flow direction. Plaques examined "as molded" revealed a 0.3 mm skin at each edge, as shown in Fig. 5.1. The remainder of the plaque, shown in the same figure, was lacking in fibrous texture. When the plaque was deformed isothermally at 190°C and then quenched the samples changed considerably. The micrographs in Fig. 5.2 indicate that the center became slightly more oriented than before the deformation, but the edge no longer appeared to be fibrous in texture. Some localized melting at the surface in which the previous orientation was permitted to relax out may be responsible for this phenomenon; annealing effects at this temperature and time are negligible and thus cannot account for the decrease in properties and structure [76].

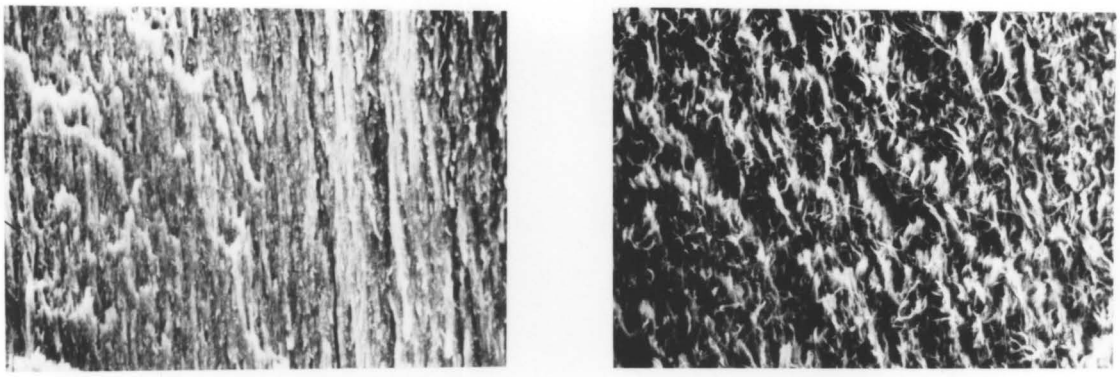

Figure 5.1 Morphology of fracture surface of injection molded plaque before deformation (x480). Flow direction is vertical, thickness direction is horizontal.

Figure 5.2 Morphology of fracture surface of injection molded plaque pressed isothermally at 190°C to 74% of its original thickness without lubrication. The left of the micrograph is the edge of the sample (x480).

Figure 5.3 Morphology of fracture surface of injection molded plaque after being cooled from 205°C during deformation to 74% of its original thickness with lubrication (x480).

In contrast, when the plaque was cooled from 205°C as it was pressed, the morphology shown in Fig. 5.3 resulted. The edge remained highly aligned in the flow direction and the core for the most part showed the same fibrous texture. Thus the deformation occurred primarily in the center region and not at the outer surface. Because of the heat transfer, the outer surface would be quenched immediately on contact with the cold platens, but the center was shown (see Appendix B) to cool to approximately 155°C by the end of the deformation, which required about 0.5 second. This finding correlates well with Fig. 2.15 in which one can see that the elastic modulus is still in the processible region at 160°C on the cooling curve for this material.

These morphological results correlate well with the mechanical properties of the samples. By increasing the fraction of the plaque that is fibrous and aligned in the flow direction, the modulus in the MD is improved. When the orientation at the surface is destroyed the flexure properties, which predominantly reflect the outer edge structure, likewise decrease. Clearly, thermal as well as deformation history is critical in determining the structure and properties of these materials.

Two additional comments should be made concerning the mechanical property and SEM results. First, no general trend was found in regard to the effect of lubrication.

Although the plaques tended to deform only along the MD without lubrication and more uniformly with the oil (the purpose of the oil was to ensure a biaxial deformation), no difference in the morphology or properties could be noted. Second, pressing the samples 26% instead of 10% did not significantly alter their morphology or properties. Thus, no more than 10% reduction in thickness is required to alter the structure and properties if the plaques are non-isothermally deformed.

Injection molded plaques of HBA/HNA were also pressed 10% and 26% under isothermal and nonisothermal conditions. Isothermal pressing was done with and without lubrication at 265°C; nonisothermal processing occurred while cooling from 295°C for the same nominal thickness reductions. The tensile and flexure results are shown in Tables 5.3 and 5.4, respectively. Although the pressed plaques showed an increase in tensile modulus in the MD from 3.0 to about 3.5 GPa, this change was not significant. However, for the 26% reduction, the maximum stress in the MD declined by 50% or more, from about 150 MPa to 50-75 MPa for both the isothermal and nonisothermal cases. The smaller reduction in thickness resulted in no appreciable change in the strength of the material. Likewise, transverse direction modulus and strength showed no significant change from initial values of 1.6 GPa and 47 MPa, respectively, for the nonisothermal pressings. However, if the

TABLE 5.3: Tensile Properties - HBA/HNA Plaques

Conditions	Direction	E_T (MPa)	σ_{Break} (MPa)
As molded	MD	2980 (230)	147 (15.5)
295°, no press	MD	2730 (120)	145 (16.0)
295°CP,NL,26%	MD	1730 (100)	62.2 (10.5)
295CP,L,26%	MD	3050 (300)	75.3 (18.3)
295CP,NL,10%	MD	3220 (510)	149 (23.0)
295CP,L,10%	MD	3560 (410)	126 (38.9)
265,NL,26%	MD	3800 (630)	51.2 (9.76)
265,L,26%	MD	3580 (440)	51.2 (27.7)
265,NL,10%	MD	3760 (250)	74.0 (31.8)
265,L,10%	MD	3310 (30)	122 (22.5)
As molded	TD	1580 (136)	46.9 (4.46)
295°, no press	TD	1400 (60)	48.6 (3.65)
295°CP,NL,26%	TD	1930 (320)	58.7 (13.9)
295CP,L,26%	TD	2050 (140)	71.3 (5.70)
295CP,NL,10%	TD	1650 (160)	54.1 (3.92)
295CP,L,10%	TD	1760 (190)	70.9 (9.81)
265,NL,26%	TD	1210 (290)	4.68 (1.07)
265,L,26%	TD	1960 -	4.72 -
265,NL,10%	TD	1480 (210)	11.0 (12.2)
265,L,10%	TD	1790 (430)	11.7 (9.20)

Here, CP indicates cooled-while-pressing, L and NL indiate lubricated and not lubricated, respectively. The percentage nominal reduction is also given. Standard deviations are given in parentheses.

TABLE 5.4: Flexure Properties - HBA/HNA Plaques

Conditions	Direction	E_B (MPa)	σ_{Break} (MPa)
As molded	MD	13000 (820)	165 (3.5)
295°, no press	MD	7210 (310)	122 (7.8)
295°CP,NL,26%	MD	2990 (190)	44.2 (10.7)
295CP,L,26%	MD	5110 (300)	78.9 (5.67)
295CP,NL,10%	MD	7100 (50)	109 (1.53)
295CP,L,10%	MD	9470 (710)	125 (4.58)
265,NL,26%	MD	7020 (185)	72.1 (14.2)
265,L,26%	MD	8910 (350)	105 (13.7)
265,NL,10%	MD	10280 (185)	106 (27.9)
265,L,10%	MD	10070 (920)	105 (12.0)

Here, CP indicates cooled-while-pressing, L and NL indiate lubricated and not lubricated, respectively. The percentage nominal reduction is also given. Standard deviations are given in parentheses.

LCP was deformed isothermally at 265°C, the transverse direction strength declined by an order of magnitude. Importantly, no change in tensile properties was observed if the plaque was simply heated to 295°C without any deformation.

Flexural results were uniformly poor, with modulus and strength in the machine direction declining under all presssing conditions. Moduli of undeformed plaques of 13 GPa and strength of 165 MPa were reduced by as much as 50%. These effects were exacerbated for the 26% reduction as compared to the more mild deformation of 10%. Unlike the tensile results, the plaque that was heated without being subjected to deformation showed a significant decrease in both modulus and strength from 13 GPa to 7.2 GPa and from 165 MPa to 122 MPa, respectively. Causes for these adverse effects will now be examined in terms of SEM and WAXS results.

The next several figures contain micrographs of fracture surfaces of injection molded plaques of HBA/HNA. In all cases the flow direction in the mold is horizontal and the thickness direction is vertical. The "as molded" plaque is seen in Fig. 5.4. Both the edge (a) and center (b) are fibrillar in texture with fiber diameters on the order of one micrometer. The only difference between the center and the edge is that the center shows fibers that seem to have less of a preferred orientation. The fibers

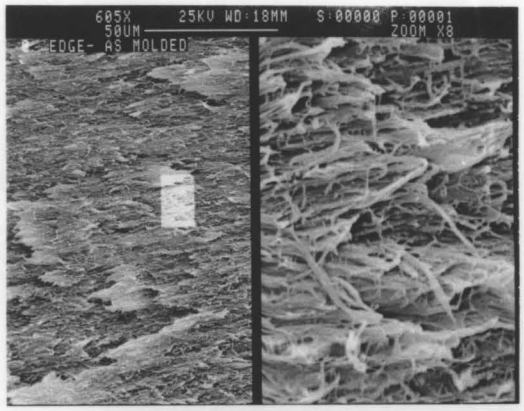

a

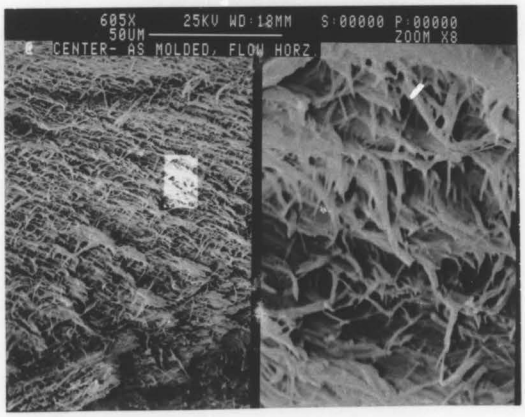

b

Figure 5.4 SEM micrographs of the edge (a) and center (b) of plaques of HBA/HNA as molded. MD is horizontal, thickness is vertical.

at the edge, on the other hand, appear to be highly aligned in the flow direction.

In Fig. 5.5 the micrographs of the edge and center of the plaque that was heated without being pressed are shown. Although the edge still has some firbrillar texture, the fibers do not appear to be as well-aligned as the "as molded" sample. The center has also changed to an isotropic collection of droplets ranging in size from one to tens of microns.

The next two figures, 5.6 and 5.7, contain micrographs of samples which were pressed to 74% of their original thickness nonisothermally. The top figure (a) in these and succeeding figures was taken at the very edge of the plaque, the middle (b) from one photo width in from the edge (about 150μm), and the bottom (c) from the center of the plaque. With no lubrication (Fig. 5.6), the edge loses its fibrillar character altogether, being replaced by a rather amorphous looking texture. The fibers do remain to some extent in b and c, but are not as prominant as in the undeformed sample. Under this particular deformation, the bending modulus, which reflects the structure of the outermost fibers, is reduced to only about 25% of its undeformed value (to 3 GPa).

In contrast, the photos in Fig. 5.7 show only a modest reduction in "fibrosity." Partially mutilated fibers are in evidence at the outermost edge (a), and they seem to be

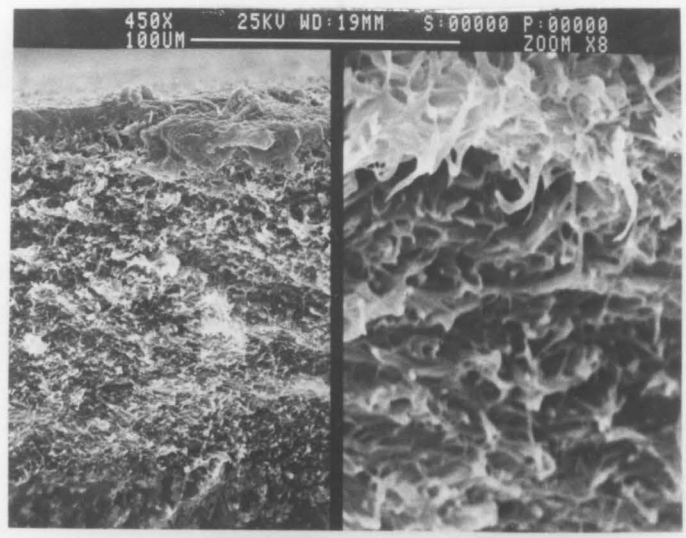

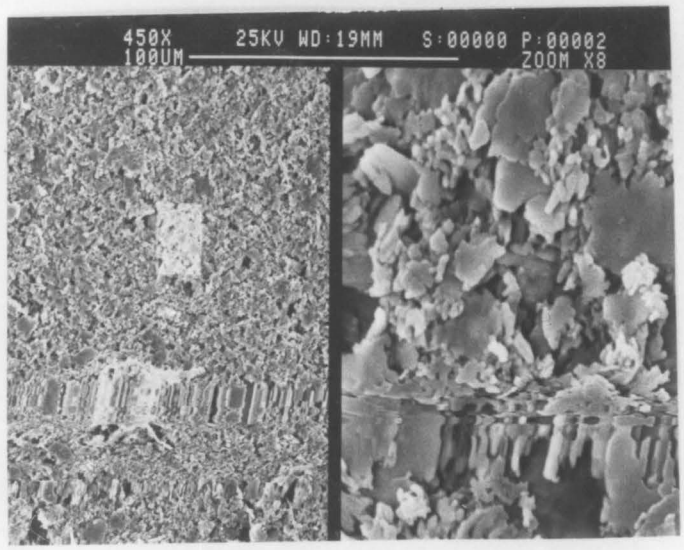

Figure 5.5 SEM micrographs of HBA/HNA plaque heated to 295°C without deformation: top is the edge and bottom is the center of the plaque.

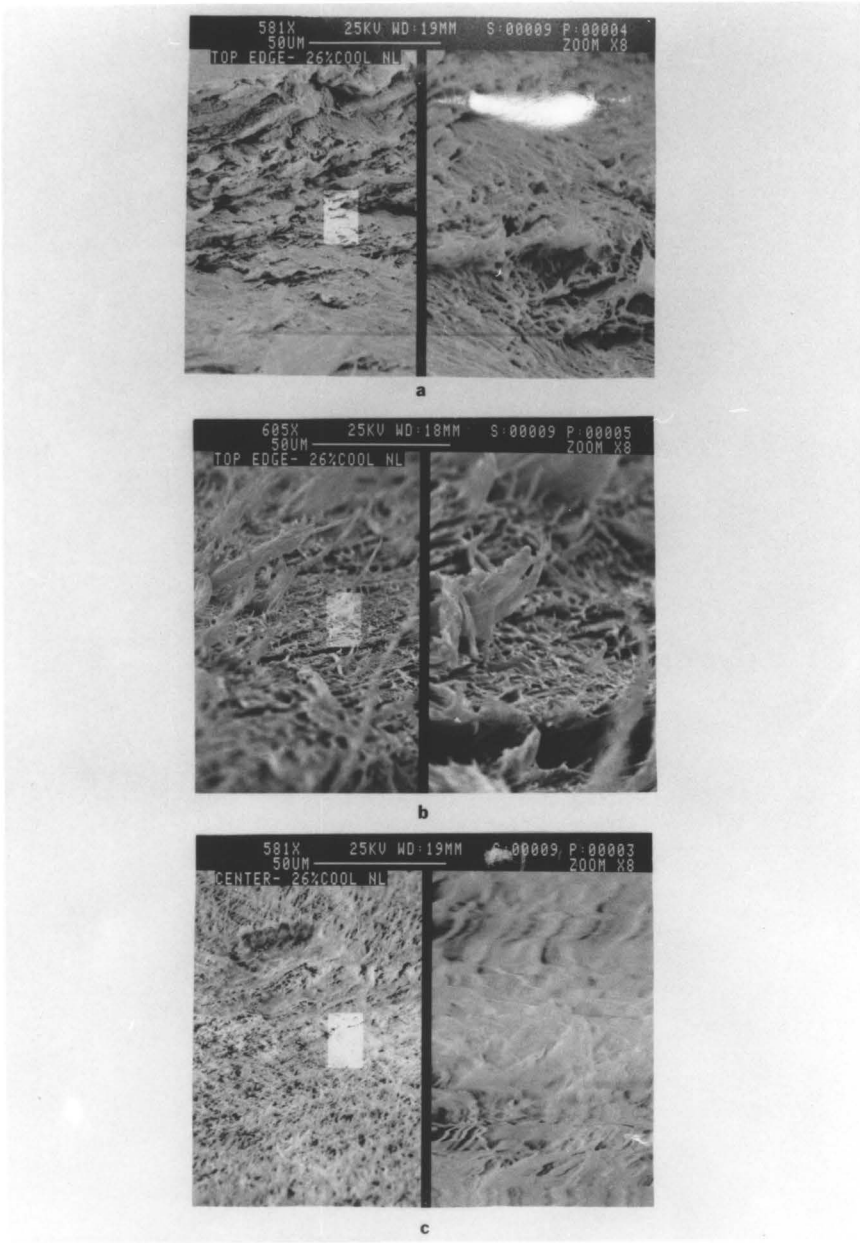

Figure 5.6 SEM micrographs of plaques of HBA/HNA pressed 26% from 295°C nonisothermally without lubrication: a) top edge; b) 150μm in from the edge; c) center. MD is horizontal and thickness is vertical.

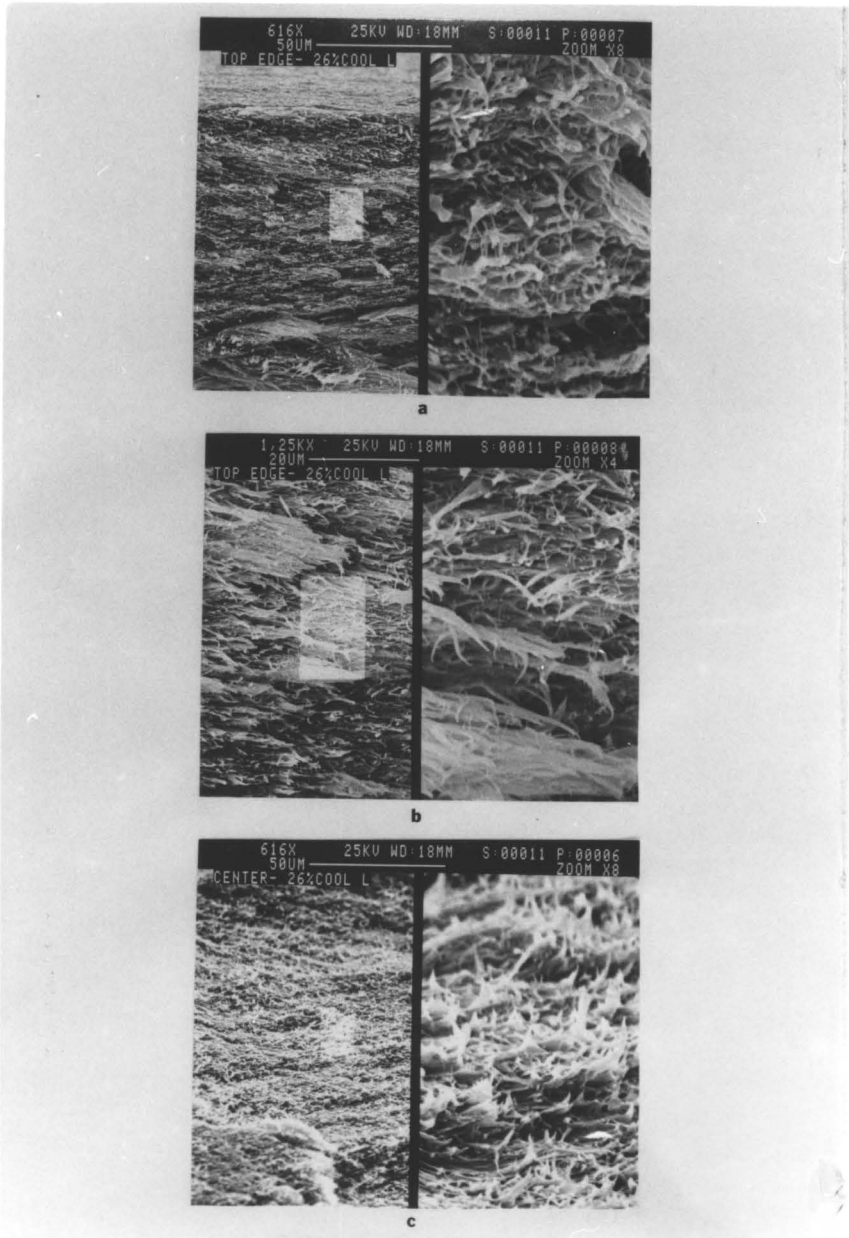

Figure 5.7 SEM micrographs of plaques of HBA/HNA pressed 26% from 295°C nonisothermally with lubrication: a) top edge; b) 150μm in from the edge; c) center. MD is horizontal and thickness is vertical.

relatively undisturbed 150μm in from the edge. The center remains a mat of relatively unoriented fibers. Here the modulus is over 5 GPa, still less than half the initial modulus before deformation but significantly better than under the same deformation without lubrication (Fig. 5.6) in which the outer structure was wholly destroyed.

The nonisothermal pressings of 10% thickness reduction were not as catastrophic in terms of structural changes as were the 26% thickness reductions. In Figs. 5.8 and 5.9 these results may be seen. In both cases the very edge of the samples show mutilated fibers, which are relatively undisturbed 150μm in from the surface of the plaque. The center in both instances was little changed from the undeformed state. The decrease in modulus and strength, although significant, was not as severe as for the samples which underwent the greater thickness reduction.

The structure of the isothermally pressed specimens was somewhat different. The outermost fibers (about 30-50μm) appear to be melted or fused together, as shown in Figs. 5.10a, 5.11a, and 5.12a. The micrograph taken about 150μm in from the edge shows fibers similar to those at the edge of the undeformed samples (Figs. 5.11b and 5.12b). The center remained largely fibrillar (Figs. 5.10b and 5.12c), but portions tended to lose their structure as viewed under the electron microscope (Figs. 5.10c and 5.11c). This phenomenon might be associated with

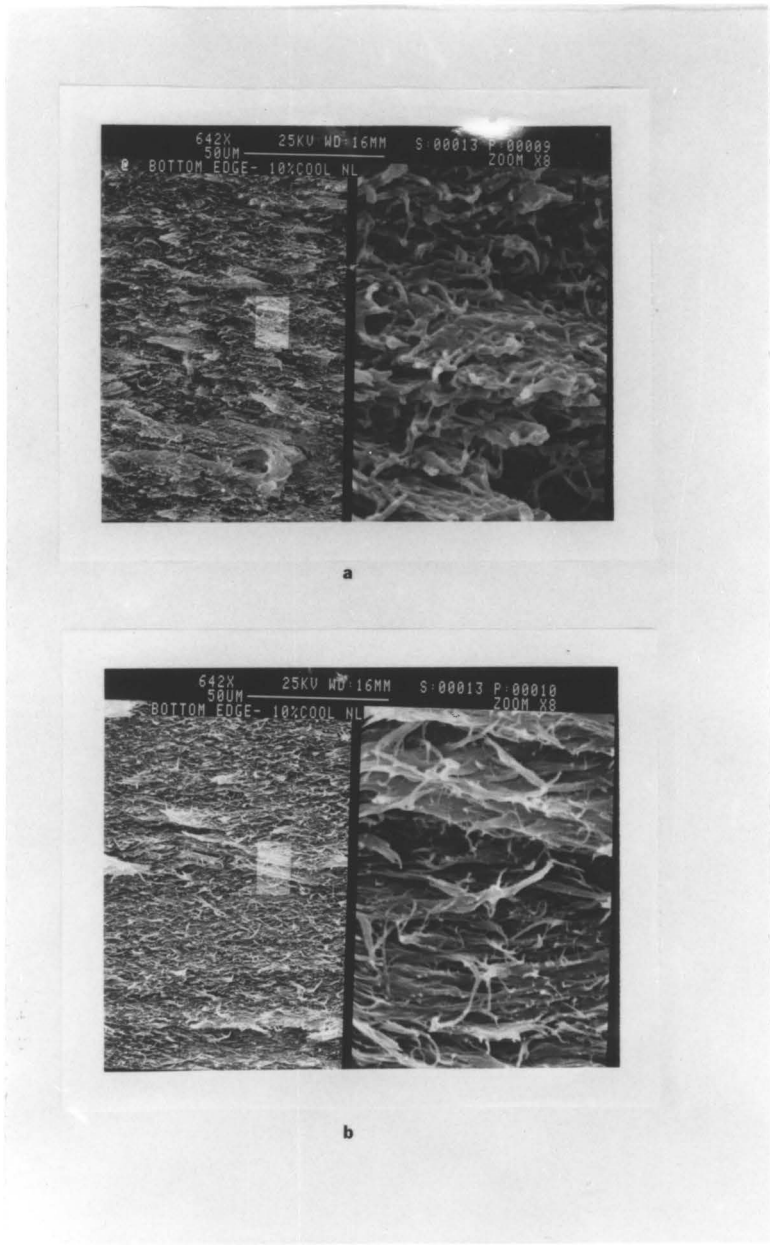

Figure 5.8 SEM micrographs of plaques of HBA/HNA pressed 10% from 295°C nonisothermally without lubrication: a) top edge; b) 150μm in from the edge. MD is horizontal and thickness is vertical.

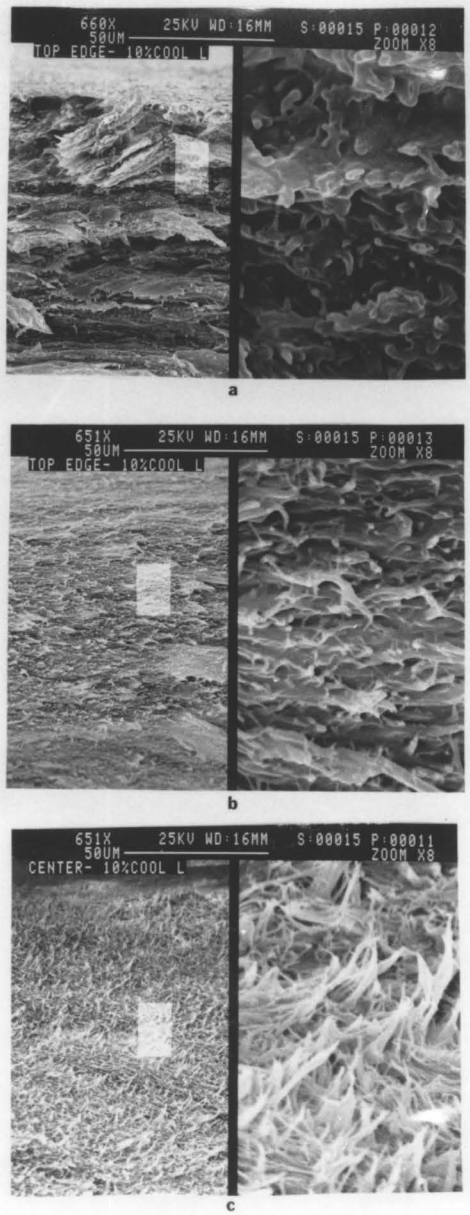

Figure 5.9 SEM micrographs of plaques of HBA/HNA pressed 10% from 295°C nonisothermally with lubrication: a) top edge; b) 150µm in from the edge; c) center. MD is horizontal and thickness is vertical.

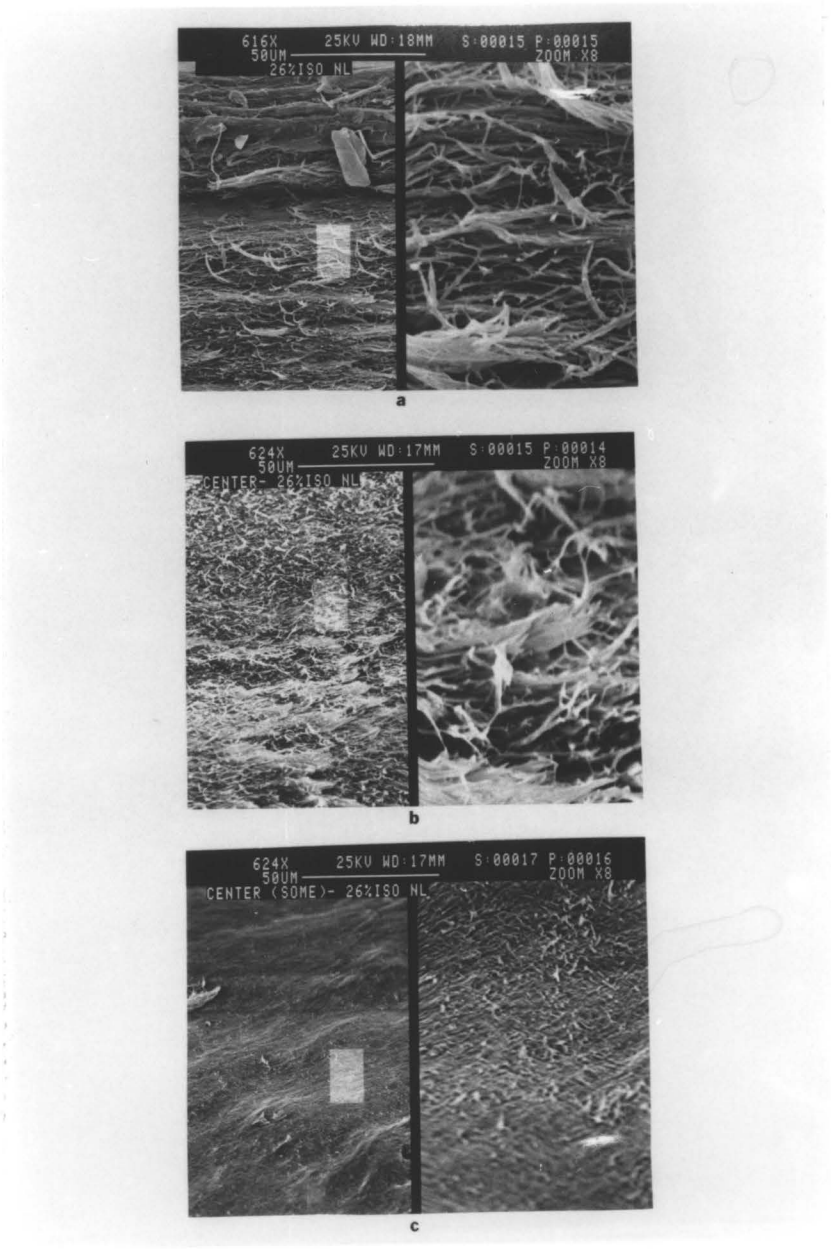

Figure 5.10 SEM micrographs of plaques of HBA/HNA pressed 26% from 265°C isothermally without lubrication: a) top edge; b) center (some); c) center (most). MD is horizontal and thickness is vertical.

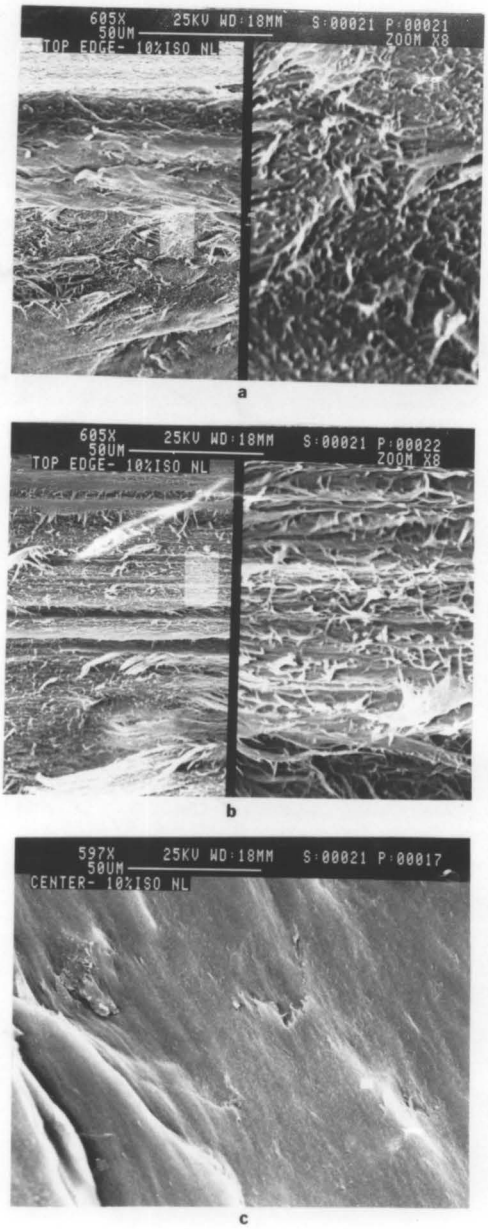

Figure 5.11 SEM micrographs of plaques of HBA/HNA pressed 10% from 265°C isothermally without lubrication: a) top edge; b) 150μm in from the edge; c) center. MD is horizontal and thickness is vertical.

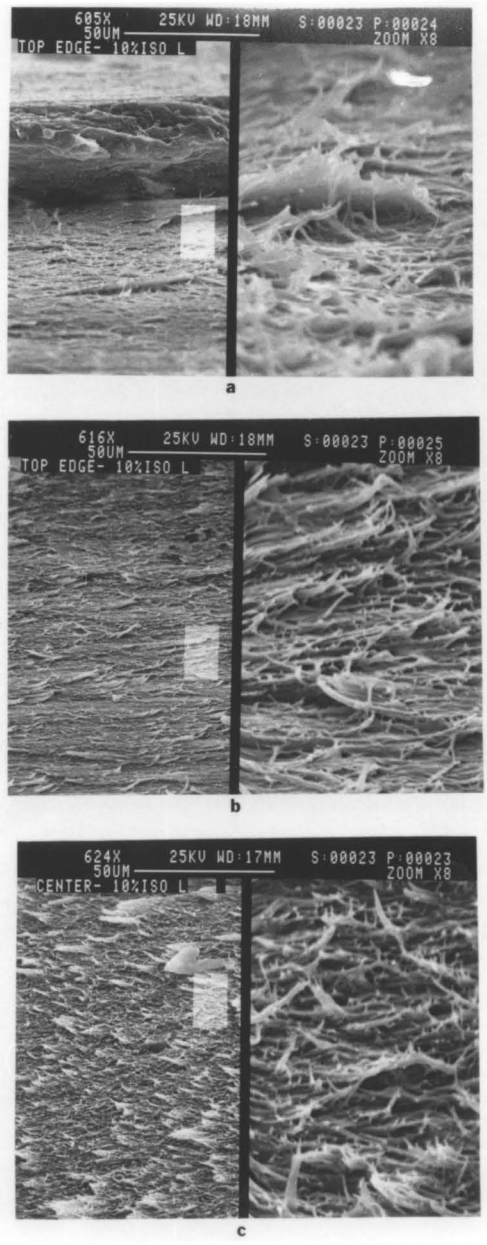

Figure 5.12 SEM micrographs of plaques of HBA/HNA pressed 10% from 265°C isothermally with lubrication: a) top edge; b) 150µm in from the edge; c) center. MD is horizontal and thickness is vertical.

localized melting of the core in some instances. The smaller amount of structural disruption evident in the isothermally pressed samples is reflected in better flexural modulus values, particularly for the 10% reduction. Strength values were inferior for all pressing conditions compared to the unpressed samples, but this was most probably due to small surface imperfections which caused premature failure of the specimens.

Wide angle x-ray results normal to the surface of the pressed plaques are shown in Figs. 5.13-5.15. In the first of these three figures the pattern of the as molded plaque is shown (machine direction vertical and transverse direction horizontal). A significant degree of molecular alignment in the flow direction in the mold is evidenced by the equatorial scattering from the specimen. The non-isothermally pressed plaques were characterized by WAXS in Fig. 5.14. For the 10% reduction some preferential orientation in the machine direction remains (c and d), but that order is removed upon further pressing. The top two patterns (a and b) were obtained from plaques squeezed to 74% of their initial thickness. With lubrication (b) no significant degree of azimuthal intensity dependence is noticeable. If the sample is squeezed with a lubricating oil, however (a), a slight transverse direction orientation becomes noticeable. The tensile properties reflect the molecular orientation: the less machine direction

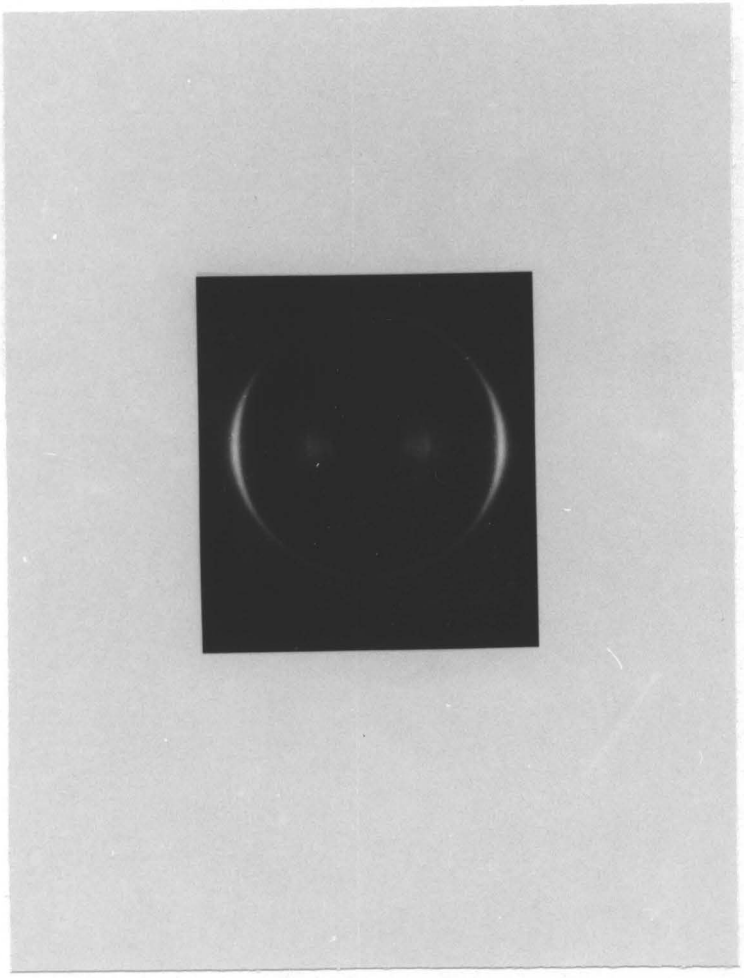

Figure 5.13 WAXS diffraction pattern for plaques of HBA/HNA as molded. MD is vertical, TD is horizontal.

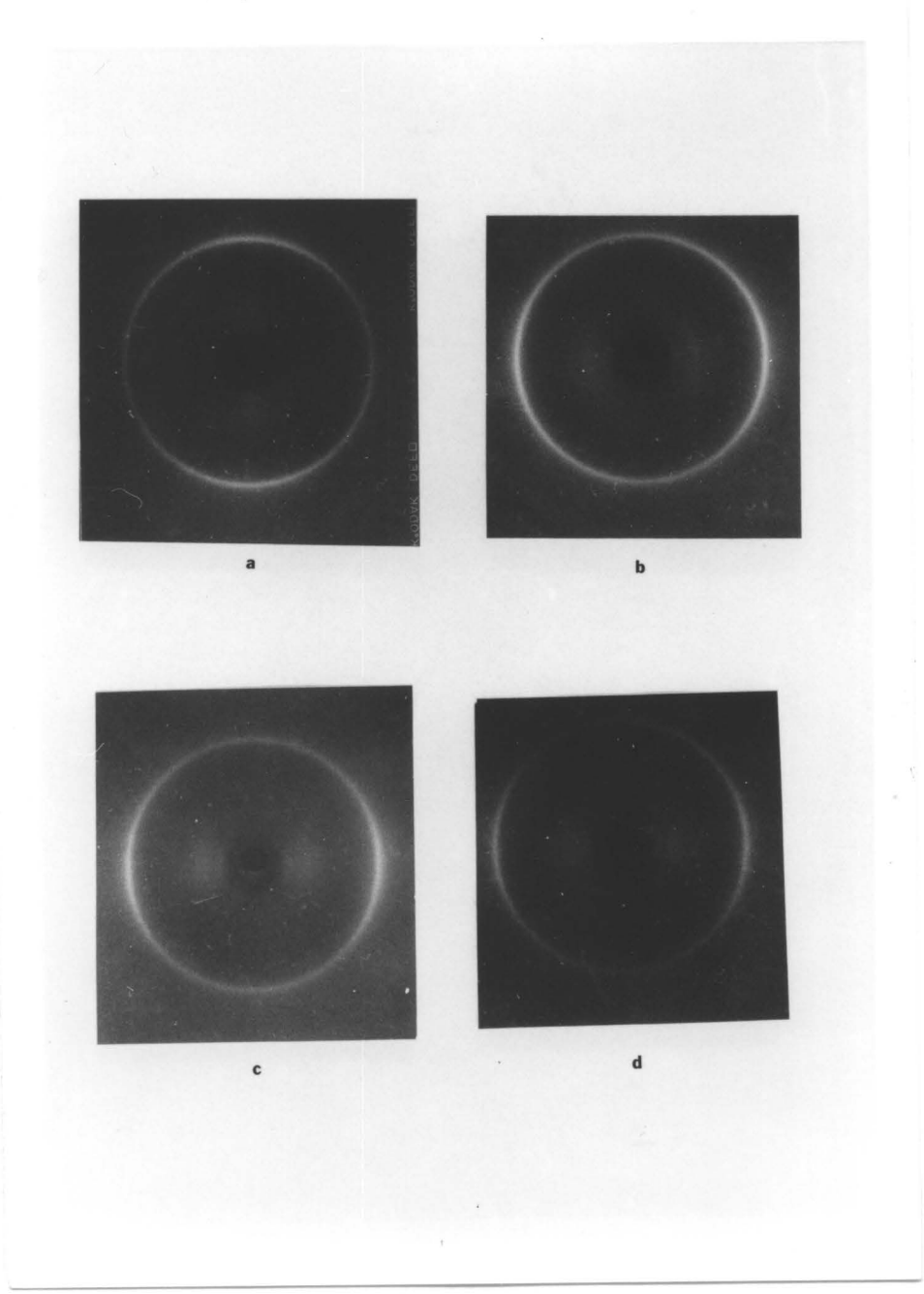

Figure 5.14 WAXS patterns for plaques of HBA/HNA pressed while cooling from 295°C: a) 26%, no lube; b) 26%, lube; c) 10%, no lube; d) 10%, lube.

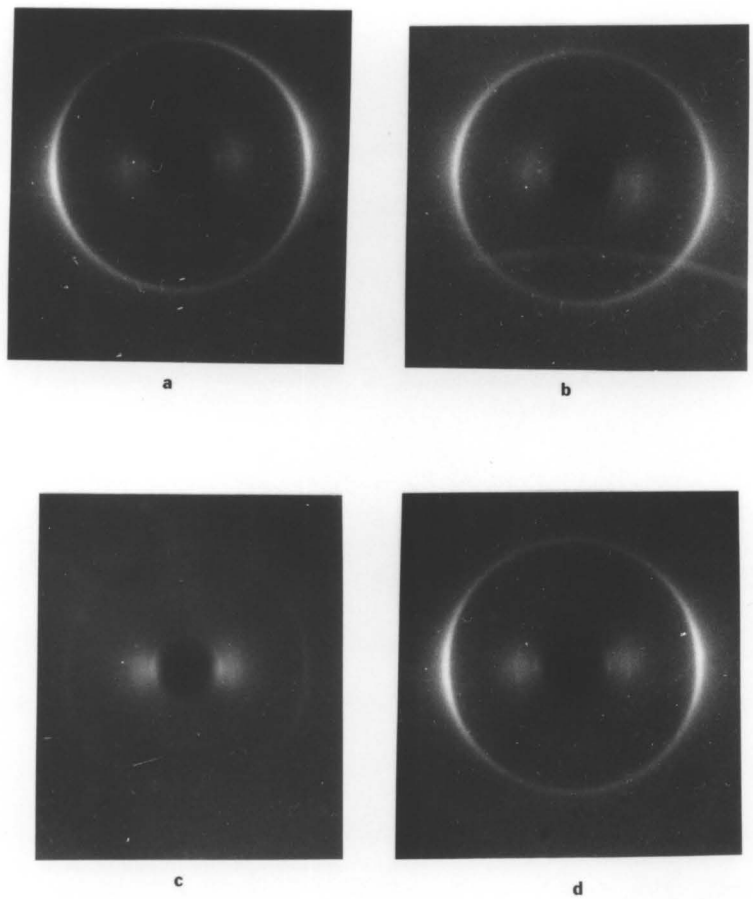

Figure 5.15 WAXS patterns for plaques of HBA/HNA pressed isothermally at 265°C: a) 26%, no lube; b) 26%, lube; c) 10%, no lube; d) 10%, lube.

orientation present, the less different the MD and TD modulus and strength. For the 26% reduction in thickness without lubrication, the transverse properties are identical (within error) to those in the machine direction.

The x-ray results for the isothermally pressed plaques show no significant change in molecular orientation with pressing (Fig. 5.15). Mechanical properties confirm this finding, showing no increase in transverse properties as with the nonisothermally pressed plaques. Hence the mechanical properties may be correlated with molecular orientation as well as structural and textural changes observed with electron microscopy.

The difference in the microscopy and mechanical results between the two copolyesters is intriguing. For the HBA/PET system, the properties and structure became more uniaxial in nature, whereas for the naphthoic copolyester a balance of properties was observed, particularly when the sample was nonisothermally pressed. This difference may be attributed to the fact that in the former case no fibrillar texture was present in the center of the sample prior to deformation. Thus, during the nonisothermal pressing, this region tended to deform without disturbing the surrounding fibrils: in other words parallel to their long axes. The result was an increase in the uniaxial nature of the plaque. In contrast, the HBA/HNA material was initially fibrous throughout the plaque,

although the center region did not appear to be as highly aligned. Even before the nonisothermal deformation at 295°C occurred, though, the thermal treatment tended to decrease the order present in the outermost fibers as well as radically alter the structure of the core. Thus, some degree of biaxiality could be imparted during the deformation. Overall the mechanical properties declined significantly more than would be expected based solely on the orientation of the molecules. The electron microscopy results chronicled the adverse effect the deformation had on the structure of the fibers.

Some of the difference between the two copolyesters may be explained by the fact that for the HBA/PET system, the deformation occurred below the melting point for this material where annealing effects were minimal for the time of the deformation. In contrast, the temperature to which the material was initially heated for nonisothermal deformation had to be greater than the melting point in order to induce any deformation while cooling. Thus, the isothermal results, which took place at a temperature below T_m, were superior to those of the nonisothermally deformed plaques. Calculations similar to those for the HBA/PET polymer indicated that the temperature reached 215°C by the conclusion of the deformation process, also in agreement with the cooling curves in Fig. 2.15 (see Appendix B).

In this section the experimental results obtained from pressing injection molded plaques were analyzed in terms of the effect of deformation and thermal history on the structure and properties of the material. Next, the effect of varying the thermal history on properties and orientation of extrusion blow molded bottles of both copolyesters will be examined.

5.2 Extrusion Blow Molding

Another method of imparting biaxial orientation in polymers during processing is blow molding. In this process a parison is extruded through an annular die, a mold clamped around it, and air blown into the mold, expanding the parison against the mold walls. Although it was difficult to accurately control the deformation and thermal histories with the laboratory setup employed, this method proved effective in obtaining a variety of structures and orientations in the final product - a bottle.

Wide angle x-ray (WAXS) diffraction patterns, SEM micrographs, and tensile property data were obtained on extrusion blow molded bottles of both copolyesters under consideration. First the Instron results will be presented, followed by the microscopy and x-ray data together to facilitate comparisons between the two techniques.

All data points reproduced in Table 5.5 for blow molded bottles of HBA/PET represent the average of at least three samples and sometimes as many as five. Transverse (hoop direction) values could not be obtained for all barrel and die temperatures because of gross non-uniformity in thickness in some instances. It should be noted that all specimens were taken from the midsection of the bottle; although SEM and WAXS were done on other portions of each bottle, mechanical test specimens could

TABLE 5.5

Tensile Properties of
Extrusion Blow Molded Bottles of HBA/PET

(Axial Direction)

Barrel/Die Temp. °C	E_T MPa	σ_{max} MPa	Elongation %
220/180	2800 (336)	50.5 (6.70)	10.9 (3.5)
220/190	1760 (134)	38.5 (6.23)	33.0 (4.7)
220/200	2620 (356)	54.0 (2.50)	10.2 (4.6)
260/190	5150 (668)	81.5 (16.6)	6.6 (3.1)
260/200	3490 (338)	58.7 (23.7)	7.1 (4.2)
275/190	6130 (1039)	98.2 (37.9)	7.5 (4.2)
275/200	4000 (907)	73.2 (16.0)	7.8 (1.7)

(Transverse or Hoop Direction)

220/190	4260 (660)	84.9 (24.4)	7.4 (1.4)
260/200	1750 (111)	43.7 (2.89)	16.1 (2.0)
275/190	1390 (283)	29.8 (13.3)	19.4 (11.2)

Standard deviations are given in parentheses.

only be obtained from the midddle of the blow molded bottle (see Fig. 5.16 for a schematic representation of a blown bottle).

When the barrel temperature was either 260 or 275°C the tensile properties of the resulting bottle were indicative of uniaxial orientation in the direction of the long axis of the parison (z direction). The properties of the bottle obtained with a barrel temperature of only 220°C were quantitatively different. The axial modulus was about half that of the high temperature extruded bottles, at about 2.50 GPa. A strength of 50 MPa was somewhat less also, but the difference was not as dramatic.

The notable exception to the above results of bottles extruded at 220°C occurred with a 190°C die temperature, at which point the bottle tended to show properties much greater in the hoop direction than in the axial direction. Modulus and strength in the axial direction were in the same range as those obtained in the transverse direction at the two highest barrel temperatures, about 1.75 GPa and 40 MPa, respectively.

Scanning electron microscopy and x-ray analysis reinforced the mechanical property data. The orientation observed in the diffraction patterns and the morphology seen under the microscope are also in qualitative agreement with each other. The axial, or z direction, is vertical in both SEM and WAXS diffraction patterns. SEM

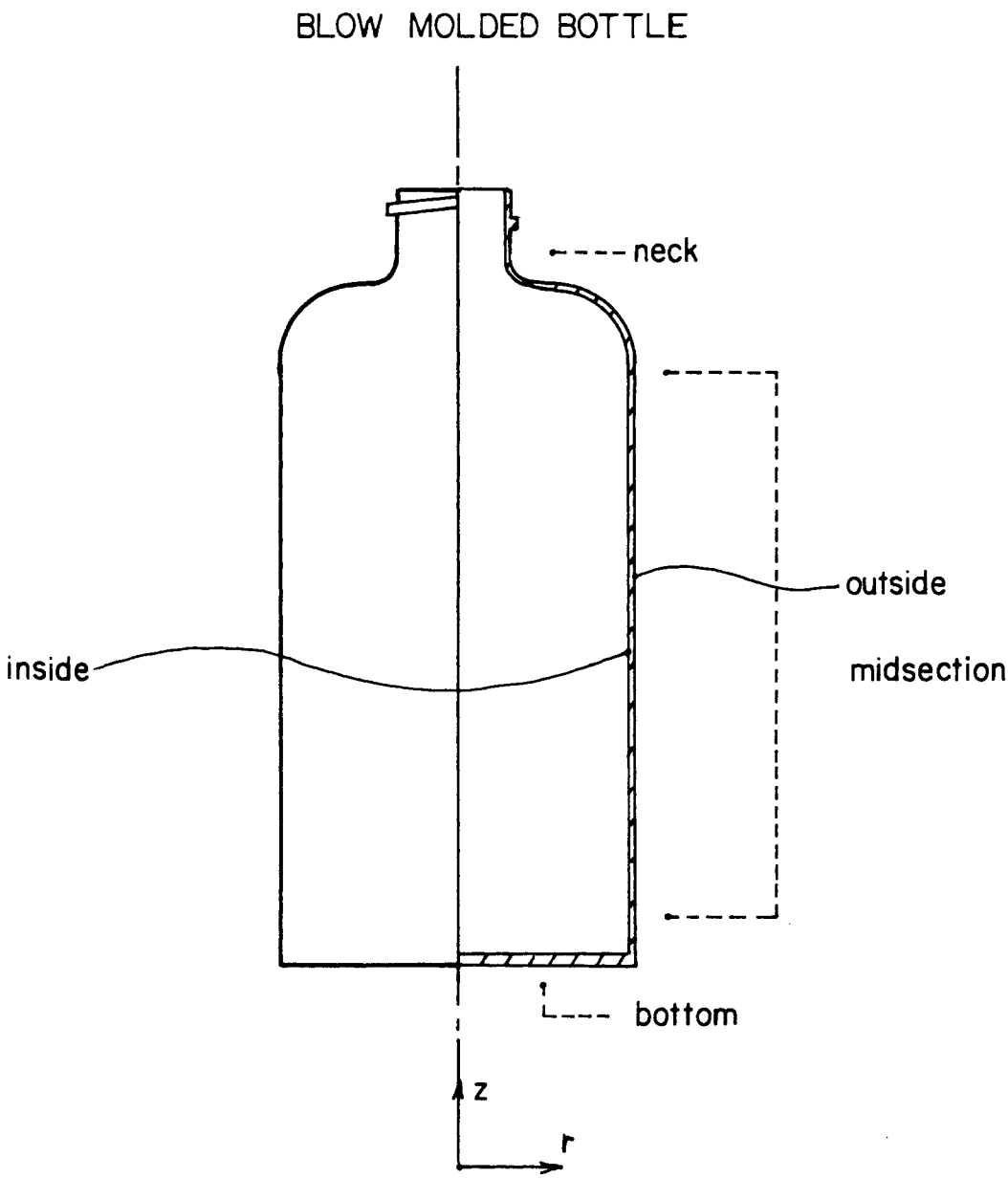

Figure 5.16 Schematic representation of a blown bottle, showing the locations from which SEM and WAXS samples were taken.

photographs were taken of both the inside and the outside surfaces of the bottle (see Fig. 5.15). Also shown are the neck and bottom regions from which additional samples for analysis were taken in some instances. WAXS patterns were taken through the thickness of each bottle (no microtoming), and thus represent an average orientation.

First, the results obtained from the midsection of each bottle will be discussed, followed by the patterns obtained from the neck and bottom regions, unblown parisons, and free blown specimens (in the latter case no mold was used and the material was permitted to air cool).

In Fig. 5.17 SEM photos and the corresponding WAXS patterns are shown for the bottles extruded at a 275°C barrel temperature and a 190°C die temperature. The orientation is uniaxial along the z direction, which is vertical in all instances. The morphology is fibrillar, particularly at the outer surface. The results from the bottle with the same barrel temperature and a 200°C die temperature were somewhat different, as may be seen in Fig. 5.18. The lower degree of orientation present may be due to greater relaxation of structure at the higher exit temperature.

Similarly, die temperature had only a slight effect on the morphology and orientation of bottles extruded with a barrel temperature of 260°C. The higher barrel temperature resulted in a sample with with a slightly more dif-

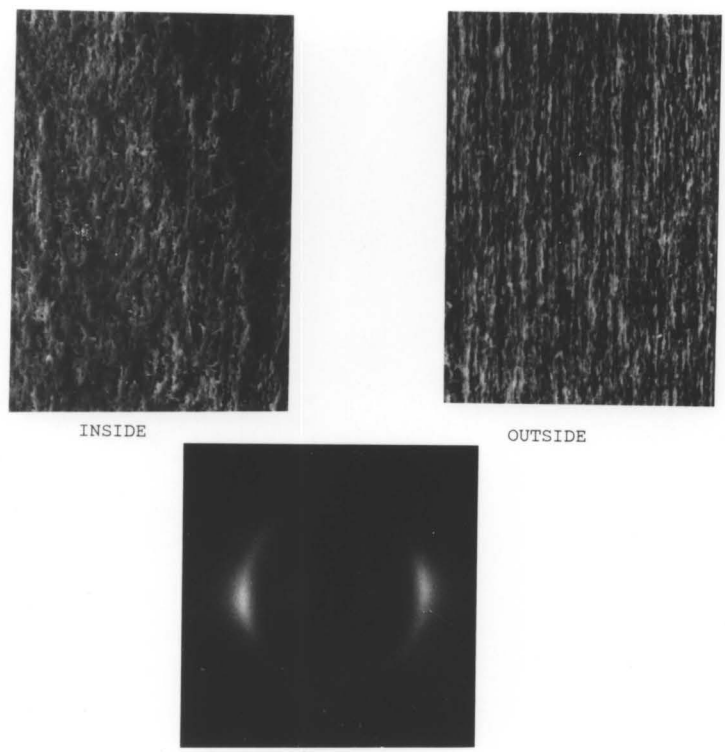

Figure 5.17 SEM micrographs of etched surfaces and WAXS patterns of blow molded bottles of HBA/PET 60/40; T_b=275, T_d=190°C. Micrographs (x480) and WAXS patterns have z direction vertical.

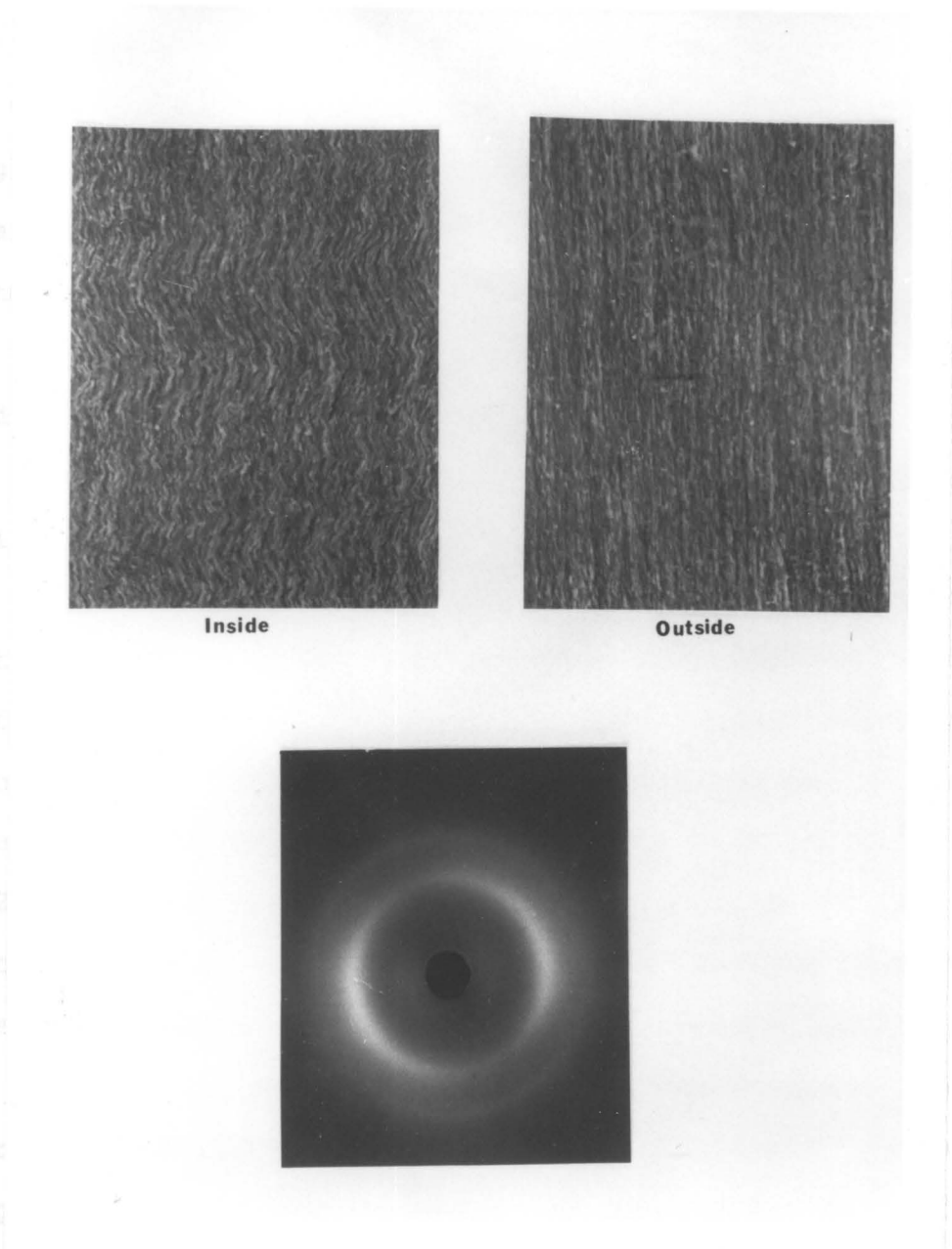

Figure 5.18 SEM micrographs of etched surfaces and WAXS patterns of blow molded bottles of HBA/PET 60/40; T_b=275, Td=200°C. Micrographs (x480) and WAXS patterns have z direction vertical.

fuse diffraction pattern, but no noticeable difference in the texture of the samples (compare Figs. 5.19 and 5.20). As with the 275° barrel temperature, the bottles showed a higher degree of z direction orientation on the outside than on the inside, probably due to more relaxation occurring during extrusion of the parison on the inside because of the quenching effect of the cold mold walls on the outside of the bottle.

While the uniaxial orientation shown by WAXS was not quite as strong at the intermediate barrel temperature as it was at a 275°C extrusion temperature, the results obtained at the lowest barrel temperature were strikingly different. With a 220°C barrel and 200°C die temperature, the specimens exhibited biaxial orientation, as shown by the four lobes of high intensity on the WAXS photo in Fig. 5.21. The SEM micrographs show a fibrous texture on the outside and a "transversely stretched" fibrous texture on the inside surface. Almost identical results may be seen in Fig. 5.22 at the 180°C die temperature and the low barrel temperature. Here the inner surface SEM photo is magnified only 200x instead of 480x as are each of the other micrographs to better show the long range texture of the bottle.

The bottles extruded at a die temperature of 190°C (T_B=220°C) are startlingly different, as seen in Fig. 5.23. The WAXS pattern for a thick sample shows a pro-

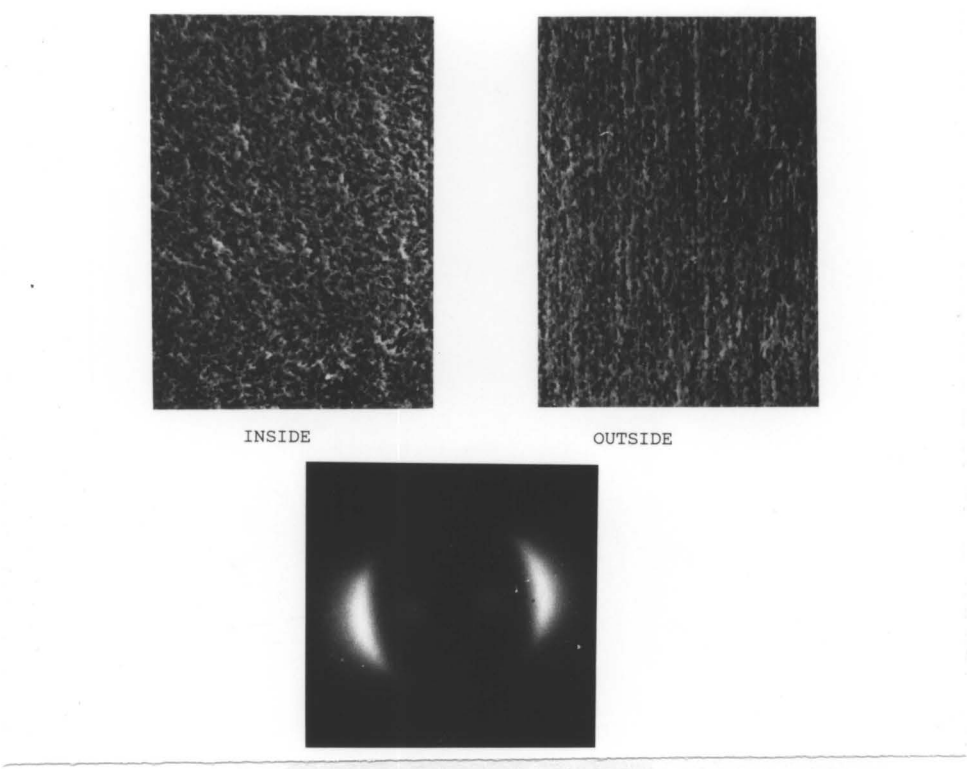

Figure 5.19 SEM micrographs of etched surfaces and WAXS patterns of blow molded bottles of HBA/PET 60/40; T_b=260, T_d=190°C. Micrographs (x480) and WAXS patterns have z direction vertical.

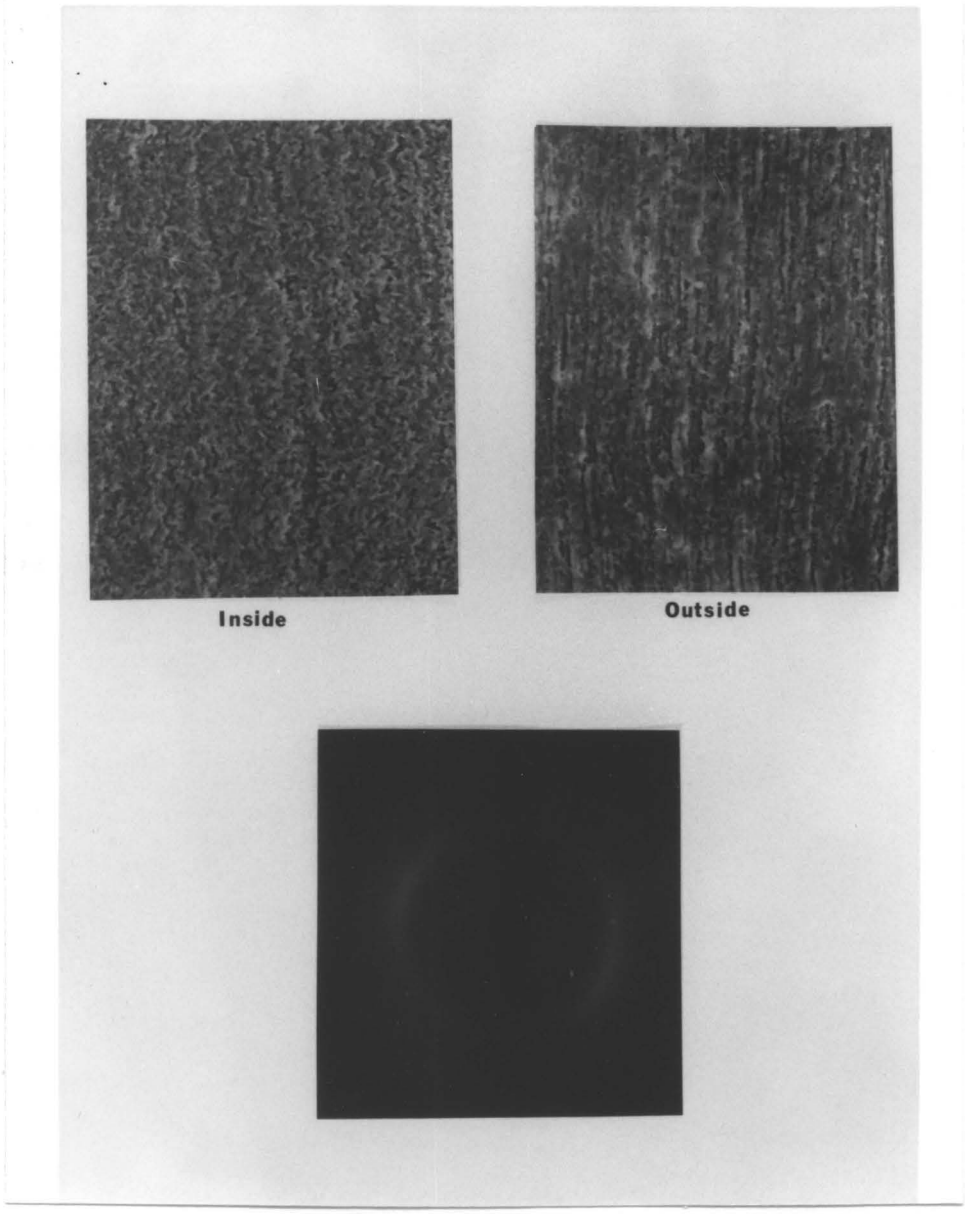

Figure 5.20 SEM micrographs of etched surfaces and WAXS patterns of blow molded bottles of HBA/PET 60/40; T_b=260, Td=200°C. Micrographs (x480) and WAXS patterns have z direction vertical.

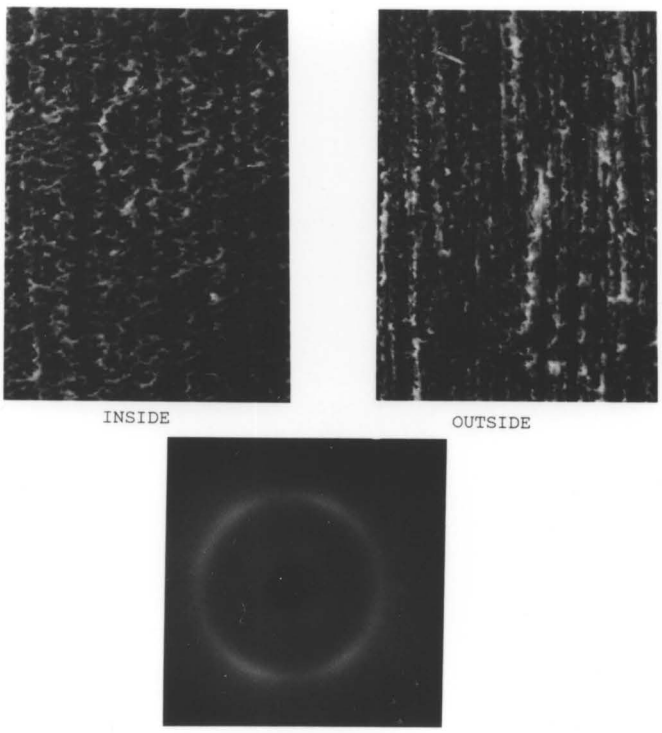

Figure 5.21 SEM micrographs of etched surfaces and WAXS patterns of blow molded bottles of HBA/PET 60/40; T_b=220, T_d=200°C. Micrographs (x480) and WAXS patterns have z direction vertical.

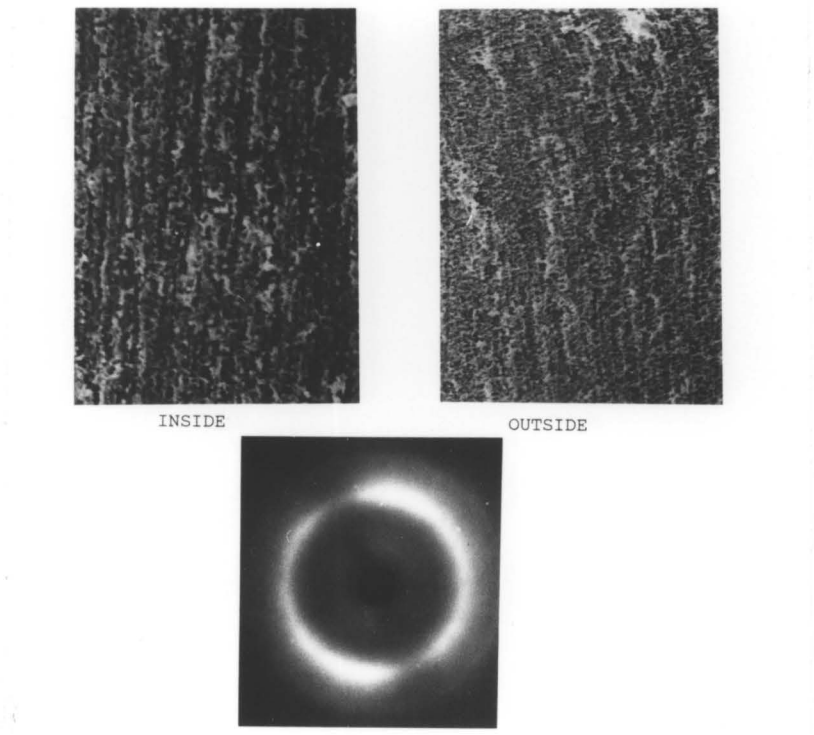

Figure 5.22 SEM micrographs of etched surfaces and WAXS patterns of blow molded bottles of HBA/PET 60/40; T_b=220, Td=180°C. Micrographs (x480) and WAXS patterns have z direction vertical.

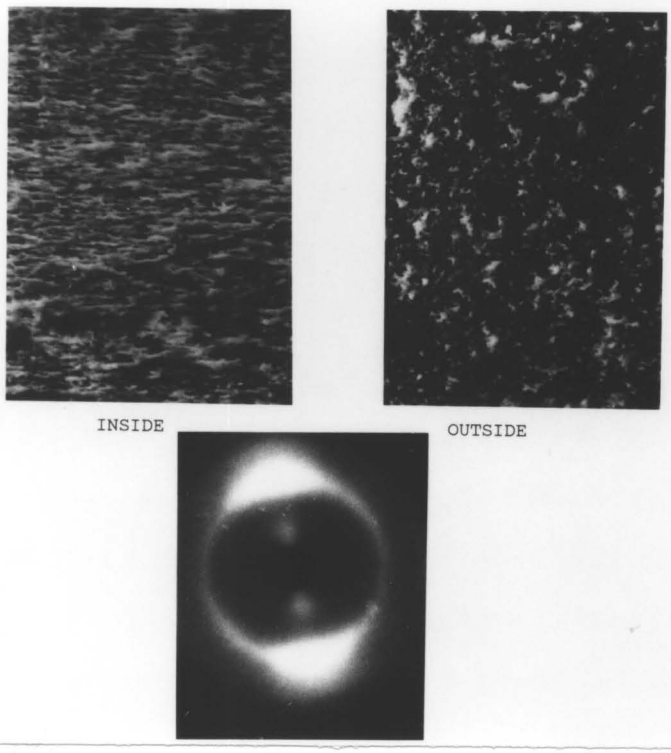

Figure 5.23 SEM micrographs of etched surfaces and WAXS patterns of blow molded bottles of HBA/PET 60/40; T_b=220, T_d=190°C. Micrographs (x480) and WAXS patterns have z direction vertical.

nounced orientation in the hoop (Θ) direction. The micrograph of the inside surface reinforces the x-ray result, showing a fibrous texture perpendicular to the axial direction. The micrograph of the outside surface shows relatively little preferential alignment of the copolyester.

Wide angle x-ray micrographs were taken parallel to the surface of the bottle in the midsection region in order to determine whether there existed a planar molecular orientation. In Fig. 5.24 these results are shown for three different thermal histories. As can be seen, there is a fairly high correlation of orientation in the plane of the surface in all cases, irrespective of the order shown when the x-rays impinge normal to the surface. Hence samples with biaxial or uniaxial alignment in either the transverse direction or the machine direction have a high degree of orientation in the plane of the surface of the bottle.

The mechanical property data, shown in Table 5.5, agree well with the microscopy and the x-ray results. The lowest axial direction modulus and strength occur where the orientation was seen in the hoop direction. The biaxially oriented specimens have significantly higher modulus and strength, and those that gave a uniaxial diffraction pattern indicating z direction orientation have the highest values. Among these latter, the bottles

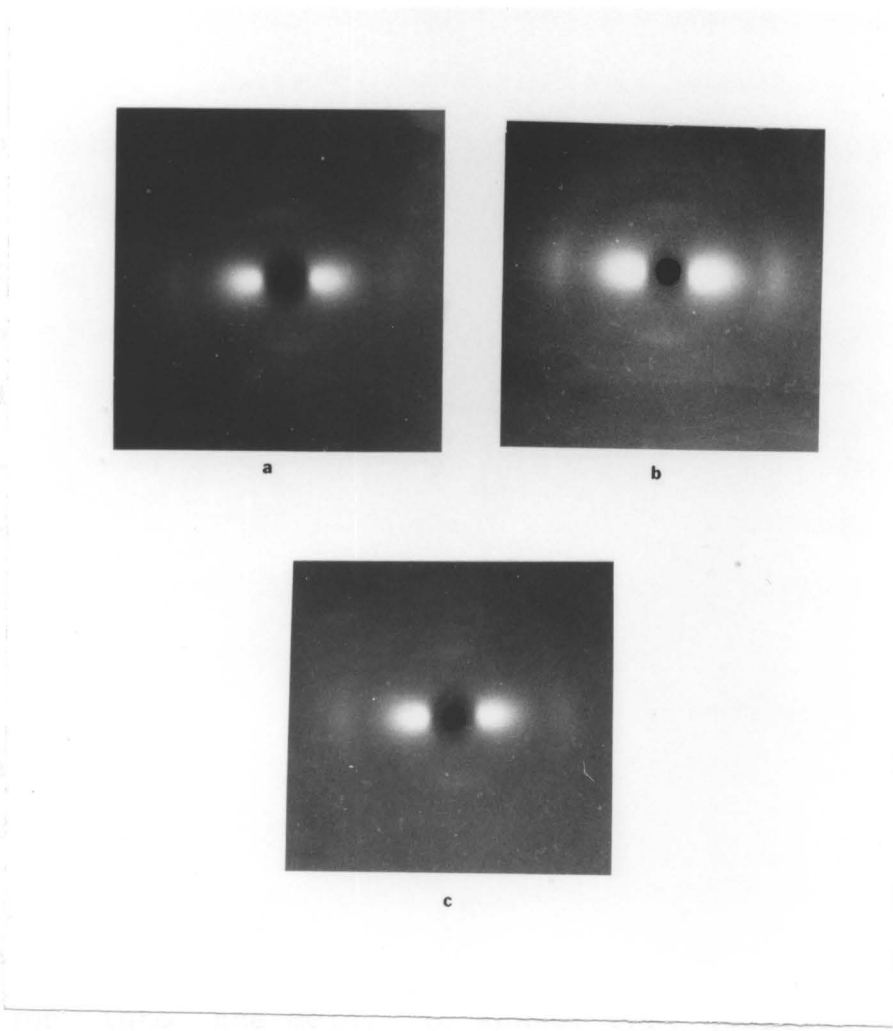

Figure 5.24 WAXS micrographs of extrusion blow molded bottles taken parallel to surface: a) T_b = 220°C, Td = 190°; b) T_b = 220°, Td = 200°; c) Tb = 260°, Td = 190°. Thickness (r) direction is vertical, z direction is horizontal.

extruded through the 190° die exhibit the most fibrillar structure and the narrowest bands of azimuthal intensity, and have modulus values over 5 GPa and strengths approaching 100 MPa. Likewise, the transverse direction tensile properties agree well with the SEM and WAXS results.

To explain the results summarized in detail above, one must account for the effects of both the thermal and deformation histories on the bottles. In extrusion blow molding these bottles, the deformation history was not varied so that the effects of differing thermal histories could be more readily analyzed. Given the similar deformation history in each case (see experimental chapter), the effect of changing the temperature in both the barrel and die heating zones was studied. Despite the limitations on the die temperatures, a complete spectrum of structures resulted in the bottles.

The question ramained, however, whether the structure observed had been imparted during or prior to blowing the parison into the mold. To answer that question, further work was done on unblown parisons and on other portions of each bottle (see Fig. 5.16).

For bottles extruded at a 220°C barrel temperature, WAXs and SEMS were taken on unblown parisons and on the bottoms of the bottles in order to compare the structure and orientation with the midsection of the bottle. At a 190°C die temperature, the results in Figs. 5.25 and 5.26

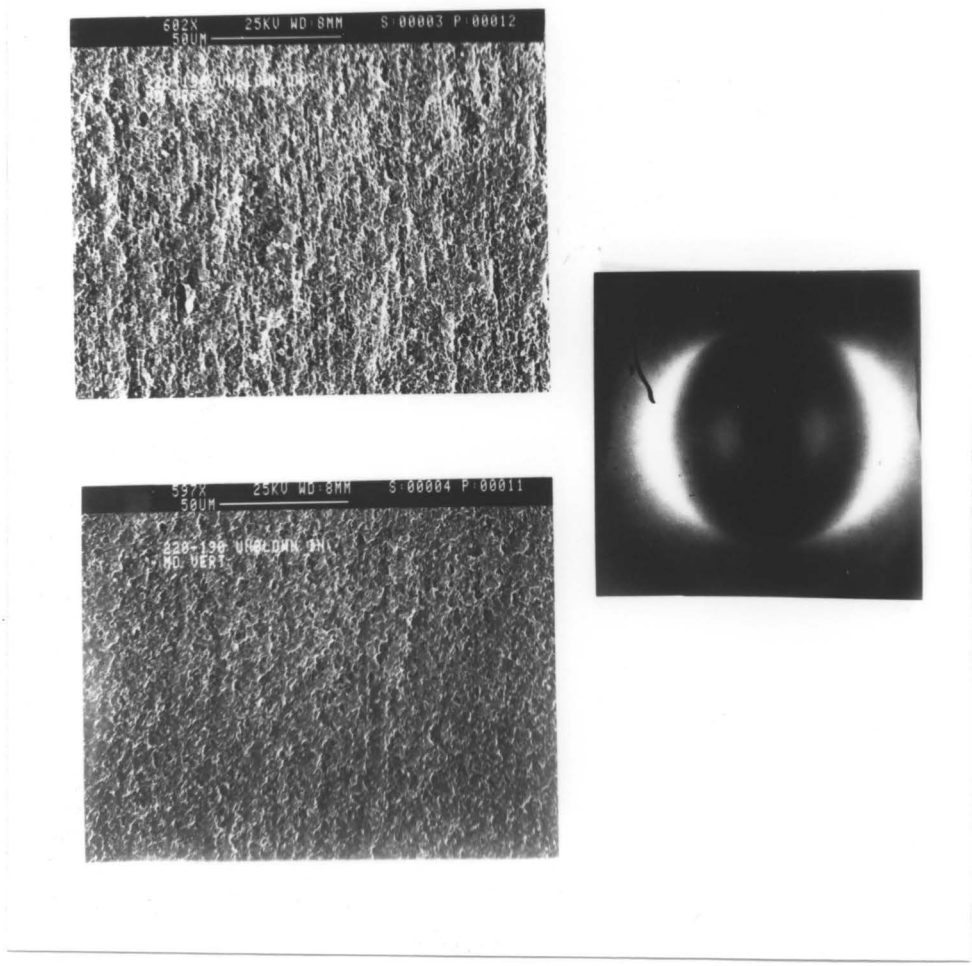

Figure 5.25 WAXS patterns and SEM micrographs of unblown parisons for the 220°-190° extrusion blow molded bottles: top micrograph is inside surface, bottom is outside surface. MD is vertical, Θ direction horizontal.

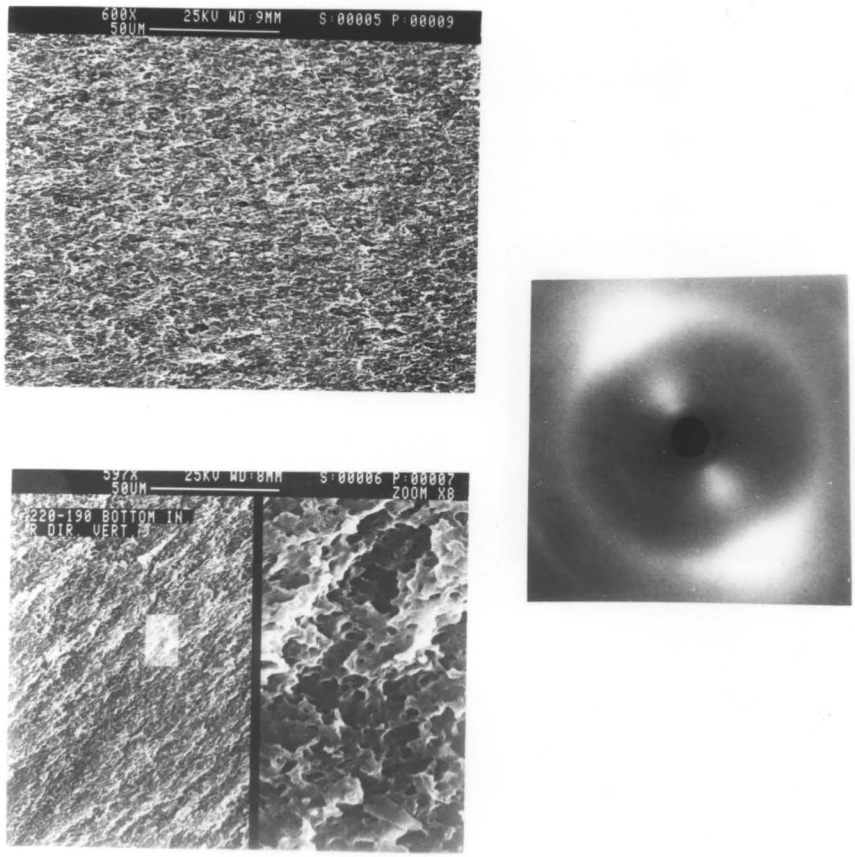

Figure 5.26 WAXS and SEM results of the bottom of the 220°-190° extrusion blow molded bottles: top micrograph is outside surface, bottom is inside surface. R direction is vertical, Θ direction is horizontal.

were obtained. The unblown parison showed a relatively high degree of z-direction orientation as indicated by WAXS and a fibrillar texture in that direction, particularly on the outside, but it was also noticeable on the inside of the specimen (Fig. 5.25). Thus, the hoop direction orientation and texture observed for the midsection of this bottle must be imparted during the blowing process. The bottom of the bottle showed an orientation intermediate between the r and Θ directions, as seen in Fig. 5.26. This structure is especially evident on the inside of the bottle.

Similarly, the orientation present in the midsection of the bottle extruded through a 200°C die appears to be imparted during the blowing process itself - essentially a planar extensional deformation. In Fig. 5.27 the orientation of the unblown parison is seen to be fairly high in the z (vertical) direction. Thus the biaxial structure in evidence in Fig. 5.19 must arise during blowing into the mold. The bottom of the bottle, seen in Fig. 5.28, shows an orientation intermediate between the r and Θ directions, similar to the bottle extruded through a 190°C die (Fig. 5.26). The difference between the two morphological textures and molecular orientation may be due to the higher stress developed at the lower die temperature causing a greater amount of molecular and structural change: hence the transverse orientation can develop.

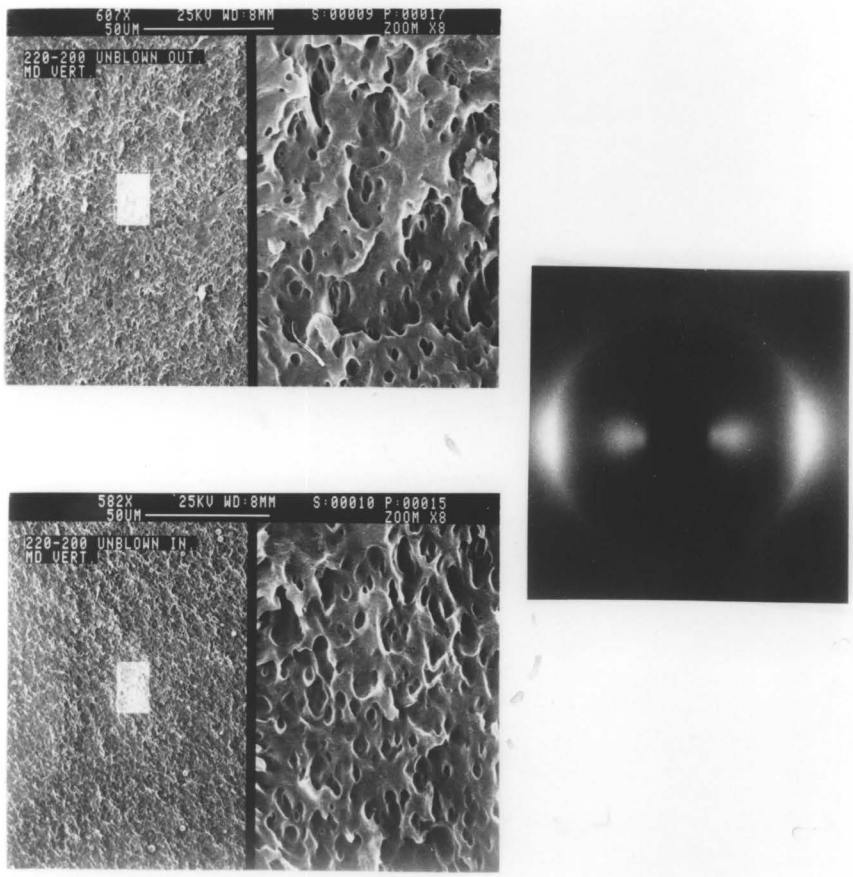

Figure 5.27 WAXS patterns and SEM micrographs of unblown parisons taken normal to the surface for the 220°-200° extrusion blow molded bottles: top micrograph is inside surface, bottom is outside surface. MD is vertical, Θ direction is horizontal.

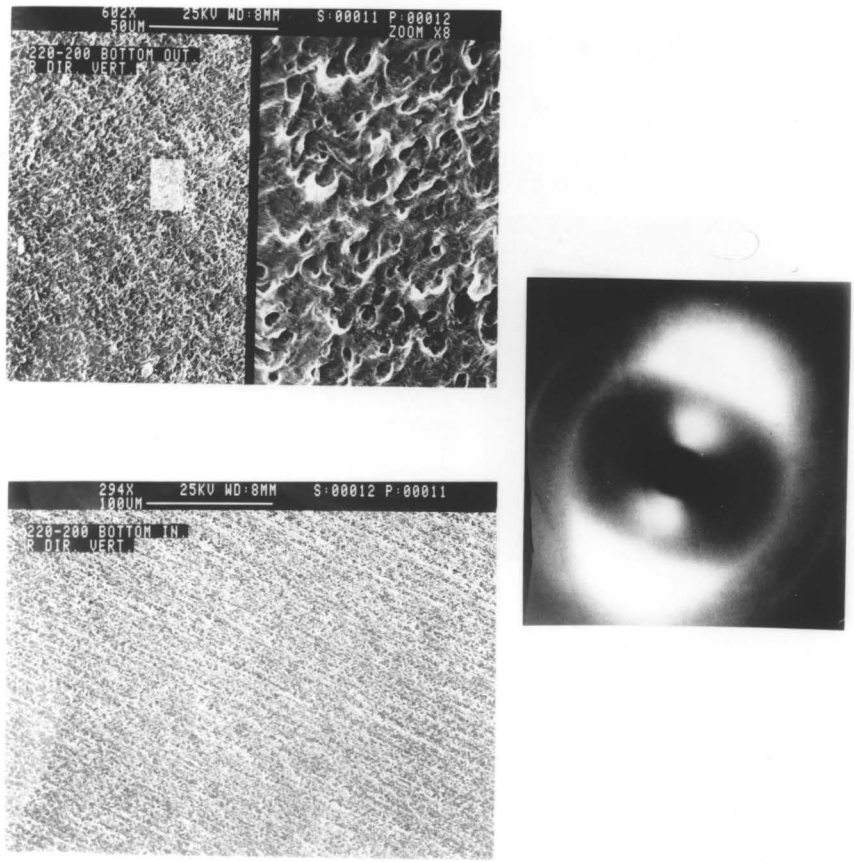

Figure 5.28 WAXS and SEM results of the taken normal to the bottom of the 220°-200° extrusion blow molded bottles: top micrograph is outside surface, bottom is inside surface. R direction is vertical, Θ direction is horizontal.

Parisons of HBA/PET were also free blown in order to analyze the effect of that deformation compared to blowing into a cold mold. In Table 5.6 the tensile properties of both this material and the Vectra copolyester which resulted from this process are shown. Machine and transverse direction values were not significantly different: the modulus and strength were about 5 GPa and 110 MPa, respectively. These values approach uniaxial properties, possibly because the film was only on the order of 0.1 mm in thickness, and hence contained little core structure. In Fig. 5.29 the resulting SEM and WAXS patterns are shown. The electron micrographs, particularly on the outside surface of the blown bubble, show little structural order. The WAXS pattern corresponds to this texture, with only a slight ordering of the molecules present, as shown by a nominal amount of azimuthal intensity dependence in a direction intermediate between the machine and transverse directions. This elimination of z-direction order possible in blown LCPs gave impetus to examining the structural development arising during free film blowing, the topic of section 5.4.

The HBA/HNA system was also blow molded under different barrel and die temperatures. Tensile results in both the machine and hoop directions are given in Table 5.7. The modulus and strength, although higher in the machine than in the transverse direction, was only 4.1 GPa and

TABLE 5.6

Tensile Properties of Free Blown Copolyesters

Copolyester	Direction	E_T (GPa)	σ_{max} (MPa)
HBA/PET (220°/200°)	MD	4.34 (1.18)	101 (28)
HBA/PET (220°/200°)	TD	6.09 (0.62)	125 (6.6)
HBA/HNA (300°/290°)	MD	5.94 (0.14)	157 (30)
HBA/HNA (300°/290°)	TD	6.47 (0.68)	139 (38)

Standard deviations are given in parentheses

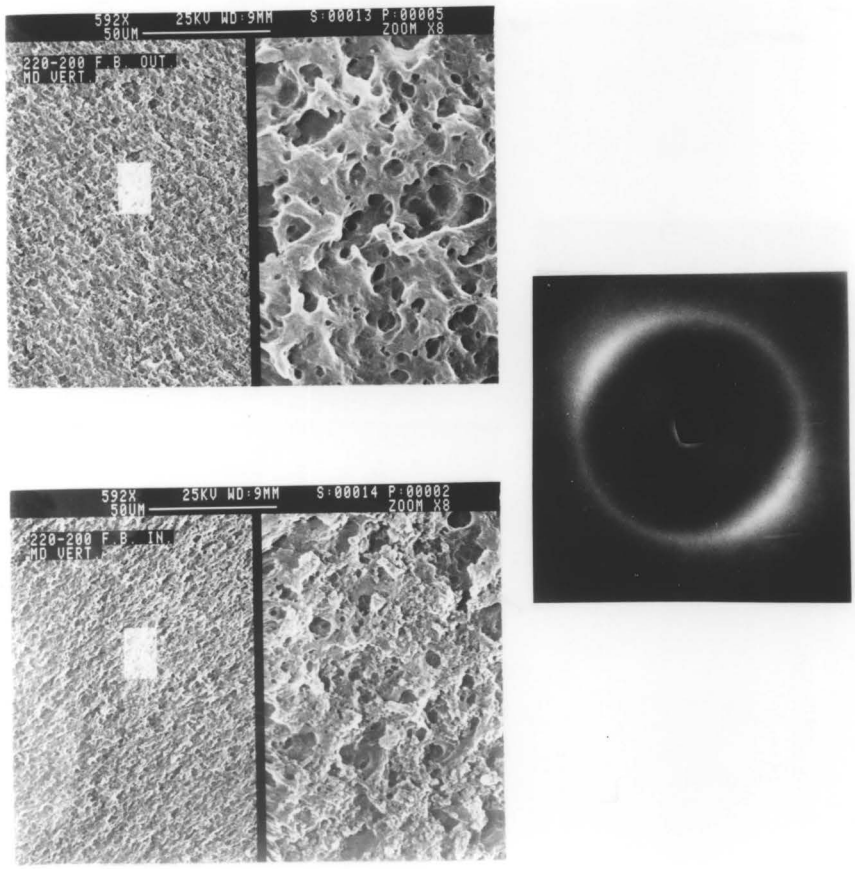

Figure 5.29 WAXS and SEM taken normal to the surface of free blown bubble of HBA/PET (220°-200°): top micrograph is outside surface, bottom is inside surface. MD is vertical, Θ direction is horizontal.

TABLE 5.7

Tensile Properties of HBA/HNA Bottles

Temp.,°C (Barrel/Die)	Direction	E_T (GPa)	σ_{max} (MPa)
300/290	MD	5.69 (.62)	130 (21.9)
320/300	MD	4.11 (0)	97.1 (8.2)
300/290	TD	4.50 (.89)	97.0 (4.9)
320/300	TD	3.00 (.69)	68.4 (4.7)

Standard deviations are given in parentheses.

97 MPa for the 320°C barrel temperature (300°C die temperature). Hoop direction values were somewhat less, but this difference was usually not significant. For the 300°C barrel temperature (290°C die), the properties improved somewhat, to 5.7 GPA and 130 MPa in the machine direction and 4.5 GPa and 97 MPa in the transverse direction. These values in the transverse direction are quite respectable and are supported qualitatively by SEM and WAXS results.

Figs. 5.30-5.33 summarize the results of the microscopy and the x-ray diffraction on the Vectra bottles. For both processing conditions given in Table 5.6, the midsections of the bottles give little preferential orientation as evidenced by WAXS. Similarly, the etched micrographs show a texture that is for the most part directionally independent, as shown in Figs. 5.30 and 5.32. In contrast, the specimens taken from the unblown parisons and the bottoms of the bottles show for both thermal histories a z direction texture (r direction for the bottoms). The WAXS data (Figs. 5.31 and 5.33) support the SEM results qualitatively, showing some (although not a high degree of) azimuthal intensity dependence of the diffraction patterns.

The tensile property results, even where significantly different, indicate only slight machine direction orientation in the midsection of each bottle. Characterization

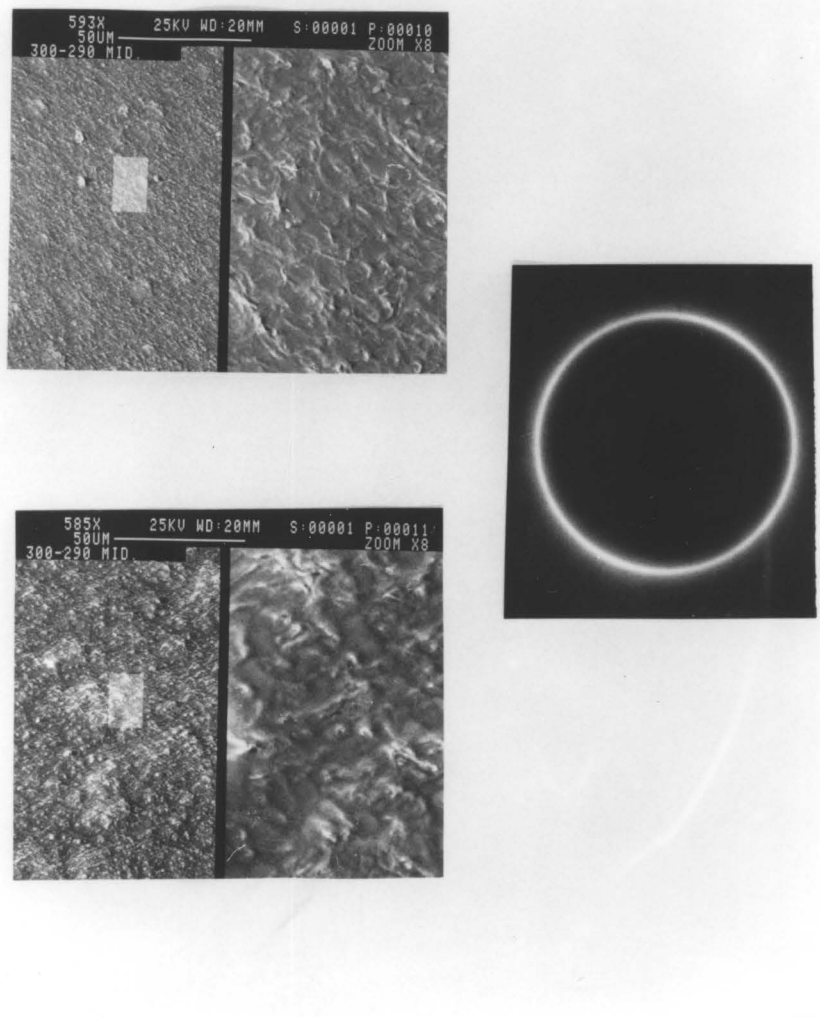

Figure 5.30 SEM and WAXS normal to the surface of blow molded HBA/HNA bottles (T_b = 300°C; T_d = 290°): top micrograph is outside surface, bottom is inside surface. MD is vertical, Θ direction is horizontal.

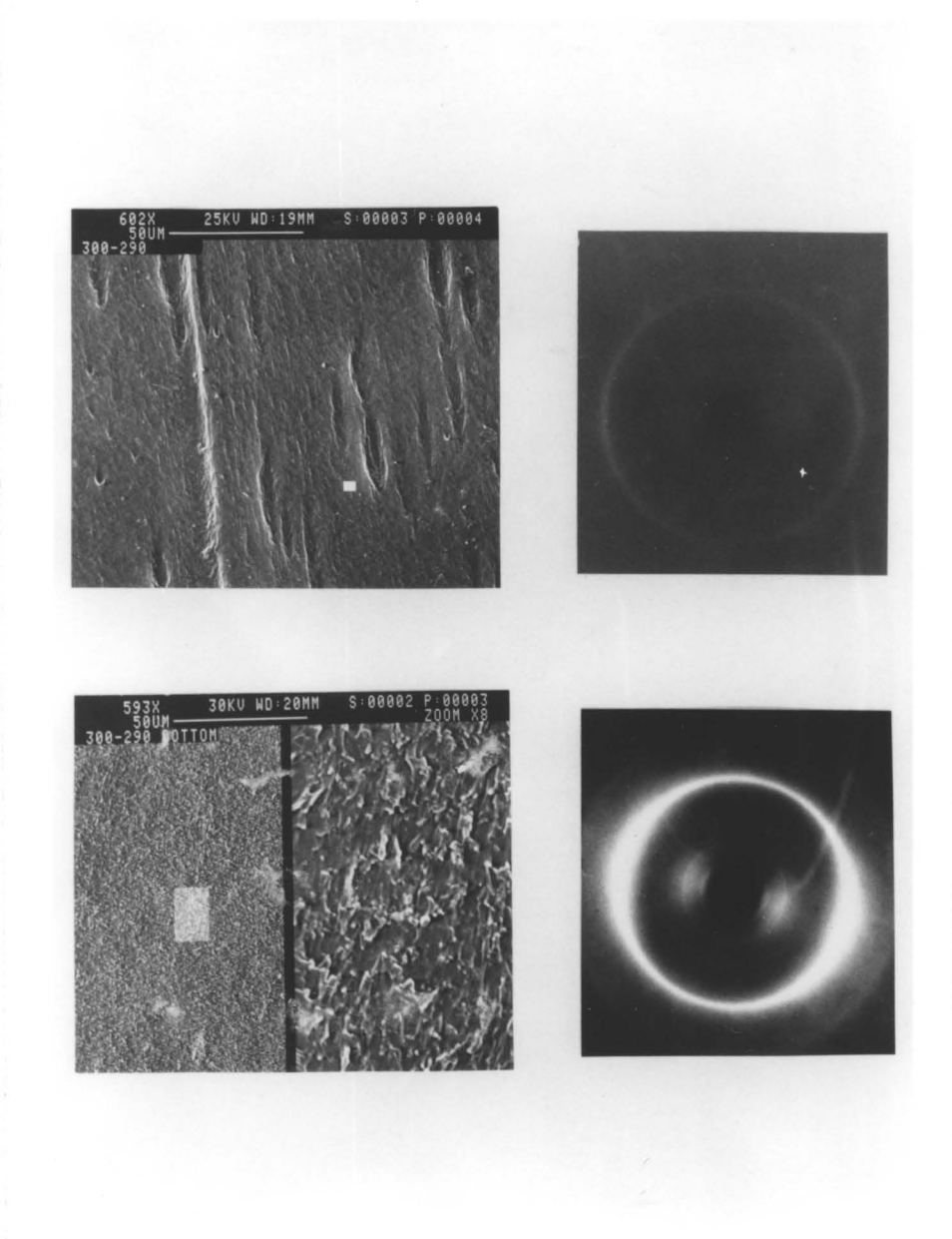

Figure 5.31 SEM micrographs and corresponding WAXS patterns for the unblown parisons (top) and the bottoms (bottom) for the same bottles as in Fig. 5.30. MD is vertical, Θ direction horizontal for the unblown parisons. MD is vertical and R direction horizontal for the bottoms.

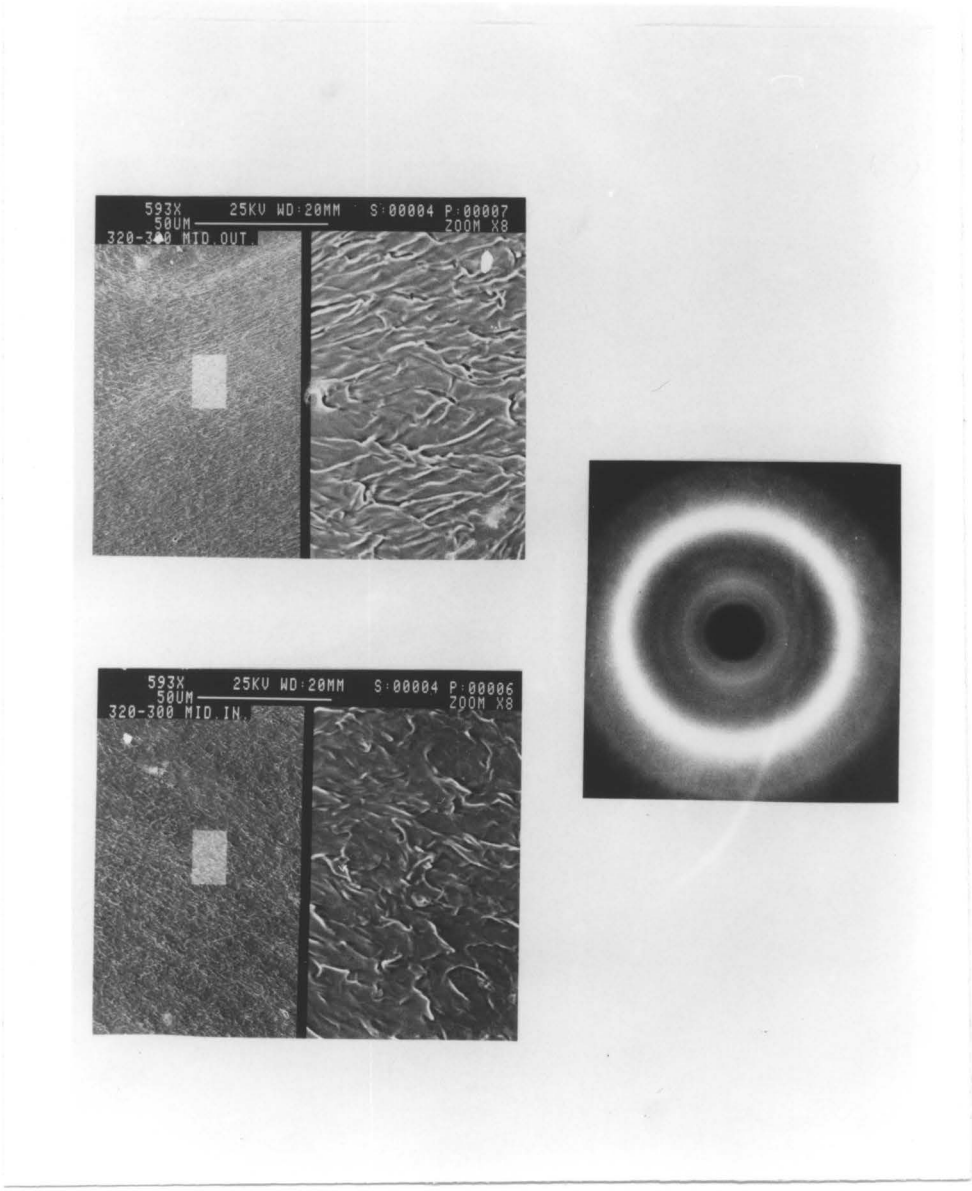

Figure 5.32 SEM and WAXS results of blow molded HBA/HNA bottles (T_b = 320°C; Td = 300°): top micrograph is outside surface, bottom is inside surface. MD is vertical, Θ direction is horizontal.

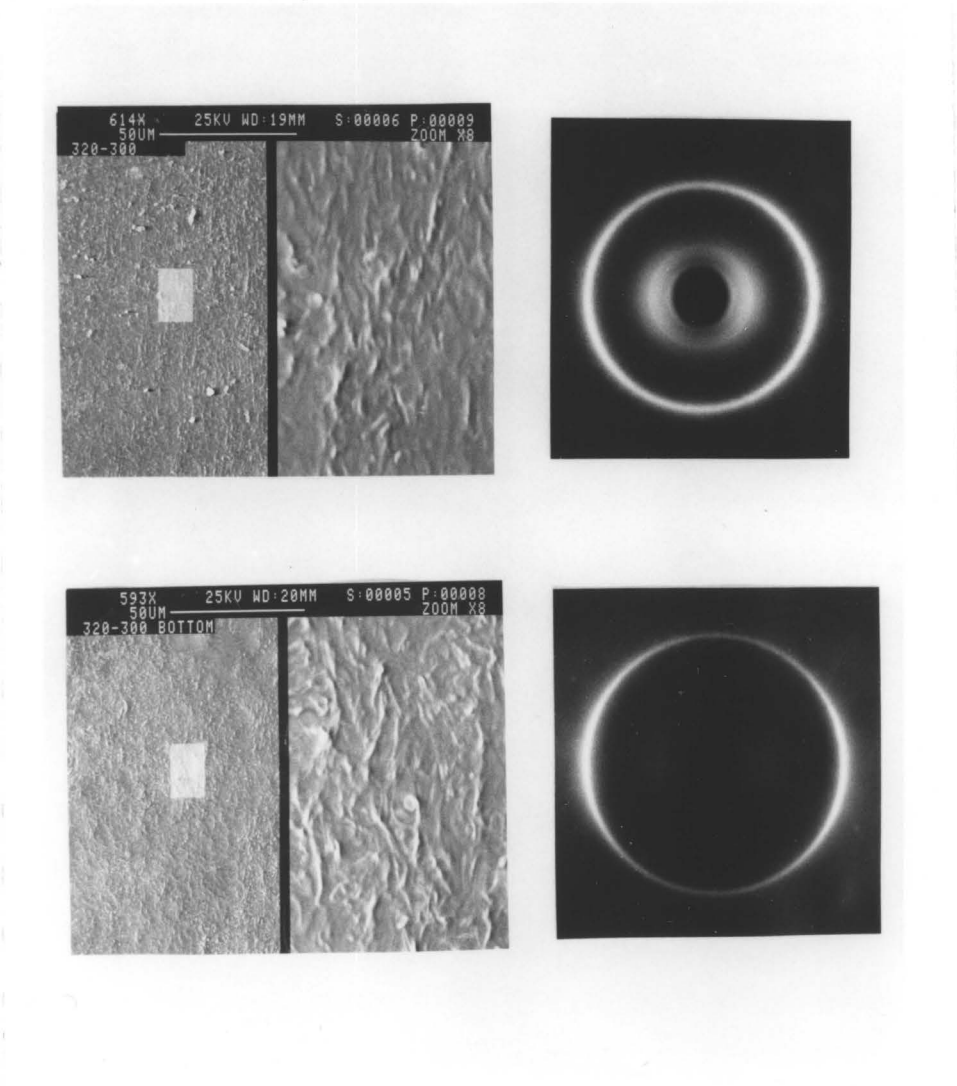

Figure 5.33 SEM micrographs and corresponding WAXS patterns for the unblown parisons (top) and the bottoms (bottom) for the same bottles as in Fig. 5.32. Taken normal to the surface.

by WAXS and SEM is not capable of resolving this slight difference, except to show that no high degree of orientation is present with either thermal history.

The HBA/HNA was also free blown as mentioned previously. The mechanical property results are shown in Table 5.6. Both axial and hoop direction properties are identical: the modulus is about 6.5 GPa and stress at break is about 150 MPa. Wide angle x-ray patterns (not shown) revealed no preferential orientation of the molecules. The promising results on the free blown bubbles, although not showing biaxial orientation with WAXS, indicated that processing uniaxial material in this manner could result in a product with superior properties in more than one direction.

Comparing blown bottles of the two copolyesters studied under the limited conditions that were possible, one sees both similarities and differences. The parisons took about 17 seconds to hang for the HBA/PET system, during which time the temperature of the bottom portion cooled to 141°C and 156°C for the 190°C and 200°C die temperatures, respectively. Likewise for the HBA/HNA hang times of about 14 seconds resulted in final temperatures of 214°C and 223°C for die temperatures of 290°C and 300°C, respectively. These temperatures agree well with the cooling curve presented in the literature review (Fig. 2.15). The deformation tends to occur at the point on the curve where

the elastic modulus increases to 104 Pa.

For both materials the outside of the bottle tended to be more highly aligned in the z-direction than the inside due to the quenching effect of the mold walls. Or ientation of all but the outside skin, though, was imparted in both materials during the blowing process itself. The lower the processing temperature employed, the greater the reorganization which occurred, perhaps because of the higher stress levels that developed and the greater elasticity exhibited by the copolyesters. Also, bubbles that were free blown showed similar diffraction patterns and mechanical property results for both materials. With this process, most of the orientation present in the parison could be removed and yet the mechanical properties remained relatively high.

Despite these similarities, a major difference remained. Under no temperature profile studied could any semblance of biaxial orientation (as evidenced by WAXS) be imparted to the blown bottles of Vectra. Since lower temperatures could not be used due to freeze off in the die, it is doubtful that such a structure was possible with this material and the limitations of the equipment.

In this section the experimental results of blow molded bottles of HBA/PET and HBA/HNA were presented and analyzed in terms of the effect of varying the thermal history on the properties and orientation of the resulting

bottles. Although biaxial orientation and properties were possible, the complex deformation kinematics were not possible to define nor vary precisely. Thus, film stretching was chosen as a biaxial deformation in which the kinematics are better known. These results will be presented in the next section.

5.3 Film Stretching

Extruded film of the 60 mole% HBA/PET was stretched on a T.M Long device as an alternative method of producing biaxial orientation. Since the material was already oriented in the machine direction, stretching was performed in the transverse direction. The stretched film was analyzed with WAXS and SEM as well as by measuring the resulting film properties. The results for the HBA/PET system are discussed in the next few paragraphs.

In Table 5.7 the tensile results for both the film originally extruded with a 230°C and with a 220°C die temperature are summarized. The average and standard deviation of five samples were calculated for each stretch condition; the findings are similar for both film die temperatures. Properties as a function of transverse stretch ratio are shown in Figs. 5.34 and 5.35. Up to a stretch ratio of 2.5 (150% elongation) the machine direction modulus (Fig. 5.34) and strength (Fig. 5.35) remained relatively constant while the stress at break and initial modulus in the transverse direction increase gradually. With a 1X3 stretch, however, the tensile properties became biaxial in nature, with a significant deterioration in the MD: under these conditions decreased from 7 GPa to about 3.5 GPa. The decrease of strength in the MD is not as dramatic, but still is significant.

TABLE 5.8 Tensile properties of HBA/PET extruded films

Stretch (MDXTD)	Dir.	E_T (MPa)	σ_{max} (MPa)
		Die Temp. = 230°C	
1 X 1	MD	6150 (900)	120 (6.7)
1 X 1.5	MD	5820 (530)	131 (8.3)
1 X 2	MD	5900 (420)	126 (6.4)
1 X 2.5	MD	7220 (390)	139 (9.1)
1 X 3	MD	3110 (400)	100 (9.4)
1 X 1	TD	1340 (150)	22.1 (0.6)
1 X 1.5	TD	1500 (230)	27.2 (4.1)
1 X 2	TD	2030 (290)	35.9 (4.9)
1 X 2.5	TD	2710 (360)	47.7 (6.6)
1 X 3	TD	3880 (1000)	73.0 (10.3)
		Die Temp. = 220°C	
1 X 1	MD	6980 (490)	128 (11.3)
1 X 1.5	MD	6340 (800)	142 (4.4)
1 X 2	MD	6690 (570)	152 (4.1)
1 X 2.5	MD	7580 (510)	156 (4.4)
1 X 1	TD	1090 (100)	18.8 (2.5)
1 X 1.5	TD	1440 (110)	30.3 (1.4)
1 X 2	TD	2600 (270)	47.2 (3.3)
1 X 2.5	TD	2470 (350)	47.7 (7.5)

Standard deviations are given in parentheses.

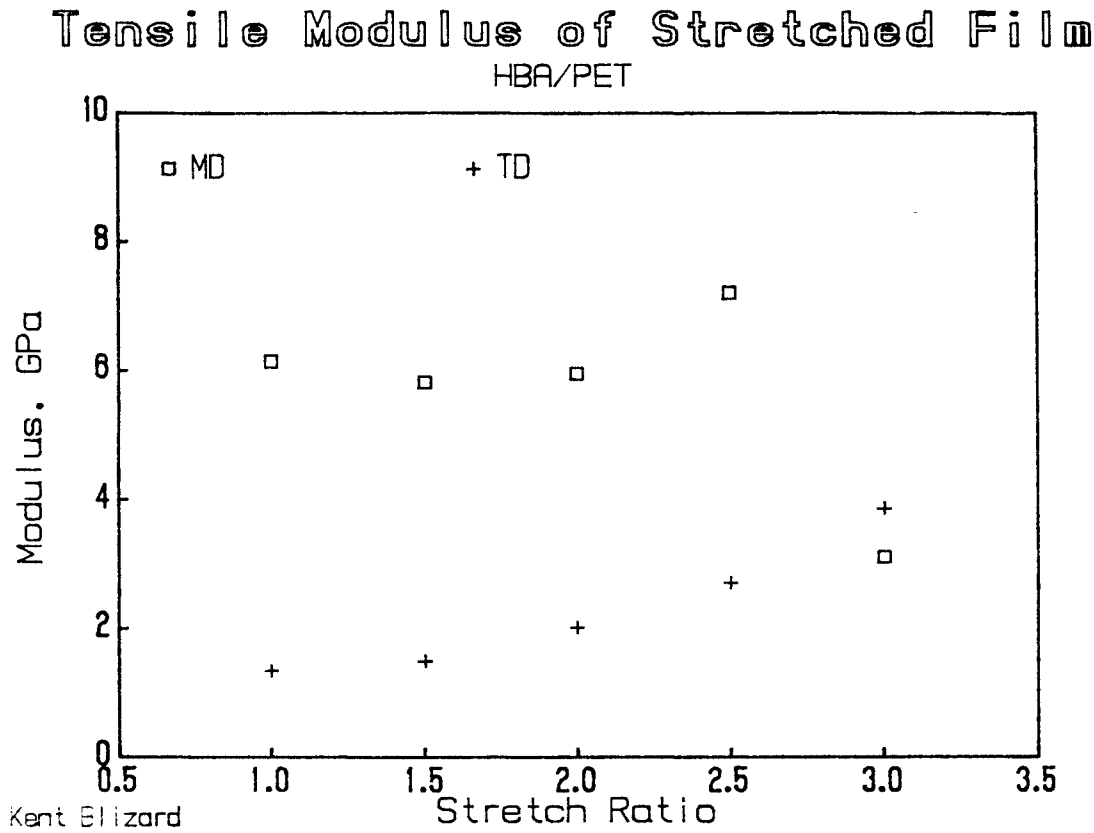

Figure 5.34 Tensile modulus as a function of transverse stretch ratio on the T.M. Long device for 60% HBA/PET

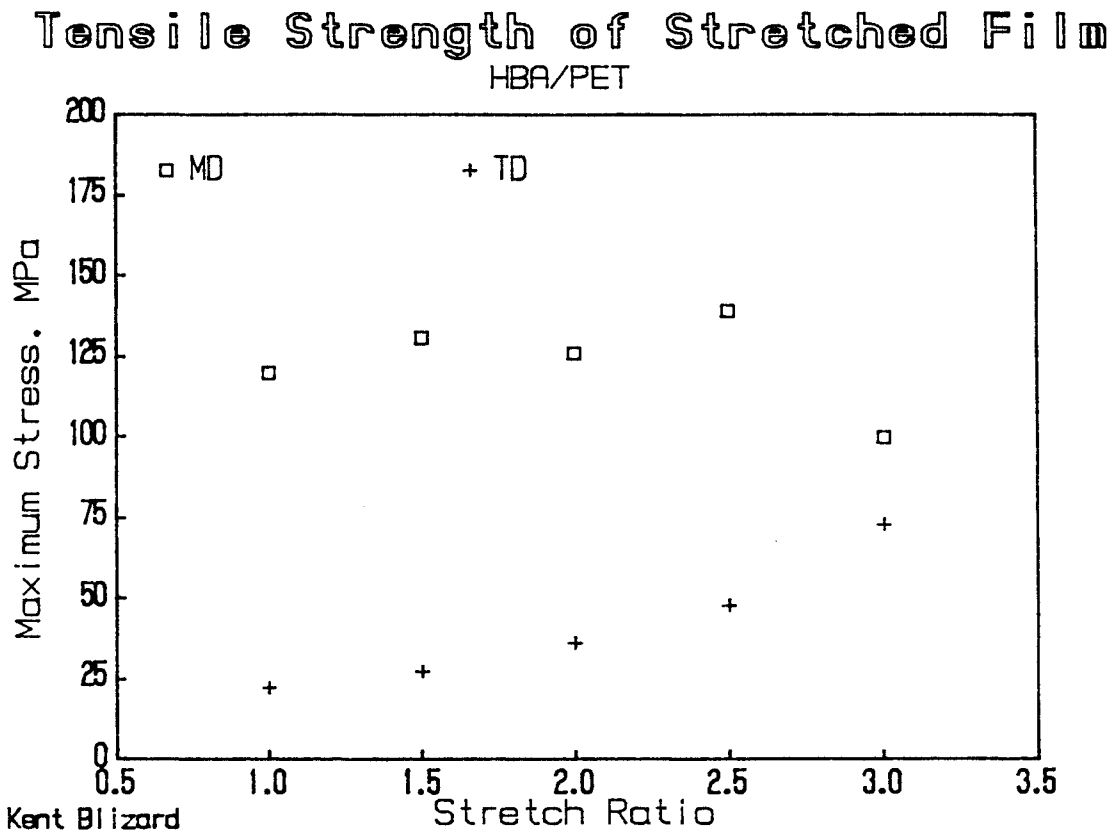

Figure 5.35 Tensile strength as a function of transverse stretch ratio on the T.M. Long device for 60% HBA/PET

The x-ray patterns in general support the mechanical property results. In Fig. 5.36 the WAXS patterns for the film extruded with a die temperature of 230°C and then stretched are shown. The as-extruded sample appears to be fairly highly oriented in the machine direction; the azimuthal intensity is not reduced significantly until the 200% elongation. This final pattern indicates no preferential MD or TD orientation in the film.

The electron micrographs of stretched film that was etched and then examined normal to the surface of the film is shown in Fig. 5.37. Viewed at about 450x magnification the texture is sponge-like for all stretch ratios. Only for the case of no transverse stretch being applied does the texture show any anisotropy. In this instance some preferential alignment in the machine direction appears, and is noticeable at low magnification.

The WAXS and SEM results indicate that the orientation induced in this material is random within what is essentially the same plane for sufficient transverse strains. The biaxial orientation seen in the blown bottles, on the other hand, was the result of a laminated structure where the orientation varied throughout the layers of the material.

In the next section the effect of kinematics and thermal history on the orientation and properties of blown film of the copolyesters will be discussed.

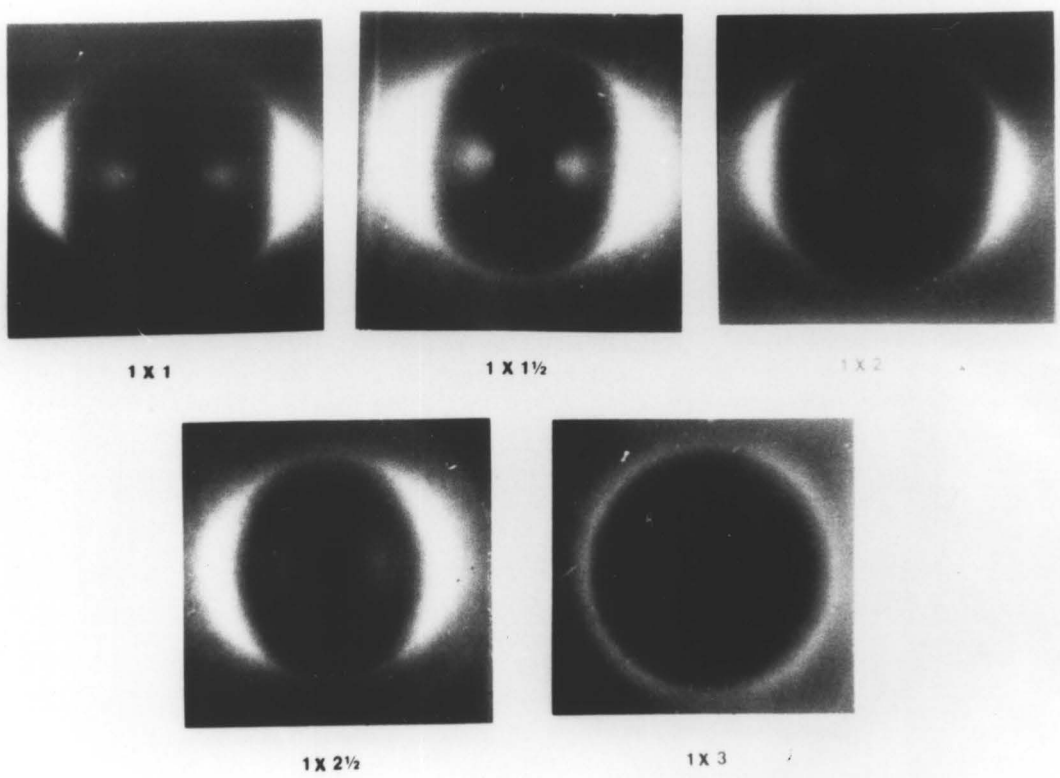

Figure 5.36 WAXS diffraction patterns as a function of stretch ratio on the T.M. Long device for 60% HBA/PET

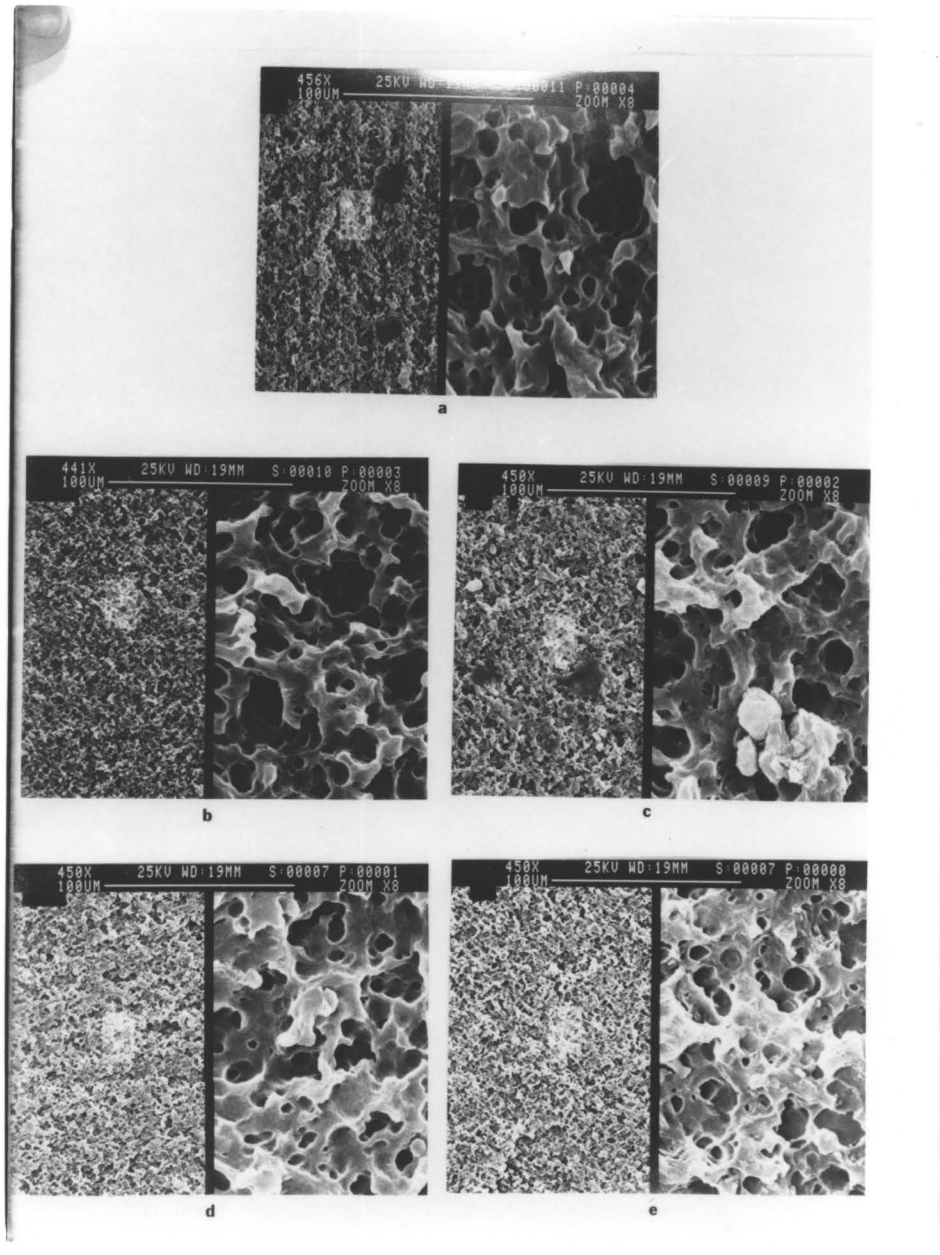

Figure 5.37 SEM micrographs of HBA/PET extruded and stretched on the T.M. Long device as a function of transverse ratio: a) 1x1; b) 1x1.5; c) 1x2; d) 1x2.5; e) 1x3.

5.4 Film Blowing

In order to more fully characterize the effect of deformation history, in particular biaxial deformation, on the orientation development of these copolyesters, the materials were blown as thin films (see experimental chapter for details). The present section is essentially restricted to the mechanical property results since the wide angle x-ray results on the film will be presented along with the predictions of Doi's theory in section 5.5.

Tensile measurements were made both parallel and perpendicular to the machine (or axial) direction for a variety of blow up ratios (BUR) and different barrel temperatures for both of the thermotropes studied. In Fig. 5.38 three typical BURs are shown for the HBA/PET copolyester and in Fig. 5.39 three different BURs are shown for HBA/HNA. The mechanical property results are reproduced in tabular form in Table 5.9. In Figs. 5.40-5.43 the modulus and maximum stress are plotted as a function of the blow up ratio in each material to better observe the effect of that parameter on the mechanical properties.

Machine direction modulus (Fig. 5.40) was not significantly altered from about 10 GPa for the PET copolyester and 13 GPa for the HNA material as the BUR was increased, although WAXS patterns do show a slight decrease in the

TABLE 5.9 Tensile Properties of Blown Film

Direction	T_b (°C)	BUR	ET (GPa)	σmax (MPa)
		HBA/PET		
MD	267	1.45	11.2	171
MD	267	2.30	10.6	247
MD	267	3.10	9.16	297
MD	247	1.30	10.7	231
TD	267	1.45	1.13	20.6
TD	267	2.30	1.29	25.3
TD	267	3.10	1.86	36.7
TD	247	1.30	1.07	19.9
		HBA/HNA		
MD	337	1.0	13.3	264
MD	337	1.95	14.8	360
MD	337	2.60	12.4	378
MD	319	1.35	12.4	342
MD	319	2.30	12.4	391
TD	337	1.0	1.08	16.1
TD	337	1.95	1.71	31.1
TD	337	2.60	3.08	69.8
TD	319	1.35	1.32	30.8
TD	319	2.30	1.93	57.5

Average standard deviations were 1.94 and 0.18 for the MD and TD moduli and 37.0 and 2.37 for the MD and TD maximum stresses.

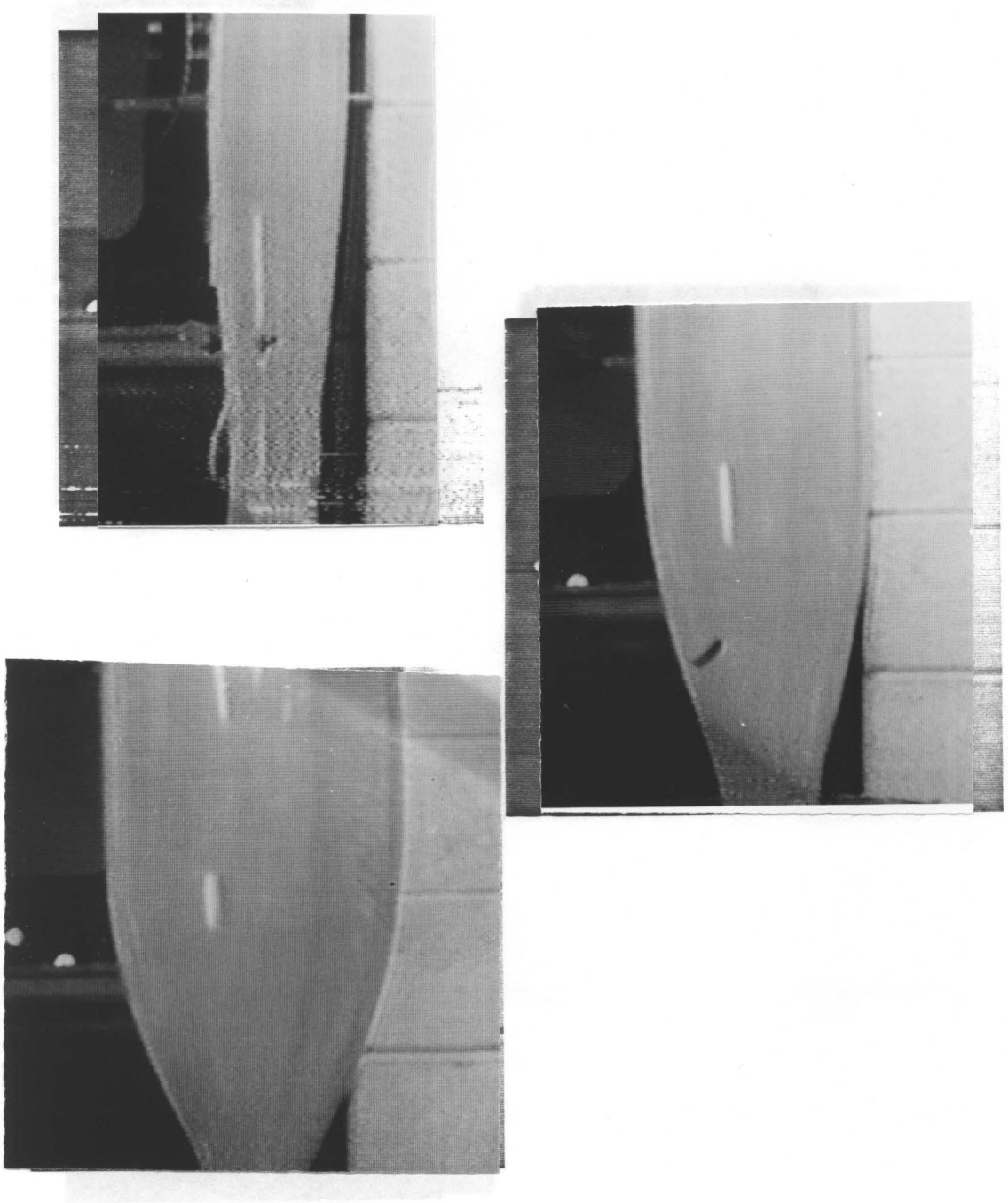

Figure 5.38 Typical blown film of HBA/PET. Top to bottom are BURs: 1.45, 2.3, and 3.1. T_b = 267°C.

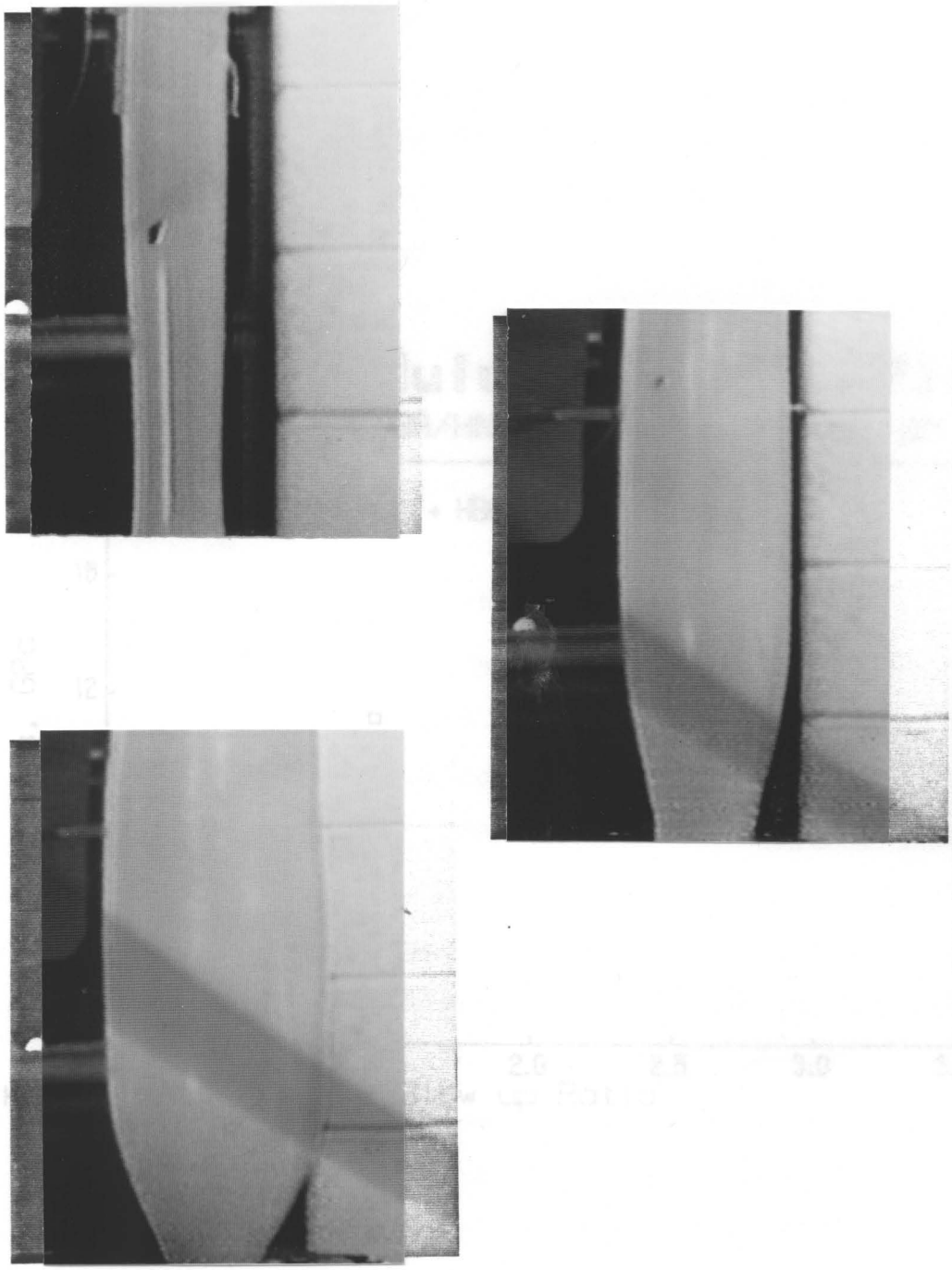

Figure 5.39 Typical blown film of HBA/HNA. Top to bottom are BURs: 1.0, 1.95, and 2.6. T_b = 267°C.

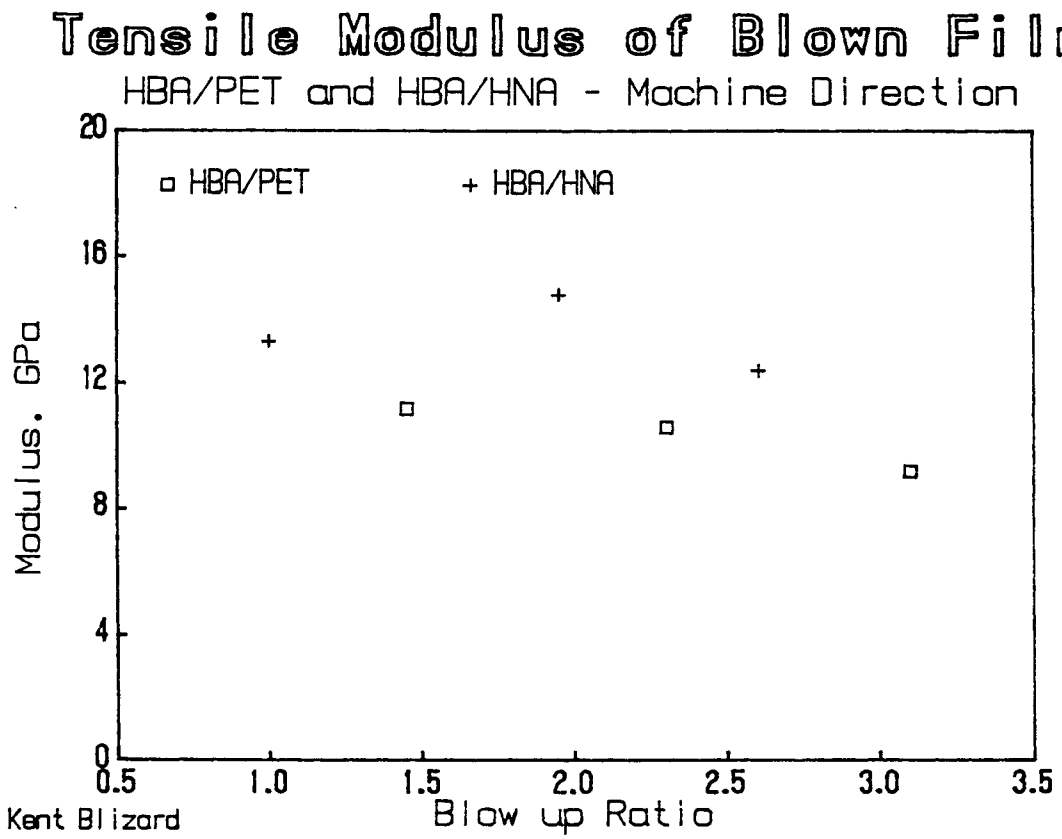

Figure 5.40 Machine direction tensile moduli of blown film of HBA/PET (T_b = 267°) and HBA/HNA (Tb = 337°).

degree of axial orientation (see Fig. 5.48). Significant improvement in the TD modulus, however, may be observed in Fig. 5.41. The modulus nearly doubled in the case of HBA/PET and trebled for HBA/HNA as the BUR was increased from 1.45 to 3.1 in the former case and from 1.0 to 2.6 in the latter instance. Even so, the transverse direction values remained at best one fourth of those in the machine direction. Indeed, the WAXS patterns (Fig. 5.49) revealed that even at the highest BUR preferential axial orientation remains.

Tensile strength, on the other hand, improved in both the MD and TD when the BUR was increased, as may be observed in Figs. 5.42 and 5.43. Fifty percent increases in the axial direction occur, to 300 MPa for HBA/PET and to almost 400 MPa for HBA/HNA! Similarly, in the TD values of strength increased from 20 to 37 MPa and from 16 to 70 MPa, respectively, for the PET and the HNA polymers. Despite these improvements, though, MD strengths remained about 5 times those in the transverse direction.

One last note on the mechanical property results is that the effect of decreasing barrel temperature (while maintaining a constant die temperature) is ambiguous. Although the kinematics of the deformation change somewhat, as will be seen in the next section, mechanical property differences were in general not significant (see Table 5.9).

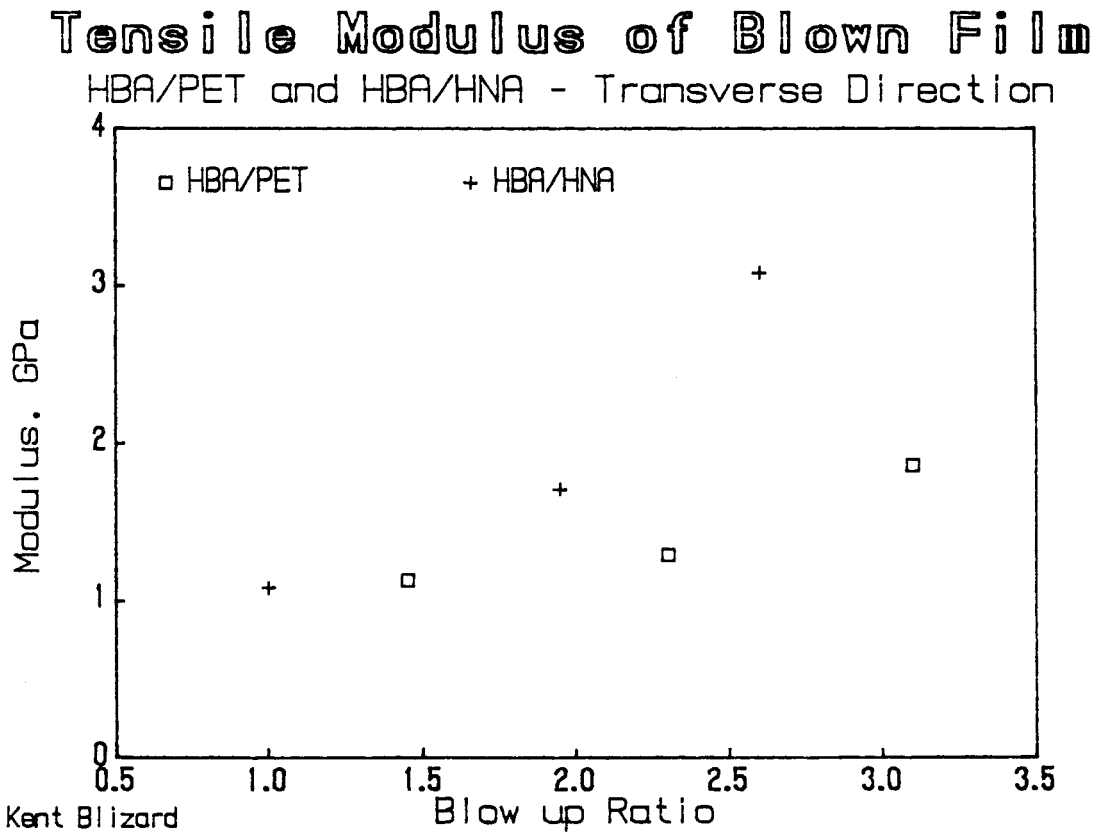

Figure 5.41 Transverse direction tensile moduli of blown film of HBA/PET (T_b = 267°) and HBA/HNA (T_b = 337°).

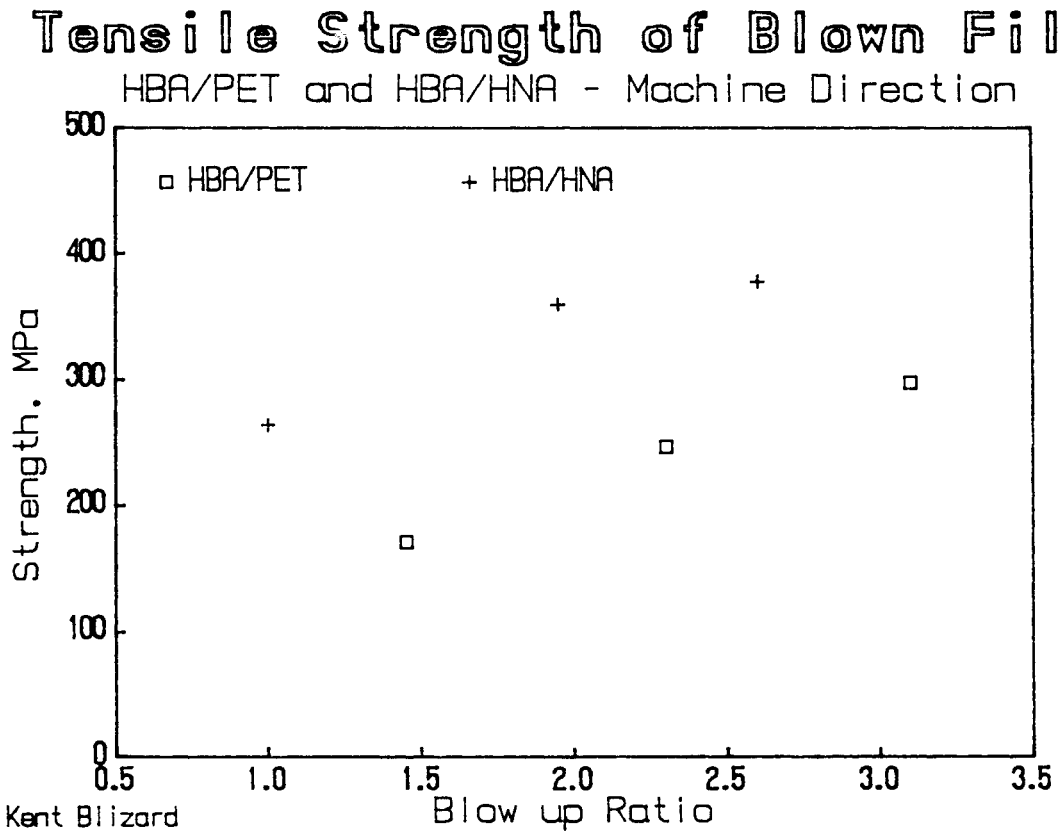

Figure 5.42 Machine direction tensile strengths of blown film of HBA/PET (T_b = 267°) and HBA/HNA (Tb = 337°).

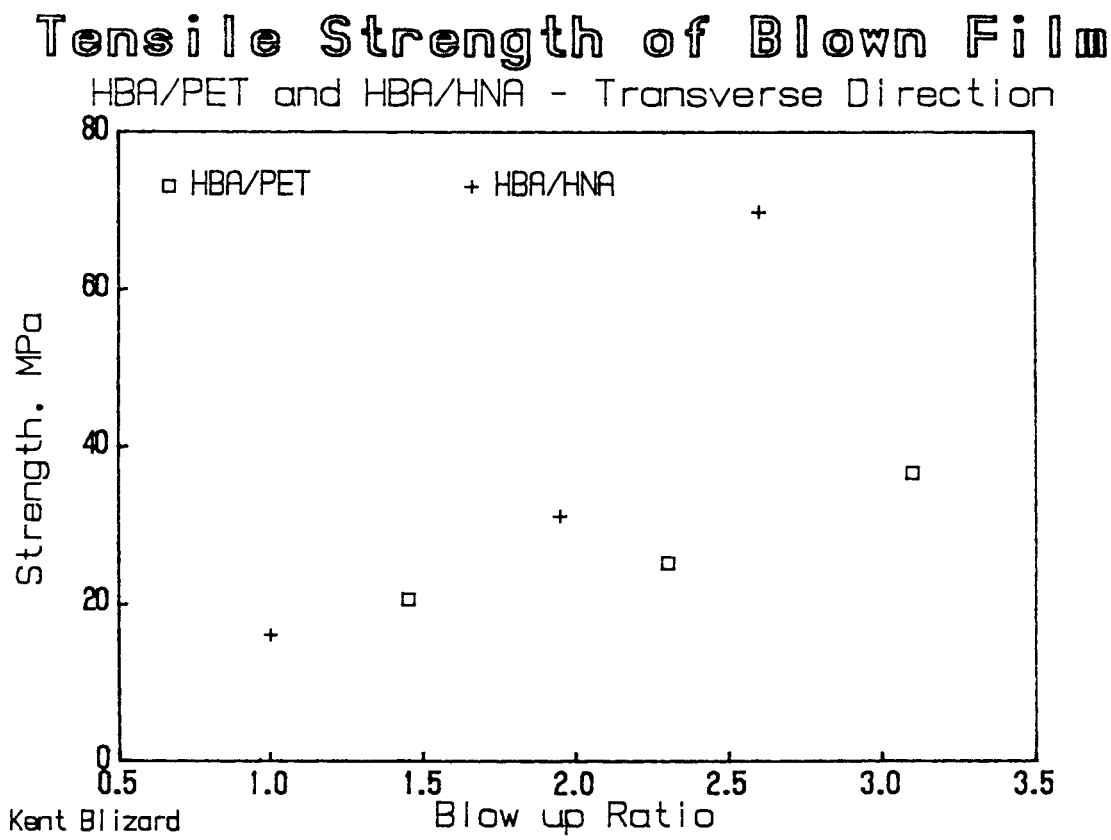

Figure 5.43 Transverse direction tensile strengths of blown film of HBA/PET (T_b = 267°) and HBA/HNA (T_b = 337°).

Although the x-ray patterns do not indicate an extremely high degree of axial orientation, the mechanical properties were exceptional in that direction in comparison, for example, to injection molded plaques with similar x-ray diffraction patterns. The predominant reason for this result is that since the films were on the order of 0.10 mm in thickness it may be assumed that the skin-core effect evident in thicker cross sections was absent, and the mechanical properties were correspondingly increased.

In this section the experimental results of the blown film process were analyzed. Next the predictions of Doi's theory for orientation development in the blown film process will be given, along with WAXS patterns as experimental corroboration.

5.5 Comparison of Theory to Experiment: Film Blowing

A major thrust of this work has been not only to produce biaxial orientation and properties in thermotropic liquid crystalline polymers but also to predict this through the use of Doi's theory. Toward this end his theory for monodomain rigid rod nematics was summarized in the literature review and transient predictions then made in Chapter 3. At that point it was also proposed to modify the theory to account for the behavior of thermotropes. In the present section the orientation predictions made for general inhomogeneous biaxial flows will be adjusted to fit the kinematics of the blown film deformation.

The deformation rates for the blown film process in the axial and transverse directions were calculated from equations given in the literature review. The video camera was used in conjunction with the VHS recorder to determine the bubble shape as a function of the axial coordinate and also to determine the velocity of a particle on the surface as a function of that same coordinate. The process consisted of obtaining both bubble radius as a function of z and marker position as a function of time from the video monitor screen. Polynomial regressions were then employed to provide a means of calculating surface velocities; the plots are reproduced

in Appendix C and a source listing of a typical program in Appendix A.

One difficulty that immediately becomes apparent in implementing the solution of the differential equations is what initial value should be chosen for the orientation parameter tensor components. The initial position of a hypothetical particle was taken as the outlet from the annular die: one may suspect that some nonzero value of S_{11}, for instance, is already present. Experimentally obtaining this value in situ, however, is no simple task. Thus, the practical solution of varying this initial value and thereby determining its effect on the equations was taken. Although any quantitative value of the theory is lost, it is questionable (as will be seen for predictions of the PPT/H_2SO_4 system in section 5.6) whether any existed in the first place. In addition, the nature of the WAXS diffraction patterns is only qualitative. As will be seen, the final orientation for different BURs remained in the same relative order regardless of the initial orientation chosen. In addition, the shape of the S_{11} versus time curve for each deformation remained essentially unchanged.

The trends shown in Figs. 5.44 and 5.45 occurred for each thermotrope when the equations were solved with the arbitrary assumption of $S_{11(0)}=0$. The final orientation at the freeze line (about 6-8 seconds) decreases with an

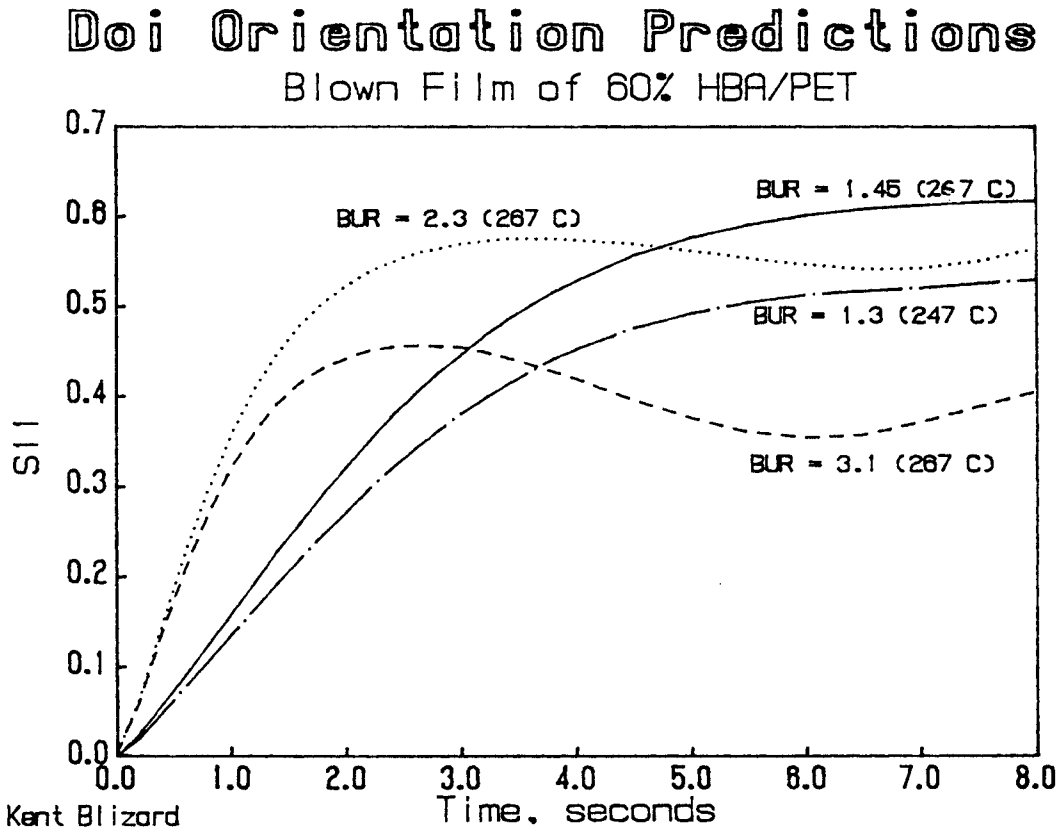

Figure 5.44 Transient orientation (S_{11}) predictions for blown film of HBA/PET at different blow up ratios. $S_{11}(0)=0$.

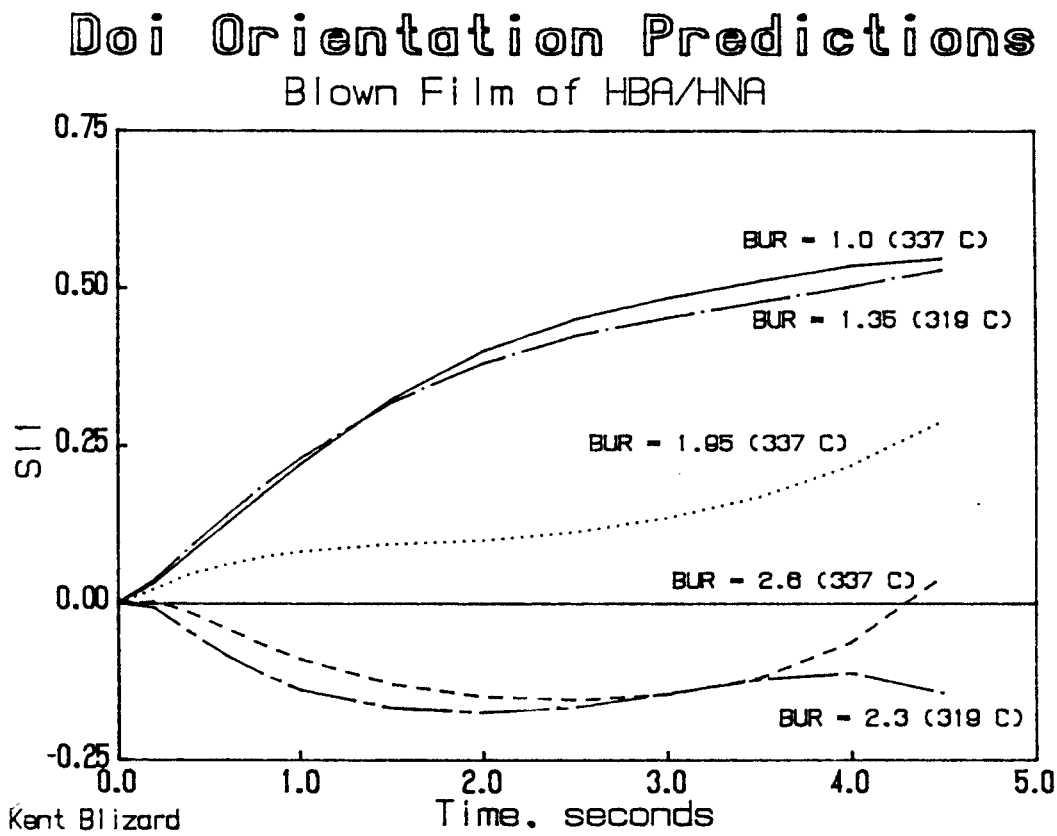

Figure 5.45 Transient orientation (S_{11}) predictions for blown film of HBA/HNA at different blow up ratios. $S_{11}(0)=0$

increase in BUR at a given barrel temperature from .62 to .56 to .41 for the HBA/PET (BURs of 1.45, 2.3, and 3.1) and from .55 to .29 to .04 for the HBA/HNA. For the latter material 3-4 seconds were required for a hypothetical particle to reach the freeze line (the difference in time between the two materials is due to different nip roll speeds). The calculations for the naphthoic copolyester indicate that the material becomes transversely oriented at high BUR, particularly if the barrel temperature is lowered. This finding will be shown to be an artifact of the assumption of an "isotropic" initial orientation in the nematic.

The assumption of $S_{11(0)}=0.332$ was made for comparison purposes. The resulting orientation development may be seen in Figs. 5.46 and 5.47. The shape and relative rank of the final orientation present in the films remained unchanged - only the quantitative value of the orientation order parameter tensor components increased when the initial orientation was increased.

Numerical values of freeze line orientation are plotted as a function of BUR for both materials in Figs. 5.48 and 5.49 for $S_{11(0)}=0.332$. Also shown are the corresponding x-ray patterns. For HBA/PET (Fig. 5.48) a nominal reduction in S_{11} from .65 to .56 occurs as the BUR is increased to 3.1. The corresponding WAXS patterns show little difference, as would be expected. A slight broad-

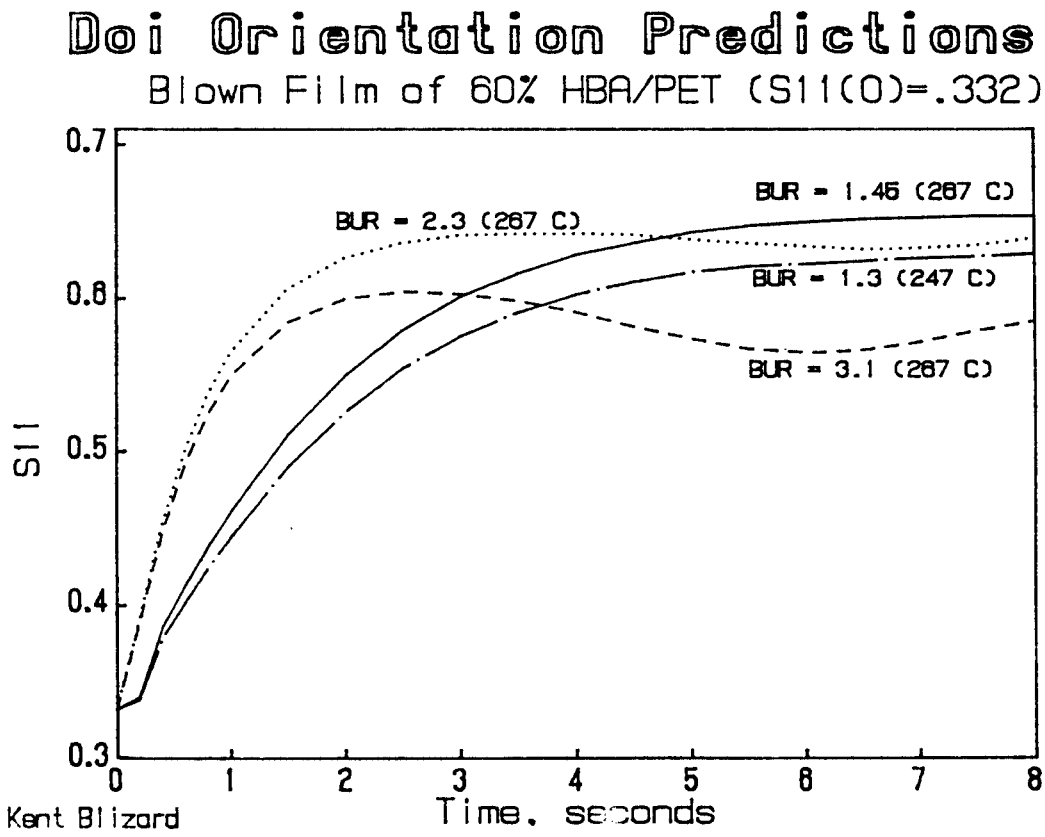

Figure 5.46 Transient orientation (S_{11}) predictions for blown film of HBA/PET at different blow up ratios. $S_{11}(0)=0.332$

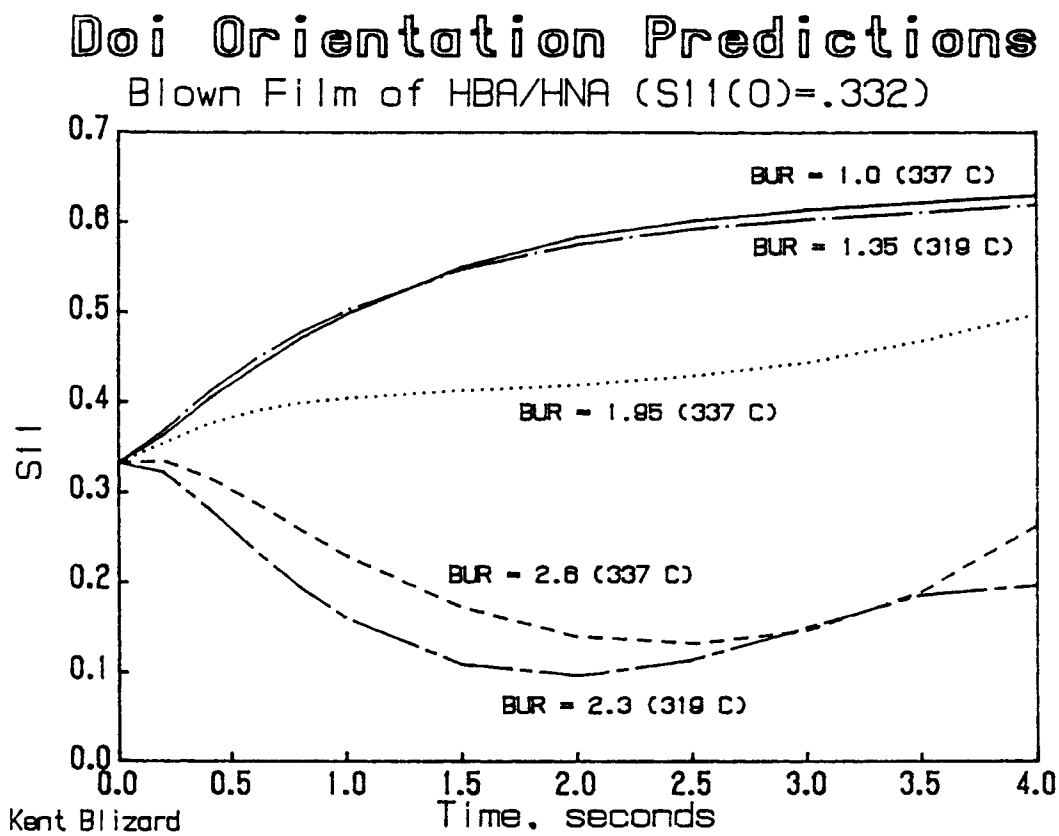

Figure 5.47 Transient orientation (S_{11}) predictions for blown film of HBA/HNA at different blow up ratios. $S_{11}(0)=0.332$

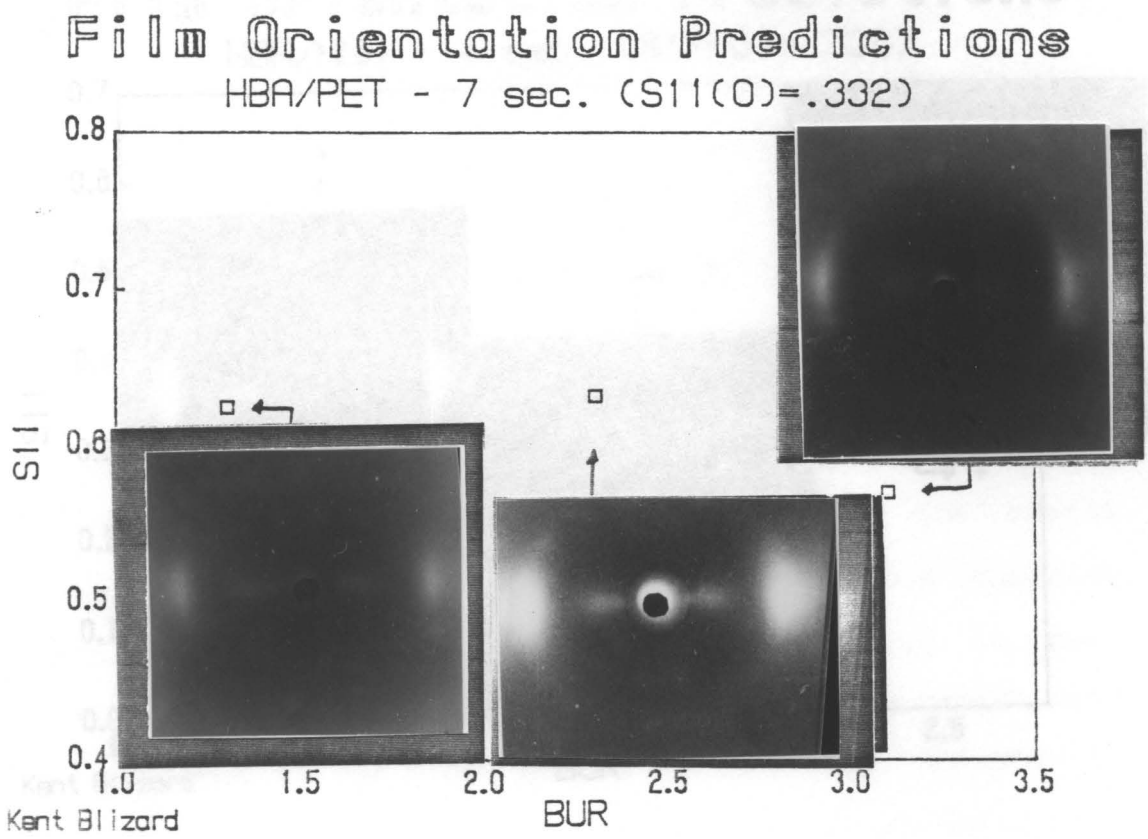

Figure 5.48 Blown film orientation as a function of BUR for HBA/PET.

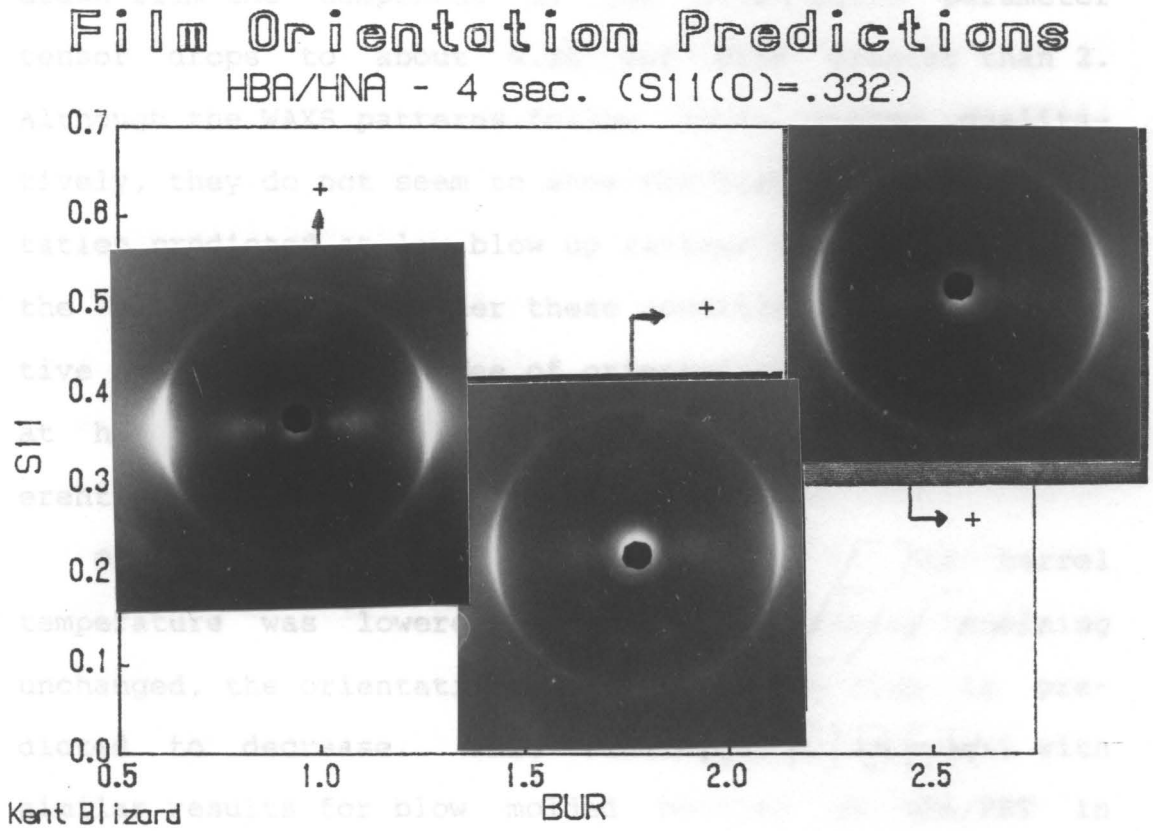

Figure 5.49 Blown film orientation as a function of BUR for HBA/HNA.

ening of the equatorial peak is, however, observed for the highest BUR film. The orientation for the HBA/HNA film is predicted by Doi's theory to decrease much more when the blow up ratio is increased. From $S_{11}=0.63$ for uniaxially drawn film the component of the orientation parameter tensor drops to about 0.20 for BURs greater than 2. Although the WAXS patterns follow these trends qualitatively, they do not seem to show the high degree of orientation predicted at low blow up ratios: the scattering of the equatorial peak under these conditions is not indicative of such a high degree of orientation. The scattering at higher BURs does indicate only a small degree of preferential orientation in the axial direction.

One interesting prediction was that if the barrel temperature was lowered, the other variables remaining unchanged, the orientation of the resulting film is predicted to decrease. This finding is in agreement with similar results for blow molded bottles of HBA/PET in which the axial orientation, as observed directly from WAXS and indirectly evidenced by tensile modulus and SEM micrographs, showed a similar decrease. In particular if the nominal barrel temperature was decreased from 275°C to 260°C a broadening of the equatorial scattering peak was observed in blown bottles. Similarly, the WAXS photos of film blown at lower barrel temperatures in Figs. 5.48 and 5.49 do exhibit less preferential orientation than do

those of blown film extruded at higher temperatures.

These last results may be explained by Fig. 2.16 in which HBA/PET was preheated above its melt temperature and then cooled to 190°C, at which point the storage modulus was measured as a function of time. Without such preheating the modulus and viscosity values are higher by at least an order of magnitude [23]. Thus, if the material is processed without preheating above its melt temperature, it will have higher rheological properties compared to processing within a few seconds of cooling to 190°C. This increase in turn results in higher stresses being developed during the deformation process, whether it be blowing into a cold mold or free film blowing. These higher stresses then cause a greater degree of reorientation in the material when a transverse deformation is imposed.

In section 5.5 the blown film results have been compared to the orientation predictions of Doi's theory. Experimental limitations, however, restricted comparisons to being only qualitative in nature. In the next section Doi's predictions for the stress development on the start up of a steady shear flow will be compared to the experimental results on the lyotropic system of PPT/H_{2SO4}. Thus it is hoped to provide a more quantitative comparison between theory and experiment than is afforded in the case of the thermotropic systems considered heretofore.

5.6 Comparison of Theory to Experiment: Transient Shear Rheology of PPT/H_2SO_4

As was seen in the previous section, the orientation predictions of the Doi model for the blown film process for both thermotropes of interest were at least in qualitative agreement with experimental results. However, because of experimental limitations it was not possible to examine the transient orientation development. Nor was it reasonable to expect quantitative agreement given the numerous assumptions inherent in the theory. The shortcomings and successes of the theory will therefore be considered in more detail for a lyotrope in the present section. In particular, the stress growth predictions of Doi's theory at the inception of steady shear will be applied to a nominal 12% (mass) anisotropic solution of poly(phenylene terephthalamide) in 100% sulfuric acid.

5.6.1 Experiment

Numerous rheological tests were made on both 4 wt% and 12 wt% solutions on the RMS as detailed in the experimental chapter. The 4% (3.9% by coagulation measurements) was chosen since it represents a concentrated isotropic solution, and the 12% (11.1% actual) an anisotropic solution. Only two results, however, are of interest in this

section: dynamic (and steady shear viscosity) and the stress growth after the imposition of steady shear at various rates. The frequency sweep of dynamic viscosity is shown in Fig. 5.50 for both 4% and 12% solutions. The 4% solution shows a zero shear rate viscosity of 1.2E4 Pa-sec., which is in agreement with its steady shear viscosity at 0.01 sec-1 (not shown). No such zero shear rate viscosity has been deduced from the rate sweeps of the 12% solution because of instrument limitations at the lower frequencies.

Shear stress at the inception of steady shear is shown in Fig. 5.51 for five different shear rates, from 0.5 to 50 sec-1 for the anisotropic solution. As may be seen, the initial overshoot increased dramatically at higher rates, but even at 0.5 sec-1 some overshoot occurred. Although the shear stress at long time remained about 1000 Pa., as the rate is increased the maximum in the overshoot increased from 1200 to about 9000 Pa. This maximum occurs at about 3 seconds for the lowest rate, and decreases to one second or less at the higher rates. The exact point of this maximum is ambiguous, however, since short time resolution was not good (experiments were actually carried out to several hundred seconds).

In contrast, stress growth for the isotropic 4% solution is shown in Fig. 5.52. Shear stress values at a given shear rate are approximately one half of those for

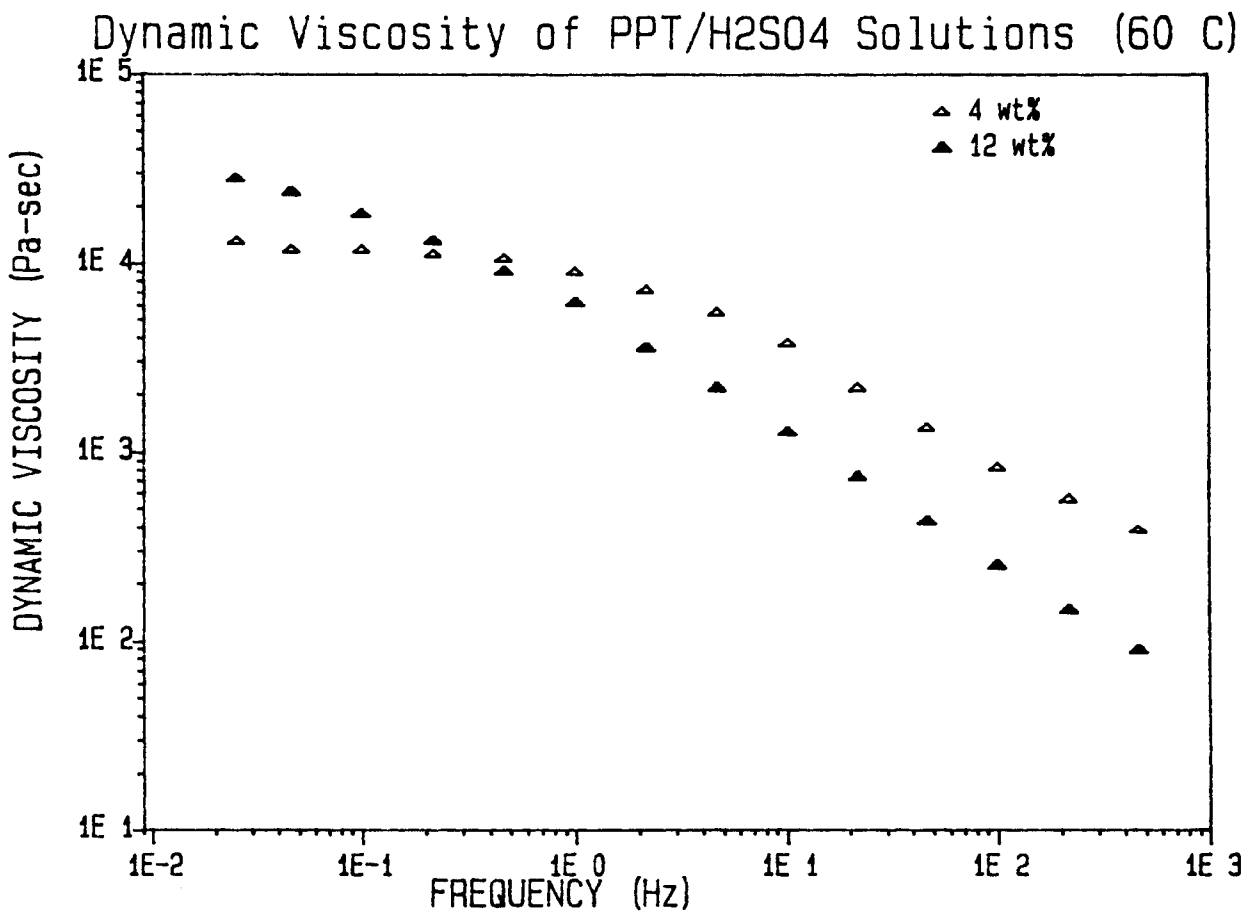

Figure 5.50 Dynamic viscosity of 4% and 12% PPT/H_2SO_4 solutions at 60°C from 0.01 to 1000 Hz.

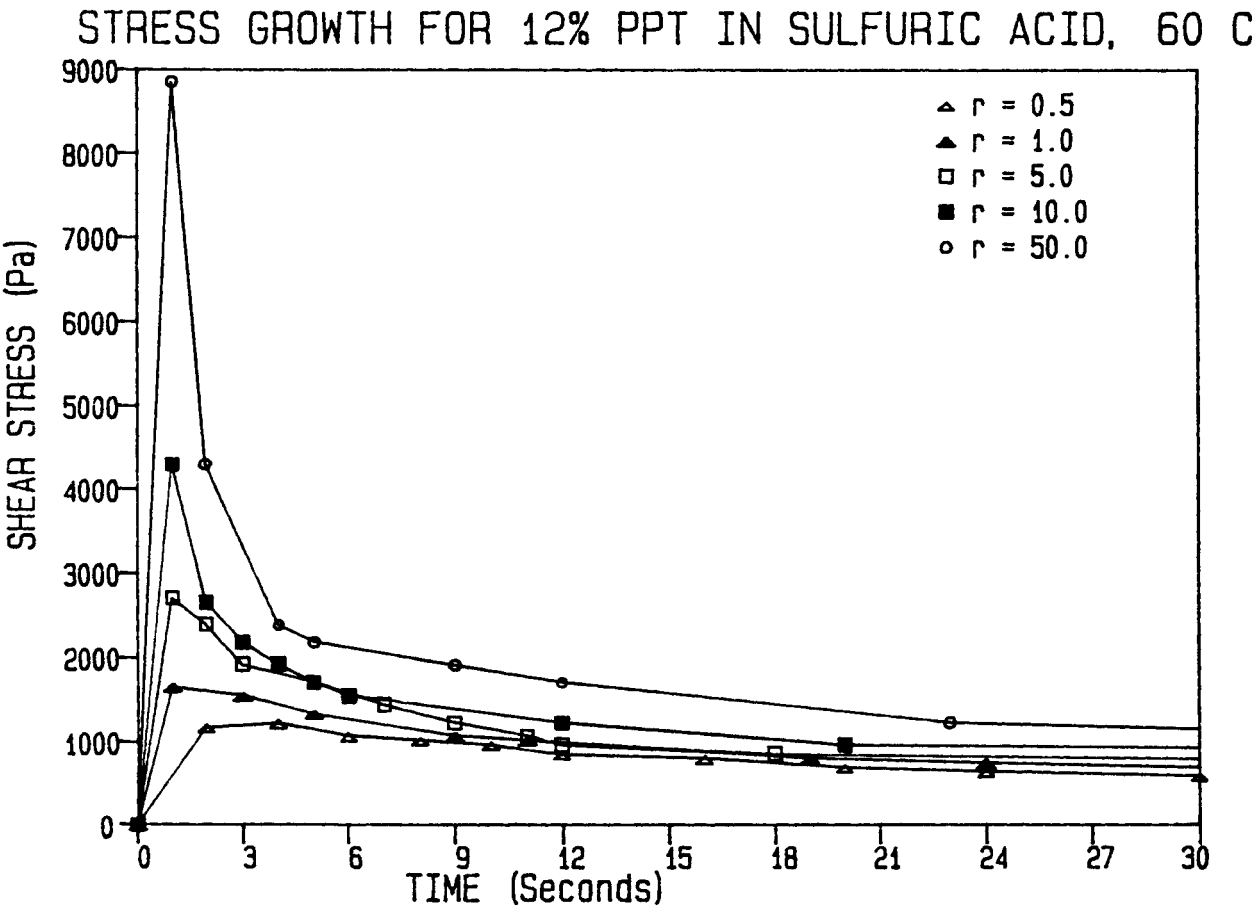

Figure 5.51 Stress growth on the inception of steady shear flow for a 12% solution of PPT/H_2SO_4 at 60°C.

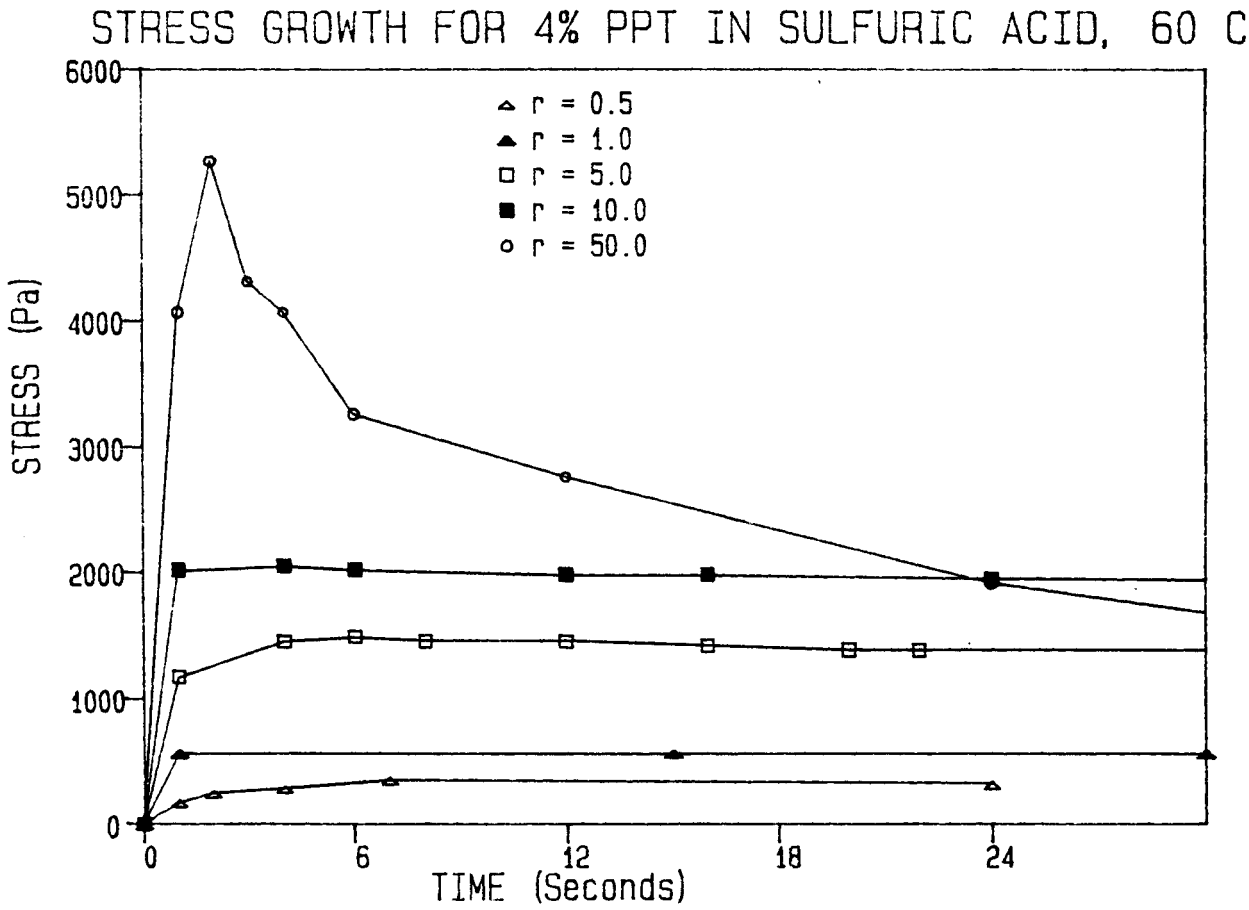

Figure 5.52 Stress growth on the inception of steady shear flow for a 4% solution of PPT/H_{2SO4} at 60°C.

the 12% solution. In addition, the degree of overshoot is substantially less - nonexistent even at the lower rates.

5.6.2 Comparison with Theory

In order to compare Doi's theory with experiment, one needs two parameters as inputs to equations 2.15 and 2.16 in the literature review: c*, the critical concentration for the formation of an anisotropic phase, and D_r, the rotational diffusivity constant of a concentrated isotropic solution. The critical concentration for this solution (Mw = 40,100, Mw/Mn = 2) may be obtained from the literature as approximately 9.0 wt% [73-75]. D_r can be obtained from the Doi-Edwards theory for concentrated isotropic solutions [62]:

$$D_r = ckT/10\mu_0$$

at a given absolute temperature and concentration. With the experimental values of μ_0 for a 4% solution, Dr was calculated to be 0.082 sec-1.

In Figs. 5.53-5.55 the transient shear stress predictions are compared with experiment for 0.5, 1.0, and 10.0 sec-1. As may be readily observed, the predictions of the theory using the experimentally obtained value of D_r drastically overshoot the experimental results at all shear rates, although long time shear stress predictions are similar to experiment at the lower two shear rates.

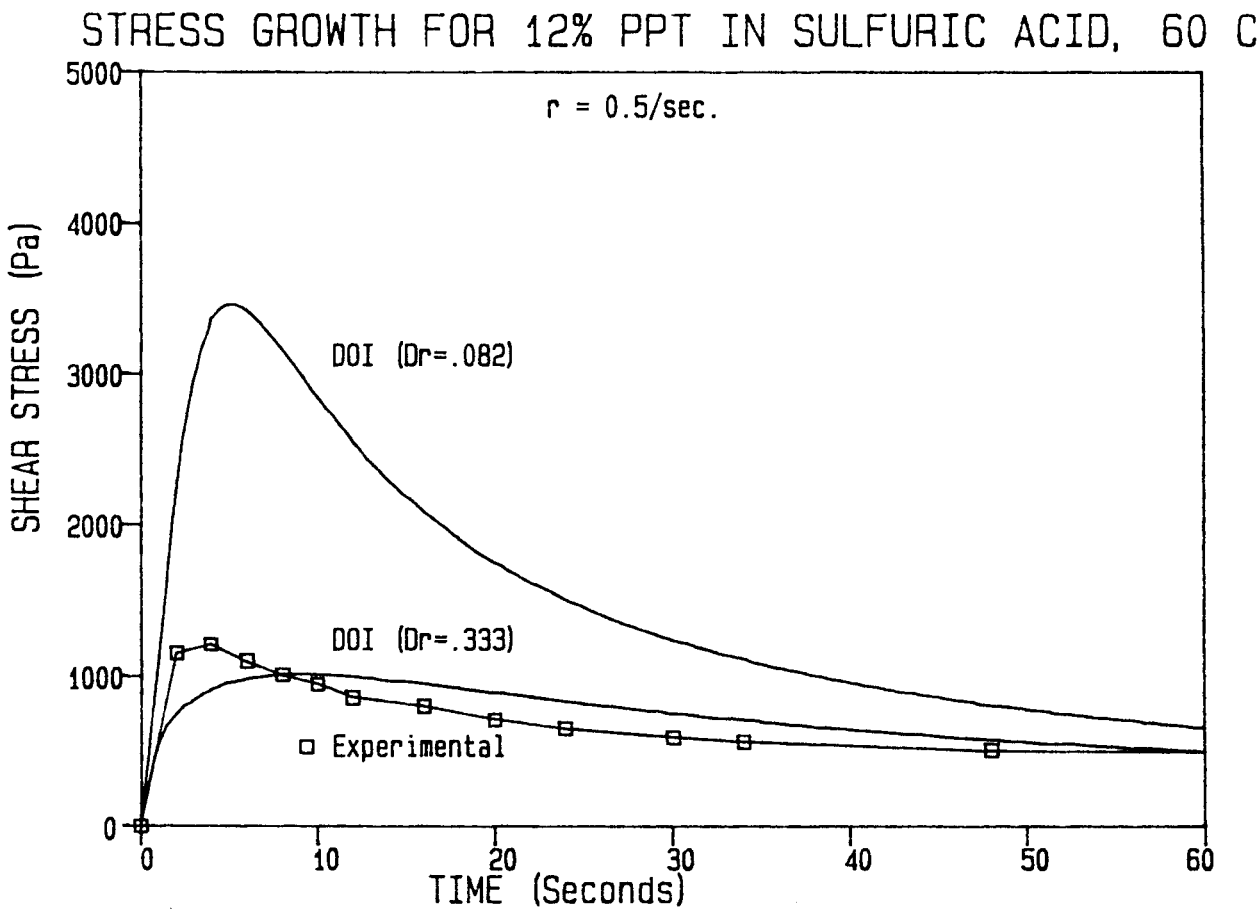

Figure 5.53 Stress growth for 12% PPT in sulfuric acid at 60°C and 0.5 sec-1: comparison with Doi's predictions.

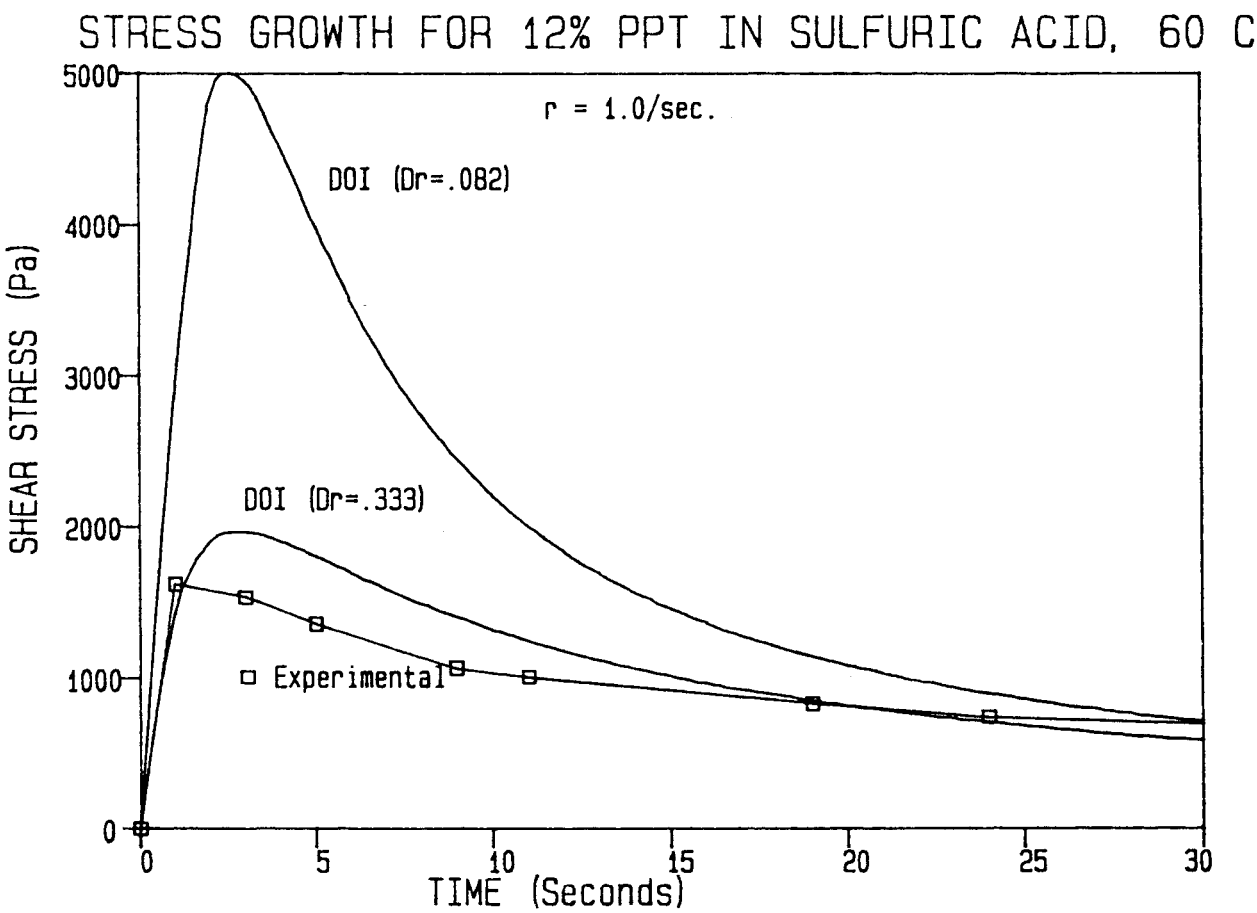

Figure 5.54 Stress growth for 12% PPT in sulfuric acid at 60°C and 1.0 sec-1: comparison with Doi's predictions.

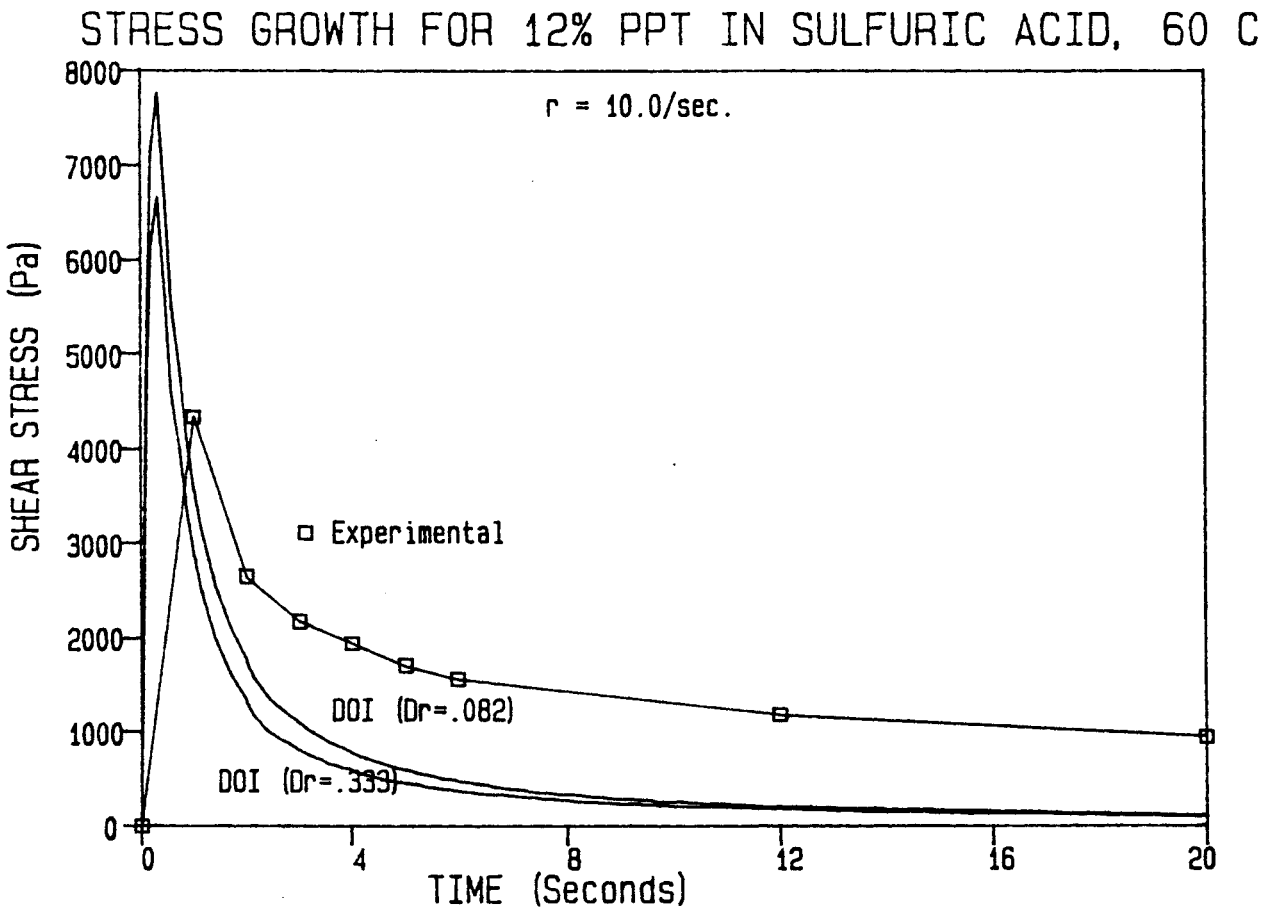

Figure 5.55 Stress growth for 12% PPT in sulfuric acid at 60°C and 10.0 sec-1: comparison with Doi's predictions.

At 10 sec-1, however, the shear stress is incorrectly predicted to rapidly approach zero or a near-zero value following its overshoot.

Since the shear stress predictions were generally poor, the input value of D_r was increased arbitrarily to determine whether the shape of the curve and the amount of overshoot could be "adjusted" to better fit the experimental data. A value of 1/3 for the diffusivity was chosen, and the results are included in the corresponding figures for each shear rate. With this modification the maximum values of stress much more closely fit the experimental ones, particularly at the two lowest rates. However, the long time predictions at 10 sec-1 remain poor.

Assuming good experimental results, this discrepancy must be considered a major shortcoming of Doi's theory as it presently stands. Thus the high rate of shear completely nullifies the non-zero diffusivity. This effect may result from dropping higher order terms when decoupling the orientation distribution in the development of the theory (see Chapter 2). Although this approximation may be valid for lower shear rates and weak velocity fields, a considerable divergence may occur at high rates and strong velocity fields.

Similarly the predictions of Doi's theory fail for a concentrated isotropic solution (4%). In Fig. 5.56 stress growth predictions are shown using the experimentally

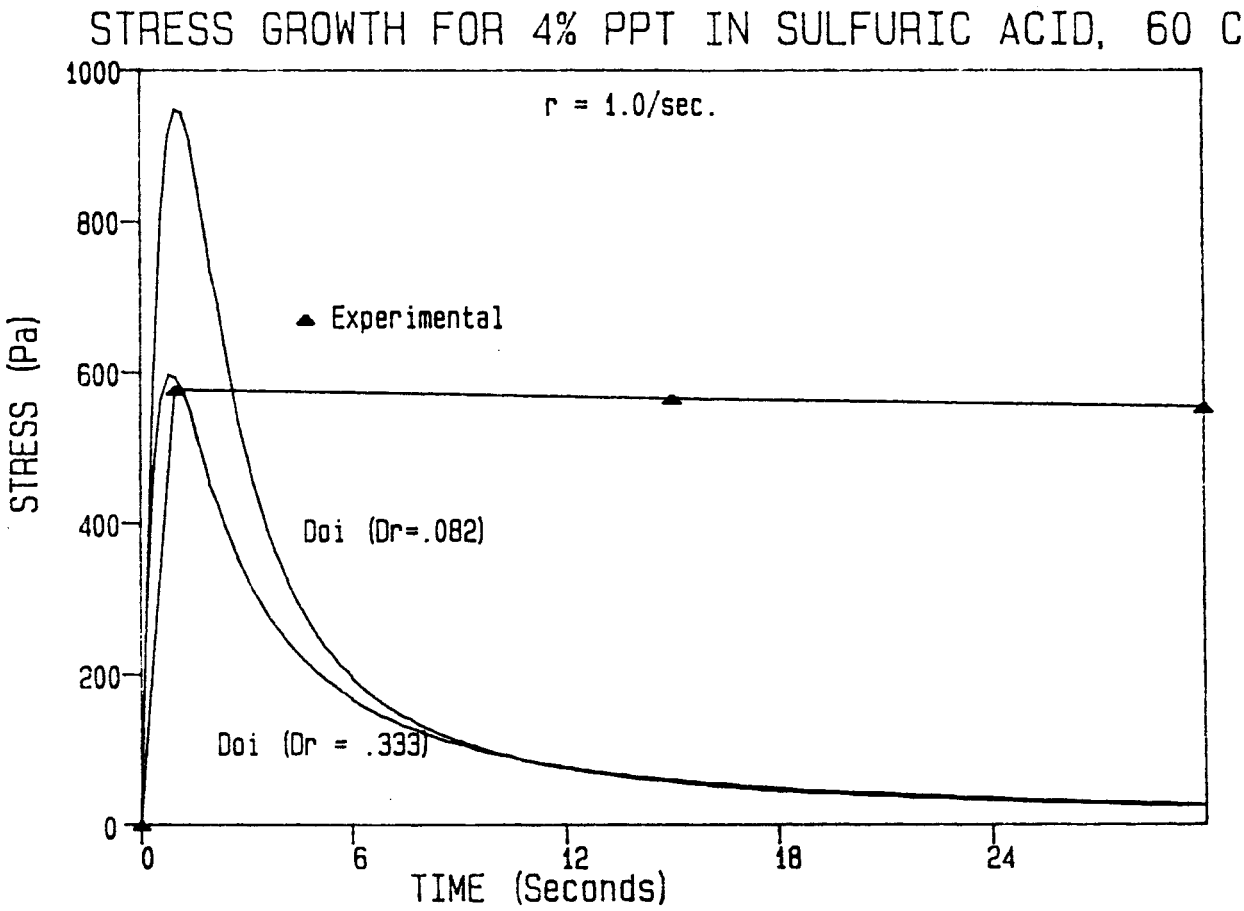

Figure 5.56 Stress growth for 4% PPT in sulfuric acid at 60°C and 1.0 sec-1: comparison with Doi's predictions.

determined diffusivity and for one four times as large, as was done for the 12% solution. Although the experimental results exhibit no overshoot at 1.0 sec-1, Doi predicts an extremely high overshoot and near zero steady state value. The same reasoning used for explaining the discrepancy for the anisotropic solution holds for the isotropic one since the identical equations were used except that the diffusivity was not modified to account for the effect of a nematic environment.

In this section the predictions of Doi's theory have been compared to experimental results for the transient stress predictions of a lyotropic system, concluding the discussion of the experimental and theoretical results. In the next chapter conclusions of this study and some recommendations for future work in this area will be made.

6. CONCLUSIONS AND RECOMMENDATIONS

An investigation into processing possibilities for achieving biaxial orientation and properties in thermotropic liquid crystalline polymers was undertaken. In addition, the orientation was predicted for these systems by utilizing Doi's theory for nematics. The following conclusions are made with regard to the results presented in Chapters 3 and 5. They may roughly be divided into two parts: conclusions from experimental work and conclusions from the theoretical predictions. Following the conclusions, several recommendations for further work, both experimental and theoretical, in this area will be made.

6.1 Processing Methods

1. Although all four processing methods considered involved biaxial deformations, only by blow molding HBA/PET was a biaxial orientation induced as evidenced by WAXS patterns.

2. In solid phase forming HBA/PET the resultant plaques showed improved mechanical properties in the MD when deformed during cooling and an overall decrease in properties when deformed isothermally. These results corresponded to the structure present. In particular, the nonisothermal deformation increased the orientation in the core and the isothermal deformation, while not affecting the core greatly, decreased the orientation in the skin region.

3. In contrast to HBA/PET, solid phase forming the HBA/HNA resulted in an increase in transverse properties although the thermal treatment tended to destroy the fibrillar texture of the skin region so machine direction properties declined dramatically.

4. In blow molding HBA/PET at 30 psig. the whole range of orientations and properties were observed, from uniaxial in the MD to biaxial to uniaxial in the TD, depending on

the barrel and die temperatures employed. In particular, the material tended to reorient during the blowing process (3:1 diameter change) if the temperatures were below 260° in the extruder.

5. It was also observed in blow molding HBA/PET that the cold mold walls had a quenching effect, locking in the orientation. In contrast to the outer surface, which had a texture similar to the unblown parison, much of the structure on the inside surface of the bottles appeared to have relaxed out.

6. In blow molding HBA/HNA, although the trends were the same as with HBA/PET, no biaxial orientation (four lobe pattern) was observed in the WAXS patterns. The blowing process tended to remove the uniaxial orientation of the parison under all conditions. It can be concluded that the viscosity and elasticity of the naphthoic copolyester were sufficient to result in a change in orientation during this planar extensional process. (Melt temperatures on the order of 220°C prior to blowing place the elastic modulus at about 104 Pa. according to Fig. 2.15).

7. Transverse stretching of HBA/PET previously extruded through a film die resulted in a decrease in its MD orientation and concomitant increase in the transverse proper-

ties. However, no biaxial orientation was observed, leading to the conclusion that the biaxial orientation present in the blown bottles was the result of a layered structure in which different layers were oriented in different directions.

8. Stretching compression molded sheets of either copolyester was not possible with the T.M. Long device because the sheet invariably tore.

9. It was not possible to induce biaxial orientation in blown film of either material. Increasing the blow up ratio from 1.35 to 3.1 for HBA/PET and from unity to 2.6 for HBA/HNA did tend to reduce the uniaxial orientation and increase the transverse properties significantly.

10. Due to the limited die temperatures which were possible during the blown film process (195°C ±5° for the PET copolyester and 250°C ±5° for the HNA copolyester) the properties in the transverse direction at best were 1/4th of those in the MD. Despite these limitations, the properties were outstanding: modulus was about 10 GPa and strength nearly 300 MPa for the ethylene terephthalate copolymer and values for the naphthoic copolyester were approximately 30% higher than these! Thus, by blowing film of both thermotropes, mechanical properties have been

obtained that are approximately 100% higher than those obtained in injection molding.

6.2 Predictions of Doi's Theory

1. In extensional flows, the transient equations of Doi, modified by approximating the diffusivity to be zero for a melt, predict saturation of orientation in one strain unit for uniaxial extension and about four S.U. for equal biaxial extension, irrespective of the initial values of $S_{\alpha\beta}$ input. In the former case, and in inhomogeneous biaxial flows, S_{11} is predicted to approach 2/3 and in equal biaxial extension 1/6 is the equilibrium value. The shear free transient stress predictions indicate no overshoot but some initial undershoot, depending on the value of dimensionless concentration, C, chosen.

2. In simple shear the S_{11} component of orientation requires 6-8 S.U. to reach its plateau value of 2/3 (for $D_r=0$). The component S_{12} as well as the shear stress σ_{12}, show some overshoot and an equilibrium value of zero or near zero as time approaches infinity. One may conclude that the higher order terms which Doi discarded are important, particularly at higher rates of deformation. If the value of diffusivity is increased from 0 to 1 sec-1 for C=4, the overshoot in σ_{12} decreases from about six times its long time value to nothing. The normal stresses exhibit no overshoot and reach a steady state in 6-8 S.U. (for $D_{r=0}$).

3. Doi's predictions for blown film of HBA/PET show a relatively uniaxially oriented final film, even at the highest BURs obtained in the laboratory. This finding is in qualitative agreement with experiment. The predictions of orientation for HBA/HNA indicate less axial orientation, particularly at higher BURs, than in the PET copolyester. This is also qualitatively corroborated by x-ray diffraction. The inability to accurately select an initial orientation (leaving the die) limited the quantitative value of the predictions.

4. It can be concluded that Doi's rheological theory (equations 2.15 and 2.16) does only a fair job of predicting stress growth in an anisotropic solution of PPT/H_2SO_4 at lower shear rates. At 10 sec^{-1} and higher the long time value of stress is predicted to approach zero, whereas the equilibrium value observed on the RMS was around 1000 Pa.

5. The stress overshoot predictions of Doi's transient equations were far greater than actually occurred using an experimentally determined diffusivity. For the isotropic solution the predictions of stress growth indicated a large initial overshoot (about 10 times its equilibrium value) although none was seen experimentally at less than 50 sec^{-1}.

6.3 Recommendations

In view of the foregoing conclusions, the following recommendations may be made for future work in this area.

1. Although it was not possible to produce biaxial structure when injection molded plaques were pressed between platens, if the flow were constrained in the machine direction by a mold, the resulting planar extension might induce more uniform properties.

2. Blow molding should be conducted on a larger machine where greater control could be exercised over the temperature profile and thus over the resultant structure and orientation. In conjunction, the infrared pyrometer could be employed to measure the parison temperature profile in situ and thus permit better correlation of thermal history with bottle properties and orientation. More accurate control over the blow pressure would also facilitate correlations between different deformation rates and resultant properties.

3. Microtoming bottles prior to analysis by x-ray scattering would give a more accurate picture of the layered texture that resulted.

4. Film stretching, although limited by the capabilities of the Long device, could be done in the transverse direction for HBA/HNA to improve TD properties if wide enough (4") extruded film could be obtained.

5. Further studies of blown film are recommended in view of the superior properties that were obtained under the limited conditions studied so far. In particular, barrel temperatures could be lowered further (in analogy to the blow molded results with lower extrusion temperatures). Blow up ratios, although limited by the material used, could conceivably be increased further. The difficulty lies primarily with the amount of material required to achieve a consistent bubble of large diameter. Also, if a larger die gap could be used biaxial orientation might be more readily obtained (in analogy to the blown bottles).

6. In order to determine some measure of the development of orientation in the blown film process, light scattering through the blown bubble might be possible. If the film were thin enough and the intervening air space properly accounted for, it may be possible to measure an aspect ratio as a function of axial position. As with the previous recommendation, polymer consumption is a prime consideration here and initial work with polyolefins is strongly encouraged.

7. One further method of producing biaxial properties in these materials should be examined. By laying up oriented sheet of these materials as prepregs for further processing, superior properties might be attained. Adhesion between layers is critical and optimizing it might reduce the resultant properties somewhat, depending on what temperatures and adhesives are necessary.

8. More work remains to be done on the transient response of nematic solutions in shearing flows as well as shear free flows. In order to predict stress growth, viscosity, and jump strain response, however, some modifications may need to be made on the present theory. In particular, at high rates of strain the predictions tend to diverge radically from experimental results. Doi's decoupling approximation of the order parameter tensor and the elimination of higher order terms should be examined in light of this disagreement.

9. In addition, it may be useful to determine the rotational diffusivity by some method other than utilizing Doi's theory and the zero shear rate viscosity since some of the discrepancy, especially in the degree of overshoot, can be attributed to this parameter.

REFERENCES

1. P.J. Flory, Proc. Roy. Soc. London, Ser. A. 234, 73(1956).

2. S.L. Kwolek, U.S. Patent No. 3,671,542 (1972).

3. "Liquid Crystalline Order in Polymers," A. Blumstein, ed., New York: Academic Press, 1978.

4. N.A. Plate and V.P. Shibaev in "Molecular and Supermolecular Order in Polymers," H. Staudinger, H. Hoecker, W. Kern-Huethig, and H. Wepf, eds. (1984).

5. "Advances in Polymer Science," vol. 60/61, M. Gordon and N.A. Plate, eds., Berlin: Springer-Verlag, 1984.

6. "Recent Advances in Liquid Crystalline Polymers," L.L. Chapoy, ed., London: Elsevier, 1985.

7. "Polymeric Liquid Crystals," A. Blumstein, ed., New York: Plenum Press, 1985.

8. T-S. Chung, Polym. Eng. Sci. 26, 901(1986).

9. G.W. Calundann and M. Jaffe, Proc. Robert Welch Conf. XXVI (1982).

10. D. Acierno, et al., Macromolecules 15, 1455(1982).

11. T-S Chung, J. Polym. Sci. Lett. 24, 299(1986).

12. Y. Ide and Z. Ophir, Polym. Eng. Sci. 23, 261(1983).

13. H. Sugiyama, et al., J. Appl. Polym. Sci. 30, 2329(1985).

14. H. Muramatsu and W.R. Krigbaum, J. Polym. Sci. Phys. 24, 1695(1986).

15. Tealdi, Ciferri, and Conio, to be published.

16. D.N. Lewis and J.F. Fellers, "Processing of Polymer Liquid Crystals," PATRA Report No. 233, April 1986.

17. W.J. Jackson and H.F. Kuhfuss, J. Polym. Sci. 14, 2043(1976).
18. W.C. Wooten, et al., in "Ultrahigh Modulus Polymers," A. Ciferri and I.M. Ward, eds., London: Applied Science Publishers, 1979.

19. Baird, Nguyen, and Joseph, SPE ANTEC Preprints 705(1982).

20. Z. Ophir and Y. Ide, Polym. Eng. Sci. 23, 792(1983).

21. D.G. Baird, et al., SPE ANTEC Preprints 508(1984).

22. Viola, Baird, and Wilkes, Polym. Eng. Sci. 25, 888(1985).

23. D. Done, PhD Thesis, Virginia Tech, 1987.

24. G.W. Farell and J.F. Fellers, J. Polym. Eng. 6, 263(1986).

25. Donald, Viney, and Windle, Polymer 24, 155(1983).

26. Viney, Donald, and Mitchell, Polymer 26, 870(1985).

27. Viney, Mitchell, and Windle, Polymer Comm. 24, 145(1983).

28. Viney and Windle, J. Mater. Sci. 17, 2661(1982).

29. Mitchell and Windle, Polymer 24, 1513(1983).

30. Donald, Viney, and Windle, Philos. Mag. B. 52, 925(1985).

31. Mitchell and Ishii, Polymer Comm. 26, 34(1985).

32. Mackley, Pinaud, and Siekmann, Polymer 22, 437(1981).

33. Zacchariades, Navard, and Logan, Mol. Cryst. Liq. Cryst. 110, 93(1984).

34. C. Viney, Polym. Eng. Sci. 26, 1021(1986).

35. Y. Ide and T-S Chung, J. Macromol. Sci. Phys. 23, 497(1984-5).

36. Tsai, Halpin, and Pagano, Composite Material Workshop, Technomic, Stamford, CT., 1968.

37. J.K. Lees, Polym. Eng. Sci. 8, 186(1968).

38. L.C. Saywer and M. Jaffe, J. Mater. Sci. 21, 1897(1986).
39. J.B. Stamatoff, Mol. Cryst. Liq. Cryst. 110, 75(1984).
40. S.L. Kwolek and R.R. Luise, Macromolecules 19, 1798(1986).
41. D.J. Blundell, Polymer 23, 359(1982).
42. D.G. Baird, in "Liquid Crystalline Order in Polymers," A. Blumstein, ed., New York: Academic Press, 1978.
43. K.F. Wissbrun, J. Rheology 25, 619(1981).
44. T. Asada and S. Onogi, Polym. Eng. Rev. 3, 323(1983).
45. D. Done and D.G. Baird, Polym. Eng. Sci. 27, 816(1987).
46. Lenz, Jin, and Freichtinger, Polymer 24, 327(1983).
47. J.R.A. Pearson and C.J.S. Petrie, J. Fluid Mech. 42, 609(1970).
48. J.R.A. Pearson and P.A. Gutteridge, J. Non-Newt. Fluid Mech. 4, 57(1972).
49. C.J.S. Petrie, Polym. Eng. Sci. 15, 708(1975).
50. C.J.S. Petrie, AIChE J. 21, 275(1975).
51. C.D. Han and J.Y. Park, J. Appl. Polym. Sci. 19, 3257(1975).
52. C.D. Han and J.Y. Park, J. Appl. Polym. Sci. 19, 3277(1975).
53. M.H. Wagner, Rheol. Acta 15, 40(1976).
54. J.R.A. Pearson, Ch. 17 in "Mechanics of Polymer Processing," London: Elsevier, 1985.
55. C.J.S. Petrie, Ch. 7 in "Computational Analysis in Polymer Processing," Pearson and Richardson, eds., London: Elsevier, 1983.
56. R. Farber and J. Dealy, Polym. Eng. Sci. 14, 435(1974).
57. P.A. Gutteridge, PhD Thesis, University of London, 1977.

58. J.L. Ericksen, in "Lecture Notes in Mathematics," New York: Springer-Verlag, 1984.
59. M.Doi, J. Polym. Sci. Phys. 19, 229(1981).

60. M. Doi and S.F. Edwards, Chs. 8-10 in "The Theory of Polymer Dynamics," Oxford: Clarended Press, 1986.

61. M. Doi, J. Phys. (Paris) 36, 607(1975).

62. M. Doi and S.F. Edwards, J. Chem. Soc. Faraday Trans. II 74, 568(1978); 74, 918(1978).

63. J.G. Kirkwood and P.L. Auer, J. Chem. Phys. 19, 281(1951).

64. L. Onsager, Ann. N.Y> Acad. Sci. 51, 627(1949).

65. W. Maier and A. Saupe, Z. Naturforschg., Teil A 13, 564(1958).

66. N. Kuzuu and M. Doi, J. Phys. Soc. Japan 52, 3486(1983).

67. J. Dealy, Polym. Eng. Sci. 11, 431(1971).

68. J.A. Castellano, "Liquid Crystals: The Fourth State of Matter," F.D. Saeva, ed., New York: Marcel Dekker, 1979.

69. J.L. White and J.E. Spruiell, Polym. Eng. Sci. 21, 859(1981).

70. G.M. Prilutski, PhD Thesis, University of Delaware, 1984.

71. Rheometrics Mechanical Spectrometer Instruction Manual

72. Joseph, Wilkes, and Baird, Polym. Eng. Sci. 25, 377(1985).

73. D.G. Baird and R.L. Ballman, J. Rheology 23, 505(1979).

74. Baird, Ballman, and Everage, Rheol. Acta 19, 183(1980).

75. D.G. Baird, American Chemical Society Polymer Preprints 23, 10(1982).

76. G.G. Viola, PhD Dissertation, Virginia Tech, 1985.

```
C     This program calculates the stresses generated at the
C     inception of steady simple shear.  It calls on the IMSL
C     routine DGEAR to solve the system of differential
C     equations.

      INTEGER N,METH,MITER,INDEX,IWK(4),IER,K
      REAL Y(4),WK(60),X,TOL,XEND,H,SIGMA(4),C,S,T
      EXTERNAL FCN,FCNJ
$DEBUG
      N = 4

C     The initial values of the components of the orientational
C     order parameter tensor will be set as the Y(N) where Y(4)
C     is the 1,2 component, Y(1) the 1,1 component, Y(2) the 2,2
C     component and Y(3) the 3,3 component.  Time, X, will also
C     be initialized.

      X = 0.
      Y(1) = 0.
      Y(2) = 0.
      Y(3) = 0.
      Y(4) = 0.0

C     The parameters for the routine DGEAR will be set.

      TOL = 0.0001
      H = 0.00001
      METH = 2
      MITER = 2
      INDEX = 1

C     The values of dimensionless concentration, C, and the pro-
C     duct ckT, given by T, will be input.

      C = 3.7
      T = 27928.0

C     The routine calling DGEAR follows.  DGEAR itself calls the
C     subroutine FCN which contains the differential equations
C     to be solved.  At the end of each run through the DO loop,
C     the values of stress, SIGMA(N) are calculated and output.
```

```
      DO 10 K=1,150
      XEND=FLOAT(K)/10.0
      CALL DGEAR (N,FCN,FCNJ,X,H,Y,XEND,TOL,METH,MITER,INDEX,IWK,WK,IER)
      IF(IER.GT.128) GOTO 20

      SIGMA(1)=T*(Y(1)*(1.-C/3.)-C*(Y(1)**2.+Y(4)**2.)+C*S*
     $(1./3.+Y(1)))
      SIGMA(2)=T*(Y(2)*(1.-C/3.)-C*(Y(2)**2.+Y(4)**2.)+C*S*(1./3.+Y(2)))
      SIGMA(3)=T*(Y(3)*(1.-C/3.)-C*Y(3)**2.+C*S*(1./3.+Y(3)))
      SIGMA(4)=T*(Y(4)*(1.-C/3.)-C*Y(4)*(Y(1)+Y(2))+C*S*Y(4))
      IOUT = 6
      CALL UGETIO(3,NIN,IOUT)
      OPEN (UNIT=IOUT,FILE='LPT1')
      WRITE(IOUT,100)X,SIGMA(1),SIGMA(2),SIGMA(3),SIGMA(4)
      100  FORMAT(10X,5F11.2)
      10  CONTINUE
      STOP
      20  CONTINUE
      STOP
      END

C     The subroutine FCN contains the differential equations to
C     be solved by DGEAR.  E is the shear rate input, and DR the
C     diffusivity.  FCNJ is a dummy subroutine required by DGEAR
C     when it calculates the Jacobian of the matrix.

      SUBROUTINE FCN(N,X,Y,YPRIME)
      INTEGER N
      REAL Y(N),YPRIME(N),X,E,D(4),C,DR,S
      E =50.0
      DR = 0.820
      D(N) = DR/(1.-1.5*Y(N)**2.)**2.
      S = Y(1)**2.+Y(2)**2.+Y(3)**2.+2.*Y(4)**2.
      YPRIME(1)=E*(4./3.*Y(4)-2.*Y(1)*Y(4))+6*D(1)*((C/3.-1.)*Y(1)+C*(Y
     $(1)**2.+Y(4)**2.)-C*S*(1./3.+Y(1)))
      YPRIME(2)=E*(-2./3.*Y(4)-2.*Y(2)*Y(4))+6*D(2)*((C/3.-1.)*Y(2)+C*(
     $Y(2)**2.+Y(4)**2.)-C*S*(1./3.+Y(2)))
      YPRIME(3)=E*(-2./3.*Y(4)-2.*Y(3)*Y(4))+6*D(3)*((C/3.-1.)*Y(3)+C*Y
     $(3)**2.-C*S*(1./3.+Y(3)))
      YPRIME(4)=E*(1./3.-2.*Y(4)**2.+Y(2))+6*D(4)*((C/3.-1.)*Y(4)+Y(4)*
     $C*(Y(1)+Y(2))-C*Y(4)*S)
      RETURN
      END
      SUBROUTINE FCNJ(N,X,Y,PD)
      INTEGER N
      REAL Y(N),PD(N,N),X
      RETURN
      END
```

```
C     This program calculates the orientation parameter tensor
C     components for inhomogeneous biaxial extension using the
C     IMSL routine DGEAR to solve the differential equations.
C     The logic and symbols are identical to the previous program
C     except that the kinematics are input to FCN for the film
C     blowing process.


$DEBUG
      IMPLICIT REAL*8 (A-H,O-Z)
      REAL Y(3),WK(42),X,TOL,XEND,H
      INTEGER N,METH,MITER,INDEX,IWK(3),IER,K
      EXTERNAL FCN,FCNJ
      N = 3
      X = 0.05
      Y(1) = 0.332
      Y(2) =-0.166
      Y(3) =-0.166
      TOL = 0.0001
      H = 0.00001
      METH = 2
      MITER = 2
      INDEX = 1
      DO 10 K=1,80
      XEND = FLOAT(K)/10.
      CALL DGEAR (N,FCN,FCNJ,X,H,Y,XEND,TOL,METH,MITER,INDEX,IWK,WK,IER)
      IF(IER.GT.128) GOTO 20
      IOUT = 6
      CALL UGETIO(3,NIN,IOUT)
      OPEN (UNIT=IOUT,FILE='LPT1')
      WRITE(IOUT,100)X,E1,E2,Y(1),Y(2),Y(3)
      100  FORMAT(10X,6F10.6)
      10  CONTINUE
      STOP
      20  CONTINUE
      STOP
      END
      SUBROUTINE FCN(N,X,Y,YPRIME)
      IMPLICIT REAL*8 (A-H,O-Z)
      REAL X,Y(N),YPRIME(N)
      INTEGER N

C     The kinematics are calculated from Z, the axial distance,
C     A, the bubble radius, V1 the local velocity parallel to the
C     surface, and psi, the angle between the axial direction and
C     the local tangent to the surface.

      Z = 0.07656+0.5962*X+0.1247*X**2.+0.00659*X**3.
      A = 2.436-0.1281*Z+0.0144*Z**2.-0.00030*Z**3.
      V1 = 0.7527+0.241*Z-0.002796*Z**2.
      DA = -0.1281+0.0288*Z-0.0009*Z**2.
      DV1 = 0.241-0.00559*Z
      PSI = DATAN(DA)
```

```
      E1 = DCOS(PSI)*DV1
      E2 = V1/A*COS(PSI)*DA
      YPRIME(1)=E1*(2./3.+4./3.*Y(1)-2.*Y(1)**2.)-E2*Y(2)*(2./3.+2.*
     $Y(1))+(E1+E2)*Y(3)*(2./3.+2.*Y(1))
      YPRIME(2)=E2*(2./3.+4./3.*Y(2)-2.*Y(2)**2.)-E1*Y(1)*(2./3.+2.*
     $Y(2))+Y(3)*(E1+E2)*(2./3.+2.*Y(2))
      YPRIME(3)=(E1+E2)*(2.*Y(3)**2.-2./3.-4./3.*Y(3))-E1*Y(1)*(2./3.+
     $2.*Y(3))-E2*Y(2)*(2./3.+2.*Y(3))
      RETURN
      END
      SUBROUTINE FCNJ(N,X,Y,PD)
      INTEGER N
      REAL Y(N),PD(N,N),X
      RETURN
      END
```

Appendix B: Calculations

Calculations were made to determine the dimensionless concentration, C, the diffusivity, D_r, and the ratio of $F_{\alpha\beta}/G_{\alpha\beta}$ for the 60 mole% HBA/PET system. Calculations of the concentration of the PPT/H_2SO_4 system (rods/volume) were also made and will be included.

C for HBA/PET

A rigid rod of length L and diameter d was assumed for each molecule. By using the C=O linkage as an effective radius of the rod and ignoring the radius of the oxygen, the diameter was obtained as:

$$d = 2[2x1.3+1.23] = 7.7 \text{ Angstroms}$$

using bond lengths and atomic radii (CRC Handbook of Chemistry, 62nd edition). Length was then determined to be 800 Angstroms from:

$$L = V/\pi r^2$$

for rigid rods where the volume of a rod, V, may be given as:

$$Mn/N_A*density$$

where Mn is the number average molecular weight and N_A is Avagadro's number. The density of this material is approximately 1.28 g/cc in the melt state (from the Instron Capillary Rheometer) and Mn≈20,000.

Using the molecular dimensions, the critical concentration for the instability of the isotropic phase may be obtained from Doi as:

$$c^* \approx 5.1/dL^2$$

Thus a critical concentration of 1.04 E18 molecules/cc was calculated. Since

$$c/c^* = C/3$$

if the actual concentration of rods is known, it is possible to obtain a dimensionless concentration. Shear stress at the start up of simple shear for this system was given in Viola's thesis. By comparing long time values with Doi's predictions for various C at 1.0 sec^{-1} and iterating one obtains:

$$1.0\ E3\ Pa \approx 0.1\ c\ (1.38\ E\text{-}23)(523K)E6$$

or,

$$c = 1.38\ E18\ molecules/cc$$

where the lefthand side of the above equation is the experimental value and the righthand side Doi's predictions at the given temperature (.1ckT). This concentration corresponds to a value of C = 4.0, which was subsequently used for the majority of predictions of Doi's equations.

D_r for HBA/PET

Using the values of d and L found above and the relevant equations from Doi and Edwards recent book (8.16, 9.16, and 10,53) D_r and D_r may be obtained. First, D_{r0} is calculated for dilute solutions from 8.16 for a given temperature if the "solvent" viscosity is known (see Chapter 3 for this equation). D_{r0} was found to be 0.424 for this sytem at 523K using a dynamic viscosity from Viola's thesis of 122 Pa-sec.

Equation 9.16 is then employed:

$$D_r = D_{r0}\ \beta\ (cL3)\text{-}2$$

where β has been obtained from experiment and is given in the literature (Doi' as about 1300. By employing the concentration and rod length already found, D_r = 1.10 E-3 was calculated.

Equation 10.53 corrects for a nematic environment:

$$D_r = Dr[1\text{-}3/2S\alpha\beta^2]\text{-}2$$

in which $S_{\alpha\beta^2}$ represents the double dot product of the orientation order parameter tensor components. This equation was used in the computer programs (Appendix A) to adjust the diffusivity as the order in the system changed.

$F_{\alpha\beta}/G_{\alpha\beta}$ for HBA/PET

To justify eliminating the $F_{\alpha\beta}$ term for thermotropic systems, one needs to calculate the relative importance of each of the terms in Doi's equations for orientation development. The $F_{\alpha\beta}$ term contains diffusivity and dimensionless concentration terms whereas the $G_{\alpha\beta}$ term contains the flow kinematics and deformation rates. This calculation was made for the 1,1 component in uniaxial deformation at 1.0 sec-1:

$$F_{11}/6D_r = (C/3-1)S_{11} - C(S_{22}^2+S_{33}^2) - C\Sigma S_{ii}^2 S_{11}$$

$$G_{11} = 2/3 + S_{11} - 3S_{11}^2$$

where the extension rate has been substituted into the latter term. For C = 4, the F_{11} term becomes:

$$F_{11} = 6D_r[S_{11}/3 - 2S_{11}^2 - 2S_{11}^3]$$

since $S_{22} = S_{33} = -\frac{1}{2}S_{11}$ for a nematic.

This ratio was then calculated for various orientation parameter tensor component values:

S_{11}	Dr	$F_{\alpha\beta}/G_{\alpha\beta}$	
0	1.1 E-3	0/.667	= 0
1/6	0.0012	-.00007/.75	= -8.87 E-5
1/3	0.0016	-.00017/.889	= -.000198
1/2	0.00282	-.00164/.417	= -.00394
2/3	0.010	-.0402/0	= -

Thus, even for $S_{11} > \frac{1}{2}$, $F_{\alpha\beta}$ is not important given Dr = 1.1 E-3 and C = 4, except at values approaching perfect orientation, $S_{11} = 2/3$.

c for PPT/H_2SO_4

Assuming a concentration of 4% by weight (which was subsequently measured to be 3.9% by coagulation of the solution in water), the concentration in molecules/cc was determined:

c = (4 g PPT/100 g soln)(1 ml PPT/1.44 g PPT)*
(1.824 g soln/1 ml soln)*[(1.44/20050)*6.022 E23]
molec PPT/ml PPT

c = 2.19 E18 molec/cc (4 wt%)

Similarly, other rod concentrations may be determined from other weight concentrations. At 60°C the ckT product was calculated:

Concentration, wt%	ckT, Pa.
3.9	9812
11.1	27928

D_r was then calculated from the Doi-Edwards relation:

$$D_r = ckT/10\mu_0$$

where μ_0 is the zero shear rate viscosity (exp.) to be 0.082 for the 3.9% solution.

Heat transfer calculations were also made to determine the centerline temperature at the conclusion of the non-isothermal deformation of plaques of HBA/PET and HBA/HNA.

Assuming a flat plate analysis for the conduction problem, one can approximate the centerline temperature in the pressed plaque subject to the boundary conditions of a constant temperature source imposed at t=0. Neglecting the conduction through the metal plates in which the plaque is sandwiched, one can use the tables in Appendix F of Welty, Wicks, and Wilson. The polymer handbook may be used to arrive at the physical constants (assuming PET):

$k = .289$ J/msK

density = 1370 kg/m^3

$C_p = 1250$ J/kgK

From the process, one obtains the following:

$T_\infty = 10°C$

$T_0 = 180°C$ for HBA/PET

$T_0 = 250°C$ for HBA/HNA

$t \approx 0.5$ seconds for the deformation

$x_1 = 0.00075$ for a 1.5 ml thick plaque

Assuming further that the heat transfer due to convection will be small compared to that due to conduction, the dimensionless parameter m will be zero. The parameter Y is read off of Figure F.7 for a given value of X:

$$X = \alpha t / x_{1/2}$$

where α is the thermal diffusivity given by:

$$\alpha = k/\text{density}*C_p$$

Substituting into the equations, one obtains Y = 0.85 for the centerline. But,

$$Y = (T-T_\infty)/(T_0-T_\infty)$$

so for the result is

T(.5 second) = 155°C for HBA/PET

T(.5 second) = 214°C for HBA/HNA

using the same approximate physical parameters for both systems.

Appendix C: Blown Film Analysis

The polynomial regressions for Figs. C.1-C.6 are given by the following equations:

Figure	BUR	Equation
C.1	1.45	$2.436-.1281z+.0144z^2-.00030z^3$
	2.30	$2.436+.1802z+.0146z^2-.0012z^3+2.24E-5*z^4$
	3.10	$2.449+.2506z+.0479z^2-.0041z^3+8.56E-5*z^4$
	1.30	$2.45-.0866z+.0132z^2-3.44E-4*z^3$
C.2	1.45	$.07656+.5962t+.1247t^2+.00659t^3$
	2.30	$.300-.207t+.6697t^2-.0334t^3$
	3.10	$.288+.2774t+.5922t^2-.0301t3$
	1.30	$-.0918+1.0609t+.1801t^2+9.93E-4*t^3$
C.3	1.45	$.7527+.241z-2.796E-3*z^2$
	2.30	$.6972+.651z-.0414z^2+8.89E-4*z^3$
	3.10	$.8363+.6467z-.0427z^2+9.29E-4*z^3$
	1.30	$1.235+.2048z-.00314z^2$
C.4	1.00	$2.458-.1535z+.0224z^2-.00107z^3+1.675E-5*z^4$
	1.95	$2.385+.2549z-.0063z^2-1.47E-5*z^3$
	2.60	$2.428+.4203z-.0115z^2+2.10E-5*z^3$
	1.35	$2.405+.0425z+.0028z^2-1.28E-4*z^3$
	2.30	$2.268+.621z-.0355z^2+5.21E-4*z^3+5.31E-5*z^4$

C.5	1.00	$-.4372+2.912t+.7228t^2$
	1.95	$-.3126+3.232t+.625t^2$
	2.60	$-.8874+4.977t+.5147t^2$
	1.35	$-.4031+2.182t+.7628t^2$
	2.30	$-.5741+4.677t+.4172t^2$
C.6	1.00	$3.32+.3316z-.00427z^2$
	1.95	$3.688+.2553z-.00233z^2$
	2.60	$5.69+.1291z-2.86E-5z^2$
	1.35	$2.752+.3777z-.00513z^2$
	2.30	$5.481+.07193z+.0014z^2$

Error in film bubble shape plots

Measuring off of the TV monitor introduces a .1 cm error due to accuracy of the ruler used. Regression deviations for HBA/PET and HBA/HNA were about .048 cm each for a total error of ±.15 cm.

Error in marker position vs. time plots

Stopwatch error (reflexes) was found from repeated runs to be .034 seconds for HBA/PET and .109 seconds for HBA/HNA. Regression deviations were .078 seconds for HBA/PET and .360 seconds for HBA/HNA. The combined error is thus ±.11 seconds for the former and ±.47 seconds for the latter. This analysis ignores the relatively small (in this case) error introduced by measurement off the TV.

Error in film surface velocity plots

The error in this plot is essentially the error in determining dz/dt. The numerator has an error of .1 cm (as determined above) and the denominator error is simply given by the time error off of the marker position vs. time chart (excluding regression deviations). Thus, for HBA/PET:

$$\text{error} = \pm \tfrac{1}{2} [(9.9/7.034)-(10.1/6.966)] = \pm 0.043 \text{ cm/s}$$

assuming a distance of 10 cm. and a time of 7 seconds to the freeze line. Similarly, for HBA/HNA:

$$\text{error} = \pm \tfrac{1}{2} [(9.9/4.109)-(10.1/3.891)] = \pm 0.186 \text{ cm/s}$$

assuming a distance of 10 cm. and a time of 4 seconds to the freeze line.

The above error estimates are reproduced in the following figures as error bars.

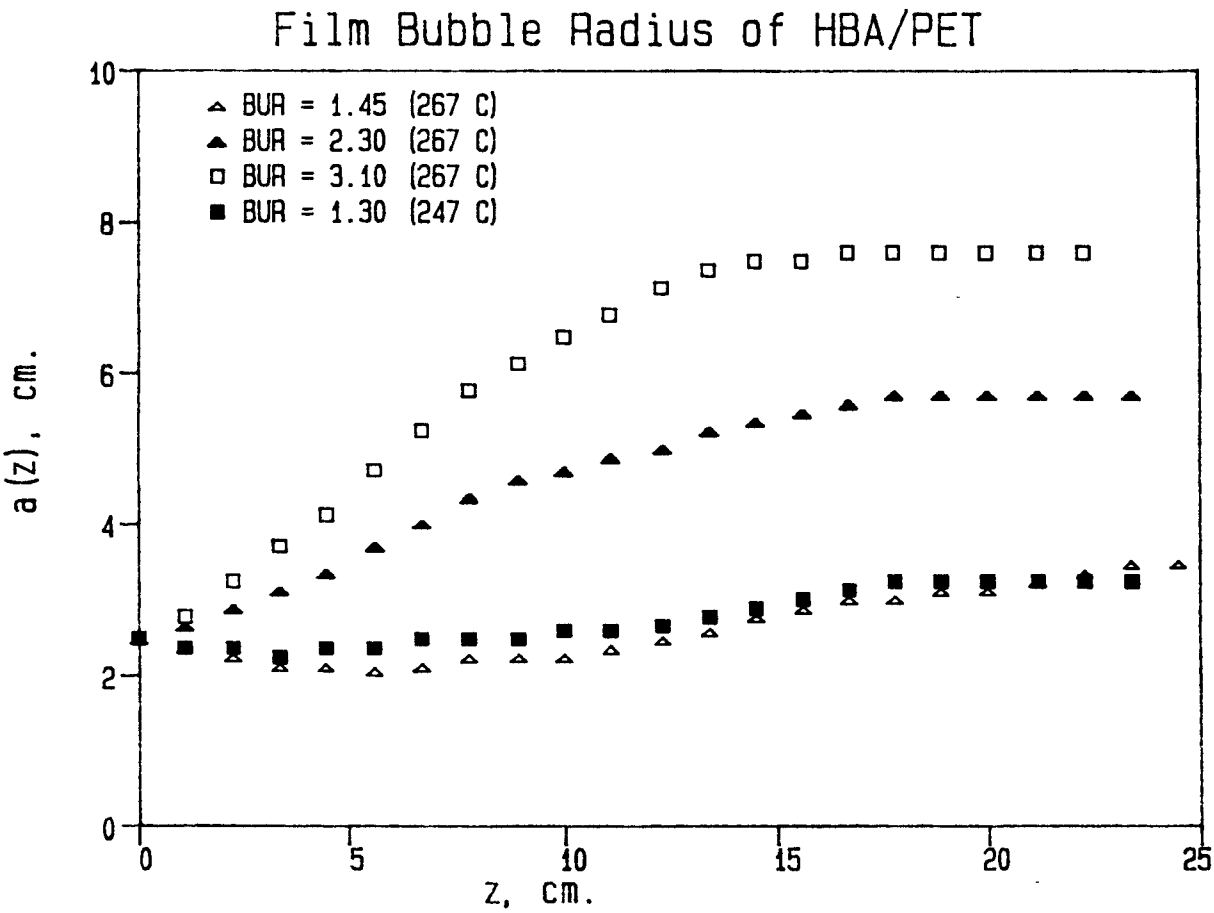

Figure C.1 Film bubble radius as a function of the axial distance for HBA/PET with different BUR.

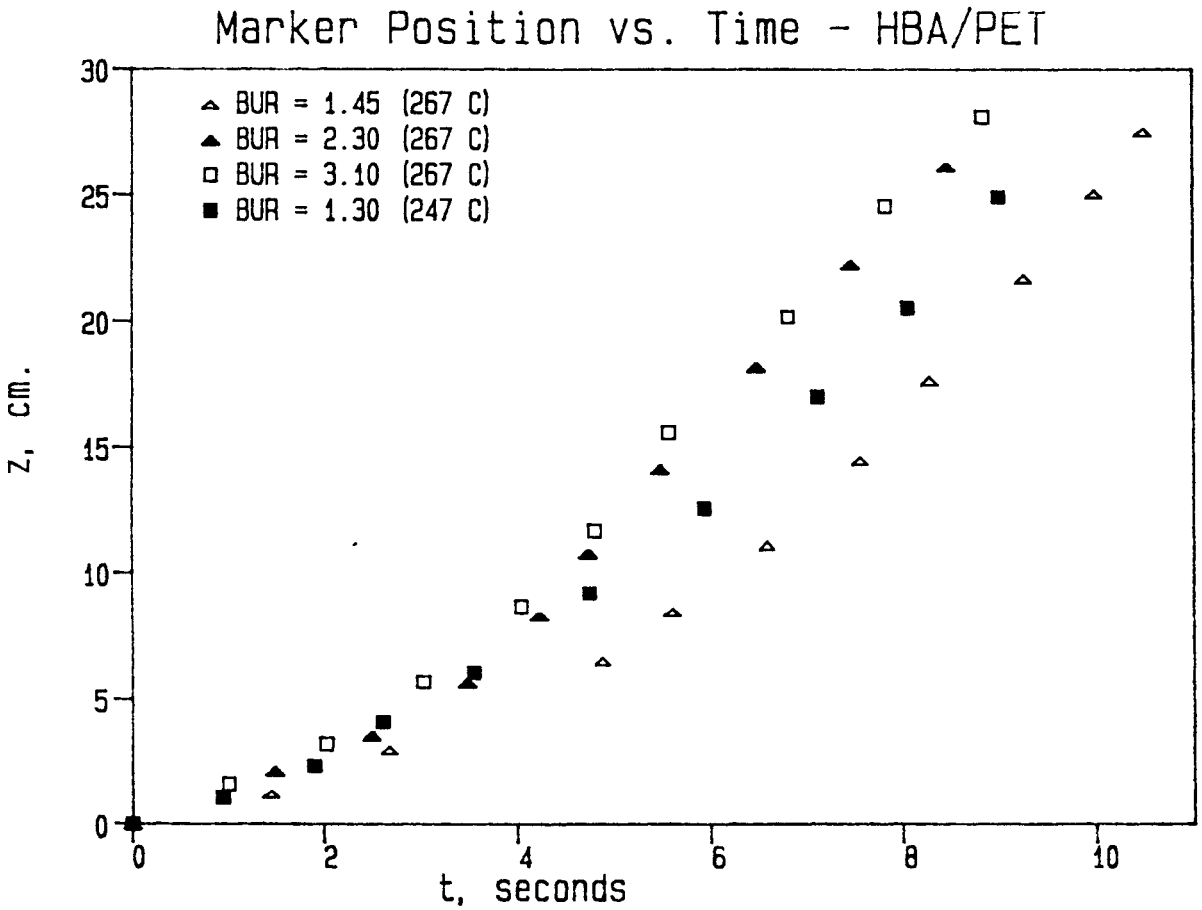

Figure C.2 Marker position as a function of time for HBA/PET with different BUR.

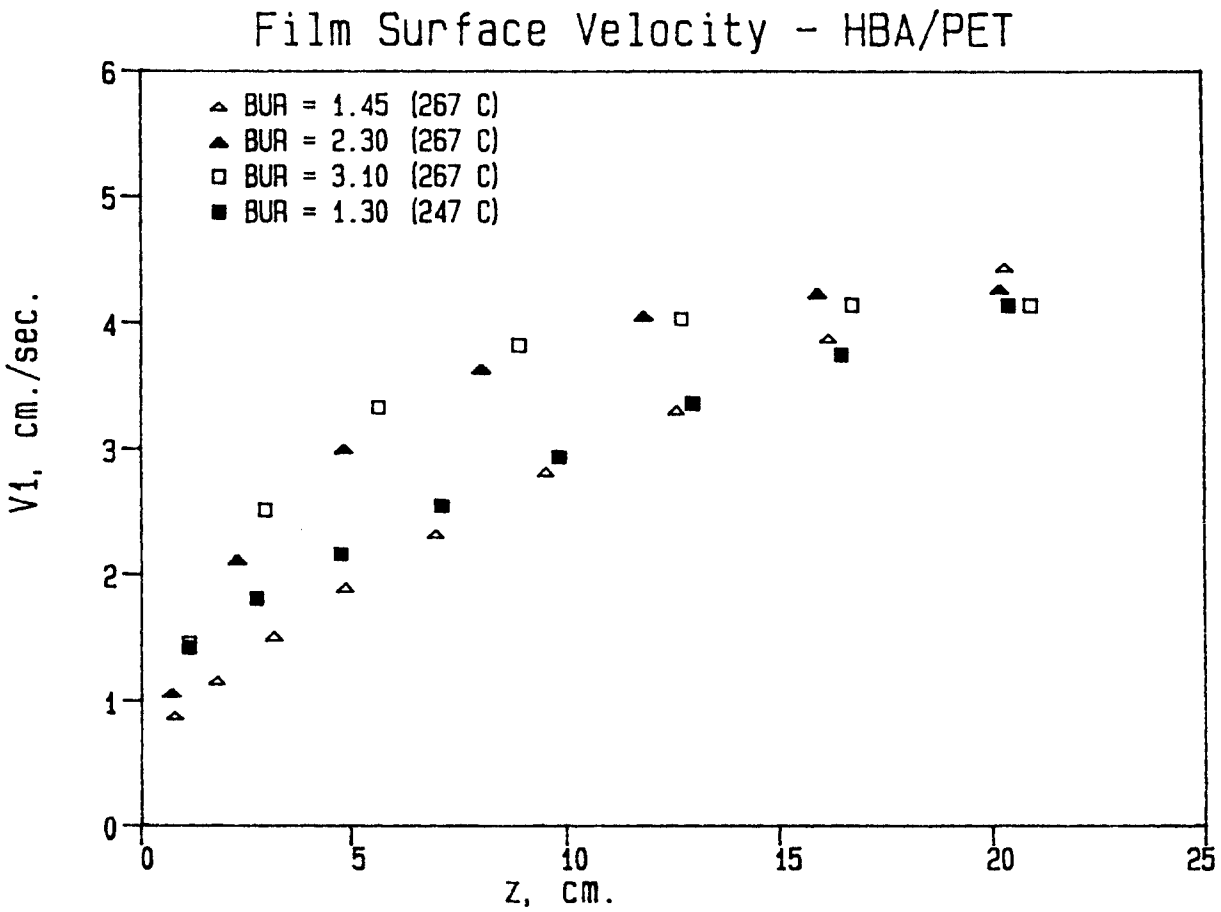

Figure C.3 Film surface velocity as a function of axial distance for HBA/PET with different BUR.

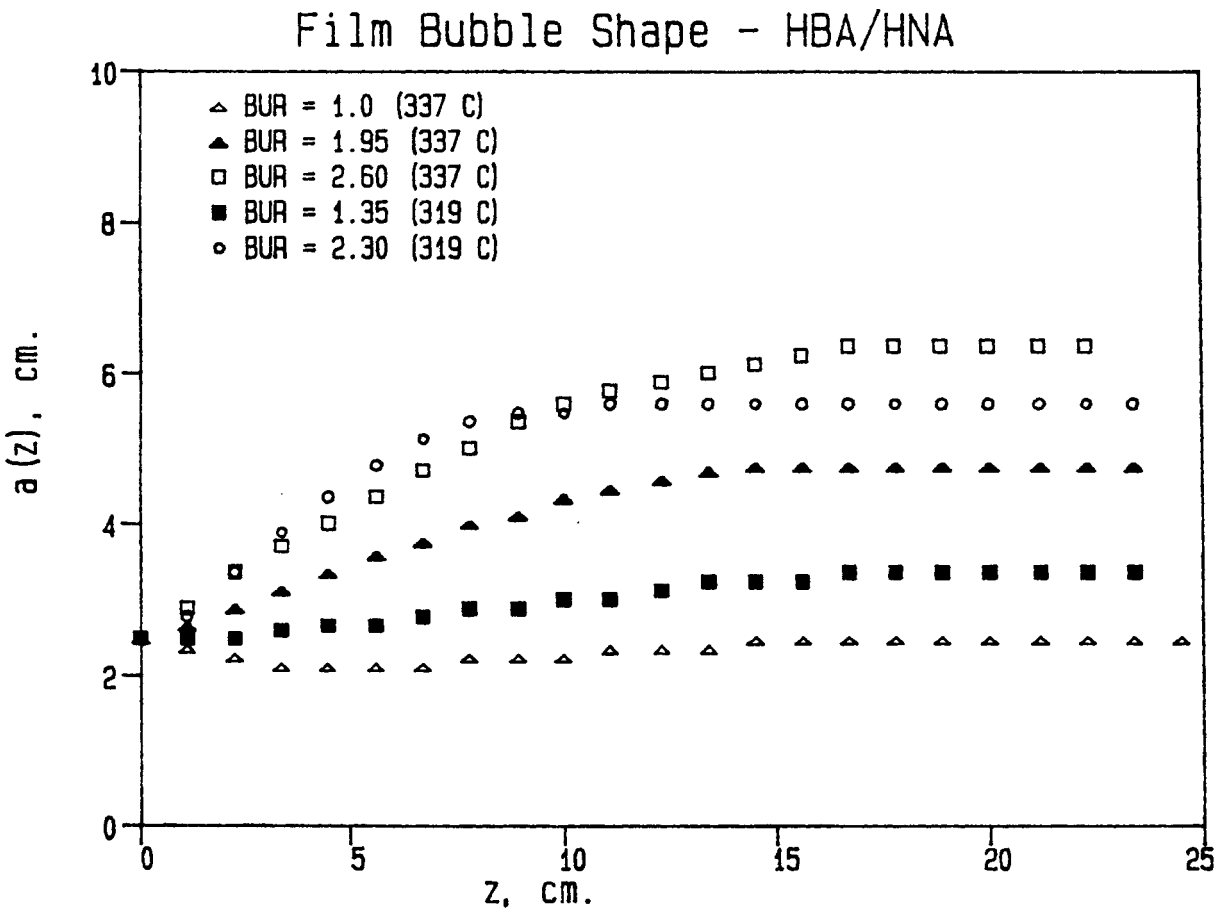

Figure C.4 Film bubble radius as a function of axial distance for HBA/HNA with different BUR.

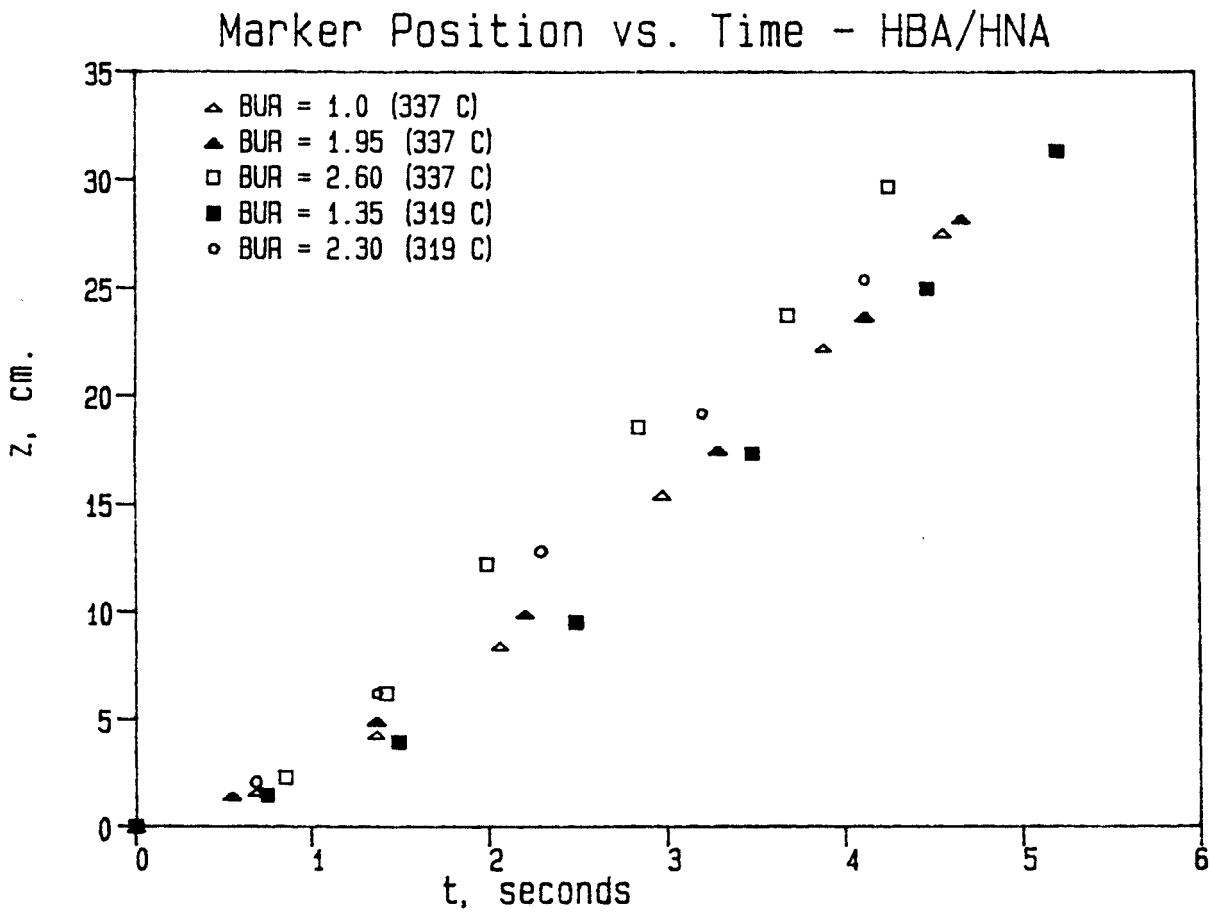

Figure C.5 Marker position as a function of time for HBA/HNA with different BUR.

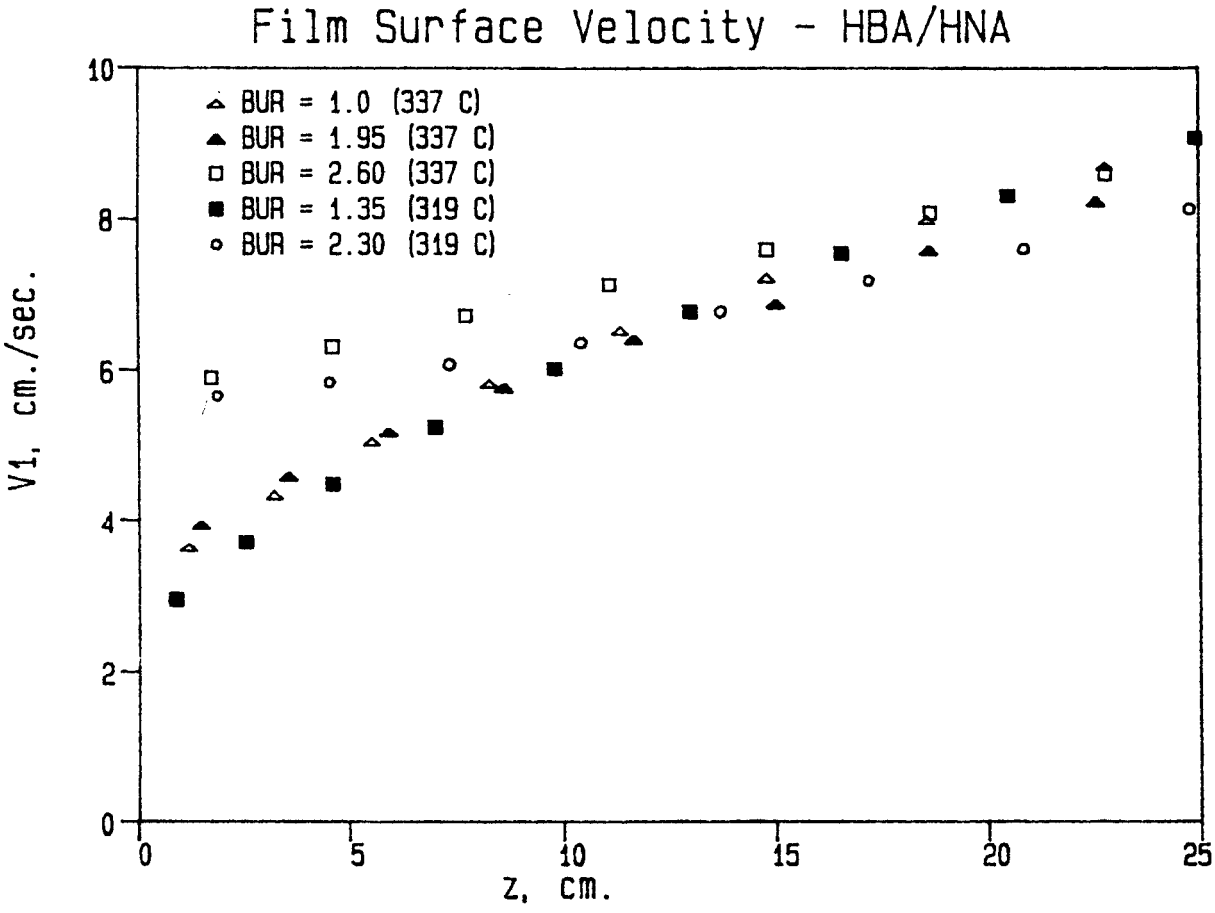

Figure C.6 Film surface velocity as a function of axial distance for HBA/HNA with different BUR.

The vita has been removed from the scanned document